# Geomorphology

## Quaternary landscape evolution in a tectonically active rift basin (paleo-lake Mweru, south-central Africa)

--Manuscript Draft--

| | |
|---|---|
| **Manuscript Number:** | GEOMOR-9528R4 |
| **Article Type:** | Research Paper |
| **Keywords:** | Landscape evolution; Morphotectonic analysis; Terrestrial cosmogenic nuclides; East African Rift System |
| **Corresponding Author:** | Spiros Olivotos<br>GFZ Potsdam<br>Potsdam, GERMANY |
| **First Author:** | Spiros Olivotos |
| **Order of Authors:** | Spiros Olivotos |
| | Samuel Niedermann |
| | Tyrel Flügel |
| | Vasiliki Mouslopoulou |
| | Silke Merchel |
| | Fenton Cotterill |
| | Bodo Bookhagen |
| | Andreas Gärtner |
| | Georg Rugel |
| | Andreas Scharf |
| | Marie-Josée Nadeau |
| | Régis Braucher |
| | Martin Seiler |
| **Abstract:** | Located between the Northern Province of Zambia and the southeastern Katanga Province of the Democratic Republic of Congo, Lakes Mweru and Mweru Wantipa are part of the southwest extension of the East African Rift System (EARS). Fault analysis reveals that, since the Miocene, movements along the active Mweru-Mweru Wantipa Fault System (MMFS) have been largely responsible for the reorganization of the landscape and the drainage patterns across the western branch of the EARS. To investigate the spatial and temporal patterns of fluvial-lacustrine landscape development, we determined in-situ cosmogenic $^{10}Be$ and $^{26}Al$ using Accelerator Mass Spectrometry. A total of twenty-six quartzitic bedrock samples were collected from knickpoints across the Mporokoso Plateau (south of Lake Mweru) and the eastern part of the Kundelungu Plateau (north of Lake Mweru). Samples from the Mporokoso Plateau and close to the MMFS provide evidence of temporary burial. By contrast, surfaces located far from the MMFS appear to have remained uncovered since their initial exposure as they show consistent $^{10}Be$ and $^{26}Al$ exposure ages ranging up to ~830 ka. Reconciliation of the observed burial patterns with morphotectonic and stratigraphic analysis reveals the existence of an extensive paleo-lake during the Pleistocene. Through hypsometric analyses of the dated knickpoints, the potential maximum water level of the paleo-lake is constrained to ~1200 m asl. High denudation rates (up to ~40 mm $ka^{-1}$) along the eastern Kundelungu Plateau suggest that footwall uplift, resulting from normal faulting, caused rapid river incision, thereby controlling paleo-lake drainage. The complex exposure histories recorded by $^{10}Be$ and $^{26}Al$ may be explained because of lake water-level fluctuations caused by active normal faulting along the MMFS coupled with intense climate variations across southeastern Africa. |

## Highlights

- Explores existence of a Quaternary paleo-lake Mweru, SW East African rift system
- Applies exposure ages of knickpoints, fault analyses and geomorphic investigations
- Cosmogenic nuclides retrieve a landscape history of burial, exposure and denudation
- Faulting and lake-river knickpoints indicate a paleo-lake level at ~1200 m asl
- Lake dynamics linked to recurring neotectonics and regional climate variation

## Abstract

Located between the Northern Province of Zambia and the southeastern Katanga Province of the Democratic Republic of Congo, Lakes Mweru and Mweru Wantipa are part of the southwest extension of the East African Rift System (EARS). Fault analysis reveals that, since the Miocene, movements along the active Mweru-Mweru Wantipa Fault System (MMFS) have been largely responsible for the reorganization of the landscape and the drainage patterns across the western branch of the EARS. To investigate the spatial and temporal patterns of fluvial-lacustrine landscape development, we determined in-situ cosmogenic $^{10}Be$ and $^{26}Al$ using Accelerator Mass Spectrometry. A total of twenty-six quartzitic bedrock samples were collected from knickpoints across the Mporokoso Plateau (south of Lake Mweru) and the eastern part of the Kundelungu Plateau (north of Lake Mweru). Samples from the Mporokoso Plateau and close to the MMFS provide evidence of temporary burial. By contrast, surfaces located far from the MMFS appear to have remained uncovered since their initial exposure as they show consistent $^{10}Be$ and $^{26}Al$ exposure ages ranging up to ~830 ka. Reconciliation of the observed burial patterns with morphotectonic and stratigraphic analysis reveals the existence of an extensive paleo-lake during the Pleistocene. Through hypsometric analyses of the dated knickpoints, the potential maximum water level of the paleo-lake is constrained to ~1200 m asl. High denudation rates (up to ~40 mm $ka^{-1}$) along the eastern Kundelungu Plateau suggest that footwall uplift, resulting from normal faulting, caused rapid river incision, thereby controlling paleo-lake drainage. The complex exposure histories recorded by $^{10}Be$ and $^{26}Al$ may be explained because of lake water-level fluctuations caused by active normal faulting along the MMFS coupled with intense climate variations across southeastern Africa.

# Quaternary landscape evolution in a tectonically active rift basin (paleo-lake Mweru, south-central Africa)

Spiros Olivotos[1], Samuel Niedermann[1], Tyrel Flügel[2], Vasiliki Mouslopoulou[3], Silke Merchel[4], Fenton Cotterill[2], Bodo Bookhagen[5], Andreas Gärtner[4], Georg Rugel[4], Andreas Scharf[4], Marie-Josée Nadeau[6], Régis Braucher[7], Martin Seiler[6]

Affiliations

(1) Deutsches GeoForschungsZentrum GFZ, Section 3.1, Telegrafenberg, 14473 Potsdam, Germany.

(2) Stellenbosch University, Matieland, 7602, Stellenbosch, South Africa.

(3) National Observatory of Athens, Institute of Geodynamics, Lofos Nimfon, Athens, 11810, Greece.

(4) Helmholtz-Zentrum Dresden-Rossendorf (HZDR), Bautzner Landstraße 400, 01328 Dresden, Germany.

(5) Institut für Geowissenschaften, University of Potsdam, Karl-Liebknecht-Str. 24-25, 14476 Potsdam, Germany.

(6) The National Laboratory for Age Determination, NTNU University Museum, Sem Sælands vei 5, 7491 Trondheim, Norway.

(7) CEREGE, Aix Marseille Univ., CNRS, Collège de France, IRD, INRAE, Plateau de l'Arbois, 13545 Aix en Provence, France

**Keywords:** Landscape evolution; Morphotectonic Analysis; Terrestrial cosmogenic nuclides; East African Rift System.

## Highlights

- Explores existence of a Quaternary paleo-lake Mweru, SW East African rift system
- Applies exposure ages of knickpoints, fault analyses and geomorphic investigations~~Applies cosmogenic dates of knickpoints, fault analysis and geomorphic investigations~~
- Cosmogenic nuclides retrieve a landscape history of burial, exposure and denudation
- Faulting and lake-river knickpoints indicate a paleo-lake level at ~1200 m asl
- Lake dynamics linked to recurring neotectonics and regional  climate variation
- ~~Explores existence of a Quaternary palaeo-lake Mweru, SW East African rift system~~
- ~~Applies cosmogenic nuclide dating, fault analysis and geomorphic investigations~~
- ~~Cosmogenic data show spatial-temporal patterns of burial, exposure and denudation~~

**Formatted:** Font: (Default) Times New Roman, 12 pt

**Formatted:** Line spacing: Double

**Formatted:** Font: (Default) Times New Roman, 12 pt

**Formatted:** Font: (Default) Times New Roman, 12 pt

**Formatted:** Line spacing: Double, Bulleted + Level: 1 + Aligned at: 0.25" + Indent at: 0.5"

~~Faulting and lake-river knickpoints indicate a paleo-lake level at ~1200 m asl~~

~~Lake development linked to active faulting and regional SE Africa climate variation~~

- ~~$^{10}Be$ and $^{26}Al$ dating reveals an extended paleo-lake Mweru during the Quaternary~~
- ~~Morphotectonic analysis indicate a paleo-lake level at ~1200 m asl~~
- ~~Two waterfalls have exceptionally high minimum exposure ages of 524 and 833 ka~~
- ~~Normal faulting forces increased river incision NW of paleo-lake Mweru~~
- ~~Striking differences in denudation rates among the surrounding plateaus~~

**Formatted:** List Paragraph, Bulleted + Level: 1 + Aligned at: 0.25" + Indent at: 0.5"

**Formatted:** Normal, Left, Space After: 0 pt, Line spacing: single, No bullets or numbering

**Commented [A1]:** These read well but perhaps they do not capture te story you have told completely.

**Formatted:** Space After: 10 pt, Line spacing: Multiple 1.15 li

## Abstract

Located between the Northern Province of Zambia and the southeastern Katanga Province of the Democratic Republic of Congo, Lakes Mweru and Mweru Wantipa are part of the southwest extension of the East African Rift System (EARS). Fault analysis reveals that, since the Miocene, ~~the~~ movements ~~at~~ along the active Mweru-Mweru Wantipa Fault System (MMFS) have been largely responsible for the reorganization of the landscape and the drainage patterns across the western branch of the EARS. ~~In order to~~To investigate the spatial and temporal patterns of fluvial-lacustrine landscape development, we determined in-situ cosmogenic $^{10}$Be and $^{26}$Al using Accelerator Mass Spectrometry. A total of twenty-six quartzitic bedrock samples were collected from knickpoints across the Mporokoso Plateau (south of Lake Mweru) and the eastern part of the Kundelungu Plateau (north of Lake Mweru). Samples from the Mporokoso Plateau and close to the MMFS provide evidence of temporary burial. By contrast, surfaces located far from the MMFS appear to have remained uncovered since their initial exposure as they show consistent $^{10}$Be and $^{26}$Al exposure ages ranging up to ~830 ka. Reconciliation of the observed burial patterns with morphotectonic and stratigraphic analysis reveals the existence of an extensive paleo-lake during the Pleistocene. Through hypsometric analyses of the dated knickpoints, the potential maximum water level of the paleo-lake is constrained to ~1200 m asl. High denudation rates (up to ~40 mm ka$^{-1}$) along the eastern Kundelungu Plateau suggest that footwall uplift, resulting from normal faulting, caused ~~fast~~ rapid river incision, thereby controlling paleo-lake drainage. The complex exposure histories recorded by $^{10}$Be and $^{26}$Al may be explained ~~as a result of~~because of lake water-level fluctuations caused by active normal faulting along the MMFS coupled with intense climate variations across southeastern Africa.

# 1. Introduction

The East African Rift System (EARS) is one of Earth's best studied active intracontinental rifts (e.g., Ebinger, 1989; Delvaux, 1991; Delvaux et al., 1992; Ring, 1994; Schlüter, 1997; Chorowicz, 2005; Braile et al., 2006; Stamps et al., 2008; Macgregor, 2015). The combination of the EARS length (> 3,000 km) and longevity (active throughout the Neogene, ~25 Ma) provides a unique opportunity to study the evolution of continental rifting; from initial crustal break-up (via normal faulting) to incipient oceanic rifting and, eventually, the opening of future oceans. Overall, the EARS can be considered to have had a dominant control on the landscape evolution of eastern Africa during the last ~30 Ma (e.g., Chorowicz, 1989, 2005; Macgregor, 2015). The northern and central parts of the EARS have been previously investigated and linkages between tectonic activity, climatic variations and (paleo) lake formation have been established (Bergner et al., 2009). However, there are limited constraints on the landscape evolution of the Western Branch of the EARS.

The interplay of faulting, climatic and fluvial processes have resulted in the development of a series of lakes that extend over a thousand kilometers along the EARS (Fig. 1 inset). The existence of large and deep paleo-lakes within the Western Branch during the Plio-Pleistocene (e.g. paleo-lakes Turkana, Edward-Albert, Obweruka, Bangweulu, Magadi, Thamalakane and Tanganyika) is well established (Williamson, 1978; Hillaire-Marcel et al., 1986; Burrough and Thomas, 2008; Cotterill and de Wit, 2011; Danley et al., 2012; Cohen et al., 2016).

Our study area lies to the southwest of Lake Tanganyika, straddling the border between the Democratic Republic of Congo (DRC; Katanga Province) and Zambia (Northern Province; Fig. 1). This area (Lake Mweru) is part of the ~~fast spreading~~fast-spreading Western Branch of the EARS, and it is characterized by an ENE-WSW trending basin-and-range topography that intersects the Tanganyika Rift System perpendicularly (Fig. 1). These typical horst and graben structures formed due to normal faulting along the Mweru-Mweru Wantipa Fault System

(MMFS) and are the seismically most active faults of central east Africa. Two of these graben structures host the high-altitude present-day lakes of Lake Mweru (917 m asl) and Lake Mweru Wantipa (932 m asl; Delvaux and Barth, 2010; Daly et al., 2020). The lakes are bounded to the northwest and southeast by two high plateaus, Kundelungu and Mporokoso, respectively (Mondeguer et al., 1989; Tack et al., 2003; Daly et al., 2020; Fig. 1).

Active faulting has been proposed previously as one of the key controls in shaping of river catchments and the landscape southwest of Tanganyika (Gumbricht et al., 2001; Haddon and McCarthy, 2005; Flügel et al., 2017; Daly et al., 2020). However, detailed geomorphological and tectonic studies in the area remain scarce, with much of the literature having focused on first-order physiographic characteristics of the rift to infer tectonic correlations between these structures and the EARS (e.g., Mohr, 1974; Tiercelin et al., 1988; Mondeguer et al., 1989; Strecker et al., 1990; Delvaux, 1991; Chorowicz, 2005; Kipata et al., 2013). Yet knickpoint creation is not only correlated with tectonic activity (normal faulting) and differential denudation, but may also be associated with changes in base-level and sea-level, as well as climatic variations (Whipple and Tucker, 1999; Whipple et al., 2000). It has been argued that climatic extremes within such ~~fast spreading~~fast-spreading rifts may have played a key role in controlling lake-level fluctuations (Lavayssiere et al., 2019). The paleo-lakes Manonga (Tanzania) and Obweruka (Uganda) are considered primary examples of climate-controlled lakes in the EARS (Harrison, et al., 1996; Van Damme and Pickford, 2003). However, without geochronologic dates to constrain landscape evolution rates in the Western Branch, determining the controlling factors acting on the landscape remains challenging. A secondary, albeit key, consideration of this study is that large knickpoints are important biogeographic controls, acting as natural barriers to species dispersal, especially fish. These landforms often result in divergent evolution between upstream and downstream populations of biota (Cotterill and de Wit, 2011;

Schwarzer et al., 2011). Thus, direct age estimates of knickpoints may inform on biogeographical histories of the region.

Dixey (1944) inferred a “greater” Lake Mweru based primarily on lacustrine deposits that are abandoned at ~1030 m asl, about 100 m higher than the present-day lake level. Moreover, Bos et al. (1995, 2006) suggested that patches of sands along the present-day Zambian (southern and southeastern) shores of Lake Mweru may indicate a migration of the Luapula River (Fig. 1). This is evidenced by sedimentary deposits that lie more to the west than its current position (Bos et al., 1995). Several studies propose that the initial Lake Mweru formed a large impoundment that extended over the lower part of the Northern Province of Zambia. No fieldwork and/or geomorphological analysis have hitherto explored the precise extent and duration of a larger paleo-lake Mweru (Dixey, 1946; Bos et al., 1995; Cotterill and de Wit, 2011).

This study attempts to identify and, where possible, quantify key factors and mechanisms that control the landscape evolution proximal to Lake Mweru. By doing so, we aim to test whether a precursor of Lake Mweru formed a big impoundment, inundating a larger portion of the Northern Province of Zambia at its lower elevations. Collectively, our study aims to explore the impact of normal fault growth on the formation of the paleo-lake and the drainage around the present-day Lake Mweru by combining tectonic and geomorphologic analyses of the study area with the application of terrestrial cosmogenic nuclides to dating and the magnitude of denudation~~by combining tectonic and geomorphologic analysis of the study area with terrestrial cosmogenic nuclides dating method~~. By interpreting a network of surface exposure dates of key landforms (river knickpoints, fault scarps, and ~~river beds~~riverbeds) across the two high plateaus (Mporokoso and Kundelungu Plateaus) that surround and delimit the current lake, we deduce the age of formation of the paleo-lake. By doing so, we constrain the extent and depth of the paleo-lake Mweru and estimate its life ~~span, and~~span and explore possible mechanisms that reduced its Pleistocene high stand. Direct geochronological derivations of the timing of the onset of the paleo-lake - and its tenure - contribute new information toward resolving the landscape evolution of the southwestern part of the Western Branch. Moreover, constraining the tenure of this Late Cenozoic depocenter reveals important information relating to the drainage evolution of the Congo-Kalahari Watershed during the Pleistocene (Flügel et al., 2015, 2017).

**Commented [A2]:** This reads well, but when reading the results later on you have tectonic fault analysis data, geomorpholgical data (KPs and hypsometry), and cosmo denudation data, alongside the cosmo exposure ages. These need to be captured more explicitly in the narrative...perhaps just add a few words or a sentence ot two at most?

**Commented [A3R2]:** Explanatory sentence added.

## 2. Geomorphic and Geologic Setting

The MMFS has a length of ~ 400 km, a width of ~ 200 km and is divided into eastern and western parts. The eastern part is characterized by an elongated ENE-WSW trend, almost perpendicular to the NW-SE trend of the Mpulungu basin (southern Lake Tanganyika; Tiercelin and Lezzar, 2002). Small and parallel grabens form shallow depressions, characterized by wetland environments (Mondeguer et al., 1989). To the west, two major troughs with NNE-SSW trend form the two main shallow lakes (Lakes Mweru and Mweru Wantipa). The majority of the faults follow a NNE-SSW trend, while few faults that mainly confine the end of the basins have a vertical trend of WNW-ESE (Mondeguer et al., 1989). The deviation in the fault trend near the Mpulungu basin results from the competency contrast with ~~of~~ the relatively stable Bangweulu ~~block~~ Block (Mondeguer et al., 1989; Fig. 1). The rotation of the extension direction reactivated earlier dip-slip faults, since strain accumulated in the same pre-Pleistocene inherited crustal structures (Ring, 1994; Morley, 2002; Saria et al., 2014). Furthermore, earthquake fault plane solutions from the area indicate an extensional displacement around the WNW axis (Delvaux and Barth, 2010). Recent modeling studies suggest that the extension direction changes from ~60° to 90°, while a left-lateral motion is applied on two domains with NE-E oriented weaknesses in between them (Molnar et al., 2019 and references therein).

Lake Mweru (situated at ~9° S and ~29° E) forms part of the south-eastern extension of the Congo Basin, being fed from the south by the Luapula River and drained to the northwest by the Luvua River (Fig. 1). The drainage of the Lake Mweru sub-basin is mostly sub-dendritic, representing the interaction of rivers flowing on Precambrian basement and regional faulting (Deffontaines and Chorowicz, 1991, Flügel et al., 2015). The extensive delta of the Luapula River suggests rapid denudation of the high plateaus between Lake Mweru and Lake Bangweulu (Fig. 1). In addition, the accumulation of Quaternary sediments with a thickness of 400 m uncomformably overlying the Neoproterozoic basement (Bos et al., 2006; Daly et al., 2020) can be interpreted as further evidence of rapid denudation of the surrounding highlands. Quaternary sediments are absent from Kilwa Island, a Neoproterozoic clastic rock outcrop, north of the delta (Shudofsky, 1985; Tiercelin and Lezzar, 2002; Daly et al., 2020). In the north, the outflowing Luvua River runs through a steep valley path with several large waterfalls, suggesting rapid incision (Flügel et al., 2017). The Kalungwishi River, a major tributary, feeds Lake Mweru from the east. This river drains its own highland sub-basin and has several large knickpoints on its course. The inflowing rivers allow the lake to maintain a surface area of ~ 5100 km$^2$ ~~year round~~year-round (Bos et al., 2006).

Along the eastern shore of Lake Mweru, a~~n~~ ~10 m high beach terrace indicates an actively uplifted coastline controlled by a long major fault line (Fault 16 in Fig. 1) across the southern borders of the Kundelungu Plateau (Daly et al., 2020). The southeastern border of the lake is delimited by a major fault (Fault 23 in Fig. 1) parallel to the trend of the Mporokoso Plateau, creating Lake Mweru that is 27 m at its deepest (Bos et al., 2006). This rectangular lake is surrounded by uplifted rift margins, ~~and~~ with the lake geometry and bathymetry ~~is~~ being controlled by ~~subsided~~ basin~~s~~ subsidence. The structural control of this setting is described in further detail below.

Southeast of Lake Mweru, a large basin of sub-horizontal sedimentary cover (Mporokoso Plateau) is developed onto the Archean-Paleoproterozoic cratonic Bangweulu ~~block~~ Block (Mondeguer et al., 1989; De Waele et al., 2009; Fig. 1). The Mporokoso Plateau consists mostly of undeformed fluvial and lacustrine sediments (De Waele and Fitzsimons, 2007). Unrug (1984) characterized the Mporokoso Plateau as the late Palaeoproterozoic to late Mesoproterozoic pre-Katangan succession to the northwest and northeast of the Bangweulu Block. A thick sedimentary bedrock succession, called the Kundelungu Plateau, forms the half graben structure that delimits the lake to the northwest (Fig 1). The Kundelungu Plateau is a part of the larger Neoproterozoic (<883 Ma to ~573 Ma; Master et al., 2005) Katangan Supergroup, ~~and it consists of~~comprising ~~carbonatic~~ carbonate and siliciclastic sequences which were deposited in a wider basin. The bedded red sand- and siltstones of the Kundelungu Plateau are exposed at the northwest corner of Lake Mweru due to incision along the Luvua River (Kipata et al., 2013).

The interplay of faulting and erosion in the broader Lake Mweru region has resulted in two relatively flat but vertically offset surfaces: the Lake Mweru valley bottom and the surrounding plateaus. In general terms, the valley bottom (~ 900 m asl) is approximately 600 m lower than the flat plateau tops (~ 1500 m asl). The amagmatic character of the tectonism, combined with an indistinct sedimentation sequence across the southwestern extension of the EARS, does not allow precise dating of the initiation of faulting in the study area. The formation of the extended denudational surface of the Central African Plateau is estimated at around late Miocene to early Pliocene times (Daly et al., 2020). The absence of Neogene sedimentation across the Central African basin suggests that the tectonic activity must have been initiated after, or during, the uplift of the Central African Plateau, thereby constraining the onset of the MMFS to the late Pliocene - early Pleistocene (~2.6 Ma; Daly et al., 2020).

# 3. Material and Methods

## 3.1. Sampling and Sample Grouping

In this study, we aim to provide temporal control to derive rates for landscape evolution. We focus on surface exposure dating of geomorphic markers using two cosmogenic radionuclides ($^{10}$Be, $^{26}$Al; the intended inclusion of stable $^{21}$Ne did not provide meaningful results, see Appendix). ~~In order to~~To ensure sufficient sample material (i.e., quartz) to undertake surface exposure dating, the field sampling mostly targeted bedrock quartzites due to their abundance in quartz. Sampling sites were located at or near waterfalls (knickpoints) as these are sites of exposed rock and considered key features in a river's development. Samples were taken from two broader areas, the Mporokoso Plateau and the northeastern Lake Mweru (Fig 1). Twenty-one samples, from seven waterfalls, were collected across the Mporokoso Plateau (Table 1), mostly from vertical or subvertical (45-90°) surfaces (Fig. 2A), downstream of the present-day knickpoint position. Where possible, samples were also taken from the waterfalls themselves to determine the minimum exposure age of the knickpoint at its current position (Fig. 2B, 2C). Dating two or more samples at different distances from the present knickpoint enables us, in principle, to estimate knickpoint retreat rates (Fig. A1). ~~In order to~~To determine maximum denudation rates, samples from horizontal surfaces (from above and below the knickpoints) were also collected (Table 1; Fig. 2B).

Five additional quartz-rich samples were obtained from the northwest shore of Lake Mweru: two from horizontal and two from vertical surfaces located along river channels (Fig. 2D) and one directly from the fault that bounds the MMFS to the north (Fig. 2E). See Table 1 for sample information and the Appendix (Fig. A1) for a more detailed description of the sampling process.

Based on their location relative to the MMFS, we subdivide our samples into three main groups: Group A samples are from south and southeast of Lake Mweru within the MMFS, Group B samples are from southeast of Lake Mweru but situated outside the MMFS, and Group C samples derive from north of Lake Mweru, along the northern margin of the MMFS (Table 1; Fig. 1).

#### *3.1.1. Group A*

The ~25 m high Kundabikwa Waterfalls (elevation ~1043 m asl) have incised quartzitic bedrock to form one of the two main knickpoints along the Kalungwishi River. Three pairs of vertical and horizontal samples (KUN01/02, KUN03/04 and KUN05/06) were taken from the right bank at different distances downstream of the present waterfalls. An additional sample (KUN07) was collected from the ~~river bank~~riverbank immediately above the waterfalls.

The Lumangwe Waterfall (~1159 m asl), located ca. 37 km upstream of the Kundabikwa Waterfalls, forms the most prominent knickpoint along the Kalungwishi River, with a height of ~40 m and a width of ~160 m (Fig. 2C). At Lumangwe Waterfall, the main bedrock is interbedded quartzite, with layers of red siltstones. Due to the vegetation density and the large amount of water, sampling this waterfall was challenging. Therefore, only one siltstone sample from a vertical face (LUM01) and a pair of quartzitic samples from vertical (LUM02) and horizontal (LUM03) surfaces were taken. Due to the very low amount of appropriately sized quartz grains, LUM01 could not be analyzed.

The cascade of the Ntumbachushi Waterfalls (~1160 m asl) is about 30 m high and is located on the Ng'ona River. Three samples were collected from these waterfalls, of which NTU01 and NTU03 were taken from the right vertical bank downstream of the current knickpoint, while NTU02 was collected above NTU01 from the corresponding horizontal bank.

The Mumbuluma Waterfalls (~1186 m asl) are situated on the Mumbuluma River and cascade down over two discrete steps. They will be denoted Mumbuluma I Waterfalls hereafter to distinguish them from the equally named waterfall on the Luongo River (section 3.1.2). MUM01 and MUM04 were collected from a vertical and a horizontal surface, respectively, of the top cascade, while the samples MUM02 (horizontal) and MUM03 (vertical) were taken from the lower step of the waterfalls.

#### *3.1.2. Group B*

The Lupupa Waterfall is located on the Mukubwe River and has a height of approximately 90 m. The highest set of cascades is located at about 1360 m asl. Due to difficulties associated with the steepness of the waterfall, we only managed to collect one sample (LUP01) close to the top of the vertical cliff.

The Luongo River is one of the dominant rivers of the Northern Province in Zambia. We collected two samples from inclined surfaces of the Mumbuluma Waterfall (hereafter denoted Mumbuluma II to distinguish it from the falls on the Mumbuluma River; section 3.1.1.), which lies at ~1370 m asl with ~10 m height.

The Lunzua Waterfalls form a series of cascades along the Lunzua River. The waterfalls are close to the town of Mpulungu at the southern shore of Lake Tanganyika (Fig. 1) and are situated at ~1300 m asl. Two vertical samples (LUZ01 and LUZ02) were collected from the banks of the Lunzua River downstream of the cascades.

#### *3.1.3. Group C*

Due to the extreme inaccessibility of waterfalls caused mainly by vegetation along the northwestern side of Lake Mweru, no samples from waterfalls were collected in that area. Rather, they were taken from ~~river beds~~riverbeds and banks comprising mostly quartzitic bedrock. MWE01 derived from an almost vertical (80°) face that forms the surface expression of a normal fault scarp (Fig. 1; Fig. 2E). Two samples (ME04, ME05) were collected from the vertical walls of the gorge along the Luvua River, close to where it discharges from Lake Mweru (Fig. 1; Fig. 2D). The samples ME06 and ME09 were collected from horizontal bank surfaces along the Misefwe and Lwilwa rivers, two small tributaries northwest of Lake Mweru.

### *3.2. Sample Processing*

Samples were crushed and sieved to 250–500 µm. Quartz grains were separated by the standard methods of heavy liquid and Frantz magnetic separation (Kohl and Nishiizumi, 1992). ~~In order to~~To dissolve all non-quartz minerals, samples were treated with dilute HCl and $H_2SiF_6$ (Brown et al., 1991). Afterwards, HF was used to remove any contribution of meteoric $^{10}Be$ by partially dissolving the quartz grains. A small fraction from each sample (~2 g) was kept for $^{21}$Ne analyses, while the remaining ~25-50 g were used for $^{10}$Be and $^{26}$Al analyses. Preparation and processing of the samples took place at the Helmholtz-Zentrum Dresden-Rossendorf (HZDR) following a modified version of the method described by Merchel and Herpers (1999) and at the University of Potsdam following the sample preparation manual of the UC Santa Barbara Cosmogenic Nuclide Preparation Facility (http://www.geog.ucsb.edu/~bodo/pdf/bookhagen_chemSeparation_UCSB.pdf), which is based on modifications of previous studies (e.g., Kohl and Nishiizumi, 1992; von Blanckenburg et al., 2004). The samples from the Kundabikwa Waterfalls (KUN) were prepared at HZDR, while the rest of the samples were prepared at University of Potsdam. For the radionuclide extraction, a known amount (~0.3 mg) of $^{9}$Be carrier was added to each sample, whilst ~1 mg Al carrier was added only to the blank samples (Table A1). Concentrated HF was used for digestion of the samples. After evaporation of the HF and the addition of $HClO_4$, ICP-AES (Inductively Coupled Plasma Atomic Emission Spectroscopy) or ICP-MS (Inductively Coupled Plasma Mass Spectrometry) measurements were done from aliquots, which were dissolved in HCl, in order to quantify the total Al concentration (Appendix Table A1). Be and Al were separated via ion exchange columns and precipitated as hydroxides. The last step before the target pressing was the ignition to oxides (900-1000 °C). Be isotope ratios were measured by Accelerator Mass Spectrometry (AMS) at the DREAMS facility of HZDR (Rugel et al., 2016; Table 2) and the National Laboratory of Age Determination of the Norwegian University of Science and Technology (NTNU), Trondheim (Seiler et al., 2018; Table 2). Al isotope ratio measurements were performed at HZDR (Rugel et al., 2016; Table 2) and at the French national facility Accélérateur pour les Sciences de la Terre, Environnement, Risques (ASTER, CEREGE, Aix-en-Provence; Arnold et al., 2010; Table 2). All processing values are provided in the Appendix (Table A1) and are one to three orders of magnitude lower than sample values.

### 3.3. *Calculation of Exposure and Burial Ages and Denudation Rates*

Waterfalls are dynamic systems that undergo geomorphological changes through time. The rate at which knickpoints migrate upstream along a river is dependent on a combination of lithology, elevation, morphology, climatic conditions, and tectonic activity (Howard et al., 1994; Whipple and Tucker, 1999; Whipple et al., 2000; Brocklehurst, 2010). Their complexity means waterfalls can be a challenge to date, even with cosmogenic nuclides. Nevertheless, useful parameters such as denudation rates, periods of burial, minimum exposure ages and sequential exposure can be estimated for knickpoints and their surrounding landscape.

To calculate exposure ages and denudation rates, sea level high latitude (SLHL) spallogenic production rates of 4.01 atoms $g^{-1}$ $a^{-1}$ for $^{10}Be$ and 27.93 atoms $g^{-1}$ $a^{-1}$ for $^{26}Al$ were used (Borchers et al., 2016). Minimum ages and maximum denudation rates were calculated with CosmoCalc 3.0 (Vermeesch, 2007), using Lal (1991) scaling factors and default values for all parameters except the SLHL production rates. The density used for the calculations is 2.65 g $cm^{-3}$ for all samples. Values were corrected according to sample thickness (1-10 cm) and geometric shielding. All $^{10}Be/^{9}Be$ ratios were normalized to the in-house standard material "SMD-Be-12" with a weighted mean value of $(1.704\pm0.030)\times10^{-12}$ (Akhmadaliev et al., 2013). The "SMD-Be-12" has been cross-calibrated to the NIST SRM 4325 standard, which has a $^{10}Be/^{9}Be$ ratio of $(2.79 \pm0.03)\times10^{-11}$ (Nishiizumi et al., 2007). $^{26}Al/^{27}Al$ ratios measured at DREAMS were normalized to the in-house standard "SMD-Al-11", with a $^{26}Al/^{27}Al$ ratio of $(9.66 \pm 0.14)\times10^{-12}$ (Rugel et al., 2016), while the Al ratios measured at ASTER were normalized to "SM-Al-11" with a $^{26}Al/^{27}Al$ ratio of $(7.401\pm0.064)\times10^{-12}$ (Arnold et al., 2010). Both Al standards are traceable via cross-calibration to the same primary standards (MB04-A, MB04-B, MB04-D) from a $^{26}Al$ round-robin exercise (Merchel and Bremser, 2004). For samples with $^{10}Be$ and $^{26}Al$ ages agreeing within error limits, error-weighted mean ages were also calculated.

Since the attenuation length of terrestrial cosmogenic nuclide (TCN) production is smaller at low angles than in a vertical direction (Dunne et al., 1999), the TCN concentration decreases faster perpendicularly beneath an inclined surface than beneath a horizontal surface. This ~~has to~~must be taken into account when calculating denudation rates of inclined or vertical surfaces and, therefore, a slope dependent correction (Hermanns et al., 2004) was applied to such surfaces.

In general, discordance between $^{10}$Be and $^{26}$Al ages may be due to long exposure (when $^{26}$Al production equals decay, i.e. after a few $^{26}$Al half-lives), denudation which has not been taken into account, or shielding from cosmic rays after initial exposure (e.g. Lal, 1991; Gosse and Phillips, 2001; Goethals et al., 2009). To reveal complex exposure histories, $^{10}$Be concentrations can be plotted against $^{26}$Al/$^{10}$Be ratios. In such two-nuclide plots, samples which lie between the "steady state denudation line" and the "constant exposure line" have experienced simple exposure histories, i.e. a combination of surface exposure and denudation. In contrast, samples plotting beneath the steady state field indicate burial after initial exposure. The calculation of burial ages (Lal, 1991) is based on the assumption that a surface has once been irradiated by cosmic rays up to steady ~~state, and~~state and was later buried until the present. This assumption is obviously not correct in our study, as all samples were taken from presently exposed surfaces. If such samples indicate burial, they must have been re-exposed sometime in the past, and only minimum burial ages can be calculated from them.

### *3.4. Normal Fault Analysis*

We used a Shuttle Radar Topography Mission (SRTM) digital surface model (DSM), Google Earth$^{TM}$ imagery, and the ArcGIS software (version 10.6) to map the traces of 63 normal faults in the area, from west of Lake Mweru to the southern shorelines of Lake Tanganyika (Fig. 1). This area largely includes faults of the MMFS, while at its eastern edge it comprises elements of the EAR (Fig. 1).

We focused our analysis on two fault parameters that, collectively, provide important information on the fault system's activity and growth: the fault length (L) and the fault displacement (D). Fault length represents an important parameter in estimating the seismic potential (including earthquake magnitude and single-event displacement) on each studied fault (Wells and Coppersmith, 1994; Wesnousky, 2008). It should be noted that several of the identified faults contain numerous parallel or sub-parallel strands (e.g. faults 30, 38, 44, 46, 49, etc. in Fig. 1) or along-strike segments (e.g. 1, 2, 7, 16, 43, etc.) which are either hard or soft linked (Walsh and Watterson, 1991). Here, these elements are thought to represent a single coherent fault that ruptures along its entirety; however, it remains possible that individual earthquakes rupture these faults or fault segments only partially. The maximum vertical displacement (or throw) on each normal fault derives by averaging numerous (>10) scarp height measurements from fault perpendicular topographic profiles collected proximal to the fault's centre. Fault lengths and displacements represent direct measurements drawn on the DSM and are presented in Table A2 together with the faults' geometries. Indirect earthquake attributes (e.g. earthquake magnitude, average recurrence interval, etc.) associated with each studied fault derive from Wells and Coppersmith's (1994) and Wesnousky's (2008) empirical relations and are also included in Table A2 (see caption of Table A2 in the Appendix for details).

Measurement of active fault lengths and displacements can be subject to significant uncertainties (Wesnousky, 2008; Mouslopoulou et al., 2012; Nicol et al., 2016a, 2020a). This is because fault scarps are prone to denudation and/or burial, especially at fault tips, where displacements are often too small to be detected with conventional mapping methods (such as aerial photo or DSM analysis, field mapping, etc.; Begg and Mouslopoulou, 2010). In this study, fault lengths and displacements should be considered as minimum values as fault scarps of < 2 m are not resolvable on the available DSM, and also because fault scarps of any size may be partly or entirely modified by denudation and/or burial (see Nicol et al., 2020a for detailed discussion on sampling biases). Rifting across the MMFS is thought to have initiated at about

2.6 Ma (late Pliocene-early Pleistocene; Tiercelin and Lezzar, 2002; Molnar et al., 2019; Daly et al., 2020), thus, fault displacement rates are calculated over this time-period (~2.6 Ma) (Table A2).

### *3.5. Digital Topography Analyses*

We analyzed selected domains of the 30-m NASADEM (NASA JPL, 2020). We have delineated the catchment of Lake Mweru using standard procedures implemented in TopoToolbox (Schwanghart and Scherler, 2014). Elevation lows (pits) were filled, a hydrological-corrected DEM has been calculated, and the catchment extents were visually verified. Our catchment extent, using the higher resolution NASADEM data, is similar to that calculated in the HydroBASINs dataset (Lehner and Grill, 2013). The catchment extent was used to extract the hypsometric curve, showing the surface area for each elevation bin. Further, we identified river knickpoints using previously published approaches (Neely et al., 2017). This entailed deriving longitudinal river profiles, converting them to Chi coordinates, and identifying knickpoint lips and bases based on positive or negative distance above a best-fit Chi profile (Neely et al., 2017). Chi profiles are area-normalized profiles where the distance coordinate has been normalized by an averaged river profile following an exponential function (Perron and Royden, 2012). The resulting profile, when in steady state, will follow a straight line. We analyze profile deviation above and below an averaged line to identify knickpoints. More detailed analysis steps are described in Neely et al. (2017). ~~In order to~~To avoid small knickpoints and remove noise inherent in the DEM, we focus on knickpoints with magnitudes (i.e., distances from the average Chi profile line) exceeding 30 m. Field observations suggest that major waterfalls associated with past lake-level highstands are generally higher than 30 m.

## 4. Results

We present our results as three components, starting with the determinations of the terrestrial cosmogenic nuclides. Second, the findings of tectonics analyses are reported, summarizing the fault geometries and kinematics of the faulted topography. Third, we present a geomorphic analysis of northeast Zambia and the adjacent Katanga Province. In the subsequent section 5 we will focus on reconstructed scenarios informed from the TCN results, which are classified according to respective landscape history, including ~~elevation~~elevation, and contrasting tectonic regimes.

## 4.1. *Terrestrial Cosmogenic Nuclides*

While the $^{10}$Be and $^{26}$Al results indicate extended periods of burial for many samples (see section 4.1.1.), there is no straightforward way to interpret the $^{21}$Ne data along with $^{10}$Be and $^{26}$Al. Due to their inconclusive nature, we do not discuss them further but present and describe them in the Appendix (Table A3 and Fig. A3, A4). Below we present the $^{10}$Be and $^{26}$Al results (shown in Table 2) by sample groups.

### 4.1.1. *$^{10}$Be and $^{26}$Al minimum exposure ages*

#### 4.1.1.1. *Group A*

Vertical samples KUN01 and KUN04 from Kundabikwa Waterfalls yield $^{10}$Be minimum ages of ~510 and ~580 ka, respectively, while $^{26}$Al minimum ages are younger, ~240 and ~360 ka. The horizontal samples KUN03, KUN05 and KUN07 show consistently younger minimum $^{10}$Be ages than the vertical samples (~320-370 ka) and $^{26}$Al minimum ages in a similar range (~170-360 ka). The horizontal KUN02 ($^{10}$Be: ~150 ka; $^{26}$Al: ~80 ka) and vertical KUN06 ($^{10}$Be: ~90 ka; $^{26}$Al: ~70 ka) samples show much younger minimum ages compared to the other Kundabikwa samples. The Lumangwe Waterfall samples LUM02 and LUM03 yielded minimum $^{10}$Be ages of ~230 and ~200 ka, respectively, and minimum $^{26}$Al ages of ~180 and ~190 ka. One vertical sample from Ntumbachushi Waterfall (NTU01) yielded a very young minimum $^{10}$Be and $^{26}$Al mean age of ~20 ka. The $^{10}$Be minimum age of the horizontal sample NTU02 is similar to those derived from the horizontal surface proximal to the Kundabwika Waterfalls (~380 ka) while its $^{26}$Al age (~340 ka) is slightly younger. NTU03, which was derived from a vertical surface, returns much younger $^{10}Be$ and $^{26}Al$ minimum ages of ~110 and ~100 ka, respectively. The samples MUM01 (vertical) and MUM04 (horizontal) from the top cascade of the Mumbuluma I Waterfalls yield minimum $^{10}Be$ ages of ~70 and ~110 ka, respectively, while $^{26}Al$ minimum ages are slightly younger (~60 and ~90 ka). The horizontally positioned sample MUM02 shows minimum ages of $^{10}Be$ (~270 ka) and $^{26}Al$ (~240 ka) which are older than for the vertical sample MUM03 (~110 and ~100 ka, respectively).

##### *4.1.1.2. Group B*

For the single sample collected from Lupupa Waterfall, the minimum $^{10}Be$ and $^{26}Al$ ages are in excellent agreement at a mean of 42.4±1.1 ka. The Mumbuluma II Waterfall sample LUO01 yields a minimum $^{10}Be$ and $^{26}Al$ mean age of 76.8±2.2 ka, which is an order of magnitude younger than the exceptionally old minimum mean age of LUO02 of 833±17 ka. Sample LUZ01, taken within a narrow river gorge of the Lunzua River, shows a minimum $^{10}Be$ and $^{26}Al$ mean age of 524±12 ka. LUZ02 was collected only about 2.4 m below the top surface and yields a mean age of 102.2±2.7 ka.

##### *4.1.1.3. Group C*

Sample MWE01 yielded minimum $^{10}Be$ and $^{26}Al$ ages which are in agreement at 7.79±0.60 ka. Samples ME04 and ME05 return minimum $^{10}Be$ and $^{26}Al$ mean ages of 12.29±0.81 ka and 11.56±0.72 ka, respectively, while ME06 and ME09 yielded minimum $^{10}Be$ and $^{26}Al$ mean ages of 42.8±1.6 and 45.7±2.0 ka, respectively.

#### *4.1.2. Maximum denudation rates*

For several samples that derive from Groups B and C, maximum denudation rates are also reported (Table 3). Samples from the eastern part of the Kundelungu Plateau yield maximum denudation rates ranging from ~15 to ~40 mm $ka^{-1}$ (samples MWE01, ME04, ME05, ME06 and ME09), while denudation rates associated with the Mporokoso Plateau are much lower and range from ~0.4 to ~6 mm $ka^{-1}$ (samples LUO01, LUO02, LUZ01 and LUZ02). Even though the denudation rates reported in this study are local ones, they indicate general differences in denudation history of both studied plateaus.

## *4.2. Tectonic Analysis*

### *4.2.1. Fault kinematics and scaling relationships*

We mapped 63 lineaments that we interpreted to represent the surface expressions of active normal faulting at depth (Fig. 1; Appendix Table A2). Fifty-three faults are located within the MMFS, while ten are located within the Mpulungu basin (southern Lake Tanganyika). The faults in the southern MMFS strike NE-SW while the northeast section of the fault system swings its strike clockwise to an ENE-WSW orientation (Table A2), intersecting, at high angles (~90°), the NW to SW trending normal faults around Lake Tanganyika. Fault lengths (L) in our dataset range from 12 km to 168 km, whereas maximum vertical fault displacements (D) range from 10 m to 700 m (Fig. 3A). Fault displacement rates (DR) are typically low, ranging from 0.004 mm $a^{-1}$ to 0.27 mm $a^{-1}$ (Fig. 3C). This, in turn, corresponds to an average earthquake recurrence for the faults in the MMFS of ~120 ka (Table A2). In order to understand the impact of normal faulting on the formation of the past and current landscape proximal to Lake Mweru, we explore the D-L relationship on the 53 normal faults in the MMFS (Table A2).

The D-L relation may provide important information on the growth and scaling properties of faults (Fig. 3; Walsh and Watterson, 1988; Bilham and Bodin, 1992; Cowie and Scholz, 1992; Schlische et al., 1996; Kim and Sanderson, 2005; Schultz et al., 2008; Nicol et al., 2010, 2020a). The graphs in Figures 3A and 3C indicate a positive D-L and DR-L relationship for the faults in the MMFS, suggesting that larger faults have accommodated more displacement and have moved faster than smaller faults (Nicol et al., 1997, 2005). Similar graphs, which indicate positive relationships between fault displacements/displacement rates and length, have been recorded on several other active and inactive fault systems globally (Kim and Sanderson, 2005; Mouslopoulou et al., 2009; Nicol et al., 2020a, b). Despite the overall positive D-L trend for most fault systems globally, the D values at a given L value and the slope of the best-fit line in these graphs may vary between fault systems (but also between different sampling periods in the same fault system), with the slope typically ranging from 0.5 to 1.5 (Schlische et al., 1996; Walsh et al., 2002; Kim and Sanderson, 2005; Nicol et al., 2010; Torabi and Berg, 2011, Nicol et al., 2020b). This variability in the D-L scaling may be due to biases arising from the time-window of observation, the age of the faulted horizons, the strain accommodated by each fault system, the mechanical properties of the faulted rocks and/or the degree of fault interactions (Watterson et al., 1996; Bailey et al., 2005; Mouslopoulou et al., 2009; Nicol et al., 2010; Rotevatn et al., 2019).

To better understand the growth of the faults in the MMFS with respect to other fault systems globally, we have plotted their D-L trend against a global dataset of inactive normal faults (Fig. 3D; Nicol et al., 2016c and references therein). Comparison shows that the faults in the MMFS plot in agreement with the global dataset occupying, however, the lower part of the global population (slopes of ~0.92 vs. ~0.99, respectively; Fig. 3D). To explore further the growth of the faults in Africa, we have also plotted in Figure 3D the single-event displacement rupture lengths from a global compilation of historic normal fault earthquakes (Wesnousky, 2008). As expected, single earthquakes clearly plot below the average trend of the global dataset (including the MMFS), their slope is significantly less than 1 (~0.3) and their scatter greater than that of the global dataset ($R^2$ values of 0.25 vs. 0.85; Fig. 3D). These features collectively suggest that each fault in the MMFS has accommodated numerous earthquakes, the number of which scales with fault length.

The approximate number of earthquakes accommodated by each fault in the MMFS, together with their earthquake magnitude and recurrence interval, has been calculated using Wesnousky's (2008) scaling relationships (Table A2). First, we calculate the single event displacement (SED) for each fault in the MMFS from the fault length (L) and subsequently the earthquake recurrence interval on each fault (Table A2). The recurrence interval is subsequently used, in conjunction with the 2.6 Ma displacement rate (time-period that rifting is thought to have initiated), to estimate the number of earthquakes accommodated by each fault (Table A2 and Fig. A2). We find that the faults in the MMFS ~~have~~ are likely to have accommodated ~2,000 ground-rupturing earthquakes since the rift's onset (~35 events per fault), with earthquake magnitudes ranging from M6.7 to M7.2 (Table A2 and Figure A2).

#### *4.2.2. Faulted topography*

To explore the relationship between the faulted topography, the available TCN ages and the current extents of Lakes Mweru and Mweru Wantipa, we generated five rift-perpendicular topographic profiles (Fig. 4) and one rift-parallel profile (Fig. 5). The profiles 1-3, across the southern MMFS and the modern Lake Mweru, reveal a strongly asymmetric rift (Fig. 4A-C). To characterize the distribution of strain along the rift, we have calculated the cumulative throw across the five profiles illustrated in Figure 4. Furthermore, to better visualize the landscape when rifting in the area was about to commence, we subtracted from the identified faults the throw measured along the topographic profiles 1-8 (Fig. 6), that is the displacement accrued on each fault since the initiation of faulting at 2.6 Ma.

Our analysis shows a three-fold increase in the cumulative throw, trending northeastwards along the rift (from ~800 m across profile 1 to ~2180 m across profile 5), with the southeast dipping faults having accommodated almost twice as much displacement (4550 m) compared to the northwest dipping faults (2690 m; Fig. 4). The dominance of the southeast dipping faults is persistent along the entire length of the MMFS, where these faults appear to have locally (e.g., see profile 5) accommodated up to 4 times more throw compared to the northwest dipping faults. The northeastward increase in extension, which is manifested by the greater number of active faults and the more confined rift axis, is not surprising as the MMFS at its northernmost extension approaches (and intersects) the fast spreading (~1 mm $a^{-1}$) EARS (Fig. 1; Fernandes et al., 2004: Calais et al., 2006; Omenda et al., 2016).

Topographic analysis suggests that the faults which are largely responsible for the formation of the modern landscape within the MMFS are faults 8, 9, 16, 17, 23 and 28 in the south, and faults 38, 40, 46 and 48 in the north. The profile along Lake Mweru (profile 6 in Fig. 5) reveals a shallow topographic basin (within <100 m from the modern lake) which is bounded at its northern side by the Kundelungu Plateau and to the south by steep hilly country formed by sediments of the Luapula River's delta (Fig. 4A). Profile 7 runs along Lake Mweru Wantipa and displays the high topographic relief between the Mporokoso Plateau and the Mpulungu basin, while profile 8 reveals the impact of normal faulting on the landscape associated with the Kundelungu Plateau (Fig. 6). These profiles are discussed in detail in Section 6.

### 4.3. *Geomorphic Analysis*

We identified a total of 61 river knickpoints from individual stream profiles that corroborate the paleo-shoreline observation (Fig. 7A). In a second step, we analyzed the hypsometry of the Lake Mweru catchment to delineate the impact of paleo-lake Mweru on the elevation distribution. The hypsometric curve of the catchment (Fig. 7B, blue and black lines) reveals large areas characterized by gentle slopes, which we interpret to correspond to areas confining the paleo-lake Mweru. They all lie at elevations between 920-930 m asl, 990-1100 m asl and 1170-1190 m asl, which align with the sampled waterfalls at 1050 and 1160 m asl. We observe additional areas with low slopes at varying elevations, but focus our analyses on the most prominent elevations. We have furthermore excluded slope angles above 3° to better show terrain associated with lake-erosion processes (Fig. 7B, blue line). In the same elevation framework, we plot the number of knickpoints observed at a specific elevation. Knickpoints cluster at specific elevations and delineate the remnant paleo-shorelines in a more refined spatial pattern, indicating three abandoned shorelines at elevations of ~925 m asl, ~1000 m asl and ~1180 m asl, respectively (Fig. 7B).

# 5. Reconstructed Scenarios for the Principal Sets of TCN Results

Overall, our TCN samples record a pattern of temporary burial over parts of the region studied. As discussed earlier (Section 1), stratigraphic evidence suggests that during the Pleistocene the study area hosted an enlarged lake, approximately 130 km wide and 300 km long (~40,000 km$^2$), centered around the (much smaller) present-day Lake Mweru (~5000 km$^2$). TCN production is completely blocked (except for some minor production by muons) when a surface is ≥10 m below the lake level. Therefore, interpreting the Plio–Pleistocene tectonic history of ~~south central~~south-central Africa, we suggest that the burial patterns recorded by our samples most likely reflect the existence of a paleo-lake that inundated a much larger depocenter.

## *5.1. Group A*

~~The majority of~~Most of the samples from Group A indicate burial (Fig. 1; Fig. 8). A few significant age discrepancies arising from samples collected from a single waterfall are also evident. The fact that all waterfalls in Group A are located within the MMFS and at elevations <1200 m asl (that is, significantly lower than Group B samples which are all located >1200 m asl) indicates that faulting and uplift may have played an important role in the burial of the landscape. Below we discuss separately the likely exposure scenarios for each waterfall in Group A.

### *5.1.1. Kundabikwa Waterfalls*

Samples from the Kundabikwa Waterfalls indicate burial over a continuous period for at least 250 ka (Fig. 8A). The significantly younger minimum exposure ages (Section 4.1.1.) of samples KUN02 and KUN06 probably indicate enhanced surface denudation or rockfalls/landslides (e.g. mechanical failure of exposed rock outcrop leading to fresh exposure). In addition, two of the three pairs of samples (KUN01/KUN02 and KUN03/KUN04) indicate older $^{10}$Be and $^{26}$Al minimum ages (Table 2) for the vertical face compared to the top horizontal surface. The fact that the top horizontal surface (KUN02, KUN03 and KUN05) of the area is younger than the vertical sections (KUN01, KUN04) is intriguing and requires further examination.

Based on the relative $^{10}Be$ and $^{26}Al$ minimum age estimates, we reconstruct the complex exposure-burial history of Kundabikwa Waterfalls and paleo-lake Mweru over six sequential stages (Fig. 9). The pre-lake stage (T1) represents the initial state of the river. In order to record a burial ~~signal~~signal, the studied surfaces must have been exposed prior to burial. ~~Thus~~Thus, the knickpoint must have already existed during stage T1. The vertical faces of the banks are gradually exposed through sequential knickpoint retreat. During this stage, channel denudation dominates. The denudation rate is relatively low on the top-horizontal surface. Most geomorphologic characteristics from this stage are assumed to have been erased by today. The second stage (T2) is defined by the onset of the lake-level rise (flooding). Water starts to cover the vertical ~~river banks~~riverbanks. Denudation decreases as the base-level increases, leading to slower knickpoint migration. Denudation is minimal (but probably not zero) as the top horizontal surfaces are flooded and lake sedimentation initiates. During T3, the lake reaches its greatest depth. Water and sediments now shield the sampled surfaces from cosmic ray irradiation, entirely blocking $^{10}Be$ and $^{26}Al$ production. Lacustrine sedimentation occurs mostly on the horizontal surfaces. The lake-level is now the base-level, resulting in the interruption of denudation.

Denudation recommences with the onset of lake drainage and associated drop of the water-level (stage T4). Localized denudation occurs on the sediment-covered horizontal surfaces while the vertical faces remain under water, with TCN production still being absent for all submerged areas. Consequent to paleo-lake outflow (T5) via the Luvua River, regional denudation of the sediments that blanket the horizontal surfaces occurs. This period of new equilibrium may have been characterized by low energy environments, which can be described, for example, as a changing complex of small wetlands, oxbow lakes and meandering channel systems, similar to the current situation in the upper reaches of ~~present-day~~present-day Lake Mweru. Lacustrine sediments are now confined to the top horizontal banks, as in the channel the sediments are eroded. The subsequent lowering of base level as the lake drains sees the rejuvenation of the waterfalls. In the last stage (T6), ~~the majority of~~most of the lacustrine sediments have been removed from all surfaces and the top horizontal surfaces are re-exposed and TCN production resumes. Back- and downwearing of the vertical bank faces leads to further denudation of the bedrock surfaces. We note that gradual rising and lowering of the lake's water-level between stages T2 and T4 should have lasted thousands or even tens of thousands of years in order to induce a detectable difference between the cosmogenic nuclide concentrations of different (horizontal vs. vertical) sampled surfaces. Indeed, previous studies of other paleo-lakes have revealed long-term lake fluctuations spanning time-intervals from 2 to >20 ka (Masters et al., 1991; Gamrod, 2009; Shuman et al., 2009; Trauth et al., 2010).

#### *5.1.2. Lumangwe Waterfall*

According to Figure 8B, ~~the~~ sample LUM03 does not show an unequivocal burial signal, in contrast to LUM02 that clearly underwent ~~clearly~~ a complex exposure history. One possible explanation is that LUM02 (1150 m asl) was covered by lake water, while LUM03 (1159 m asl) was not (or it was only slightly covered so the cosmogenic nuclide production did not stop completely). Such a scenario implies that the Lumangwe cascades marked the eastern shore of the paleo-lake. Another possibility is that the LUM02 rock face was covered by a recent landslide or rockfall. ~~However~~However, no physical evidence of such an event can be found, suggesting that if it did occur, the Kalungwishi River has subsequently removed any such debris. A minimum burial time of 300 ka is estimated for LUM02 (Fig. 8B).

### 5.1.3. *Ntumbachushi Waterfalls*

Samples NTU01 and NTU02 do not indicate a clear burial signal. The weathered profile of the NTU01 surface and the very young minimum $^{10}$Be and $^{26}$Al mean age (~20 ka) most likely indicate a recent rockfall. Although NTU03 does indicate burial of ~400 ka (Fig. 8C), this age is questionable due to the young minimum $^{10}$Be and $^{26}$Al ages (~100 and ~80 ka, respectively) that derive from the same sample and which, coupled with the highly weathered and fractured nature of the sampled surface, make it unlikely to record an ancient pre-lake stage.

### 5.1.4. *Mumbuluma I Waterfalls (Mumbuluma River)*

All results from the Mumbuluma I falls indicate a clear burial signal at 1σ confidence level, though not at 2σ (Fig. 8D). The top cascade yields younger minimum $^{10}$Be ages (MUM01, MUM04) than the second cascade downstream (MUM02, MUM03), suggesting that the lower waterfall formed before the top one. Also, the top horizontal surface (MUM04; minimum $^{10}$Be age 113 ka) seems to have undergone more intense denudation than the lower surface (MUM02; 271 ka). A rockfall may explain the young minimum $^{10}$Be age of the vertical sample MUM01 (~70 ka). The approximate minimum burial time of the area is ~350 ka (Fig. 8D), an age which is in good agreement with the duration of burial recorded at the Lumangwe falls.

## 5.2. Group B

Samples in Group B date waterfalls which are situated outside the MMFS (Fig. 1). $^{10}$Be and $^{26}$Al minimum ages are in good agreement for most samples, indicating that these surfaces have not been buried since their initial exposure (Fig. 10). Thus, it appears that these locations were not flooded by the paleo-lake. Minimum exposure ages and maximum denudation rates within this group are discussed below.

### *5.2.1. Lupupa Waterfall*

LUP01 shows very young minimum $^{10}$Be and $^{26}$Al ages, which probably do not reflect the actual age of the waterfall but a rockfall event. For such recent events, no burial signal is expected (Fig. 10A).

### *5.2.2. Mumbuluma II Waterfall (Luongo River)*

Both samples from the Luongo's Mumbuluma II Waterfall are from sub-vertical (45°-50°) surfaces and show no clear $^{10}$Be-$^{26}$Al burial signal (Fig. 10B). This cascade was formed on a bedrock contact between quartzites and sandstones. The development of the cascade is clearly controlled by differential denudation between the overlying softer sandstone and the harder quartzite. Maximum denudation rates of ~6 mm ka$^{-1}$ for the sandstone (LUO01) and of ~0.4 mm ka$^{-1}$ for the quartzite (LUO02) are calculated (Table 3). The large difference in the denudation rates of the two lithologies further highlights the role of differential denudation in the formation of this cascade. Sample LUO02 plots exactly on the no denudation line in Figure 5b, indicating a minimum $^{10}$Be and $^{26}$Al mean exposure age of 833±17 ka. This age, which is the oldest recorded minimum exposure age among the studied waterfalls, indicates a very old formation age of the Mumbuluma II knickpoint. It is worth mentioning that this is an exceptionally old age for an inclined surface located within the zone of an actively incising river channel.

### *5.2.3. Lunzua Waterfalls*

Both samples from Lunzua Waterfalls show no $^{10}$Be-$^{26}$Al burial signal (Fig. 10C). LUZ01 yields a very old minimum age for a vertical surface, which indicates that it was constantly exposed since at least 524±12 ka. In terms of a steady denudation rate, this age would correspond to a local rate of receding of the rock face (in horizontal direction) of ~0.4 mm ka$^{-1}$. LUZ02 yields a much younger minimum $^{10}$Be and $^{26}$Al mean age (102.2±2.7 ka). It is unclear whether the age difference between the two samples reflects the retreat of the waterfall or is just due to more intense denudation near the top.

### 5.3. Group C

Samples from the northwest side of Lake Mweru (Group C) were located at lower elevations than those from groups A and B and their minimum $^{10}$Be and $^{26}$Al ages are distinctly younger and more comparable to one another (Table 2). The sample that derives from a vertical surface of the fault no. 16 (MWE01; Fig. 1) implies a fast but steady denudation rate of ~40 mm ka$^{-1}$ (Table 3) or a rockfall on the fault surface <10 ka ago. Additionally, two further samples (ME04, ME05) from vertical sections along the Luvua River show rather young minimum $^{10}$Be and $^{26}$Al mean ages (12.29±0.81 and 11.56±0.72 ka, respectively). As the paleo-lake Mweru was drained via the Luvua River, during the Pleistocene (Cotterill and de Wit, 2011), it is possible that these young ages reflect rockfall events or steady and fast incision, but obviously they do not represent the age of paleo-lake drainage. Fast denudation of the northeastern section of the Kundelungu Plateau is further supported by two samples which were collected from horizontal surfaces along the Misefwe and Lwilwa rivers (ME06 and ME09; Fig. 1), yielding maximum $^{10}$Be denudation rates of ~16 mm ka$^{-1}$ (Table 3). In summary, Group C samples show no $^{10}$Be-$^{26}$Al burial signals and relatively young minimum ages due to recent rockfalls and/or fast eroding surfaces (Fig. 11; Tables 2, 3). However, these young ages do not contradict the assumed extension of the paleo-lake Mweru over this section of the Kundelungu Plateau. Rather, they suggest that pre paleo-lake surfaces have not been preserved due to faster denudation. Such rates could be related to a potential uplifting caused by the activity of fault no. 16 (Fig. 1). Further investigation of this activity is required.

## 6. Discussion

Our results explore the landscape evolution of the Mweru rift system, the southwest extension of the EARS, since the late Neogene. The establishment of paleo-lake Mweru initiated a new drainage network feeding the paleo-lake until the penultimate capture of this depocenter by an Upper Congo headwater. Here we discuss the implications of these new insights with respect to the southward and westward propagation of rifting.

### *6.1. Onset of Active Faulting and the Formation of the Paleo-Lake Mweru*

Rifting in the study area is thought to have commenced by at least ~2.6 Ma (Tiercelin and Lezzar, 2002; Decrée et al., 2010; Molnar et al., 2019; Daly et al., 2020). Overall, analysis of the faulted topography within the MMFS reveals that individual faults have played a pivotal role in forming the two depressions that host the Lakes Mweru and Mweru Wantipa. Active faulting and associated footwall uplift ~~is~~are also responsible for the wide ridge that extends today between the two lakes (Fig. 1). The landscape reconstruction through subtraction of the 2.6 Ma fault throws (Fig. 6) displays a mild relief across the extended area of the MMFS, revealing that the landscape was similar to the flat East African erosion surface. During the early Pleistocene, the average topographic altitude was formerly higher, though it is possible that the relative height difference between the Kundelungu and Mporokoso Plateaus has not changed significantly since the onset of rifting. A low energy environment, such as a shallow wetland, and associated meandering rivers probably extended over this landscape, which was related to the extensive and relatively long-lived paleo-Chambeshi drainage system (Cotterill, 2005).

The southern part of the MMFS (profiles 1 and 6; Fig. 6A, 6F) hosts deltaic deposits associated with the Luapula River (Fig. 1). The primary faults that bound the depression that hosts ~~today~~ Lake Mweru today to the west are (from south to north) faults 8, 9, 10 and 16 (Fig. 1). The total throw on these southeast dipping faults is ~640 m as opposed to the 200 m of cumulative throw recorded on the northwest dipping faults (i.e., 23 and 28) that bound this depression to the southeast. This geometry reveals a highly asymmetric rift tilted to the southeast. Profiles in Figure 6A and 6F suggest that faults 8 and 23 contributed drastically to the lowering of the landscape between the two horsts by a total throw of ~700 m. During the early Pleistocene, the southern part of the Mporokoso Plateau was about 250 m lower than the Kundelungu Plateau. It is known that during this period, the Luapula River captured the paleo-Chambeshi River, which led to the ~~present day~~present-day linkage between the Bangweulu and Mweru lakes (Cotterill, 2003, 2005). This interpretation, which is not described by the tectonic analysis presented here, suggests that the proto-Luapula River was flowing southward towards Lake Bangweulu (as suggested previously; Cotterill, 2005, 2006; Cotterill and de Wit, 2011; Moore et al., 2012). The onset of tectonic activity, together with the southward knickpoint retreat of the proto-Luapula River, may have contributed to the separation of the previously topographically connected Mporokoso and Kundelungu Plateaus.

Moving northwards, to profiles 2 and 6 (Figs. 6B, 6F), the elevation difference between the two shoulders of the rift is more distinct. The southeast dipping faults of the Kundelungu Plateau sum a total throw of almost 800 m, while faults along the Mporokoso Plateau have a total throw of ~300 m. It appears that the Mporokoso Plateau stood around 1400-1500 m asl during the late Pliocene. The basement of the lake was clearly higher than today, standing at ~1000 m asl, while the Kundelungu Plateau maintained its high elevation at ~1700 m asl. Faults 9, 16, 23, 24, 28 and 32 were the main contributors of downfaulting. In this area, the wetland was deeper (Kilwa Island did not exist) and the clastic bedrock was the main dominant rock type of the wetland's bottom. According to profiles 3 and 6 (Figs. 6C, 6F), the local average altitude of the landscape was lower, reaching the highest point of ~1350 m asl on the Kundelungu Plateau. The maximum altitude of the Mporokoso Plateau was ~1250 m asl, minimizing the elevational difference between the two shoulders of the rift. The total throw of the southeast dipping faults is ~500 m, while the northwest dipping faults' total displacement is 400 m, creating an almost symmetric section in a generally asymmetric structure. Considering Figure 6C, the reconstructed landscape during the early Pleistocene had a relatively low relief.

Both these plateaus seem to have had an approximately similar local height (~1400 m asl), and the lowest point was probably close to the ~~present day~~present-day location of the Kundabwika Waterfalls, which was controlled by Fault 44.

Cotterill (2006) discussed the possibility that part of the Kalungwishi River, today flowing north, was redirected from the south, as the Kalungwishi River was formerly a major headwater of the proto-Luongo River (Fig. 1). Geobiological estimates of evolutionary events can be applied from the genomic record of extant fishes. These estimates of speciation events confer an independent chronology of these drainage links (Cotterill and de Wit, 2011). A pertinent example is the Early Pleistocene speciation of a killifish, *Nothobranchius ostergaardi*, confined within the eastern Mweru Wantipa basin; this species diverged from 0.46 to 1.11 Ma from its closest living relatives, which today occur south of the Congo-Zambezi watershed (van der Merwe et al., 2021). Their origin is attributed to the breakup of the paleo-Chambeshi River, and this event overlaps with independent pulses of fish speciation within the Mweru graben, as well as TCN dates constraining the tenure of paleo-lake Mweru. The onset of the MMFS (deepening of the paleo-lake Mweru) then disrupted the paleo-drainage of the Luongo-Kalungwishi system, contributing gradually to its disconnection from the paleo-Chambeshi drainage (Cotterill, 2006; Cotterill and de Wit, 2011).

Compared to Lake Mweru (917 m asl), Lake Mweru Wantipa stands at a higher elevation (932 m asl), and it is characterized by a high relief landscape. According to profiles 4 and 5 (Fig. 4), the total throw of the southeast dipping faults along the Kundelungu Plateau reaches up to 1720 m, while the northeast dipping faults have a maximum total throw of 460 m. Despite the approximately four-fold difference of the throw measured on the southeast and northwest faults, the rift here does not appear to be strongly asymmetric. This can be rationalized if we consider that the former faults are distributed across a distance of ~140 km whereas the latter ones span only 10 km across the rift’s shoulder. From a geomorphological ~~point of~~

~~view~~perspective, the Mweru Wantipa depression hosts the seismically most active structures of the Southwestern Extension of the EARS (Daly et al., 2020). This is also supported by the DEM fault analysis that suggests a denser fault network of fresh discontinuous traces between the Lakes Mweru Wantipa and Tanganyika. The extended landscape around the modern Lake Mweru Wantipa during the early Pleistocene was also characterized by high relief, while the base of the wetland was standing at ~1150 m asl (Fig. 6D). The Kundelungu Plateau was standing at a maximum altitude of > 2000 m asl, while the Mporokoso Plateau had a maximum elevation of ~1900 m asl (Fig. 6E). The modern lowlands (cross ~~hachure~~ hatching in the east in Fig. 12) on the borders between Lake Mweru Wantipa and the Mpulungu basin have currently an average elevation <1200 m asl. During the Pleistocene (Fig. 6G), the elevation was just ~50 m higher, with the lowest point ~1200 m asl. However, this elevation difference was sufficient to prevent the merging of paleo-lake Mweru and paleo-lake Tanganyika and suggests that these lakes have never been linked.

The western margin of the paleo-lake was defined by the long and high Kundelungu Plateau. The depression (cross ~~hachure~~ hatching in the west in Fig. 12) that separates the main part of the plateau from its eastern continuity did not exist during the Pleistocene. Based on Figure 6H, the two parts of the plateau were connected, and the average elevation of the linking crest was ~1400 m. Faults 16a and 17 downfaulted the intervening landscape by ~200 m, resulting in the separation of the southwestern and northeastern sections of the Kundelungu Plateau. There is no evidence of a sudden tectonic event that created this depression, so we assume that it was dominated by gradual lowering of the landscape due to normal faulting and denudation activity across the Kundelungu Plateau, as implied also by the TCN data.

Interestingly, the transition from Pliocene to Pleistocene (2.6 Ma) is characterized by a major climatic change in the southern hemisphere, from warm and humid conditions to aridification until 1.8 Ma, which is invoked as a driver of contraction and expansion of the lakes

(Cohen et al., 1997). The lakes that were already flooded since ~3.6 Ma experienced contractions around 1.1 Ma (Cohen et al., 1997). Lavayssiere et al. (2019) reported that Lake Tanganyika dried down to the point it was divided into three contracted paleo-lakes, limited within the sub basins of the rift, which possibly caused fish speciation. The lake levels were restored gradually until 550 ka, while fluctuations in levels occurred, possibly linked to alterations in Pleistocene paleo-climates (Cohen et al., 1997; Trauth et al., 2005, 2010; Lavayssiere et al., 2019). Indeed, TCN dating suggests water level fluctuations across the paleo-lake Mweru during the Pleistocene (Section 5.1.1.), which attests to complex interactions between past climates and tectonics.

### 6.2. *The Drainage of Paleo-Lake Mweru*

At Kundabikwa Waterfalls, three samples (KUN01, 02, 03) yield burial ages of ~1 Ma (Fig. 8A). The minimum burial ages of the other four samples (KUN04, 05, 06, 07) are lower (~500 ka). This may be explained by a higher contribution of post-burial production, which shifts data points in the two-nuclide plot (Fig. 8A) from the burial area towards the steady-state field again. Therefore, it is the oldest burial age among all samples that provides a minimum estimate for the time the Kundabikwa Waterfalls have been covered, i.e. >1 Ma. Indeed, it is possible that the paleo-lake Mweru existed much longer than that. If the lake (including the various lake fluctuations) actually lasted more than ~2 Ma, essentially all $^{26}$Al present in a sample today would have been produced after the drainage of the paleo-lake (as the half-life of $^{26}$Al is 705 ka and after three half-lives almost 90% will have decayed; Norris et al., 1983). Under such an assumption, the highest minimum $^{26}$Al age of all samples showing burial would provide a time constraint for when the paleo-lake was drained to a level below the elevation of the waterfalls. Sample KUN04 of the Kundabikwa Waterfalls records the highest $^{26}$Al minimum age among all samples that indicate burial, constraining the timing of lake drainage to ~350 ka (i.e. middle Pleistocene). Variable denudation and tectonic rates within the study area can explain the observed variations in minimum ages between different locations. Nevertheless, all samples from Group A are consistent with an inferred lake drainage at ~200-400 ka, with age differences most likely representing lake level fluctuations.

The reconstruction of key features that formed the landscape at ~350 ka is required to determine potential waterways allowing for the drainage, and consequent lowering, of the paleo-lake. To achieve this, we calculated, assuming constant displacement rates over these timescales (Mouslopoulou et al. 2009), the throw accrued on each fault since 350 ka and we subsequently subtracted it from its total displacement (Table A2). The modified faulted topography is assessed via profiles 1-8 (cross sections in Fig. 1), the results of which are illustrated in Figure A5 in the Appendix. The restored topography at 350 ka reveals minor, albeit crucial, readjustments that appear to have impacted on the size of the paleo-lake. According to the profiles in Figure 4, faults 8, 9 and 16 are the largest displacement faults that formed the asymmetrical half-graben structure that hosted the paleo-lake. Faults 16a and 17 also contributed to the formation of the depression west of present-day Lake Mweru and across the Kundelungu Plateau (Fig. A5c). This depression might have played a key role in the lowering of the paleo-lake's water level as it aided its tapping to the west (Fig. 12). Faster denudation rates in the north (~40 mm $ka^{-1}$; Group C) compared to the south (~6 mm $ka^{-1}$; Groups A, B) were forced by footwall uplift across Fault 16, resulting in fast incision along the northward flowing Luvua River (Fig. 1).

Dramatic lake level fluctuations have been reported throughout the late Pleistocene (14-450 ka) across Lake Tanganyika, Lake Malawi and the southwest extension of the EARS, which are related to tectonic factors and/or aridification periods (Danley et al., 2012; Ivory et al., 2016). From 450 to 350 ka, a regional ~~dropping~~ lowering of the temperature and ~~the~~ global sea level is directly correlated with the low stand of the lake levels across the Western Branch (Bakker and Mercer, 1986). In addition, a major dry period across the Congo basin occurred between ~270

**Commented [A4]:** You do mean sea level don't you and not lake level?

**Commented [A5R4]:** Indeed yes. Sea leve it is.

and 180 ka, resulting in an additional lowering of the water level (Gasse et al., 1989). The evidence for the drainage of paleo-lake Mweru based on $^{10}$Be and $^{26}$Al data, together with tectonic analyses and the evidence for intensive climatic variation during the Pleistocene, indicate a gradual shrinking of the paleo-lake rather than a sudden tectonic event. The outflow of the paleo-lake through the Luvua River was most likely one of the main events that drained the lake (Dixey, 1944; Bos et al., 2006; Goodier et al., 2011; Cotterill and de Wit, 2011; Fig. 1). However, evaporation, especially in arid periods, may have further accelerated contraction of the paleo-lake, notably across the vast, shallow depression located between the two sections of the Kundelungu Plateau (Fig. 12).

### *6.3. Paleo-Lake Mweru During the Late Neogene-Quaternary*

Assuming that the paleo-lake Mweru ~~lasted~~ existed for a minimum of ~2 Ma, the burial ages constrain its formation to the late Pliocene-early Pleistocene. This assumption is supported by the high species endemism of the extant fish fauna of Lake Mweru (Cotterill, 2005; Meier et al., 2019). More specifically, recent molecular clock analyses have estimated respective timings of origin of several radiations of endemic fish clades (Family Cichlidae) confined within Lake Mweru. Four of these clades have evolved diverse species flocks, whose origins are estimated at 270–350, 430–560, 270–940, and 720–940 ka, constrained by a molecular clock calibrated for the Cichlidae (Meier et al., 2019). Thus, depending on the applied calibration scheme, the mean genetic divergence of the most common recent ancestors provides a date of 0.27-1.04 Ma and their actual speciation dates (i.e. timing of completed lineage divergence) was likely more recent (Meier et al., 2019). The second line of geobiotic evidence comprises the "Mweru Complex" of killifishes, genus *Nothobranchius*. The timing of radiation of its seven species is significant, because their ecology confines them within the floodplains that formed after the shrinkage of the larger lake. The independently constrained molecular clock of

*Nothobranchius* estimates the origin of this complex between 0.48 and 1.01 Ma (van der Merwe et al., 2021).

Our data inform a schematic map that estimates the maximum size of the paleo-lake Mweru through the Pleistocene (Fig. 12). The maximum lake level is constrained via TCN dating at 1200 m asl, while the minimum level should be the elevation of the Kundabikwa Waterfalls (~1050 m asl). The estimate of a 1200 m asl lake level is supported by the hypsometric and knickpoint analysis (~1180 m asl). The Lumangwe and Ntumbachushi Waterfalls are assumed to represent the eastern shorelines of this paleo-lake. This inference is confirmed by the heights of the dominant knickpoints at the same elevation mapped throughout the catchment (Fig. 7). The southern border of the paleo-lake likely coincided closely with the Mumbuluma I waterfalls which, together with preliminary molecular phylogenetic analyses (Cotterill, 2004, 2005), suggest that the southern section of the Kundelungu Plateau was connected with the Mporokoso Plateau during the Pliocene (and prior to the formation of the Luapula River; Tack et al., 2003; Cotterill and de Wit, 2011; Guillocheau et al., 2015).

Red siltstones from the Kundelungu Plateau are possibly correlated with the upper red beds of the Luapula Beds, implying that the Luapula River eroded the once connected Kundelungu and Mporokoso Plateaus (Abraham, 1959; Thieme, 1971). The western bank of the paleo-lake is defined by the Kundelungu Plateau that rises to ~1700 m asl. Paleo-lake Mweru was likely connected to the Mweru Wantipa wetlands as suggested by the relationships of *Pseudocrenilabrus* (family: Cichlidae) species from these two waterbodies (Egger et al., 2015). However, it appears unlikely that it was linked with the Mpulungu graben of Lake Tanganyika due to the highly distinct fish fauna of these two lakes. This is in agreement with Dixey (1944, 1946), who proposed that the Lakes Mweru and Mweru Wantipa were once connected, a hypothesis re-affirmed by Cotterill and de Wit (2011). Finally, the northern banks are defined by the edge of the extensive plateau between the Mweru Wantipa wetlands and Lake Tanganyika (Fig. 12).

## 7. Conclusions

Terrestrial cosmogenic nuclides results coupled with tectonic and digital topographic analyses reveal the existence of a large paleo-lake Mweru. This paleo lake exceeded the sizes of the present-day Lakes Mweru and Mweru Wantipa. We identified the following evidence for lake size and timing:

As estimated previously, our results indicate the onset of the paleo-lake at around 2.6 Ma. The timing of lake existence is consistent with the phylogenetic molecular clock analyses of endemic fish species, which also constrain the formation of the paleo-lake at the late Pliocene - early Pleistocene. Formation of this lake is correlated with the onset of the Mweru-Mweru Wantipa Fault System in the Early Pleistocene and likely established an estimated maximum shoreline at ~1200 m asl. The extent of the paleo-lake was also identified by river knickpoint and hypsometric analysis to constrain its paleo-shorelines at ~1180 m.

Intense normal faulting and associated footwall uplift at the northwestern paleo-lake boundary must have forced fast river incision in the eastern section of the Kundelungu Plateau. In contrast, two exceptionally old minimum $^{10}$Be and $^{26}$Al exposure ages of 524 and 833 ka were obtained from vertical/sub-vertical surfaces besides active river courses across the Mporokoso Plateau, possibly reflecting the actual exposure ages of these surfaces. These ages illustrate the stability of the plateau, which is also reflected by the low maximum denudation rates (~0.4 to ~6 mm ka$^{-1}$). The deepening/flooding of the paleo-lake, which was probably due to the active extension and associated normal faulting, continued at least until the Middle Pleistocene (~350 ka), resulting in complex exposure histories observed at the knickpoints on the Mporokoso Plateau.

## Acknowledgements

This study is part of the interdisciplinary project “Exploiting the Genomic Record of Living Biota to Reconstruct the Landscape Evolution of South Central Africa” funded by the Volkswagen Foundation (VolkswagenStiftung) [grant number 88732]. Parts of this research were carried out at the Ion Beam Centre (IBC) at the Helmholtz-Zentrum Dresden-Rossendorf e.V., a member of the Helmholtz Association. We would like to thank Enzio Schnabel, Heike Rothe, Sabine Tonn and Hella Wittmann (GFZ Potsdam) as well as Daniel Gorzawski, Antje Musiol, Julia Artel, Milena Wöller and Konstanze Stübner (University of Potsdam) for their help and assistance with laboratory processes and analyses. We would also like to thank Sabrina Beutner (HZDR) for ICP-MS measurements and the DREAMS operator team for their assistance with AMS measurements. The ASTER Team (G. Aumaître, D. Bourlès and K. Keddadouche) is acknowledged for assistance with AMS measurements at CEREGE, Aix-en-Provence. The ASTER AMS national facility is supported by the INSU/CNRS, the ANR through the “Projets thématiques d'excellence” program for the “Equipements d'excellence” ASTER-CEREGE action and IRD. John G. Begg is warmly thanked for discussions associated with active faulting within the MMFS and its impact on the landscape evolution. We are grateful for comments to the manuscript by Ulrich Schliewen and Frederic Schedel (Zoologische Staatssammlung München). We sincerely thank Christian Mwabanua Mutabi and Bauchet Manda (University of Lubumbashi) and Boniface, George and Kelvin for their enthusiastic assistance in the field. Last but not least, we are grateful to the Editor Martin Stokes, to Laura Evenstar ~~(University of Brighton)~~ and ~~an~~ an anonymous reviewer for their constructive comments that improved this manuscript significantly.

# References

Abraham, D. (1959). The stratigraphical and structural relationship of the Kundelungu System, Plateau Series and basement rocks in the Mid-Luapula valley, Northern Rhodesia. D. Phil. Thesis, Univ. Leeds, 152 pp.

Akhmadaliev, S., Heller, R., Hanf, D., Rugel, G. and Merchel, S. (2013). The new 6 MV AMS-facility DREAMS at Dresden. Nuclear Instruments and Methods in Physics Research Section B: Beam Interactions with Materials and Atoms, 294, 5-10. https://doi.org/10.1016/j.nimb.2012.01.053

Arnold, M., Merchel, S., Bourlès, D. L., Braucher, R., Benedetti, L., Finkel, R. C. Aumaître, G., Gottdang, A. and Klein, M. (2010). The French accelerator mass spectrometry facility ASTER: improved performance and developments. Nuclear Instruments and Methods in Physics Research Section B: Beam Interactions with Materials and Atoms, 268(11-12), 1954-1959. https://doi.org/10.1016/j.nimb.2010.02.107

Bailey, W. R., Walsh, J. J. and Manzocchi, T. (2005). Fault populations, strain distribution and basement fault reactivation in the East Pennines Coalfield, UK. Journal of Structural Geology, 27(5), 913-928. https://doi.org/10.1016/j.jsg.2004.10.014

Bakker, E. M. V. Z. and Mercer, J. H. (1986). Major late Cainozoic climatic events and palaeoenvironmental changes in Africa viewed in a worldwide context. Palaeogeography, Palaeoclimatology, Palaeoecology, 56(3-4), 217-235. https://doi.org/10.1016/0031-0182(86)90095-7

Begg, J. G. and Mouslopoulou, V. (2010). Analysis of late Holocene faulting within an active rift using lidar, Taupo Rift, New Zealand. Journal of Volcanology and Geothermal Research, 190(1-2), 152-167. https://doi.org/10.1016/j.jvolgeores.2009.06.001

Bergner, A. G., Strecker, M. R., Trauth, M. H., Deino, A., Gasse, F., Blisniuk, P., and Duehnforth, M. (2009). Tectonic and climatic control on evolution of rift lakes in the Central Kenya Rift, East Africa. Quaternary Science Reviews, 28(25-26), 2804-2816. https://doi.org/10.1016/j.quascirev.2009.07.008

Bilham, R. and Bodin, P. (1992). Fault zone connectivity: Slip rates on faults in the San Francisco Bay area, California. Science, 258(5080), 281-284. https://doi.org/10.1126/science.258.5080.281

Borchers, B., Marrero, S., Balco, G., Caffee, M., Goehring, B., Lifton, N., Nishiizumi, K., Phillips, F., Schaefer, J. and Stone, J. (2016). Geological calibration of spallation production rates in the CRONUS-Earth project. Quaternary Geochronology, 31, 188-198. https://doi.org/10.1016/j.quageo.2015.01.009

Bos, A. R., van Zwieten, P. A. M. and Ngula, E. S. (1995). A limnological survey on Lake Mweru, Zambia. DoF/ML/Report No. 27, Department of Fisheries, Nchelenge, Zambia, 90 pp.

Bos, A. R., Kapasa, C. K. and van Zwieten, P. A. (2006). Update on the bathymetry of Lake Mweru (Zambia), with notes on water level fluctuations. African Journal of Aquatic Science, 31(1), 145-150. https://doi.org/10.2989/16085910609503882

Braile, L. W., Keller, G. R., Wendlandt, R. F., Morgan, P. and Khan, M. A. (2006). The East African rift system. In Developments in Geotectonics (Elsevier), Vol. 25, 213-III. https://doi.org/10.1016/S0419-0254(06)80013-3

Brocklehurst, S. H. (2010). Tectonics and geomorphology. Progress in Physical Geography, 34(3), 357-383. https://doi.org/10.1177/0309133309360632

Brown, E. T., Edmond, J. M., Raisbeck, G. M., Yiou, F., Kurz, M. D. and Brook, E. J. (1991). Examination of surface exposure ages of Antarctic moraines using in situ produced $^{10}$Be and $^{26}$Al. Geochimica et Cosmochimica Acta, 55(8), 2269-2283. https://doi.org/10.1016/0016-7037(91)90103-C

Burrough, S. L. and Thomas, D. S. G. (2008). Late Quaternary lake-level fluctuations in the Mababe Depression: Middle Kalahari palaeolakes and the role of Zambezi inflows. Quaternary Research, 69(3), 388-403. https://doi.org/10.1016/j.yqres.2008.02.003

Calais, E., Ebinger, C., Hartnady, C. and Nocquet, J. M. (2006). Kinematics of the East African Rift from GPS and earthquake slip vector data. Geological Society, London, Special Publications, 259(1), 9-22. https://doi.org/10.1144/GSL.SP.2006.259.01.03

Chorowicz, J. (1989). Transfer and transform fault zones in continental rifts: examples in the Afro-Arabian rift system. Implications of crust breaking. Journal of African Earth Sciences (and the Middle East), 8(2-4), 203-214. https://doi.org/10.1016/S0899-5362(89)80025-9

Chorowicz, J. (2005). The East African rift system. Journal of African Earth Sciences, 43(1-3), 379-410. https://doi.org/10.1016/j.jafrearsci.2005.07.019

Cohen, A. S., Lezzar, K. E., Tiercelin, J. J. and Soreghan, M. (1997). New palaeogeographic and lake-level reconstructions of Lake Tanganyika: implications for tectonic, climatic and biological evolution in a rift lake. Basin research, 9(2), 107-132. https://doi.org/10.1046/j.1365-2117.1997.00038.x

Cohen, A.S., Gergurich, E.L., Kraemer, B.M., McGlue, M.M., McIntyre, P.B., Russell, J.M., Simmons, J.D. and Swarzenski, P.W. (2016). Climate warming reduces fish production and benthic habitat in Lake Tanganyika, one of the most biodiverse freshwater ecosystems. Proceedings of the National Academy of Sciences, 113(34), 9563-9568. https://doi.org/10.1073/pnas.1603237113

Cotterill, F. P. D. (2003). A biogeographic review of tsessebe antelopes *Damaliscus lunatus* (Bovidae: Alcelaphini) in south-Central Africa. Durban Museum Novitates, 28, 45-55.

Cotterill, F. P. D. (2004). Drainage evolution in south-central Africa and vicariant speciation in swamp-dwelling weaver birds and swamp flycatchers. The Honeyguide, 25(1), 7-25.

Cotterill, F. P. D. (2005). The Upemba lechwe, *Kobus anselli*: an antelope new to science emphasizes the conservation importance of Katanga, Democratic Republic of Congo. Journal of Zoology, 265(2), 113-132. https://doi.org/10.1017/S0952836904006193

Cotterill, F. P. (2006). The Evolutionary History and Taxonomy of the *Kobus leche* species complex of south-central Africa in the context of Palaeo-Drainage Dynamics.

Cotterill, F. P. D. and de Wit, M. J. (2011). Geoecodynamics and the Kalahari epeirogeny: linking its genomic record, tree of life and palimpsest into a unified narrative of landscape evolution. South African Journal of Geology, 114(3-4), 489-514. https://doi.org/10.2113/gssajg.114.3-4.489

Cowie, P. A. and Scholz, C. H. (1992). Displacement-length scaling relationship for faults: data synthesis and discussion. Journal of Structural Geology, 14(10), 1149-1156. https://doi.org/10.1016/0191-8141(92)90066-6

Daly, M. C., Green, P., Watts, A. B., Davies, O., Chibesakunda, F. and Walker, R. (2020). Tectonics and Landscape of the Central African Plateau and their Implications for a Propagating Southwestern Rift in Africa. Geochemistry, Geophysics, Geosystems, 21(6), e2019GC008746. https://doi.org/10.1029/2019GC008746

Danley, P. D., Husemann, M., Ding, B., DiPietro, L. M., Beverly, E. J. and Peppe, D. J. (2012). The impact of the geologic history and paleoclimate on the diversification of East African cichlids. International Journal of Evolutionary Biology. https://doi.org/10.1155/2012/574851

De Waele, B. and Fitzsimons, I. C. W. (2007). The nature and timing of Palaeoproterozoic sedimentation at the southeastern margin of the Congo Craton; zircon U–Pb geochronology of plutonic, volcanic and clastic units in northern Zambia. Precambrian Research, 159(1-2), 95-116. https://doi.org/10.1016/j.precamres.2007.06.004

De Waele, B., Fitzsimons, I. C. W., Wingate, M. T. D., Tembo, F., Mapani, B. and Belousova, E. A. (2009). The geochronological framework of the Irumide Belt: a prolonged crustal history along the margin of the Bangweulu Craton. American Journal of Science, 309(2), 132-187. https://doi.org/10.2475/02.2009.03

Decrée, S., Deloule, É., Ruffet, G., Dewaele, S., Mees, F., Marignac, C., Yans, J. and De Putter, T. (2010). Geodynamic and climate controls in the formation of Mio–Pliocene world-class oxidized cobalt and manganese ores in the Katanga province, DR Congo. Mineralium Deposita, 45, 621-629. https://doi.org/10.1007/s00126-010-0305-8

Deffontaines, B. and Chorowicz, J. (1991). Principles of drainage basin analysis from multisource data: application to the structural analysis of the Zaire Basin. Tectonophysics, 194(3), 237-263. https://doi.org/10.1016/0040-1951(91)90263-R

Delvaux, D. (1991). The Karoo to Recent rifting in the western branch of the East-African Rift System: A bibliographical synthesis. Mus. Roy. Afr. Centr., Tervuren (Belg.), Dépt. Géol. Min., Rapp. ann. 1989–1990, 63–83.

Delvaux, D. and Barth, A. (2010). African stress pattern from formal inversion of focal mechanism data. Tectonophysics, 482(1-4), 105-128. https://doi.org/10.1016/j.tecto.2009.05.009

Delvaux, D., Levi, K., Kajara, R. and Sarota, J. (1992). Cenozoic paleostress and kinematic evolution of the Rukwa-North Malawi rift valley (East African rift system). Bulletin des Centres de Recherche Exploration-Production Elf-Aquitaine, 16(2), 383-406.

Dixey, F. (1944). The geomorphology of northern Rhodesia. South African Journal of Geology, 47(Transactions 1944), 9-45.

Dixey, F. (1946). Erosion and tectonics in the East African rift system. Quarterly Journal of the Geological Society, 102(1-4), 339-388. https://doi.org/10.1144/GSL.JGS.1946.102.01-04.16

Dunne, J., Elmore, D. and Muzikar, P. (1999). Scaling factors for the rates of production of cosmogenic nuclides for geometric shielding and attenuation at depth on sloped surfaces. Geomorphology, 27, 3-11. https://doi.org/10.1016/S0169-555X(98)00086-5

Ebinger, C. J. (1989). Tectonic development of the western branch of the East African rift system. Geological Society of America Bulletin, 101(7), 885-903. https://doi.org/10.1130/0016-7606(1989)101<0885:TDOTWB>2.3.CO;2

Egger, B., Klaefiger, Y., Indermaur, A., Koblmüller, S., Theis, A., Egger, S., Näf, T., Van Steenberge, M., Sturmbauer, C., Katongo, C. and Salzburger, W. (2015). Phylogeographic and phenotypic assessment of a basal haplochromine cichlid fish from Lake Chila, Zambia. Hydrobiologia, 748(1), 171-184.

Fernandes, R. M. S., Ambrosius, B. A. C., Noomen, R., Bastos, L., Combrinck, L., Miranda, J. M. and Spakman, W. (2004). Angular velocities of Nubia and Somalia from continuous GPS data: implications on present-day relative kinematics. Earth and Planetary Science Letters, 222(1), 197-208. https://doi.org/10.1016/j.epsl.2004.02.008

Flügel, T. J., Eckardt, F. D. and Cotterill, F. P. (2015). The present day drainage patterns of the Congo river system and their Neogene evolution. In Geology and resource potential of the Congo Basin, 315-337. Springer, Berlin, Heidelberg.

Flügel, T. J., Eckardt, F. D. and Cotterill, W. F. P. (2017). The geomorphology and river longitudinal profiles of the Congo-Kalahari Watershed. The African Neogene-Climate, Environments and People: Palaeoecology of Africa 34, 31-52. DOI: 10.1201/9781315161808-4.

Gamrod, J. L. (2009). Paleolimnological records of environmental change preserved in Paleo-Lake Mababe, northwest Botswana. Doctoral dissertation, Oklahoma State University.

Gasse, F., Stabell, B., Fourtanier, E. and van Iperen, Y. (1989). Freshwater diatom influx in intertropical Atlantic: relationships with continental records from Africa. Quaternary Research, 32(2), 229-243. https://doi.org/10.1016/0033-5894(89)90079-3

Goethals, M.M., Hetzel, R., Niedermann, S., Wittmann, H., Fenton, C.R., Kubik, P.W., Christl, M. and von Blanckenburg, F. (2009). An improved experimental determination of cosmogenic $^{10}Be/^{21}Ne$ and $^{26}Al/^{21}Ne$ production ratios in quartz. Earth and Planetary Science Letters, 284(1-2), 187-198. https://doi.org/10.1016/j.epsl.2009.04.027

Goodier, S. A., Cotterill, F. P., O'Ryan, C., Skelton, P. H. and de Wit, M. J. (2011). Cryptic diversity of African tigerfish (Genus *Hydrocynus*) reveals palaeogeographic signatures of linked Neogene geotectonic events. PloS one, 6(12), e28775. https://doi.org/10.1371/journal.pone.0028775

Gosse, J. C. and Phillips, F. M. (2001). Terrestrial in situ cosmogenic nuclides: theory and application. Quaternary Science Reviews, 20(14), 1475-1560. https://doi.org/10.1016/S0277-3791(00)00171-2

Guillocheau, F., Chelalou, R., Linol, B., Dauteuil, O., Robin, C., Mvondo, F., Callec, Y. and Colin, J. P. (2015). Cenozoic landscape evolution in and around the Congo Basin: constraints from sediments and planation surfaces. In Geology and Resource Potential of the Congo Basin. Springer, Berlin, Heidelberg, 271-313. https://doi.org/10.1007/978-3-642-29482-2_14

Gumbricht, T., McCarthy, T.S. and Merry, C.L. (2001). The topography of the Okavango Delta, Botswana, and its tectonic and sedimentological implications. South African Journal of Geology, 104, 243-264. https://doi.org/10.2113/1040243

Haddon, I.G. and McCarthy, T.S. (2005). The Mesozoic–Cenozoic interior sag basins of Central Africa: the Late-Cretaceous–Cenozoic Kalahari and Okavango basins. Journal of African Earth Sciences, 43, 316-333. https://doi.org/10.1016/j.jafrearsci.2005.07.008

Harrison, T., Mbago, M.L., and Msuya, C.P. (1996). Stratigraphy and vertebrate palaeontology of late Neogene sites in the Manonga Valley, north–central Tanzania. Kaupia, 6: 291–295.

Hermanns, R. L., Niedermann, S., Ivy-Ochs, S. and Kubik, P. W. (2004). Rock avalanching into a landslide-dammed lake causing multiple dam failure in Las Conchas valley (NW Argentina) – evidence from surface exposure dating and stratigraphic analyses. Landslides, 1(2), 113-122. https://doi.org/10.1007/s10346-004-0013-5

Hillaire-Marcel, C., Carro, O. and Casanova, J. (1986). 14C and ThU dating of Pleistocene and Holocene stromatolites from East African paleolakes. Quaternary Research, 25(3), 312-329. https://doi.org/10.1016/0033-5894(86)90004-9

Howard, A. D., Dietrich, W. E. and Seidl, M. A. (1994). Modeling fluvial erosion on regional to continental scales. Journal of Geophysical Research: Solid Earth, 99(B7), 13971-13986. https://doi.org/10.1029/94JB00744

Ivory, S. J., Blome, M. W., King, J. W., McGlue, M. M., Cole, J. E. and Cohen, A. S. (2016). Environmental change explains cichlid adaptive radiation at Lake Malawi over the past 1.2 million years. Proceedings of the National Academy of Sciences, 113(42), 11895-11900. https://doi.org/10.1073/pnas.1611028113

Kim, Y. S. and Sanderson, D. J. (2005). The relationship between displacement and length of faults: a review. Earth-Science Reviews, 68(3-4), 317-334. https://doi.org/10.1016/j.earscirev.2004.06.003

Kipata, M. L., Delvaux, D., Sebagenzi, M. N., Cailteux, J. and Sintubin, M. (2013). Brittle tectonic and stress field evolution in the Pan-African Lufilian arc and its foreland (Katanga, DRC): from orogenic compression to extensional collapse, transpressional inversion and transition to rifting. Geologica Belgica, 16(1), 1-17.

Kohl, C. P. and Nishiizumi, K. (1992). Chemical isolation of quartz for measurement of in-situ-produced cosmogenic nuclides. Geochimica et Cosmochimica Acta, 56(9), 3583-3587. https://doi.org/10.1016/0016-7037(92)90401-4

Lal, D. (1991). Cosmic ray labeling of erosion surfaces: in situ nuclide production rates and erosion models. Earth and Planetary Science Letters, 104(2-4), 424-439. https://doi.org/10.1016/0012-821X(91)90220-C

Lavayssiere, A., Drooff, C., Ebinger, C., Gallacher, R., Illsley- Kemp, F., Oliva, S. J. and Keir, D. (2019). Depth extent and kinematics of faulting in the southern Tanganyika rift, Africa. Tectonics, 38(3), 842-862. https://doi.org/10.1029/2018TC005379

Lehner, B. and Grill, G. (2013). Global river hydrography and network routing: baseline data and new approaches to study the world's large river systems. Hydrological Processes, 27(15), 2171-2186. https://doi.org/10.1002/hyp.9740

Macgregor, D. (2015). History of the development of the East African Rift System: A series of interpreted maps through time. Journal of African Earth Sciences, 101: 232–252. https://doi.org/10.1016/j.jafrearsci.2014.09.016

Master, S., Rainaud, C., Armstrong, R. A., Phillips, D. and Robb, L. J. (2005). Provenance ages of the Neoproterozoic Katanga Supergroup (Central African Copperbelt), with implications for basin evolution. Journal of African Earth Sciences, 42(1-5), 41-60. https://doi.org/10.1016/j.jafrearsci.2005.08.005

Masters, L. S., Burkhardt, J. W. and Tausch, R. (1991). The geomorphic process: effects of base level lowering on riparian management. Rangelands Archives, 13(6), 280-284.

Meier, J. I., Stelkens, R. B., Joyce, D. A., Mwaiko, S., Phiri, N., Schliewen, U. K., Selz, O.M., Wagner, C.E., Katongo, C. and Seehausen, O. (2019). The coincidence of ecological opportunity with hybridization explains rapid adaptive radiation in Lake Mweru cichlid fishes. Nature communications, 10(1), 1-11. https://doi.org/10.1038/s41467-019-13278-z

Merchel, S. and Herpers, U. (1999). An update on radiochemical separation techniques for the determination of long-lived radionuclides via accelerator mass spectrometry. Radiochimica Acta, 84(4), 215-220. https://doi.org/10.1524/ract.1999.84.4.215

Merchel, S. and Bremser, W. (2004). First international $^{26}$Al interlaboratory comparison–Part I. Nuclear Instruments and Methods in Physics Research Section B: Beam Interactions with Materials and Atoms, 223, 393-400. https://doi.org/10.1016/j.nimb.2005.05.051

Mohr, P. A. (1974). ENE-trending lineaments of the African rift system. Proc. First Int. Conf. New Basement Tectonics, Utah. Geol. Ass. Publ., 5 (1974), 327-336.

Molnar, N. E., Cruden, A. R. and Betts, P. G. (2019). Interactions between propagating rifts and linear weaknesses in the lower crust. Geosphere, 15(5), 1617-1640. https://doi.org/10.1130/GES02119.1

Mondeguer, A., Ravenne, C., Masse, P. and Tiercelin, J. J. (1989). Sedimentary basins in an extension and strike-slip background; the" South Tanganyika troughs complex", East African

Rift. Bulletin de la Société géologique de France, 3, 501-522. https://doi.org/10.2113/gssgfbull.V.3.501

Moore, A. E., Cotterill, F. P. D. and Eckardt, F. D. (2012). The evolution and ages of Makgadikgadi palaeo-lakes: consilient evidence from Kalahari drainage evolution south-central Africa. South African Journal of Geology, 115(3), 385-413. https://doi.org/10.2113/gssajg.115.3.385

Morley, C. K. (2002). Evolution of large normal faults: Evidence from seismic reflection data. AAPG bulletin, 86(6), 961-978. https://doi.org/10.1306/61EEDBFC-173E-11D7-8645000102C1865D

Mouslopoulou, V., Walsh, J. J. and Nicol, A. (2009). Fault displacement rates on a range of timescales. Earth and Planetary Science Letters, 278(3-4), 186-197. https://doi.org/10.1016/j.epsl.2008.11.031

Mouslopoulou, V., Nicol, A., Walsh, J. J., Begg, J. G., Townsend, D. B. and Hristopulos, D. T. (2012). Fault-slip accumulation in an active rift over thousands to millions of years and the importance of paleoearthquake sampling. Journal of Structural Geology, 36, 71-80. https://doi.org/10.1016/j.jsg.2011.11.010

NASA JPL (2020). NASADEM Merged DEM Global 1 arc second V001 [Data set]. NASA EOSDIS Land Processes DAAC. Last accessed September 2020. https://doi.org/10.5067/MEaSUREs/NASADEM/NASADEM_HGT.001

Neely, A. B., Bookhagen, B. and Burbank, D. W. (2017). An automated knickzone selection algorithm (KZ- Picker) to analyze transient landscapes: Calibration and validation. Journal of Geophysical Research: Earth Surface, 122(6), 1236-1261. https://doi.org/10.1002/2017JF004250

Nicol, A., Walsh, J. J., Watterson, J. and Underhill, J. R. (1997). Displacement rates of normal faults. Nature, 390(6656), 157-159. https://doi.org/10.1038/36548

Nicol, A., Walsh, J., Berryman, K. and Nodder, S. (2005). Growth of a normal fault by the accumulation of slip over millions of years. Journal of Structural Geology, 27(2), 327-342. https://doi.org/10.1016/j.jsg.2004.09.002

Nicol, A., Walsh, J. J., Villamor, P., Seebeck, H. and Berryman, K. R. (2010). Normal fault interactions, paleoearthquakes and growth in an active rift. Journal of Structural Geology, 32(8), 1101-1113. https://doi.org/10.1016/j.jsg.2010.06.018

Nicol, A., Van Dissen, R., Stirling, M. and Gerstenberger, M. (2016a). Completeness of the paleoseismic active fault record in New Zealand. Seismological Research Letters, 86, 1299-1310. doi:10.1785/0220160088

Nicol, A., Robinson, R., Van Dissen, R. J. and Harvison, A. (2016b). Variability of recurrence interval and single-event slip for surface-rupturing earthquakes in New Zealand. New Zealand Journal of Geology and Geophysics, 59(1), 97-116. https://doi.org/10.1080/00288306.2015.1127822

Nicol, A., Childs, C., Walsh, J.J., Manzocchi, T. and Schöpfer, M.P.J. (2016c). Interactions and growth of faults in an outcrop-scale system. In: The Geometry and Growth of Normal Faults. (Edited by Childs, C., Holdsworth, R. E., Jackson, C. A.-L., Manzocchi, T., Walsh, J. J. & Yielding, G.). Geological Society of London, Special Publication, 439, doi.org/10.1144/SP439.9

Nicol, A., Mouslopoulou, V., Begg, J. and Oncken, O. (2020a). Paleoearthquakes, sampling biases and growth of active normal faults on the eastern Mediterranean island of Crete. Geochemistry, Geophysics, Geosystems (in press).

Nicol, A., Walsh, J., Childs, C. and Manzocchi, T. (2020b). The growth of faults. In Understanding Faults (pp. 221-255). Elsevier. https://doi.org/10.1016/B978-0-12-815985-9.00006-0

Nishiizumi, K., Imamura, M., Caffee, M. W., Southon, J. R., Finkel, R. C. and McAninch, J. (2007). Absolute calibration of $^{10}$Be AMS standards. Nuclear Instruments and Methods in Physics Research Section B: Beam Interactions with Materials and Atoms, 258(2), 403-413. https://doi.org/10.1016/j.nimb.2007.01.297

Norris, T. L., Gancarz, A. J., Rokop, D. J. and Thomas, K. W. (1983). Half-life of $^{26}$Al. Journal of Geophysical Research: Solid Earth, 88(S01), B331-B333. https://doi.org/10.1029/JB088iS01p0B331

Omenda, P., Ebinger, C., Nelson, W., Delvaux, D., Cumming, W., Marini, L., Halldórsson, S., Varet, J., Árnason, K., Ruempker, G. and Alexander, K. (2016). Characteristics and important factors that influence the development of geothermal systems in the western branch of East African Rift System". In 6th African Rift Geothermal Conference 2016.

Perron, J. T. and Royden, L. (2012). An integral approach to bedrock river profile analysis. Earth Surface Processes and Landforms, 38(6), 570-576. https://doi.org/10.1002/esp.3302

Ring, U. (1994). The influence of preexisting structure on the evolution of the Cenozoic Malawi rift (East African rift system). Tectonics, 13(2), 313-326. https://doi.org/10.1029/93TC03188

Rotevatn, A., Jackson, C. A. L., Tvedt, A. B., Bell, R. E. and Blækkan, I. (2019). How do normal faults grow?. Journal of Structural Geology, 125, 174-184. https://doi.org/10.1016/j.jsg.2018.08.005

Rugel, G., Pavetich, S., Akhmadaliev, S., Baez, S. M. E., Scharf, A., Ziegenrücker, R. and Merchel, S. (2016). The first four years of the AMS-facility DREAMS: Status and developments for more accurate radionuclide data. Nuclear Instruments and Methods in Physics Research B, 370, 94-100. https://doi.org/10.1016/j.nimb.2016.01.012

Saria, E., Calais, E., Stamps, D. S., Delvaux, D. and Hartnady, C. J. H. (2014). Present-day kinematics of the East African Rift. Journal of Geophysical Research: Solid Earth, 119(4), 3584-3600. https://doi.org/10.1016/0301-9268(84)90032-9

Schlische, R. W., Young, S. S., Ackermann, R. V. and Gupta, A. (1996). Geometry and scaling relations of a population of very small rift-related normal faults. Geology, 24(8), 683-686. https://doi.org/10.1130/0091-7613(1996)024<0683:GASROA>2.3.CO;2

Schlüter, T. (1997). Geology of East Africa. In: Bender, F., Jacobshagen, V. and Lüttig, G. (Eds.), Beiträge zur Regionalen Geologie der Erde, Band 27. Gebrüder Borntraeger, Berlin, Stuttgart, 484 pp.

Schultz, R. A., Soliva, R., Fossen, H., Okubo, C. H. and Reeves, D. M. (2008). Dependence of displacement–length scaling relations for fractures and deformation bands on the volumetric changes across them. Journal of Structural Geology, 30(11), 1405-1411. https://doi.org/10.1016/j.jsg.2008.08.001

Schwanghart, W. and Scherler, D. (2014). TopoToolbox 2–MATLAB-based software for topographic analysis and modeling in Earth surface sciences. Earth Surface Dynamics, 2(1), 1-7. doi:10.5194/esurf-2-1-2014

Schwarzer, J., Misof, B., Ifuta, S. N. and Schliewen, U. K. (2011). Time and origin of cichlid colonization of the lower Congo rapids. Plos one, 6(7), e22380. https://doi.org/10.1371/journal.pone.0022380

Seiler, M., Anjar, J., Værnes, E., Nadeau, M. J. and Scognamiglio, G. (2018). First $^{10}$Be measurements at Trondheim 1 MV AMS. Nuclear Instruments and Methods in Physics, B 437, 123-129. https://doi.org/10.1016/j.nimb.2018.08.013

Shudofsky, G. N. (1985). Source mechanisms and focal depths of East African earthquakes using Rayleigh-wave inversion and body-wave modelling. Geophysical Journal International, 83(3), 563-614. https://doi.org/10.1111/j.1365-246X.1985.tb04328.x

Shuman, B., Henderson, A. K., Colman, S. M., Stone, J. R., Fritz, S. C., Stevens, L. R., Power, M. J. and Whitlock, C. (2009). Holocene lake-level trends in the Rocky Mountains, USA. Quaternary Science Reviews, 28(19-20), 1861-1879. https://doi.org/10.1016/j.quascirev.2009.03.003

Stamps, D. S., Calais, E., Saria, E., Hartnady, C., Nocquet, J. M., Ebinger, C. J. and Fernandes, R. M. (2008). A kinematic model for the East African Rift. Geophysical Research Letters, 35(5), L05304. https://doi.org/10.1029/2007GL032781

Strecker, M. R., Blisniuk, P. M. and Eisbacher, G. H. (1990). Rotation of extension direction in the central Kenya Rift. Geology, 18(4), 299-302. https://doi.org/10.1130/0091-7613(1990)018<0299:ROEDIT>2.3.CO;2

~~Šujan, M., Lačný, A., Braucher, R., Magdolen, P., Aumaître, A. T. G., Bourlès, D. and Keddadouche, K. (2017). Early Pleistocene age of fluvial sediment in the Stará Garda Cave revealed by $^{26}$Al/$^{10}$Be burial dating: implications for geomorphic evolution of the Malé Karpaty Mts. (Western Carpathians). Acta Carsologica, 46(2-3), 251-264.~~

Formatted: Highlight

Tack, L., Fernandez-Alonso, M., Trefois, P., Lavreau, J. and Cailteux, J. L. H. (2003). New data raise new questions on the regional geology of the Katanga Province as figured on the 1974 Geological Map (1/2000000) of the Democratic Republic of Congo (DRC). In Proterozoic Base

Metal Deposits of Western Gondwana. 3rd IGCP-450 Conference and Guide Book of the Field Workshop, Lumbumbashi, Congo, 78-82.

Thieme, J.G. (1971). The Geology of Musonda Falls Area, Explanation of Sheet 1028, SE Quarter. Geological Survey of Zambia, Report No. 32, 25.

Tiercelin, J. J. and Lezzar, K. E. (2002). A 300 million years history of rift lakes in Central and East Africa: an updated broad review. In The East African great lakes: limnology, palaeolimnology and biodiversity. Springer, Dordrecht, 3-60. https://doi.org/10.1007/0-306-48201-0_1

Tiercelin, J. J., Chorowicz, J., Bellon, H., Richert, J. P., Mwanbene, J. T. and Walgenwitz, F. (1988). East African Rift System: offset, age and tectonic significance of the Tanganyika-Rukwa-Malawi intracontinental transcurrent fault zone. Tectonophysics, 148(3-4), 241-252. https://doi.org/10.1016/0040-1951(88)90133-3

Torabi, A. and Berg, S. S. (2011). Scaling of fault attributes: A review. Marine and Petroleum Geology, 28(8), 1444-1460. https://doi.org/10.1016/j.marpetgeo.2011.04.003

Trauth, M. H., Maslin, M. A., Deino, A. and Strecker, M. R. (2005). Late Cenozoic moisture history of East Africa. Science, 309(5743), 2051-2053. https://doi.org/10.1126/science.1112964

Trauth, M. H., Maslin, M. A., Deino, A. L., Junginger, A., Lesoloyia, M., Odada, E. O., Olago, D. O., Olaka, L.A., Strecker, M. R. and Tiedemann, R. (2010). Human evolution in a variable environment: the amplifier lakes of Eastern Africa. Quaternary Science Reviews, 29(23-24), 2981-2988. https://doi.org/10.1016/j.quascirev.2010.07.007

Unrug, R. (1984). The mid-Proterozoic Mporokoso Group of northern Zambia: stratigraphy, sedimentation and regional position. Precambrian Research, 24(2), 99-121.

Van Damme, D. and Pickford, M. (2003). The late Cenozoic Thiaridae (Mollusca, Gastropoda, Cerithioidea) of the Albertine Rift Valley (Uganda-Congo) and their bearing on the origin and evolution of the Tanganyikan thalassoid malacofauna. Hydrobiologia, 498(1-3), 1-83. https://doi.org/10.1023/A:1026298512117

van der Merwe, P.D., Cotterill, F.P.D., Kandziora, M., Watters, B.R., Nagy, B., Genade, T., Flügel, T.J., Svendsen D. and Bellstedt, D. U. (2021). Genomic Fingerprints of Palaeogeographic History: The tempo and mode of Rift tectonics across tropical Africa has shaped the diversification of the killifish genus *Nothobranchius* (Teleostei: Cyprinodontiformes). Molecular Phylogenetics and Evolution, In Press. https://doi.org/10.1016/j.ympev.2020.106988

Vermeesch, P. (2007). CosmoCalc: An Excel add-in for cosmogenic nuclide calculations. Geochemistry, Geophysics, Geosystems, 8(8), https://doi.org/10.1029/2006GC001530

von Blanckenburg, F., Hewawasam, T. and Kubik, P. W. (2004). Cosmogenic nuclide evidence for low weathering and denudation in the wet, tropical highlands of Sri Lanka. Journal of Geophysical Research: Earth Surface, 109(F3), F03008. https://doi.org/10.1029/2003JF000049

Walsh, J. J. and Watterson, J. (1988). Analysis of the relationship between displacements and dimensions of faults. Journal of Structural geology, 10(3), 239-247. https://doi.org/10.1016/0191-8141(88)90057-0

Walsh, J. J., Nicol, A. and Childs, C. (2002). An alternative model for the growth of faults. Journal of Structural Geology, 24(11), 1669-1675. https://doi.org/10.1016/S0191-8141(01)00165-1

Walsh, J. J. and Watterson, J. (1991). Geometric and kinematic coherence and scale effects in normal fault systems. Geological Society, London, Special Publications, 56(1), 193-203. https://doi.org/10.1144/GSL.SP.1991.056.01.13

Watterson, J., Walsh, J. J., Gillespie, P. A. and Easton, S. (1996). Scaling systematics of fault sizes on a large-scale range fault map. Journal of Structural Geology, 18(2-3), 199-214. https://doi.org/10.1016/S0191-8141(96)80045-9

Wells, D. L. and Coppersmith, K. J. (1994). New empirical relationships among magnitude, rupture length, rupture width, rupture area, and surface displacement. Bulletin of the seismological Society of America, 84(4), 974-1002.

Wesnousky, S. G. (2008). Displacement and geometrical characteristics of earthquake surface ruptures: Issues and implications for seismic-hazard analysis and the process of earthquake rupture. Bulletin of the Seismological Society of America, 98(4), 1609-1632. https://doi.org/10.1785/0120070111

Whipple, K. X. and Tucker, G. E. (1999). Dynamics of the stream- power river incision model: Implications for height limits of mountain ranges, landscape response timescales, and research needs. Journal of Geophysical Research: Solid Earth, 104(B8), 17661-17674. https://doi.org/10.1029/1999JB900120

Whipple, K. X., Snyder, N. P. and Dollenmayer, K. (2000). Rates and processes of bedrock incision by the Upper Ukak River since the 1912 Novarupta ash flow in the Valley of Ten Thousand Smokes, Alaska. Geology, 28(9), 835-838. https://doi.org/10.1130/0091-7613(2000)28<835:RAPOBI>2.0.CO;2

Williamson, P. G. (1978). Evidence for the major features and development of Rift Palaeolakes in the Neogene of East Africa from certain aspects of Lacustrine Mollusc assemblages. Geological Society, London, Special Publications, 6(1), 507-527. https://doi.org/10.1144/GSL.SP.1978.006.01.35

## Figure Captions

Figure 1: Morphotectonic map of the Mweru-Mweru Wantipa Fault System (MMFS) in the southern East African Rift System. Normal faults are indicated by black lines while ticks indicate downfaulted side. Numbers next to each fault correspond to entries in Table A2 in the Appendix. Red lines indicate topographic profiles presented in Figures 4, 5 and 6. Green circles, yellow triangles and blue squares indicate sampling locations of the three different sampling groups. Inset shows location of study area in Africa. KUN: Kundabikwa Waterfalls; LUM: Lumangwe Waterfall; NTU: Ntumbachushi Waterfalls; MUM: Mumbuluma I Waterfalls; LUP: Lupupa Waterfall; LUO: Mumbuluma II Waterfall; LUZ: Lunzua Waterfalls.

Figure 2: A) Sampling of KUN01 from a vertical face on the banks of Kalungwishi River, downstream of Kundabikwa Waterfalls, Zambia; B) Sampling of bedrock (MUM04) directly from the horizontal surface of the knickpoint at Mumbuluma I Waterfalls, Zambia; C) View of Lumangwe Waterfall, Zambia; D) Sample location of ME09, Lwilwa River, DRC; E) Sampling of MWE01 from the face of fault 16, DRC.

Figure 3: A) Log-log plot illustrating the relationship between topographic fault length and total displacement for the faults in the MMFS (grey circles) and the Mpulungu basin (southern Tanganyika Fault System; black circles). B) Same as (a) but illustrating separately the NW dipping (circles) and the SE dipping (triangles) faults in the MMFS. C) Log-log plot illustrating the relationship between topographic fault length and the displacement rate for the faults in the MMFS (grey circles) and the Mpulungu basin (black circles). D) Global dataset of displacement vs. fault length (shaded area; Nicol et al., 2016b). Black circles show data for the same faults as in Figure 3A while white triangles represent single-event displacement rupture lengths for historical earthquakes (Wesnousky, 2008). Least squares lines of best fit and R2 values are also indicated for each dataset.

**Commented [A6]:** Fig 3 is quite pixelated and seems to be of low quality, can you make some efforts to improve it's appearance?

**Commented [A7R6]:** Perhaps problem while uploading the file. The original figure is high quality.

Figure 4: Five topographic profiles approximately perpendicular to the trend of the MMFS (for locality of the profiles see Figure 1). The SE dipping faults are indicated with red lines while the NW dipping faults with blue lines. Sample locations are indicated with yellow circles. Numbers with F next to faults correspond to numbered faults in Figure 1 and entries in Table A2 in the Appendix. Plain numbers next to the faults indicate the throw (m) of the respective fault. The total fault throw as well as the throw of the NW (blue) and SE (red) dipping faults are indicated on each profile. Blue dashed line indicates the potential water level of the paleo-lake Mweru.

**Commented [A8]:** Can you make the Distance label the same point size as the elevation on for consistency?

**Commented [A9R8]:** Done

Figure 5: Topographic profile along the trend of the MMFS. See Figure 1 for profile location and Figure 4 for explanations.

Figure 6: Reconstructed landscape based on the topographic profiles presented in Figures 4 and 5 and two additional profiles (Profiles 7 and 8) which are depicted in Figure 1. Subtracted throw resulted assuming a constant fault displacement rate (see Table A2 for values) during the last 2.6 Ma. Dashed black lines represent the current landscape. Grey dashed line indicates the approximate elevation of the reconstructed landscape about 2.6 Ma (rift's onset), while black solid line is the average elevation of the reconstructed landscape. The SE dipping faults are indicated by red triangles while blue circles indicate the NW dipping faults. The SW dipping faults are presented as green rhombuses, while yellow squares show the NE dipping faults.

Figure 7: A) Locations of river knickpoints for the Lake Mweru catchment. Symbol colours indicate knickpoint elevations and symbol sizes show knickpoint magnitudes (lips minus base elevation). Only river knickpoints with elevations between 900 and 1200 m asl are shown. Note the clustering of river knickpoints at ~925 (dark blue), ~1000, and ~1180 m asl that correspond to paleo-shorelines of paleo-lake Mweru. B) Hypsometric curve of Lake Mweru derived from a 30 m SRTM DEM (NASA JPL, 2020). All grid cells within the Lake Mweru catchment were binned into 10 m elevation bins and their respective surface areas were calculated (black line).

The elevations were filtered to only show hillslope angles < 3° (blue line). Note the two distinctive peaks at ~925 m asl and ~1180 m asl that show the elevations of the paleo-lake Mweru. Knickpoint elevation shows a high number of river knickpoints at paleo-lake shorelines (only river knickpoints with at least 30 m offset are shown).

Figure 8: Two-nuclide diagrams showing $^{10}$Be concentrations (atoms/g, corrected for total shielding and scaled to common elevation) versus $^{26}$Al/$^{10}$Be ratios for samples of Group A. The black dashed line indicates the “steady state denudation line” and the solid black line the “constant exposure line” (e.g. Lal, 1991). Red lines show the temporal evolution of data at constant denudation rates and subsequent burial. Green lines indicate duration of burial under the assumption that samples were first exposed and later completely buried until present. Samples are indicated with black error ellipses (1σ shown). Underlined labels indicate samples taken from vertical surfaces. A) Kundabikwa Waterfalls; B) Lumangwe Waterfall; C) Ntumbachushi Waterfalls; D) Mumbuluma I Waterfalls.

**Commented [A10]:** This figure was not included in the R2/R3 submission.

**Commented [A11R10]:** Problem with uploading. It is included this time.

Figure 9: Schematic figure of successive landscape stages of Kalungwishi River at Kundabikwa Waterfalls and paleo-lake Mweru. T1: Initial river state with waterfall already in place. T2: Onset of paleo-lake Mweru below Kundabikwa Waterfalls. Areas downstream of the knickpoint are covered with water and sediment, while denudation at and upstream of the waterfalls is reduced due to lower energy environment. T3: Full establishment of paleo-lake Mweru resulting in water cover and sediment deposition on top horizontal surfaces. T4: Drainage of the paleo-lake, resulting in exposure of areas above the knickpoint with concomitant incision of lacustrine sediments at the waterfalls and deposition of these sediments into the remaining lake below the waterfalls. T5: Paleo-lake Mweru is completely drained and sediments deposited during T3 and T4 are removed through regional denudation, resulting in differential bedrock exposure. T6: Present day river course with limited sedimentary cover and ongoing down- and backwearing through increased denudation.

**Commented [A12]:** There is a problem with this figure as the diagrams are appearing as black boxes.

**Commented [A13R12]:** Again perhaps problem with the uploading. Let me know if there is any further issue.

Figure 10: Two-nuclide diagrams showing $^{10}$Be concentrations (atoms/g) versus $^{26}$Al/$^{10}$Be ratios for samples of Group B. See Figure 8 for explanations. A) Lupupa Waterfall; B) Mumbuluma II Waterfall (Luongo River); C) Lunzua Waterfalls.

Figure 11: Two-nuclide diagram showing $^{10}$Be concentration (atoms/g) versus $^{26}$Al/$^{10}$Be ratios for samples of Group C. See Figure 8 for explanations.

Figure 12: Schematic representation of the possible maximum extent of paleo-lake Mweru during the Plio-Pleistocene (see blue contour at 1200 m asl). Shaded areas represent reconstructed paleo-topography that was present during the Plio-Pleistocene.

# Quaternary landscape evolution in a tectonically active rift basin (paleo-lake Mweru, south-central Africa)

Spiros Olivotos[1], Samuel Niedermann[1], Tyrel Flügel[2], Vasiliki Mouslopoulou[3], Silke Merchel[4], Fenton Cotterill[2], Bodo Bookhagen[5], Andreas Gärtner[4], Georg Rugel[4], Andreas Scharf[4], Marie-Josée Nadeau[6], Régis Braucher[7], Martin Seiler[6]

Affiliations

(1) Deutsches GeoForschungsZentrum GFZ, Section 3.1, Telegrafenberg, 14473 Potsdam, Germany.

(2) Stellenbosch University, Matieland, 7602, Stellenbosch, South Africa.

(3) National Observatory of Athens, Institute of Geodynamics, Lofos Nimfon, Athens, 11810, Greece.

(4) Helmholtz-Zentrum Dresden-Rossendorf (HZDR), Bautzner Landstraße 400, 01328 Dresden, Germany.

(5) Institut für Geowissenschaften, University of Potsdam, Karl-Liebknecht-Str. 24-25, 14476 Potsdam, Germany.

(6) The National Laboratory for Age Determination, NTNU University Museum, Sem Sælands vei 5, 7491 Trondheim, Norway.

(7) CEREGE, Aix Marseille Univ., CNRS, Collège de France, IRD, INRAE, Plateau de l'Arbois, 13545 Aix en Provence, France

**Keywords:** Landscape evolution; Morphotectonic Analysis; Terrestrial cosmogenic nuclides; East African Rift System.

## Highlights

- Explores existence of a Quaternary paleo-lake Mweru, SW East African rift system
- Applies exposure ages of knickpoints, fault analyses and geomorphic investigations
- Cosmogenic nuclides retrieve a landscape history of burial, exposure and denudation
- Faulting and lake-river knickpoints indicate a paleo-lake level at ~1200 m asl
- Lake dynamics linked to recurring neotectonics and regional  climate variation

# Abstract

Located between the Northern Province of Zambia and the southeastern Katanga Province of the Democratic Republic of Congo, Lakes Mweru and Mweru Wantipa are part of the southwest extension of the East African Rift System (EARS). Fault analysis reveals that, since the Miocene, movements along the active Mweru-Mweru Wantipa Fault System (MMFS) have been largely responsible for the reorganization of the landscape and the drainage patterns across the western branch of the EARS. To investigate the spatial and temporal patterns of fluvial-lacustrine landscape development, we determined in-situ cosmogenic $^{10}Be$ and $^{26}Al$ using Accelerator Mass Spectrometry. A total of twenty-six quartzitic bedrock samples were collected from knickpoints across the Mporokoso Plateau (south of Lake Mweru) and the eastern part of the Kundelungu Plateau (north of Lake Mweru). Samples from the Mporokoso Plateau and close to the MMFS provide evidence of temporary burial. By contrast, surfaces located far from the MMFS appear to have remained uncovered since their initial exposure as they show consistent $^{10}Be$ and $^{26}Al$ exposure ages ranging up to ~830 ka. Reconciliation of the observed burial patterns with morphotectonic and stratigraphic analysis reveals the existence of an extensive paleo-lake during the Pleistocene. Through hypsometric analyses of the dated knickpoints, the potential maximum water level of the paleo-lake is constrained to ~1200 m asl. High denudation rates (up to ~40 mm $ka^{-1}$) along the eastern Kundelungu Plateau suggest that footwall uplift, resulting from normal faulting, caused rapid river incision, thereby controlling paleo-lake drainage. The complex exposure histories recorded by $^{10}Be$ and $^{26}Al$ may be explained because of lake water-level fluctuations caused by active normal faulting along the MMFS coupled with intense climate variations across southeastern Africa.

# 1. Introduction

The East African Rift System (EARS) is one of Earth's best studied active intracontinental rifts (e.g., Ebinger, 1989; Delvaux, 1991; Delvaux et al., 1992; Ring, 1994; Schlüter, 1997; Chorowicz, 2005; Braile et al., 2006; Stamps et al., 2008; Macgregor, 2015). The combination of the EARS length (> 3,000 km) and longevity (active throughout the Neogene, ~25 Ma) provides a unique opportunity to study the evolution of continental rifting; from initial crustal break-up (via normal faulting) to incipient oceanic rifting and, eventually, the opening of future oceans. Overall, the EARS can be considered to have had a dominant control on the landscape evolution of eastern Africa during the last ~30 Ma (e.g., Chorowicz, 1989, 2005; Macgregor, 2015). The northern and central parts of the EARS have been previously investigated and linkages between tectonic activity, climatic variations and (paleo) lake formation have been established (Bergner et al., 2009). However, there are limited constraints on the landscape evolution of the Western Branch of the EARS.

The interplay of faulting, climatic and fluvial processes have resulted in the development of a series of lakes that extend over a thousand kilometers along the EARS (Fig. 1 inset). The existence of large and deep paleo-lakes within the Western Branch during the Plio-Pleistocene (e.g. paleo-lakes Turkana, Edward-Albert, Obweruka, Bangweulu, Magadi, Thamalakane and Tanganyika) is well established (Williamson, 1978; Hillaire-Marcel et al., 1986; Burrough and Thomas, 2008; Cotterill and de Wit, 2011; Danley et al., 2012; Cohen et al., 2016).

Our study area lies to the southwest of Lake Tanganyika, straddling the border between the Democratic Republic of Congo (DRC; Katanga Province) and Zambia (Northern Province; Fig. 1). This area (Lake Mweru) is part of the fast-spreading Western Branch of the EARS, and it is characterized by an ENE-WSW trending basin-and-range topography that intersects the Tanganyika Rift System perpendicularly (Fig. 1). These typical horst and graben structures formed due to normal faulting along the Mweru-Mweru Wantipa Fault System (MMFS) and are the seismically most active faults of central east Africa. Two of these graben structures host the high-altitude present-day lakes of Lake Mweru (917 m asl) and Lake Mweru Wantipa (932 m asl; Delvaux and Barth, 2010; Daly et al., 2020). The lakes are bounded to the northwest and southeast by two high plateaus, Kundelungu and Mporokoso, respectively (Mondeguer et al., 1989; Tack et al., 2003; Daly et al., 2020; Fig. 1).

Active faulting has been proposed previously as one of the key controls in shaping of river catchments and the landscape southwest of Tanganyika (Gumbricht et al., 2001; Haddon and McCarthy, 2005; Flügel et al., 2017; Daly et al., 2020). However, detailed geomorphological and tectonic studies in the area remain scarce, with much of the literature having focused on first-order physiographic characteristics of the rift to infer tectonic correlations between these structures and the EARS (e.g., Mohr, 1974; Tiercelin et al., 1988; Mondeguer et al., 1989; Strecker et al., 1990; Delvaux, 1991; Chorowicz, 2005; Kipata et al., 2013). Yet knickpoint creation is not only correlated with tectonic activity (normal faulting) and differential denudation, but may also be associated with changes in base-level and sea-level, as well as climatic variations (Whipple and Tucker, 1999; Whipple et al., 2000). It has been argued that climatic extremes within such fast-spreading rifts may have played a key role in controlling lake-level fluctuations (Lavayssiere et al., 2019). The paleo-lakes Manonga (Tanzania) and Obweruka (Uganda) are considered primary examples of climate-controlled lakes in the EARS (Harrison, et al., 1996; Van Damme and Pickford, 2003). However, without geochronologic dates to constrain landscape evolution rates in the Western Branch, determining the controlling factors acting on the landscape remains challenging. A secondary, albeit key, consideration of this study is that large knickpoints are important biogeographic controls, acting as natural barriers to species dispersal, especially fish. These landforms often result in divergent evolution between upstream and downstream populations of biota (Cotterill and de Wit, 2011; Schwarzer et al., 2011). Thus, direct age estimates of knickpoints may inform on biogeographical histories of the region.

Dixey (1944) inferred a “greater” Lake Mweru based primarily on lacustrine deposits that are abandoned at ~1030 m asl, about 100 m higher than the present-day lake level. Moreover, Bos et al. (1995, 2006) suggested that patches of sands along the present-day Zambian (southern and southeastern) shores of Lake Mweru may indicate a migration of the Luapula River (Fig. 1). This is evidenced by sedimentary deposits that lie more to the west than its current position (Bos et al., 1995). Several studies propose that the initial Lake Mweru formed a large impoundment that extended over the lower part of the Northern Province of Zambia. No fieldwork and/or geomorphological analysis have hitherto explored the precise extent and duration of a larger paleo-lake Mweru (Dixey, 1946; Bos et al., 1995; Cotterill and de Wit, 2011).

This study attempts to identify and, where possible, quantify key factors and mechanisms that control the landscape evolution proximal to Lake Mweru. By doing so, we aim to test whether a precursor of Lake Mweru formed a big impoundment, inundating a larger portion of the Northern Province of Zambia at its lower elevations. Collectively, our study aims to explore the impact of normal fault growth on the formation of the paleo-lake and the drainage around the present-day Lake Mweru by combining tectonic and geomorphologic analyses of the study area with the application of terrestrial cosmogenic nuclides to dating and the magnitude of denudation. By interpreting a network of surface exposure dates of key landforms (river knickpoints, fault scarps, and riverbeds) across the two high plateaus (Mporokoso and Kundelungu Plateaus) that surround and delimit the current lake, we deduce the age of formation of the paleo-lake. By doing so, we constrain the extent and depth of the paleo-lake Mweru and estimate its life span and explore possible mechanisms that reduced its Pleistocene high stand. Direct geochronological derivations of the timing of the onset of the paleo-lake -

and its tenure - contribute new information toward resolving the landscape evolution of the southwestern part of the Western Branch. Moreover, constraining the tenure of this Late Cenozoic depocenter reveals important information relating to the drainage evolution of the Congo-Kalahari Watershed during the Pleistocene (Flügel et al., 2015, 2017).

## 2. Geomorphic and Geologic Setting

The MMFS has a length of ~ 400 km, a width of ~ 200 km and is divided into eastern and western parts. The eastern part is characterized by an elongated ENE-WSW trend, almost perpendicular to the NW-SE trend of the Mpulungu basin (southern Lake Tanganyika; Tiercelin and Lezzar, 2002). Small and parallel grabens form shallow depressions, characterized by wetland environments (Mondeguer et al., 1989). To the west, two major troughs with NNE-SSW trend form the two main shallow lakes (Lakes Mweru and Mweru Wantipa). The majority of the faults follow a NNE-SSW trend, while few faults that mainly confine the end of the basins have a vertical trend of WNW-ESE (Mondeguer et al., 1989). The deviation in the fault trend near the Mpulungu basin results from the competency contrast with the relatively stable Bangweulu Block (Mondeguer et al., 1989; Fig. 1). The rotation of the extension direction reactivated earlier dip-slip faults, since strain accumulated in the same pre-Pleistocene inherited crustal structures (Ring, 1994; Morley, 2002; Saria et al., 2014). Furthermore, earthquake fault plane solutions from the area indicate an extensional displacement around the WNW axis (Delvaux and Barth, 2010). Recent modeling studies suggest that the extension direction changes from ~60° to 90°, while a left-lateral motion is applied on two domains with NE-E oriented weaknesses in between them (Molnar et al., 2019 and references therein).

Lake Mweru (situated at ~9° S and ~29° E) forms part of the south-eastern extension of the Congo Basin, being fed from the south by the Luapula River and drained to the northwest by the Luvua River (Fig. 1). The drainage of the Lake Mweru sub-basin is mostly sub-dendritic, representing the interaction of rivers flowing on Precambrian basement and regional faulting

(Deffontaines and Chorowicz, 1991, Flügel et al., 2015). The extensive delta of the Luapula River suggests rapid denudation of the high plateaus between Lake Mweru and Lake Bangweulu (Fig. 1). In addition, the accumulation of Quaternary sediments with a thickness of 400 m uncomformably overlying the Neoproterozoic basement (Bos et al., 2006; Daly et al., 2020) can be interpreted as further evidence of rapid denudation of the surrounding highlands. Quaternary sediments are absent from Kilwa Island, a Neoproterozoic clastic rock outcrop, north of the delta (Shudofsky, 1985; Tiercelin and Lezzar, 2002; Daly et al., 2020). In the north, the outflowing Luvua River runs through a steep valley path with several large waterfalls, suggesting rapid incision (Flügel et al., 2017). The Kalungwishi River, a major tributary, feeds Lake Mweru from the east. This river drains its own highland sub-basin and has several large knickpoints on its course. The inflowing rivers allow the lake to maintain a surface area of ~ 5100 km$^2$ year-round (Bos et al., 2006).

Along the eastern shore of Lake Mweru, a ~10 m high beach terrace indicates an actively uplifted coastline controlled by a long major fault line (Fault 16 in Fig. 1) across the southern borders of the Kundelungu Plateau (Daly et al., 2020). The southeastern border of the lake is delimited by a major fault (Fault 23 in Fig. 1) parallel to the trend of the Mporokoso Plateau, creating Lake Mweru that is 27 m at its deepest (Bos et al., 2006). This rectangular lake is surrounded by uplifted rift margins, with the lake geometry and bathymetry being controlled by basin subsidence. The structural control of this setting is described in further detail below.

Southeast of Lake Mweru, a large basin of sub-horizontal sedimentary cover (Mporokoso Plateau) is developed onto the Archean-Paleoproterozoic cratonic Bangweulu Block (Mondeguer et al., 1989; De Waele et al., 2009; Fig. 1). The Mporokoso Plateau consists mostly of undeformed fluvial and lacustrine sediments (De Waele and Fitzsimons, 2007). Unrug (1984) characterized the Mporokoso Plateau as the late Palaeoproterozoic to late Mesoproterozoic pre-Katangan succession to the northwest and northeast of the Bangweulu Block. A thick sedimentary bedrock succession, called the Kundelungu Plateau, forms the half graben structure that delimits the lake to the northwest (Fig 1). The Kundelungu Plateau is a part of the larger Neoproterozoic (<883 Ma to ~573 Ma; Master et al., 2005) Katangan Supergroup, comprising carbonate and siliciclastic sequences which were deposited in a wider basin. The bedded red sand- and siltstones of the Kundelungu Plateau are exposed at the northwest corner of Lake Mweru due to incision along the Luvua River (Kipata et al., 2013).

The interplay of faulting and erosion in the broader Lake Mweru region has resulted in two relatively flat but vertically offset surfaces: the Lake Mweru valley bottom and the surrounding plateaus. In general terms, the valley bottom (~ 900 m asl) is approximately 600 m lower than the flat plateau tops (~ 1500 m asl). The amagmatic character of the tectonism, combined with an indistinct sedimentation sequence across the southwestern extension of the EARS, does not allow precise dating of the initiation of faulting in the study area. The formation of the extended denudational surface of the Central African Plateau is estimated at around late Miocene to early Pliocene times (Daly et al., 2020). The absence of Neogene sedimentation across the Central African basin suggests that the tectonic activity must have been initiated after, or during, the uplift of the Central African Plateau, thereby constraining the onset of the MMFS to the late Pliocene - early Pleistocene (~2.6 Ma; Daly et al., 2020).

# 3. Material and Methods

## *3.1. Sampling and Sample Grouping*

In this study, we aim to provide temporal control to derive rates for landscape evolution. We focus on surface exposure dating of geomorphic markers using two cosmogenic radionuclides ($^{10}$Be, $^{26}$Al; the intended inclusion of stable $^{21}$Ne did not provide meaningful results, see Appendix). To ensure sufficient sample material (i.e., quartz) to undertake surface exposure dating, the field sampling mostly targeted bedrock quartzites due to their abundance in quartz. Sampling sites were located at or near waterfalls (knickpoints) as these are sites of exposed rock and considered key features in a river's development. Samples were taken from two broader areas, the Mporokoso Plateau and the northeastern Lake Mweru (Fig 1). Twenty-one samples, from seven waterfalls, were collected across the Mporokoso Plateau (Table 1), mostly from vertical or subvertical (45-90°) surfaces (Fig. 2A), downstream of the present-day knickpoint position. Where possible, samples were also taken from the waterfalls themselves to determine the minimum exposure age of the knickpoint at its current position (Fig. 2B, 2C). Dating two or more samples at different distances from the present knickpoint enables us, in principle, to estimate knickpoint retreat rates (Fig. A1). To determine maximum denudation rates, samples from horizontal surfaces (from above and below the knickpoints) were also collected (Table 1; Fig. 2B).

Five additional quartz-rich samples were obtained from the northwest shore of Lake Mweru: two from horizontal and two from vertical surfaces located along river channels (Fig. 2D) and one directly from the fault that bounds the MMFS to the north (Fig. 2E). See Table 1 for sample information and the Appendix (Fig. A1) for a more detailed description of the sampling process.

Based on their location relative to the MMFS, we subdivide our samples into three main groups: Group A samples are from south and southeast of Lake Mweru within the MMFS, Group B samples are from southeast of Lake Mweru but situated outside the MMFS, and Group C samples derive from north of Lake Mweru, along the northern margin of the MMFS (Table 1; Fig. 1).

#### *3.1.1. Group A*

The ~25 m high Kundabikwa Waterfalls (elevation ~1043 m asl) have incised quartzitic bedrock to form one of the two main knickpoints along the Kalungwishi River. Three pairs of vertical and horizontal samples (KUN01/02, KUN03/04 and KUN05/06) were taken from the right bank at different distances downstream of the present waterfalls. An additional sample (KUN07) was collected from the riverbank immediately above the waterfalls.

The Lumangwe Waterfall (~1159 m asl), located ca. 37 km upstream of the Kundabikwa Waterfalls, forms the most prominent knickpoint along the Kalungwishi River, with a height of ~40 m and a width of ~160 m (Fig. 2C). At Lumangwe Waterfall, the main bedrock is interbedded quartzite, with layers of red siltstones. Due to the vegetation density and the large amount of water, sampling this waterfall was challenging. Therefore, only one siltstone sample from a vertical face (LUM01) and a pair of quartzitic samples from vertical (LUM02) and horizontal (LUM03) surfaces were taken. Due to the very low amount of appropriately sized quartz grains, LUM01 could not be analyzed.

The cascade of the Ntumbachushi Waterfalls (~1160 m asl) is about 30 m high and is located on the Ng'ona River. Three samples were collected from these waterfalls, of which NTU01 and NTU03 were taken from the right vertical bank downstream of the current knickpoint, while NTU02 was collected above NTU01 from the corresponding horizontal bank.

The Mumbuluma Waterfalls (~1186 m asl) are situated on the Mumbuluma River and cascade down over two discrete steps. They will be denoted Mumbuluma I Waterfalls hereafter to distinguish them from the equally named waterfall on the Luongo River (section 3.1.2). MUM01 and MUM04 were collected from a vertical and a horizontal surface, respectively, of the top cascade, while the samples MUM02 (horizontal) and MUM03 (vertical) were taken from the lower step of the waterfalls.

### *3.1.2. Group B*

The Lupupa Waterfall is located on the Mukubwe River and has a height of approximately 90 m. The highest set of cascades is located at about 1360 m asl. Due to difficulties associated with the steepness of the waterfall, we only managed to collect one sample (LUP01) close to the top of the vertical cliff.

The Luongo River is one of the dominant rivers of the Northern Province in Zambia. We collected two samples from inclined surfaces of the Mumbuluma Waterfall (hereafter denoted Mumbuluma II to distinguish it from the falls on the Mumbuluma River; section 3.1.1.), which lies at ~1370 m asl with ~10 m height.

The Lunzua Waterfalls form a series of cascades along the Lunzua River. The waterfalls are close to the town of Mpulungu at the southern shore of Lake Tanganyika (Fig. 1) and are situated at ~1300 m asl. Two vertical samples (LUZ01 and LUZ02) were collected from the banks of the Lunzua River downstream of the cascades.

#### *3.1.3. Group C*

Due to the extreme inaccessibility of waterfalls caused mainly by vegetation along the northwestern side of Lake Mweru, no samples from waterfalls were collected in that area. Rather, they were taken from riverbeds and banks comprising mostly quartzitic bedrock. MWE01 derived from an almost vertical (80°) face that forms the surface expression of a normal fault scarp (Fig. 1; Fig. 2E). Two samples (ME04, ME05) were collected from the vertical walls of the gorge along the Luvua River, close to where it discharges from Lake Mweru (Fig. 1; Fig. 2D). The samples ME06 and ME09 were collected from horizontal bank surfaces along the Misefwe and Lwilwa rivers, two small tributaries northwest of Lake Mweru.

### *3.2. Sample Processing*

Samples were crushed and sieved to 250–500 μm. Quartz grains were separated by the standard methods of heavy liquid and Frantz magnetic separation (Kohl and Nishiizumi, 1992). To dissolve all non-quartz minerals, samples were treated with dilute HCl and $H_2SiF_6$ (Brown et al., 1991). Afterwards, HF was used to remove any contribution of meteoric $^{10}Be$ by partially dissolving the quartz grains. A small fraction from each sample (~2 g) was kept for $^{21}Ne$ analyses, while the remaining ~25-50 g were used for $^{10}Be$ and $^{26}Al$ analyses. Preparation and processing of the samples took place at the Helmholtz-Zentrum Dresden-Rossendorf (HZDR) following a modified version of the method described by Merchel and Herpers (1999) and at the University of Potsdam following the sample preparation manual of the UC Santa Barbara Cosmogenic Nuclide Preparation Facility (http://www.geog.ucsb.edu/~bodo/pdf/bookhagen_chemSeparation_UCSB.pdf), which is based on modifications of previous studies (e.g., Kohl and Nishiizumi, 1992; von Blanckenburg et al., 2004). The samples from the Kundabikwa Waterfalls (KUN) were prepared at HZDR, while the rest of the samples were prepared at University of Potsdam. For the radionuclide extraction, a known amount (~0.3 mg) of $^{9}$Be carrier was added to each sample, whilst ~1 mg Al carrier was added only to the blank samples (Table A1). Concentrated HF was used for digestion of the samples. After evaporation of the HF and the addition of $HClO_4$, ICP-AES (Inductively Coupled Plasma Atomic Emission Spectroscopy) or ICP-MS (Inductively Coupled Plasma Mass Spectrometry) measurements were done from aliquots, which were dissolved in HCl, in order to quantify the total Al concentration (Appendix Table A1). Be and Al were separated via ion exchange columns and precipitated as hydroxides. The last step before the target pressing was the ignition to oxides (900-1000 °C). Be isotope ratios were measured by Accelerator Mass Spectrometry (AMS) at the DREAMS facility of HZDR (Rugel et al., 2016; Table 2) and the National Laboratory of Age Determination of the Norwegian University of Science and Technology (NTNU), Trondheim (Seiler et al., 2018; Table 2). Al isotope ratio measurements were performed at HZDR (Rugel et al., 2016; Table 2) and at the French national facility Accélérateur pour les Sciences de la Terre, Environnement, Risques (ASTER, CEREGE, Aix-en-Provence; Arnold et al., 2010; Table 2). All processing values are provided in the Appendix (Table A1) and are one to three orders of magnitude lower than sample values.

## *3.3. Calculation of Exposure and Burial Ages and Denudation Rates*

Waterfalls are dynamic systems that undergo geomorphological changes through time. The rate at which knickpoints migrate upstream along a river is dependent on a combination of lithology, elevation, morphology, climatic conditions, and tectonic activity (Howard et al., 1994; Whipple and Tucker, 1999; Whipple et al., 2000; Brocklehurst, 2010). Their complexity means waterfalls can be a challenge to date, even with cosmogenic nuclides. Nevertheless, useful parameters such as denudation rates, periods of burial, minimum exposure ages and sequential exposure can be estimated for knickpoints and their surrounding landscape.

To calculate exposure ages and denudation rates, sea level high latitude (SLHL) spallogenic production rates of 4.01 atoms $g^{-1}$ $a^{-1}$ for $^{10}Be$ and 27.93 atoms $g^{-1}$ $a^{-1}$ for $^{26}Al$ were used (Borchers et al., 2016). Minimum ages and maximum denudation rates were calculated with CosmoCalc 3.0 (Vermeesch, 2007), using Lal (1991) scaling factors and default values for all parameters except the SLHL production rates. The density used for the calculations is 2.65 g $cm^{-3}$ for all samples. Values were corrected according to sample thickness (1-10 cm) and geometric shielding. All $^{10}Be/^{9}Be$ ratios were normalized to the in-house standard material "SMD-Be-12" with a weighted mean value of $(1.704 \pm 0.030) \times 10^{-12}$ (Akhmadaliev et al., 2013). The "SMD-Be-12" has been cross-calibrated to the NIST SRM 4325 standard, which has a $^{10}Be/^{9}Be$ ratio of $(2.79 \pm 0.03) \times 10^{-11}$ (Nishiizumi et al., 2007). $^{26}Al/^{27}Al$ ratios measured at DREAMS were normalized to the in-house standard "SMD-Al-11", with a $^{26}Al/^{27}Al$ ratio of $(9.66 \pm 0.14) \times 10^{-12}$ (Rugel et al., 2016), while the Al ratios measured at ASTER were normalized to "SM-Al-11" with a $^{26}Al/^{27}Al$ ratio of $(7.401 \pm 0.064) \times 10^{-12}$ (Arnold et al., 2010). Both Al standards are traceable via cross-calibration to the same primary standards (MB04-A, MB04-B, MB04-D) from a $^{26}Al$ round-robin exercise (Merchel and Bremser, 2004). For samples with $^{10}Be$ and $^{26}Al$ ages agreeing within error limits, error-weighted mean ages were also calculated.

Since the attenuation length of terrestrial cosmogenic nuclide (TCN) production is smaller at low angles than in a vertical direction (Dunne et al., 1999), the TCN concentration decreases faster perpendicularly beneath an inclined surface than beneath a horizontal surface. This must be taken into account when calculating denudation rates of inclined or vertical surfaces and, therefore, a slope dependent correction (Hermanns et al., 2004) was applied to such surfaces.

In general, discordance between $^{10}$Be and $^{26}$Al ages may be due to long exposure (when $^{26}$Al production equals decay, i.e. after a few $^{26}$Al half-lives), denudation which has not been taken into account, or shielding from cosmic rays after initial exposure (e.g. Lal, 1991; Gosse and Phillips, 2001; Goethals et al., 2009). To reveal complex exposure histories, $^{10}$Be concentrations can be plotted against $^{26}$Al/$^{10}$Be ratios. In such two-nuclide plots, samples which lie between the "steady state denudation line" and the "constant exposure line" have experienced simple exposure histories, i.e. a combination of surface exposure and denudation. In contrast, samples plotting beneath the steady state field indicate burial after initial exposure. The calculation of burial ages (Lal, 1991) is based on the assumption that a surface has once been irradiated by cosmic rays up to steady state and was later buried until the present. This assumption is obviously not correct in our study, as all samples were taken from presently exposed surfaces. If such samples indicate burial, they must have been re-exposed sometime in the past, and only minimum burial ages can be calculated from them.

### *3.4. Normal Fault Analysis*

We used a Shuttle Radar Topography Mission (SRTM) digital surface model (DSM), Google Earth™ imagery, and the ArcGIS software (version 10.6) to map the traces of 63 normal faults in the area, from west of Lake Mweru to the southern shorelines of Lake Tanganyika (Fig. 1). This area largely includes faults of the MMFS, while at its eastern edge it comprises elements of the EAR (Fig. 1).

We focused our analysis on two fault parameters that, collectively, provide important information on the fault system's activity and growth: the fault length (L) and the fault displacement (D). Fault length represents an important parameter in estimating the seismic potential (including earthquake magnitude and single-event displacement) on each studied fault (Wells and Coppersmith, 1994; Wesnousky, 2008). It should be noted that several of the identified faults contain numerous parallel or sub-parallel strands (e.g. faults 30, 38, 44, 46, 49, etc. in Fig. 1) or along-strike segments (e.g. 1, 2, 7, 16, 43, etc.) which are either hard or soft linked (Walsh and Watterson, 1991). Here, these elements are thought to represent a single coherent fault that ruptures along its entirety; however, it remains possible that individual earthquakes rupture these faults or fault segments only partially. The maximum vertical displacement (or throw) on each normal fault derives by averaging numerous (>10) scarp height measurements from fault perpendicular topographic profiles collected proximal to the fault's centre. Fault lengths and displacements represent direct measurements drawn on the DSM and are presented in Table A2 together with the faults' geometries. Indirect earthquake attributes (e.g. earthquake magnitude, average recurrence interval, etc.) associated with each studied fault derive from Wells and Coppersmith's (1994) and Wesnousky's (2008) empirical relations and are also included in Table A2 (see caption of Table A2 in the Appendix for details).

Measurement of active fault lengths and displacements can be subject to significant uncertainties (Wesnousky, 2008; Mouslopoulou et al., 2012; Nicol et al., 2016a, 2020a). This is because fault scarps are prone to denudation and/or burial, especially at fault tips, where displacements are often too small to be detected with conventional mapping methods (such as aerial photo or DSM analysis, field mapping, etc.; Begg and Mouslopoulou, 2010). In this study, fault lengths and displacements should be considered as minimum values as fault scarps of < 2 m are not resolvable on the available DSM, and also because fault scarps of any size may be partly or entirely modified by denudation and/or burial (see Nicol et al., 2020a for detailed discussion on sampling biases). Rifting across the MMFS is thought to have initiated at about

2.6 Ma (late Pliocene-early Pleistocene; Tiercelin and Lezzar, 2002; Molnar et al., 2019; Daly et al., 2020), thus, fault displacement rates are calculated over this time-period (~2.6 Ma) (Table A2).

### 3.5. *Digital Topography Analyses*

We analyzed selected domains of the 30-m NASADEM (NASA JPL, 2020). We have delineated the catchment of Lake Mweru using standard procedures implemented in TopoToolbox (Schwanghart and Scherler, 2014). Elevation lows (pits) were filled, a hydrological-corrected DEM has been calculated, and the catchment extents were visually verified. Our catchment extent, using the higher resolution NASADEM data, is similar to that calculated in the HydroBASINs dataset (Lehner and Grill, 2013). The catchment extent was used to extract the hypsometric curve, showing the surface area for each elevation bin. Further, we identified river knickpoints using previously published approaches (Neely et al., 2017). This entailed deriving longitudinal river profiles, converting them to Chi coordinates, and identifying knickpoint lips and bases based on positive or negative distance above a best-fit Chi profile (Neely et al., 2017). Chi profiles are area-normalized profiles where the distance coordinate has been normalized by an averaged river profile following an exponential function (Perron and Royden, 2012). The resulting profile, when in steady state, will follow a straight line. We analyze profile deviation above and below an averaged line to identify knickpoints. More detailed analysis steps are described in Neely et al. (2017). To avoid small knickpoints and remove noise inherent in the DEM, we focus on knickpoints with magnitudes (i.e., distances from the average Chi profile line) exceeding 30 m. Field observations suggest that major waterfalls associated with past lake-level highstands are generally higher than 30 m.

## 4. Results

We present our results as three components, starting with the determinations of the terrestrial cosmogenic nuclides. Second, the findings of tectonics analyses are reported, summarizing the fault geometries and kinematics of the faulted topography. Third, we present a geomorphic analysis of northeast Zambia and the adjacent Katanga Province. In the subsequent section 5 we will focus on reconstructed scenarios informed from the TCN results, which are classified according to respective landscape history, including elevation, and contrasting tectonic regimes.

## 4.1. Terrestrial Cosmogenic Nuclides

While the $^{10}$Be and $^{26}$Al results indicate extended periods of burial for many samples (see section 4.1.1.), there is no straightforward way to interpret the $^{21}$Ne data along with $^{10}$Be and $^{26}$Al. Due to their inconclusive nature, we do not discuss them further but present and describe them in the Appendix (Table A3 and Fig. A3, A4). Below we present the $^{10}$Be and $^{26}$Al results (shown in Table 2) by sample groups.

### 4.1.1. $^{10}$Be and $^{26}$Al minimum exposure ages

#### 4.1.1.1. Group A

Vertical samples KUN01 and KUN04 from Kundabikwa Waterfalls yield $^{10}$Be minimum ages of ~510 and ~580 ka, respectively, while $^{26}$Al minimum ages are younger, ~240 and ~360 ka. The horizontal samples KUN03, KUN05 and KUN07 show consistently younger minimum $^{10}$Be ages than the vertical samples (~320-370 ka) and $^{26}$Al minimum ages in a similar range (~170-360 ka). The horizontal KUN02 ($^{10}$Be: ~150 ka; $^{26}$Al: ~80 ka) and vertical KUN06 ($^{10}$Be: ~90 ka; $^{26}$Al: ~70 ka) samples show much younger minimum ages compared to the other Kundabikwa samples. The Lumangwe Waterfall samples LUM02 and LUM03 yielded minimum $^{10}$Be ages of ~230 and ~200 ka, respectively, and minimum $^{26}$Al ages of ~180 and ~190 ka. One vertical sample from Ntumbachushi Waterfall (NTU01) yielded a very young minimum $^{10}$Be and $^{26}$Al mean age of ~20 ka. The $^{10}$Be minimum age of the horizontal sample NTU02 is similar to those derived from the horizontal surface proximal to the Kundabwika Waterfalls (~380 ka) while its $^{26}$Al age (~340 ka) is slightly younger. NTU03, which was derived from a vertical surface, returns much younger $^{10}$Be and $^{26}$Al minimum ages of ~110 and ~100 ka, respectively. The samples MUM01 (vertical) and MUM04 (horizontal) from the top cascade of the Mumbuluma I Waterfalls yield minimum $^{10}$Be ages of ~70 and ~110 ka, respectively, while $^{26}$Al minimum ages are slightly younger (~60 and ~90 ka). The horizontally positioned sample MUM02 shows minimum ages of $^{10}$Be (~270 ka) and $^{26}$Al (~240 ka) which are older than for the vertical sample MUM03 (~110 and ~100 ka, respectively).

##### *4.1.1.2. Group B*

For the single sample collected from Lupupa Waterfall, the minimum $^{10}$Be and $^{26}$Al ages are in excellent agreement at a mean of 42.4±1.1 ka. The Mumbuluma II Waterfall sample LUO01 yields a minimum $^{10}$Be and $^{26}$Al mean age of 76.8±2.2 ka, which is an order of magnitude younger than the exceptionally old minimum mean age of LUO02 of 833±17 ka. Sample LUZ01, taken within a narrow river gorge of the Lunzua River, shows a minimum $^{10}$Be and $^{26}$Al mean age of 524±12 ka. LUZ02 was collected only about 2.4 m below the top surface and yields a mean age of 102.2±2.7 ka.

##### *4.1.1.3. Group C*

Sample MWE01 yielded minimum $^{10}$Be and $^{26}$Al ages which are in agreement at 7.79±0.60 ka. Samples ME04 and ME05 return minimum $^{10}$Be and $^{26}$Al mean ages of 12.29±0.81 ka and 11.56±0.72 ka, respectively, while ME06 and ME09 yielded minimum $^{10}$Be and $^{26}$Al mean ages of 42.8±1.6 and 45.7±2.0 ka, respectively.

#### *4.1.2. Maximum denudation rates*

For several samples that derive from Groups B and C, maximum denudation rates are also reported (Table 3). Samples from the eastern part of the Kundelungu Plateau yield maximum denudation rates ranging from ~15 to ~40 mm ka$^{-1}$ (samples MWE01, ME04, ME05, ME06 and ME09), while denudation rates associated with the Mporokoso Plateau are much lower and range from ~0.4 to ~6 mm ka$^{-1}$ (samples LUO01, LUO02, LUZ01 and LUZ02). Even though the denudation rates reported in this study are local ones, they indicate general differences in denudation history of both studied plateaus.

## 4.2. Tectonic Analysis

### 4.2.1. Fault kinematics and scaling relationships

We mapped 63 lineaments that we interpreted to represent the surface expressions of active normal faulting at depth (Fig. 1; Appendix Table A2). Fifty-three faults are located within the MMFS, while ten are located within the Mpulungu basin (southern Lake Tanganyika). The faults in the southern MMFS strike NE-SW while the northeast section of the fault system swings its strike clockwise to an ENE-WSW orientation (Table A2), intersecting, at high angles (~90°), the NW to SW trending normal faults around Lake Tanganyika. Fault lengths (L) in our dataset range from 12 km to 168 km, whereas maximum vertical fault displacements (D) range from 10 m to 700 m (Fig. 3A). Fault displacement rates (DR) are typically low, ranging from 0.004 mm $a^{-1}$ to 0.27 mm $a^{-1}$ (Fig. 3C). This, in turn, corresponds to an average earthquake recurrence for the faults in the MMFS of ~120 ka (Table A2). In order to understand the impact of normal faulting on the formation of the past and current landscape proximal to Lake Mweru, we explore the D-L relationship on the 53 normal faults in the MMFS (Table A2).

The D-L relation may provide important information on the growth and scaling properties of faults (Fig. 3; Walsh and Watterson, 1988; Bilham and Bodin, 1992; Cowie and Scholz, 1992; Schlische et al., 1996; Kim and Sanderson, 2005; Schultz et al., 2008; Nicol et al., 2010, 2020a). The graphs in Figures 3A and 3C indicate a positive D-L and DR-L relationship for the faults in the MMFS, suggesting that larger faults have accommodated more displacement and have moved faster than smaller faults (Nicol et al., 1997, 2005). Similar graphs, which indicate positive relationships between fault displacements/displacement rates and length, have been recorded on several other active and inactive fault systems globally (Kim and Sanderson, 2005; Mouslopoulou et al., 2009; Nicol et al., 2020a, b). Despite the overall positive D-L trend for most fault systems globally, the D values at a given L value and the slope of the best-fit line in these graphs may vary between fault systems (but also between different sampling periods in the same fault system), with the slope typically ranging from 0.5 to 1.5 (Schlische et al., 1996; Walsh et al., 2002; Kim and Sanderson, 2005; Nicol et al., 2010; Torabi and Berg, 2011, Nicol et al., 2020b). This variability in the D-L scaling may be due to biases arising from the time-window of observation, the age of the faulted horizons, the strain accommodated by each fault system, the mechanical properties of the faulted rocks and/or the degree of fault interactions (Watterson et al., 1996; Bailey et al., 2005; Mouslopoulou et al., 2009; Nicol et al., 2010; Rotevatn et al., 2019).

To better understand the growth of the faults in the MMFS with respect to other fault systems globally, we have plotted their D-L trend against a global dataset of inactive normal faults (Fig. 3D; Nicol et al., 2016c and references therein). Comparison shows that the faults in the MMFS plot in agreement with the global dataset occupying, however, the lower part of the global population (slopes of ~0.92 vs. ~0.99, respectively; Fig. 3D). To explore further the growth of the faults in Africa, we have also plotted in Figure 3D the single-event displacement rupture lengths from a global compilation of historic normal fault earthquakes (Wesnousky, 2008). As expected, single earthquakes clearly plot below the average trend of the global dataset (including the MMFS), their slope is significantly less than 1 (~0.3) and their scatter greater than that of the global dataset ($R^2$ values of 0.25 vs. 0.85; Fig. 3D). These features collectively suggest that each fault in the MMFS has accommodated numerous earthquakes, the number of which scales with fault length.

The approximate number of earthquakes accommodated by each fault in the MMFS, together with their earthquake magnitude and recurrence interval, has been calculated using Wesnousky's (2008) scaling relationships (Table A2). First, we calculate the single event displacement (SED) for each fault in the MMFS from the fault length (L) and subsequently the earthquake recurrence interval on each fault (Table A2). The recurrence interval is subsequently used, in conjunction with the 2.6 Ma displacement rate (time-period that rifting is thought to have initiated), to estimate the number of earthquakes accommodated by each fault (Table A2 and Fig. A2). We find that the faults in the MMFS are likely to have accommodated ~2,000 ground-rupturing earthquakes since the rift's onset (~35 events per fault), with earthquake magnitudes ranging from M6.7 to M7.2 (Table A2 and Figure A2).

### *4.2.2. Faulted topography*

To explore the relationship between the faulted topography, the available TCN ages and the current extents of Lakes Mweru and Mweru Wantipa, we generated five rift-perpendicular topographic profiles (Fig. 4) and one rift-parallel profile (Fig. 5). The profiles 1-3, across the southern MMFS and the modern Lake Mweru, reveal a strongly asymmetric rift (Fig. 4A-C). To characterize the distribution of strain along the rift, we have calculated the cumulative throw across the five profiles illustrated in Figure 4. Furthermore, to better visualize the landscape when rifting in the area was about to commence, we subtracted from the identified faults the throw measured along the topographic profiles 1-8 (Fig. 6), that is the displacement accrued on each fault since the initiation of faulting at 2.6 Ma.

Our analysis shows a three-fold increase in the cumulative throw, trending northeastwards along the rift (from ~800 m across profile 1 to ~2180 m across profile 5), with the southeast dipping faults having accommodated almost twice as much displacement (4550 m) compared to the northwest dipping faults (2690 m; Fig. 4). The dominance of the southeast dipping faults is persistent along the entire length of the MMFS, where these faults appear to have locally (e.g., see profile 5) accommodated up to 4 times more throw compared to the northwest dipping faults. The northeastward increase in extension, which is manifested by the greater number of active faults and the more confined rift axis, is not surprising as the MMFS at its northernmost extension approaches (and intersects) the fast spreading (~1 mm $a^{-1}$) EARS (Fig. 1; Fernandes et al., 2004: Calais et al., 2006; Omenda et al., 2016).

Topographic analysis suggests that the faults which are largely responsible for the formation of the modern landscape within the MMFS are faults 8, 9, 16, 17, 23 and 28 in the south, and faults 38, 40, 46 and 48 in the north. The profile along Lake Mweru (profile 6 in Fig. 5) reveals a shallow topographic basin (within <100 m from the modern lake) which is bounded at its northern side by the Kundelungu Plateau and to the south by steep hilly country formed by sediments of the Luapula River's delta (Fig. 4A). Profile 7 runs along Lake Mweru Wantipa and displays the high topographic relief between the Mporokoso Plateau and the Mpulungu basin, while profile 8 reveals the impact of normal faulting on the landscape associated with the Kundelungu Plateau (Fig. 6). These profiles are discussed in detail in Section 6.

### 4.3. *Geomorphic Analysis*

We identified a total of 61 river knickpoints from individual stream profiles that corroborate the paleo-shoreline observation (Fig. 7A). In a second step, we analyzed the hypsometry of the Lake Mweru catchment to delineate the impact of paleo-lake Mweru on the elevation distribution. The hypsometric curve of the catchment (Fig. 7B, blue and black lines) reveals large areas characterized by gentle slopes, which we interpret to correspond to areas confining the paleo-lake Mweru. They all lie at elevations between 920-930 m asl, 990-1100 m asl and 1170-1190 m asl, which align with the sampled waterfalls at 1050 and 1160 m asl. We observe additional areas with low slopes at varying elevations, but focus our analyses on the most prominent elevations. We have furthermore excluded slope angles above 3° to better show terrain associated with lake-erosion processes (Fig. 7B, blue line). In the same elevation framework, we plot the number of knickpoints observed at a specific elevation. Knickpoints cluster at specific elevations and delineate the remnant paleo-shorelines in a more refined spatial pattern, indicating three abandoned shorelines at elevations of ~925 m asl, ~1000 m asl and ~1180 m asl, respectively (Fig. 7B).

# 5. Reconstructed Scenarios for the Principal Sets of TCN Results

Overall, our TCN samples record a pattern of temporary burial over parts of the region studied. As discussed earlier (Section 1), stratigraphic evidence suggests that during the Pleistocene the study area hosted an enlarged lake, approximately 130 km wide and 300 km long (~40,000 km$^2$), centered around the (much smaller) present-day Lake Mweru (~5000 km$^2$). TCN production is completely blocked (except for some minor production by muons) when a surface is ≥10 m below the lake level. Therefore, interpreting the Plio–Pleistocene tectonic history of south-central Africa, we suggest that the burial patterns recorded by our samples most likely reflect the existence of a paleo-lake that inundated a much larger depocenter.

## *5.1. <u>Group A</u>*

Most of the samples from Group A indicate burial (Fig. 1; Fig. 8). A few significant age discrepancies arising from samples collected from a single waterfall are also evident. The fact that all waterfalls in Group A are located within the MMFS and at elevations <1200 m asl (that is, significantly lower than Group B samples which are all located >1200 m asl) indicates that faulting and uplift may have played an important role in the burial of the landscape. Below we discuss separately the likely exposure scenarios for each waterfall in Group A.

### *5.1.1. Kundabikwa Waterfalls*

Samples from the Kundabikwa Waterfalls indicate burial over a continuous period for at least 250 ka (Fig. 8A). The significantly younger minimum exposure ages (Section 4.1.1.) of samples KUN02 and KUN06 probably indicate enhanced surface denudation or rockfalls/landslides (e.g. mechanical failure of exposed rock outcrop leading to fresh exposure). In addition, two of the three pairs of samples (KUN01/KUN02 and KUN03/KUN04) indicate older $^{10}$Be and $^{26}$Al minimum ages (Table 2) for the vertical face compared to the top horizontal surface. The fact that the top horizontal surface (KUN02, KUN03 and KUN05) of the area is younger than the vertical sections (KUN01, KUN04) is intriguing and requires further examination.

Based on the relative $^{10}Be$ and $^{26}Al$ minimum age estimates, we reconstruct the complex exposure-burial history of Kundabikwa Waterfalls and paleo-lake Mweru over six sequential stages (Fig. 9). The pre-lake stage (T1) represents the initial state of the river. In order to record a burial signal, the studied surfaces must have been exposed prior to burial. Thus, the knickpoint must have already existed during stage T1. The vertical faces of the banks are gradually exposed through sequential knickpoint retreat. During this stage, channel denudation dominates. The denudation rate is relatively low on the top-horizontal surface. Most geomorphologic characteristics from this stage are assumed to have been erased by today. The second stage (T2) is defined by the onset of the lake-level rise (flooding). Water starts to cover the vertical riverbanks. Denudation decreases as the base-level increases, leading to slower knickpoint migration. Denudation is minimal (but probably not zero) as the top horizontal surfaces are flooded and lake sedimentation initiates. During T3, the lake reaches its greatest depth. Water and sediments now shield the sampled surfaces from cosmic ray irradiation, entirely blocking $^{10}Be$ and $^{26}Al$ production. Lacustrine sedimentation occurs mostly on the horizontal surfaces. The lake-level is now the base-level, resulting in the interruption of denudation.

Denudation recommences with the onset of lake drainage and associated drop of the water-level (stage T4). Localized denudation occurs on the sediment-covered horizontal surfaces while the vertical faces remain under water, with TCN production still being absent for all submerged areas. Consequent to paleo-lake outflow (T5) via the Luvua River, regional denudation of the sediments that blanket the horizontal surfaces occurs. This period of new equilibrium may have been characterized by low energy environments, which can be described, for example, as a changing complex of small wetlands, oxbow lakes and meandering channel systems, similar to the current situation in the upper reaches of present-day Lake Mweru.

Lacustrine sediments are now confined to the top horizontal banks, as in the channel the sediments are eroded. The subsequent lowering of base level as the lake drains sees the rejuvenation of the waterfalls. In the last stage (T6), most of the lacustrine sediments have been removed from all surfaces and the top horizontal surfaces are re-exposed and TCN production resumes. Back- and downwearing of the vertical bank faces leads to further denudation of the bedrock surfaces. We note that gradual rising and lowering of the lake's water-level between stages T2 and T4 should have lasted thousands or even tens of thousands of years in order to induce a detectable difference between the cosmogenic nuclide concentrations of different (horizontal vs. vertical) sampled surfaces. Indeed, previous studies of other paleo-lakes have revealed long-term lake fluctuations spanning time-intervals from 2 to >20 ka (Masters et al., 1991; Gamrod, 2009; Shuman et al., 2009; Trauth et al., 2010).

### *5.1.2. Lumangwe Waterfall*

According to Figure 8B, sample LUM03 does not show an unequivocal burial signal, in contrast to LUM02 that clearly underwent a complex exposure history. One possible explanation is that LUM02 (1150 m asl) was covered by lake water, while LUM03 (1159 m asl) was not (or it was only slightly covered so the cosmogenic nuclide production did not stop completely). Such a scenario implies that the Lumangwe cascades marked the eastern shore of the paleo-lake. Another possibility is that the LUM02 rock face was covered by a recent landslide or rockfall. However, no physical evidence of such an event can be found, suggesting that if it did occur, the Kalungwishi River has subsequently removed any such debris. A minimum burial time of 300 ka is estimated for LUM02 (Fig. 8B).

### *5.1.3. Ntumbachushi Waterfalls*

Samples NTU01 and NTU02 do not indicate a clear burial signal. The weathered profile of the NTU01 surface and the very young minimum $^{10}$Be and $^{26}$Al mean age (~20 ka) most likely indicate a recent rockfall. Although NTU03 does indicate burial of ~400 ka (Fig. 8C), this age is questionable due to the young minimum $^{10}$Be and $^{26}$Al ages (~100 and ~80 ka, respectively) that derive from the same sample and which, coupled with the highly weathered and fractured nature of the sampled surface, make it unlikely to record an ancient pre-lake stage.

#### *5.1.4. Mumbuluma I Waterfalls (Mumbuluma River)*

All results from the Mumbuluma I falls indicate a clear burial signal at 1σ confidence level, though not at 2σ (Fig. 8D). The top cascade yields younger minimum $^{10}$Be ages (MUM01, MUM04) than the second cascade downstream (MUM02, MUM03), suggesting that the lower waterfall formed before the top one. Also, the top horizontal surface (MUM04; minimum $^{10}$Be age 113 ka) seems to have undergone more intense denudation than the lower surface (MUM02; 271 ka). A rockfall may explain the young minimum $^{10}$Be age of the vertical sample MUM01 (~70 ka). The approximate minimum burial time of the area is ~350 ka (Fig. 8D), an age which is in good agreement with the duration of burial recorded at the Lumangwe falls.

### *5.2. <u>Group B</u>*

Samples in Group B date waterfalls which are situated outside the MMFS (Fig. 1). $^{10}$Be and $^{26}$Al minimum ages are in good agreement for most samples, indicating that these surfaces have not been buried since their initial exposure (Fig. 10). Thus, it appears that these locations were not flooded by the paleo-lake. Minimum exposure ages and maximum denudation rates within this group are discussed below.

#### *5.2.1. Lupupa Waterfall*

LUP01 shows very young minimum $^{10}$Be and $^{26}$Al ages, which probably do not reflect the actual age of the waterfall but a rockfall event. For such recent events, no burial signal is expected (Fig. 10A).

### 5.2.2. *Mumbuluma II Waterfall (Luongo River)*

Both samples from the Luongo's Mumbuluma II Waterfall are from sub-vertical (45°-50°) surfaces and show no clear $^{10}$Be-$^{26}$Al burial signal (Fig. 10B). This cascade was formed on a bedrock contact between quartzites and sandstones. The development of the cascade is clearly controlled by differential denudation between the overlying softer sandstone and the harder quartzite. Maximum denudation rates of ~6 mm ka$^{-1}$ for the sandstone (LUO01) and of ~0.4 mm ka$^{-1}$ for the quartzite (LUO02) are calculated (Table 3). The large difference in the denudation rates of the two lithologies further highlights the role of differential denudation in the formation of this cascade. Sample LUO02 plots exactly on the no denudation line in Figure 5b, indicating a minimum $^{10}$Be and $^{26}$Al mean exposure age of 833±17 ka. This age, which is the oldest recorded minimum exposure age among the studied waterfalls, indicates a very old formation age of the Mumbuluma II knickpoint. It is worth mentioning that this is an exceptionally old age for an inclined surface located within the zone of an actively incising river channel.

### 5.2.3. *Lunzua Waterfalls*

Both samples from Lunzua Waterfalls show no $^{10}$Be-$^{26}$Al burial signal (Fig. 10C). LUZ01 yields a very old minimum age for a vertical surface, which indicates that it was constantly exposed since at least 524±12 ka. In terms of a steady denudation rate, this age would correspond to a local rate of receding of the rock face (in horizontal direction) of ~0.4 mm ka$^{-1}$. LUZ02 yields a much younger minimum $^{10}$Be and $^{26}$Al mean age (102.2±2.7 ka). It is unclear whether the age difference between the two samples reflects the retreat of the waterfall or is just due to more intense denudation near the top.

## 5.3. <u>*Group C*</u>

Samples from the northwest side of Lake Mweru (Group C) were located at lower elevations than those from groups A and B and their minimum $^{10}$Be and $^{26}$Al ages are distinctly younger and more comparable to one another (Table 2). The sample that derives from a vertical surface of the fault no. 16 (MWE01; Fig. 1) implies a fast but steady denudation rate of ~40 mm ka$^{-1}$ (Table 3) or a rockfall on the fault surface <10 ka ago. Additionally, two further samples (ME04, ME05) from vertical sections along the Luvua River show rather young minimum $^{10}$Be and $^{26}$Al mean ages (12.29±0.81 and 11.56±0.72 ka, respectively). As the paleo-lake Mweru was drained via the Luvua River, during the Pleistocene (Cotterill and de Wit, 2011), it is possible that these young ages reflect rockfall events or steady and fast incision, but obviously they do not represent the age of paleo-lake drainage. Fast denudation of the northeastern section of the Kundelungu Plateau is further supported by two samples which were collected from horizontal surfaces along the Misefwe and Lwilwa rivers (ME06 and ME09; Fig. 1), yielding maximum $^{10}$Be denudation rates of ~16 mm ka$^{-1}$ (Table 3). In summary, Group C samples show no $^{10}$Be-$^{26}$Al burial signals and relatively young minimum ages due to recent rockfalls and/or fast eroding surfaces (Fig. 11; Tables 2, 3). However, these young ages do not contradict the assumed extension of the paleo-lake Mweru over this section of the Kundelungu Plateau. Rather, they suggest that pre paleo-lake surfaces have not been preserved due to faster denudation. Such rates could be related to a potential uplifting caused by the activity of fault no. 16 (Fig. 1). Further investigation of this activity is required.

# 6. Discussion

Our results explore the landscape evolution of the Mweru rift system, the southwest extension of the EARS, since the late Neogene. The establishment of paleo-lake Mweru initiated a new drainage network feeding the paleo-lake until the penultimate capture of this depocenter by an Upper Congo headwater. Here we discuss the implications of these new insights with respect to the southward and westward propagation of rifting.

### 6.1. *Onset of Active Faulting and the Formation of the Paleo-Lake Mweru*

Rifting in the study area is thought to have commenced by at least ~2.6 Ma (Tiercelin and Lezzar, 2002; Decrée et al., 2010; Molnar et al., 2019; Daly et al., 2020). Overall, analysis of the faulted topography within the MMFS reveals that individual faults have played a pivotal role in forming the two depressions that host the Lakes Mweru and Mweru Wantipa. Active faulting and associated footwall uplift are also responsible for the wide ridge that extends today between the two lakes (Fig. 1). The landscape reconstruction through subtraction of the 2.6 Ma fault throws (Fig. 6) displays a mild relief across the extended area of the MMFS, revealing that the landscape was similar to the flat East African erosion surface. During the early Pleistocene, the average topographic altitude was formerly higher, though it is possible that the relative height difference between the Kundelungu and Mporokoso Plateaus has not changed significantly since the onset of rifting. A low energy environment, such as a shallow wetland, and associated meandering rivers probably extended over this landscape, which was related to the extensive and relatively long-lived paleo-Chambeshi drainage system (Cotterill, 2005).

The southern part of the MMFS (profiles 1 and 6; Fig. 6A, 6F) hosts deltaic deposits associated with the Luapula River (Fig. 1). The primary faults that bound the depression that hosts Lake Mweru today to the west are (from south to north) faults 8, 9, 10 and 16 (Fig. 1). The total throw on these southeast dipping faults is ~640 m as opposed to the 200 m of cumulative throw recorded on the northwest dipping faults (i.e., 23 and 28) that bound this depression to the southeast. This geometry reveals a highly asymmetric rift tilted to the southeast. Profiles in Figure 6A and 6F suggest that faults 8 and 23 contributed drastically to the lowering of the landscape between the two horsts by a total throw of ~700 m. During the early Pleistocene, the southern part of the Mporokoso Plateau was about 250 m lower than the Kundelungu Plateau. It is known that during this period, the Luapula River captured the paleo-Chambeshi River, which led to the present-day linkage between the Bangweulu and Mweru lakes (Cotterill, 2003, 2005). This interpretation, which is not described by the tectonic analysis presented here, suggests that the proto-Luapula River was flowing southward towards Lake Bangweulu (as suggested previously; Cotterill, 2005, 2006; Cotterill and de Wit, 2011; Moore et al., 2012). The onset of tectonic activity, together with the southward knickpoint retreat of the proto-Luapula River, may have contributed to the separation of the previously topographically connected Mporokoso and Kundelungu Plateaus.

Moving northwards, to profiles 2 and 6 (Figs. 6B, 6F), the elevation difference between the two shoulders of the rift is more distinct. The southeast dipping faults of the Kundelungu Plateau sum a total throw of almost 800 m, while faults along the Mporokoso Plateau have a total throw of ~300 m. It appears that the Mporokoso Plateau stood around 1400-1500 m asl during the late Pliocene. The basement of the lake was clearly higher than today, standing at ~1000 m asl, while the Kundelungu Plateau maintained its high elevation at ~1700 m asl. Faults 9, 16, 23, 24, 28 and 32 were the main contributors of downfaulting. In this area, the wetland was deeper (Kilwa Island did not exist) and the clastic bedrock was the main dominant rock type of the wetland's bottom. According to profiles 3 and 6 (Figs. 6C, 6F), the local average altitude of the landscape was lower, reaching the highest point of ~1350 m asl on the Kundelungu Plateau. The maximum altitude of the Mporokoso Plateau was ~1250 m asl, minimizing the elevational difference between the two shoulders of the rift. The total throw of the southeast dipping faults is ~500 m, while the northwest dipping faults' total displacement is 400 m, creating an almost symmetric section in a generally asymmetric structure. Considering Figure 6C, the reconstructed landscape during the early Pleistocene had a relatively low relief. Both these plateaus seem to have had an approximately similar local height (~1400 m asl), and the lowest point was probably close to the present-day location of the Kundabwika Waterfalls, which was controlled by Fault 44.

Cotterill (2006) discussed the possibility that part of the Kalungwishi River, today flowing north, was redirected from the south, as the Kalungwishi River was formerly a major headwater of the proto-Luongo River (Fig. 1). Geobiological estimates of evolutionary events can be applied from the genomic record of extant fishes. These estimates of speciation events confer an independent chronology of these drainage links (Cotterill and de Wit, 2011). A pertinent example is the Early Pleistocene speciation of a killifish, *Nothobranchius ostergaardi*, confined within the eastern Mweru Wantipa basin; this species diverged from 0.46 to 1.11 Ma from its closest living relatives, which today occur south of the Congo-Zambezi watershed (van der Merwe et al., 2021). Their origin is attributed to the breakup of the paleo-Chambeshi River, and this event overlaps with independent pulses of fish speciation within the Mweru graben, as well as TCN dates constraining the tenure of paleo-lake Mweru. The onset of the MMFS (deepening of the paleo-lake Mweru) then disrupted the paleo-drainage of the Luongo-Kalungwishi system, contributing gradually to its disconnection from the paleo-Chambeshi drainage (Cotterill, 2006; Cotterill and de Wit, 2011).

Compared to Lake Mweru (917 m asl), Lake Mweru Wantipa stands at a higher elevation (932 m asl), and it is characterized by a high relief landscape. According to profiles 4 and 5 (Fig. 4), the total throw of the southeast dipping faults along the Kundelungu Plateau reaches up to 1720 m, while the northeast dipping faults have a maximum total throw of 460 m. Despite the approximately four-fold difference of the throw measured on the southeast and northwest faults, the rift here does not appear to be strongly asymmetric. This can be rationalized if we consider that the former faults are distributed across a distance of ~140 km whereas the latter ones span only 10 km across the rift's shoulder. From a geomorphological perspective, the Mweru Wantipa depression hosts the seismically most active structures of the Southwestern Extension of the EARS (Daly et al., 2020). This is also supported by the DEM fault analysis that suggests a denser fault network of fresh discontinuous traces between the Lakes Mweru

Wantipa and Tanganyika. The extended landscape around the modern Lake Mweru Wantipa during the early Pleistocene was also characterized by high relief, while the base of the wetland was standing at ~1150 m asl (Fig. 6D). The Kundelungu Plateau was standing at a maximum altitude of > 2000 m asl, while the Mporokoso Plateau had a maximum elevation of ~1900 m asl (Fig. 6E). The modern lowlands (cross hatching in the east in Fig. 12) on the borders between Lake Mweru Wantipa and the Mpulungu basin have currently an average elevation <1200 m asl. During the Pleistocene (Fig. 6G), the elevation was just ~50 m higher, with the lowest point ~1200 m asl. However, this elevation difference was sufficient to prevent the merging of paleo-lake Mweru and paleo-lake Tanganyika and suggests that these lakes have never been linked.

The western margin of the paleo-lake was defined by the long and high Kundelungu Plateau. The depression (cross hatching in the west in Fig. 12) that separates the main part of the plateau from its eastern continuity did not exist during the Pleistocene. Based on Figure 6H, the two parts of the plateau were connected, and the average elevation of the linking crest was ~1400 m. Faults 16a and 17 downfaulted the intervening landscape by ~200 m, resulting in the separation of the southwestern and northeastern sections of the Kundelungu Plateau. There is no evidence of a sudden tectonic event that created this depression, so we assume that it was dominated by gradual lowering of the landscape due to normal faulting and denudation activity across the Kundelungu Plateau, as implied also by the TCN data.

Interestingly, the transition from Pliocene to Pleistocene (2.6 Ma) is characterized by a major climatic change in the southern hemisphere, from warm and humid conditions to aridification until 1.8 Ma, which is invoked as a driver of contraction and expansion of the lakes (Cohen et al., 1997). The lakes that were already flooded since ~3.6 Ma experienced contractions around 1.1 Ma (Cohen et al., 1997). Lavayssiere et al. (2019) reported that Lake Tanganyika dried down to the point it was divided into three contracted paleo-lakes, limited within the sub basins of the rift, which possibly caused fish speciation. The lake levels were restored gradually until 550 ka, while fluctuations in levels occurred, possibly linked to alterations in Pleistocene paleoclimates (Cohen et al., 1997; Trauth et al., 2005, 2010; Lavayssiere et al., 2019). Indeed, TCN dating suggests water level fluctuations across the paleo-lake Mweru during the Pleistocene (Section 5.1.1.), which attests to complex interactions between past climates and tectonics.

### *6.2. The Drainage of Paleo-Lake Mweru*

At Kundabikwa Waterfalls, three samples (KUN01, 02, 03) yield burial ages of ~1 Ma (Fig. 8A). The minimum burial ages of the other four samples (KUN04, 05, 06, 07) are lower (~500 ka). This may be explained by a higher contribution of post-burial production, which shifts data points in the two-nuclide plot (Fig. 8A) from the burial area towards the steady-state field again. Therefore, it is the oldest burial age among all samples that provides a minimum estimate for the time the Kundabikwa Waterfalls have been covered, i.e. >1 Ma. Indeed, it is possible that the paleo-lake Mweru existed much longer than that. If the lake (including the various lake fluctuations) actually lasted more than ~2 Ma, essentially all $^{26}$Al present in a sample today would have been produced after the drainage of the paleo-lake (as the half-life of $^{26}$Al is 705 ka and after three half-lives almost 90% will have decayed; Norris et al., 1983). Under such an assumption, the highest minimum $^{26}$Al age of all samples showing burial would provide a time constraint for when the paleo-lake was drained to a level below the elevation of the waterfalls. Sample KUN04 of the Kundabikwa Waterfalls records the highest $^{26}$Al minimum age among all samples that indicate burial, constraining the timing of lake drainage to ~350 ka (i.e. middle Pleistocene). Variable denudation and tectonic rates within the study area can explain the observed variations in minimum ages between different locations. Nevertheless, all samples from Group A are consistent with an inferred lake drainage at ~200-400 ka, with age differences most likely representing lake level fluctuations.

The reconstruction of key features that formed the landscape at ~350 ka is required to determine potential waterways allowing for the drainage, and consequent lowering, of the paleo-lake. To achieve this, we calculated, assuming constant displacement rates over these timescales (Mouslopoulou et al. 2009), the throw accrued on each fault since 350 ka and we subsequently subtracted it from its total displacement (Table A2). The modified faulted topography is assessed via profiles 1-8 (cross sections in Fig. 1), the results of which are illustrated in Figure A5 in the Appendix. The restored topography at 350 ka reveals minor, albeit crucial, readjustments that appear to have impacted on the size of the paleo-lake. According to the profiles in Figure 4, faults 8, 9 and 16 are the largest displacement faults that formed the asymmetrical half-graben structure that hosted the paleo-lake. Faults 16a and 17 also contributed to the formation of the depression west of present-day Lake Mweru and across the Kundelungu Plateau (Fig. A5c). This depression might have played a key role in the lowering of the paleo-lake's water level as it aided its tapping to the west (Fig. 12). Faster denudation rates in the north (~40 mm $ka^{-1}$; Group C) compared to the south (~6 mm $ka^{-1}$; Groups A, B) were forced by footwall uplift across Fault 16, resulting in fast incision along the northward flowing Luvua River (Fig. 1).

Dramatic lake level fluctuations have been reported throughout the late Pleistocene (14-450 ka) across Lake Tanganyika, Lake Malawi and the southwest extension of the EARS, which are related to tectonic factors and/or aridification periods (Danley et al., 2012; Ivory et al., 2016). From 450 to 350 ka, a regional lowering of the temperature and global sea level is directly correlated with the low stand of the lake levels across the Western Branch (Bakker and Mercer, 1986). In addition, a major dry period across the Congo basin occurred between ~270 and 180 ka, resulting in an additional lowering of the water level (Gasse et al., 1989). The evidence for the drainage of paleo-lake Mweru based on $^{10}Be$ and $^{26}Al$ data, together with tectonic analyses and the evidence for intensive climatic variation during the Pleistocene, indicate a gradual shrinking of the paleo-lake rather than a sudden tectonic event. The outflow of the paleo-lake through the Luvua River was most likely one of the main events that drained the lake (Dixey, 1944; Bos et al., 2006; Goodier et al., 2011; Cotterill and de Wit, 2011; Fig. 1). However, evaporation, especially in arid periods, may have further accelerated contraction of the paleo-lake, notably across the vast, shallow depression located between the two sections of the Kundelungu Plateau (Fig. 12).

### *6.3. Paleo-Lake Mweru During the Late Neogene-Quaternary*

Assuming that the paleo-lake Mweru existed for a minimum of ~2 Ma, the burial ages constrain its formation to the late Pliocene-early Pleistocene. This assumption is supported by the high species endemism of the extant fish fauna of Lake Mweru (Cotterill, 2005; Meier et al., 2019). More specifically, recent molecular clock analyses have estimated respective timings of origin of several radiations of endemic fish clades (Family Cichlidae) confined within Lake Mweru. Four of these clades have evolved diverse species flocks, whose origins are estimated at 270–350, 430–560, 270–940, and 720–940 ka, constrained by a molecular clock calibrated for the Cichlidae (Meier et al., 2019). Thus, depending on the applied calibration scheme, the mean genetic divergence of the most common recent ancestors provides a date of 0.27-1.04 Ma and their actual speciation dates (i.e. timing of completed lineage divergence) was likely more recent (Meier et al., 2019). The second line of geobiotic evidence comprises the "Mweru Complex" of killifishes, genus *Nothobranchius*. The timing of radiation of its seven species is significant, because their ecology confines them within the floodplains that formed after the shrinkage of the larger lake. The independently constrained molecular clock of *Nothobranchius* estimates the origin of this complex between 0.48 and 1.01 Ma (van der Merwe et al., 2021).

Our data inform a schematic map that estimates the maximum size of the paleo-lake Mweru through the Pleistocene (Fig. 12). The maximum lake level is constrained via TCN dating at 1200 m asl, while the minimum level should be the elevation of the Kundabikwa Waterfalls

(~1050 m asl). The estimate of a 1200 m asl lake level is supported by the hypsometric and knickpoint analysis (~1180 m asl). The Lumangwe and Ntumbachushi Waterfalls are assumed to represent the eastern shorelines of this paleo-lake. This inference is confirmed by the heights of the dominant knickpoints at the same elevation mapped throughout the catchment (Fig. 7). The southern border of the paleo-lake likely coincided closely with the Mumbuluma I waterfalls which, together with preliminary molecular phylogenetic analyses (Cotterill, 2004, 2005), suggest that the southern section of the Kundelungu Plateau was connected with the Mporokoso Plateau during the Pliocene (and prior to the formation of the Luapula River; Tack et al., 2003; Cotterill and de Wit, 2011; Guillocheau et al., 2015).

Red siltstones from the Kundelungu Plateau are possibly correlated with the upper red beds of the Luapula Beds, implying that the Luapula River eroded the once connected Kundelungu and Mporokoso Plateaus (Abraham, 1959; Thieme, 1971). The western bank of the paleo-lake is defined by the Kundelungu Plateau that rises to ~1700 m asl. Paleo-lake Mweru was likely connected to the Mweru Wantipa wetlands as suggested by the relationships of *Pseudocrenilabrus* (family: Cichlidae) species from these two waterbodies (Egger et al., 2015). However, it appears unlikely that it was linked with the Mpulungu graben of Lake Tanganyika due to the highly distinct fish fauna of these two lakes. This is in agreement with Dixey (1944, 1946), who proposed that the Lakes Mweru and Mweru Wantipa were once connected, a hypothesis re-affirmed by Cotterill and de Wit (2011). Finally, the northern banks are defined by the edge of the extensive plateau between the Mweru Wantipa wetlands and Lake Tanganyika (Fig. 12).

## 7. Conclusions

Terrestrial cosmogenic nuclides results coupled with tectonic and digital topographic analyses reveal the existence of a large paleo-lake Mweru. This paleo lake exceeded the sizes of the present-day Lakes Mweru and Mweru Wantipa. We identified the following evidence for lake size and timing:

As estimated previously, our results indicate the onset of the paleo-lake at around 2.6 Ma. The timing of lake existence is consistent with the phylogenetic molecular clock analyses of endemic fish species, which also constrain the formation of the paleo-lake at the late Pliocene - early Pleistocene. Formation of this lake is correlated with the onset of the Mweru-Mweru Wantipa Fault System in the Early Pleistocene and likely established an estimated maximum shoreline at ~1200 m asl. The extent of the paleo-lake was also identified by river knickpoint and hypsometric analysis to constrain its paleo-shorelines at ~1180 m.

Intense normal faulting and associated footwall uplift at the northwestern paleo-lake boundary must have forced fast river incision in the eastern section of the Kundelungu Plateau. In contrast, two exceptionally old minimum $^{10}$Be and $^{26}$Al exposure ages of 524 and 833 ka were obtained from vertical/sub-vertical surfaces besides active river courses across the Mporokoso Plateau, possibly reflecting the actual exposure ages of these surfaces. These ages illustrate the stability of the plateau, which is also reflected by the low maximum denudation rates (~0.4 to ~6 mm ka$^{-1}$). The deepening/flooding of the paleo-lake, which was probably due to the active extension and associated normal faulting, continued at least until the Middle Pleistocene (~350 ka), resulting in complex exposure histories observed at the knickpoints on the Mporokoso Plateau.

## Acknowledgements

This study is part of the interdisciplinary project “Exploiting the Genomic Record of Living Biota to Reconstruct the Landscape Evolution of South Central Africa” funded by the Volkswagen Foundation (VolkswagenStiftung) [grant number 88732]. Parts of this research were carried out at the Ion Beam Centre (IBC) at the Helmholtz-Zentrum Dresden-Rossendorf e.V., a member of the Helmholtz Association. We would like to thank Enzio Schnabel, Heike Rothe, Sabine Tonn and Hella Wittmann (GFZ Potsdam) as well as Daniel Gorzawski, Antje Musiol, Julia Artel, Milena Wöller and Konstanze Stübner (University of Potsdam) for their help and assistance with laboratory processes and analyses. We would also like to thank Sabrina Beutner (HZDR) for ICP-MS measurements and the DREAMS operator team for their assistance with AMS measurements. The ASTER Team (G. Aumaître, D. Bourlès and K. Keddadouche) is acknowledged for assistance with AMS measurements at CEREGE, Aix-en-Provence. The ASTER AMS national facility is supported by the INSU/CNRS, the ANR through the "Projets thématiques d'excellence" program for the "Equipements d'excellence" ASTER-CEREGE action and IRD. John G. Begg is warmly thanked for discussions associated with active faulting within the MMFS and its impact on the landscape evolution. We are grateful for comments to the manuscript by Ulrich Schliewen and Frederic Schedel (Zoologische Staatssammlung München). We sincerely thank Christian Mwabanua Mutabi and Bauchet Manda (University of Lubumbashi) and Boniface, George and Kelvin for their enthusiastic assistance in the field. Last but not least, we are grateful to the Editor Martin Stokes, to Laura Evenstar and an anonymous reviewer for their constructive comments that improved this manuscript significantly.

# References

Abraham, D. (1959). The stratigraphical and structural relationship of the Kundelungu System, Plateau Series and basement rocks in the Mid-Luapula valley, Northern Rhodesia. D. Phil. Thesis, Univ. Leeds, 152 pp.

Akhmadaliev, S., Heller, R., Hanf, D., Rugel, G. and Merchel, S. (2013). The new 6 MV AMS-facility DREAMS at Dresden. Nuclear Instruments and Methods in Physics Research Section B: Beam Interactions with Materials and Atoms, 294, 5-10. https://doi.org/10.1016/j.nimb.2012.01.053

Arnold, M., Merchel, S., Bourlès, D. L., Braucher, R., Benedetti, L., Finkel, R. C. Aumaître, G., Gottdang, A. and Klein, M. (2010). The French accelerator mass spectrometry facility ASTER: improved performance and developments. Nuclear Instruments and Methods in Physics Research Section B: Beam Interactions with Materials and Atoms, 268(11-12), 1954-1959. https://doi.org/10.1016/j.nimb.2010.02.107

Bailey, W. R., Walsh, J. J. and Manzocchi, T. (2005). Fault populations, strain distribution and basement fault reactivation in the East Pennines Coalfield, UK. Journal of Structural Geology, 27(5), 913-928. https://doi.org/10.1016/j.jsg.2004.10.014

Bakker, E. M. V. Z. and Mercer, J. H. (1986). Major late Cainozoic climatic events and palaeoenvironmental changes in Africa viewed in a worldwide context. Palaeogeography, Palaeoclimatology, Palaeoecology, 56(3-4), 217-235. https://doi.org/10.1016/0031-0182(86)90095-7

Begg, J. G. and Mouslopoulou, V. (2010). Analysis of late Holocene faulting within an active rift using lidar, Taupo Rift, New Zealand. Journal of Volcanology and Geothermal Research, 190(1-2), 152-167. https://doi.org/10.1016/j.jvolgeores.2009.06.001

Bergner, A. G., Strecker, M. R., Trauth, M. H., Deino, A., Gasse, F., Blisniuk, P., and Duehnforth, M. (2009). Tectonic and climatic control on evolution of rift lakes in the Central Kenya Rift, East Africa. Quaternary Science Reviews, 28(25-26), 2804-2816. https://doi.org/10.1016/j.quascirev.2009.07.008

Bilham, R. and Bodin, P. (1992). Fault zone connectivity: Slip rates on faults in the San Francisco Bay area, California. Science, 258(5080), 281-284. https://doi.org/10.1126/science.258.5080.281

Borchers, B., Marrero, S., Balco, G., Caffee, M., Goehring, B., Lifton, N., Nishiizumi, K., Phillips, F., Schaefer, J. and Stone, J. (2016). Geological calibration of spallation production rates in the CRONUS-Earth project. Quaternary Geochronology, 31, 188-198. https://doi.org/10.1016/j.quageo.2015.01.009

Bos, A. R., van Zwieten, P. A. M. and Ngula, E. S. (1995). A limnological survey on Lake Mweru, Zambia. DoF/ML/Report No. 27, Department of Fisheries, Nchelenge, Zambia, 90 pp.

Bos, A. R., Kapasa, C. K. and van Zwieten, P. A. (2006). Update on the bathymetry of Lake Mweru (Zambia), with notes on water level fluctuations. African Journal of Aquatic Science, 31(1), 145-150. https://doi.org/10.2989/16085910609503882

Braile, L. W., Keller, G. R., Wendlandt, R. F., Morgan, P. and Khan, M. A. (2006). The East African rift system. In Developments in Geotectonics (Elsevier), Vol. 25, 213-III. https://doi.org/10.1016/S0419-0254(06)80013-3

Brocklehurst, S. H. (2010). Tectonics and geomorphology. Progress in Physical Geography, 34(3), 357-383. https://doi.org/10.1177/0309133309360632

Brown, E. T., Edmond, J. M., Raisbeck, G. M., Yiou, F., Kurz, M. D. and Brook, E. J. (1991). Examination of surface exposure ages of Antarctic moraines using in situ produced $^{10}$Be and $^{26}$Al. Geochimica et Cosmochimica Acta, 55(8), 2269-2283. https://doi.org/10.1016/0016-7037(91)90103-C

Burrough, S. L. and Thomas, D. S. G. (2008). Late Quaternary lake-level fluctuations in the Mababe Depression: Middle Kalahari palaeolakes and the role of Zambezi inflows. Quaternary Research, 69(3), 388-403. https://doi.org/10.1016/j.yqres.2008.02.003

Calais, E., Ebinger, C., Hartnady, C. and Nocquet, J. M. (2006). Kinematics of the East African Rift from GPS and earthquake slip vector data. Geological Society, London, Special Publications, 259(1), 9-22. https://doi.org/10.1144/GSL.SP.2006.259.01.03

Chorowicz, J. (1989). Transfer and transform fault zones in continental rifts: examples in the Afro-Arabian rift system. Implications of crust breaking. Journal of African Earth Sciences (and the Middle East), 8(2-4), 203-214. https://doi.org/10.1016/S0899-5362(89)80025-9

Chorowicz, J. (2005). The East African rift system. Journal of African Earth Sciences, 43(1-3), 379-410. https://doi.org/10.1016/j.jafrearsci.2005.07.019

Cohen, A. S., Lezzar, K. E., Tiercelin, J. J. and Soreghan, M. (1997). New palaeogeographic and lake-level reconstructions of Lake Tanganyika: implications for tectonic, climatic and biological evolution in a rift lake. Basin research, 9(2), 107-132. https://doi.org/10.1046/j.1365-2117.1997.00038.x

Cohen, A.S., Gergurich, E.L., Kraemer, B.M., McGlue, M.M., McIntyre, P.B., Russell, J.M., Simmons, J.D. and Swarzenski, P.W. (2016). Climate warming reduces fish production and benthic habitat in Lake Tanganyika, one of the most biodiverse freshwater ecosystems. Proceedings of the National Academy of Sciences, 113(34), 9563-9568. https://doi.org/10.1073/pnas.1603237113

Cotterill, F. P. D. (2003). A biogeographic review of tsessebe antelopes *Damaliscus lunatus* (Bovidae: Alcelaphini) in south-Central Africa. Durban Museum Novitates, 28, 45-55.

Cotterill, F. P. D. (2004). Drainage evolution in south-central Africa and vicariant speciation in swamp-dwelling weaver birds and swamp flycatchers. The Honeyguide, 25(1), 7-25.

Cotterill, F. P. D. (2005). The Upemba lechwe, *Kobus anselli*: an antelope new to science emphasizes the conservation importance of Katanga, Democratic Republic of Congo. Journal of Zoology, 265(2), 113-132. https://doi.org/10.1017/S0952836904006193

Cotterill, F. P. (2006). The Evolutionary History and Taxonomy of the *Kobus leche* species complex of south-central Africa in the context of Palaeo-Drainage Dynamics.

Cotterill, F. P. D. and de Wit, M. J. (2011). Geoecodynamics and the Kalahari epeirogeny: linking its genomic record, tree of life and palimpsest into a unified narrative of landscape evolution. South African Journal of Geology, 114(3-4), 489-514. https://doi.org/10.2113/gssajg.114.3-4.489

Cowie, P. A. and Scholz, C. H. (1992). Displacement-length scaling relationship for faults: data synthesis and discussion. Journal of Structural Geology, 14(10), 1149-1156. https://doi.org/10.1016/0191-8141(92)90066-6

Daly, M. C., Green, P., Watts, A. B., Davies, O., Chibesakunda, F. and Walker, R. (2020). Tectonics and Landscape of the Central African Plateau and their Implications for a Propagating Southwestern Rift in Africa. Geochemistry, Geophysics, Geosystems, 21(6), e2019GC008746. https://doi.org/10.1029/2019GC008746

Danley, P. D., Husemann, M., Ding, B., DiPietro, L. M., Beverly, E. J. and Peppe, D. J. (2012). The impact of the geologic history and paleoclimate on the diversification of East African cichlids. International Journal of Evolutionary Biology. https://doi.org/10.1155/2012/574851

De Waele, B. and Fitzsimons, I. C. W. (2007). The nature and timing of Palaeoproterozoic sedimentation at the southeastern margin of the Congo Craton; zircon U–Pb geochronology of plutonic, volcanic and clastic units in northern Zambia. Precambrian Research, 159(1-2), 95-116. https://doi.org/10.1016/j.precamres.2007.06.004

De Waele, B., Fitzsimons, I. C. W., Wingate, M. T. D., Tembo, F., Mapani, B. and Belousova, E. A. (2009). The geochronological framework of the Irumide Belt: a prolonged crustal history along the margin of the Bangweulu Craton. American Journal of Science, 309(2), 132-187. https://doi.org/10.2475/02.2009.03

Decrée, S., Deloule, É., Ruffet, G., Dewaele, S., Mees, F., Marignac, C., Yans, J. and De Putter, T. (2010). Geodynamic and climate controls in the formation of Mio–Pliocene world-class oxidized cobalt and manganese ores in the Katanga province, DR Congo. Mineralium Deposita, 45, 621-629. https://doi.org/10.1007/s00126-010-0305-8

Deffontaines, B. and Chorowicz, J. (1991). Principles of drainage basin analysis from multisource data: application to the structural analysis of the Zaire Basin. Tectonophysics, 194(3), 237-263. https://doi.org/10.1016/0040-1951(91)90263-R

Delvaux, D. (1991). The Karoo to Recent rifting in the western branch of the East-African Rift System: A bibliographical synthesis. Mus. Roy. Afr. Centr., Tervuren (Belg.), Dépt. Géol. Min., Rapp. ann. 1989–1990, 63–83.

Delvaux, D. and Barth, A. (2010). African stress pattern from formal inversion of focal mechanism data. Tectonophysics, 482(1-4), 105-128. https://doi.org/10.1016/j.tecto.2009.05.009

Delvaux, D., Levi, K., Kajara, R. and Sarota, J. (1992). Cenozoic paleostress and kinematic evolution of the Rukwa-North Malawi rift valley (East African rift system). Bulletin des Centres de Recherche Exploration-Production Elf-Aquitaine, 16(2), 383-406.

Dixey, F. (1944). The geomorphology of northern Rhodesia. South African Journal of Geology, 47(Transactions 1944), 9-45.

Dixey, F. (1946). Erosion and tectonics in the East African rift system. Quarterly Journal of the Geological Society, 102(1-4), 339-388. https://doi.org/10.1144/GSL.JGS.1946.102.01-04.16

Dunne, J., Elmore, D. and Muzikar, P. (1999). Scaling factors for the rates of production of cosmogenic nuclides for geometric shielding and attenuation at depth on sloped surfaces. Geomorphology, 27, 3-11. https://doi.org/10.1016/S0169-555X(98)00086-5

Ebinger, C. J. (1989). Tectonic development of the western branch of the East African rift system. Geological Society of America Bulletin, 101(7), 885-903. https://doi.org/10.1130/0016-7606(1989)101<0885:TDOTWB>2.3.CO;2

Egger, B., Klaefiger, Y., Indermaur, A., Koblmüller, S., Theis, A., Egger, S., Näf, T., Van Steenberge, M., Sturmbauer, C., Katongo, C. and Salzburger, W. (2015). Phylogeographic and phenotypic assessment of a basal haplochromine cichlid fish from Lake Chila, Zambia. Hydrobiologia, 748(1), 171-184.

Fernandes, R. M. S., Ambrosius, B. A. C., Noomen, R., Bastos, L., Combrinck, L., Miranda, J. M. and Spakman, W. (2004). Angular velocities of Nubia and Somalia from continuous GPS data: implications on present-day relative kinematics. Earth and Planetary Science Letters, 222(1), 197-208. https://doi.org/10.1016/j.epsl.2004.02.008

Flügel, T. J., Eckardt, F. D. and Cotterill, F. P. (2015). The present day drainage patterns of the Congo river system and their Neogene evolution. In Geology and resource potential of the Congo Basin, 315-337. Springer, Berlin, Heidelberg.

Flügel, T. J., Eckardt, F. D. and Cotterill, W. F. P. (2017). The geomorphology and river longitudinal profiles of the Congo-Kalahari Watershed. The African Neogene-Climate, Environments and People: Palaeoecology of Africa 34, 31-52. DOI: 10.1201/9781315161808-4.

Gamrod, J. L. (2009). Paleolimnological records of environmental change preserved in Paleo-Lake Mababe, northwest Botswana. Doctoral dissertation, Oklahoma State University.

Gasse, F., Stabell, B., Fourtanier, E. and van Iperen, Y. (1989). Freshwater diatom influx in intertropical Atlantic: relationships with continental records from Africa. Quaternary Research, 32(2), 229-243. https://doi.org/10.1016/0033-5894(89)90079-3

Goethals, M.M., Hetzel, R., Niedermann, S., Wittmann, H., Fenton, C.R., Kubik, P.W., Christl, M. and von Blanckenburg, F. (2009). An improved experimental determination of cosmogenic $^{10}$Be/$^{21}$Ne and $^{26}$Al/$^{21}$Ne production ratios in quartz. Earth and Planetary Science Letters, 284(1-2), 187-198. https://doi.org/10.1016/j.epsl.2009.04.027

Goodier, S. A., Cotterill, F. P., O'Ryan, C., Skelton, P. H. and de Wit, M. J. (2011). Cryptic diversity of African tigerfish (Genus *Hydrocynus*) reveals palaeogeographic signatures of linked Neogene geotectonic events. PloS one, 6(12), e28775. https://doi.org/10.1371/journal.pone.0028775

Gosse, J. C. and Phillips, F. M. (2001). Terrestrial in situ cosmogenic nuclides: theory and application. Quaternary Science Reviews, 20(14), 1475-1560. https://doi.org/10.1016/S0277-3791(00)00171-2

Guillocheau, F., Chelalou, R., Linol, B., Dauteuil, O., Robin, C., Mvondo, F., Callec, Y. and Colin, J. P. (2015). Cenozoic landscape evolution in and around the Congo Basin: constraints from sediments and planation surfaces. In Geology and Resource Potential of the Congo Basin. Springer, Berlin, Heidelberg, 271-313. https://doi.org/10.1007/978-3-642-29482-2_14

Gumbricht, T., McCarthy, T.S. and Merry, C.L. (2001). The topography of the Okavango Delta, Botswana, and its tectonic and sedimentological implications. South African Journal of Geology, 104, 243-264. https://doi.org/10.2113/1040243

Haddon, I.G. and McCarthy, T.S. (2005). The Mesozoic–Cenozoic interior sag basins of Central Africa: the Late-Cretaceous–Cenozoic Kalahari and Okavango basins. Journal of African Earth Sciences, 43, 316-333. https://doi.org/10.1016/j.jafrearsci.2005.07.008

Harrison, T., Mbago, M.L., and Msuya, C.P. (1996). Stratigraphy and vertebrate palaeontology of late Neogene sites in the Manonga Valley, north–central Tanzania. Kaupia, 6: 291–295.

Hermanns, R. L., Niedermann, S., Ivy-Ochs, S. and Kubik, P. W. (2004). Rock avalanching into a landslide-dammed lake causing multiple dam failure in Las Conchas valley (NW Argentina) – evidence from surface exposure dating and stratigraphic analyses. Landslides, 1(2), 113-122. https://doi.org/10.1007/s10346-004-0013-5

Hillaire-Marcel, C., Carro, O. and Casanova, J. (1986). 14C and ThU dating of Pleistocene and Holocene stromatolites from East African paleolakes. Quaternary Research, 25(3), 312-329. https://doi.org/10.1016/0033-5894(86)90004-9

Howard, A. D., Dietrich, W. E. and Seidl, M. A. (1994). Modeling fluvial erosion on regional to continental scales. Journal of Geophysical Research: Solid Earth, 99(B7), 13971-13986. https://doi.org/10.1029/94JB00744

Ivory, S. J., Blome, M. W., King, J. W., McGlue, M. M., Cole, J. E. and Cohen, A. S. (2016). Environmental change explains cichlid adaptive radiation at Lake Malawi over the past 1.2 million years. Proceedings of the National Academy of Sciences, 113(42), 11895-11900. https://doi.org/10.1073/pnas.1611028113

Kim, Y. S. and Sanderson, D. J. (2005). The relationship between displacement and length of faults: a review. Earth-Science Reviews, 68(3-4), 317-334. https://doi.org/10.1016/j.earscirev.2004.06.003

Kipata, M. L., Delvaux, D., Sebagenzi, M. N., Cailteux, J. and Sintubin, M. (2013). Brittle tectonic and stress field evolution in the Pan-African Lufilian arc and its foreland (Katanga, DRC): from orogenic compression to extensional collapse, transpressional inversion and transition to rifting. Geologica Belgica, 16(1), 1-17.

Kohl, C. P. and Nishiizumi, K. (1992). Chemical isolation of quartz for measurement of in-situ-produced cosmogenic nuclides. Geochimica et Cosmochimica Acta, 56(9), 3583-3587. https://doi.org/10.1016/0016-7037(92)90401-4

Lal, D. (1991). Cosmic ray labeling of erosion surfaces: in situ nuclide production rates and erosion models. Earth and Planetary Science Letters, 104(2-4), 424-439. https://doi.org/10.1016/0012-821X(91)90220-C

Lavayssiere, A., Drooff, C., Ebinger, C., Gallacher, R., Illsley- Kemp, F., Oliva, S. J. and Keir, D. (2019). Depth extent and kinematics of faulting in the southern Tanganyika rift, Africa. Tectonics, 38(3), 842-862. https://doi.org/10.1029/2018TC005379

Lehner, B. and Grill, G. (2013). Global river hydrography and network routing: baseline data and new approaches to study the world's large river systems. Hydrological Processes, 27(15), 2171-2186. https://doi.org/10.1002/hyp.9740

Macgregor, D. (2015). History of the development of the East African Rift System: A series of interpreted maps through time. Journal of African Earth Sciences, 101: 232–252. https://doi.org/10.1016/j.jafrearsci.2014.09.016

Master, S., Rainaud, C., Armstrong, R. A., Phillips, D. and Robb, L. J. (2005). Provenance ages of the Neoproterozoic Katanga Supergroup (Central African Copperbelt), with implications for basin evolution. Journal of African Earth Sciences, 42(1-5), 41-60. https://doi.org/10.1016/j.jafrearsci.2005.08.005

Masters, L. S., Burkhardt, J. W. and Tausch, R. (1991). The geomorphic process: effects of base level lowering on riparian management. Rangelands Archives, 13(6), 280-284.

Meier, J. I., Stelkens, R. B., Joyce, D. A., Mwaiko, S., Phiri, N., Schliewen, U. K., Selz, O.M., Wagner, C.E., Katongo, C. and Seehausen, O. (2019). The coincidence of ecological opportunity with hybridization explains rapid adaptive radiation in Lake Mweru cichlid fishes. Nature communications, 10(1), 1-11. https://doi.org/10.1038/s41467-019-13278-z

Merchel, S. and Herpers, U. (1999). An update on radiochemical separation techniques for the determination of long-lived radionuclides via accelerator mass spectrometry. Radiochimica Acta, 84(4), 215-220. https://doi.org/10.1524/ract.1999.84.4.215

Merchel, S. and Bremser, W. (2004). First international $^{26}Al$ interlaboratory comparison–Part I. Nuclear Instruments and Methods in Physics Research Section B: Beam Interactions with Materials and Atoms, 223, 393-400. https://doi.org/10.1016/j.nimb.2005.05.051

Mohr, P. A. (1974). ENE-trending lineaments of the African rift system. Proc. First Int. Conf. New Basement Tectonics, Utah. Geol. Ass. Publ., 5 (1974), 327-336.

Molnar, N. E., Cruden, A. R. and Betts, P. G. (2019). Interactions between propagating rifts and linear weaknesses in the lower crust. Geosphere, 15(5), 1617-1640. https://doi.org/10.1130/GES02119.1

Mondeguer, A., Ravenne, C., Masse, P. and Tiercelin, J. J. (1989). Sedimentary basins in an extension and strike-slip background; the" South Tanganyika troughs complex", East African Rift. Bulletin de la Société géologique de France, 3, 501-522. https://doi.org/10.2113/gssgfbull.V.3.501

Moore, A. E., Cotterill, F. P. D. and Eckardt, F. D. (2012). The evolution and ages of Makgadikgadi palaeo-lakes: consilient evidence from Kalahari drainage evolution south-central Africa. South African Journal of Geology, 115(3), 385-413. https://doi.org/10.2113/gssajg.115.3.385

Morley, C. K. (2002). Evolution of large normal faults: Evidence from seismic reflection data. AAPG bulletin, 86(6), 961-978. https://doi.org/10.1306/61EEDBFC-173E-11D7-8645000102C1865D

Mouslopoulou, V., Walsh, J. J. and Nicol, A. (2009). Fault displacement rates on a range of timescales. Earth and Planetary Science Letters, 278(3-4), 186-197. https://doi.org/10.1016/j.epsl.2008.11.031

Mouslopoulou, V., Nicol, A., Walsh, J. J., Begg, J. G., Townsend, D. B. and Hristopulos, D. T. (2012). Fault-slip accumulation in an active rift over thousands to millions of years and the importance of paleoearthquake sampling. Journal of Structural Geology, 36, 71-80. https://doi.org/10.1016/j.jsg.2011.11.010

NASA JPL (2020). NASADEM Merged DEM Global 1 arc second V001 [Data set]. NASA EOSDIS Land Processes DAAC. Last accessed September 2020. https://doi.org/10.5067/MEaSUREs/NASADEM/NASADEM_HGT.001

Neely, A. B., Bookhagen, B. and Burbank, D. W. (2017). An automated knickzone selection algorithm (KZ- Picker) to analyze transient landscapes: Calibration and validation. Journal of Geophysical Research: Earth Surface, 122(6), 1236-1261. https://doi.org/10.1002/2017JF004250

Nicol, A., Walsh, J. J., Watterson, J. and Underhill, J. R. (1997). Displacement rates of normal faults. Nature, 390(6656), 157-159. https://doi.org/10.1038/36548

Nicol, A., Walsh, J., Berryman, K. and Nodder, S. (2005). Growth of a normal fault by the accumulation of slip over millions of years. Journal of Structural Geology, 27(2), 327-342. https://doi.org/10.1016/j.jsg.2004.09.002

Nicol, A., Walsh, J. J., Villamor, P., Seebeck, H. and Berryman, K. R. (2010). Normal fault interactions, paleoearthquakes and growth in an active rift. Journal of Structural Geology, 32(8), 1101-1113. https://doi.org/10.1016/j.jsg.2010.06.018

Nicol, A., Van Dissen, R., Stirling, M. and Gerstenberger, M. (2016a). Completeness of the paleoseismic active fault record in New Zealand. Seismological Research Letters, 86, 1299-1310. doi:10.1785/0220160088

Nicol, A., Robinson, R., Van Dissen, R. J. and Harvison, A. (2016b). Variability of recurrence interval and single-event slip for surface-rupturing earthquakes in New Zealand. New Zealand Journal of Geology and Geophysics, 59(1), 97-116. https://doi.org/10.1080/00288306.2015.1127822

Nicol, A., Childs, C., Walsh, J.J., Manzocchi, T. and Schöpfer, M.P.J. (2016c). Interactions and growth of faults in an outcrop-scale system. In: The Geometry and Growth of Normal Faults. (Edited by Childs, C., Holdsworth, R. E., Jackson, C. A.-L., Manzocchi, T., Walsh, J. J. & Yielding, G.). Geological Society of London, Special Publication, 439, doi.org/10.1144/SP439.9

Nicol, A., Mouslopoulou, V., Begg, J. and Oncken, O. (2020a). Paleoearthquakes, sampling biases and growth of active normal faults on the eastern Mediterranean island of Crete. Geochemistry, Geophysics, Geosystems (in press).

Nicol, A., Walsh, J., Childs, C. and Manzocchi, T. (2020b). The growth of faults. In Understanding Faults (pp. 221-255). Elsevier. https://doi.org/10.1016/B978-0-12-815985-9.00006-0

Nishiizumi, K., Imamura, M., Caffee, M. W., Southon, J. R., Finkel, R. C. and McAninch, J. (2007). Absolute calibration of $^{10}$Be AMS standards. Nuclear Instruments and Methods in Physics Research Section B: Beam Interactions with Materials and Atoms, 258(2), 403-413. https://doi.org/10.1016/j.nimb.2007.01.297

Norris, T. L., Gancarz, A. J., Rokop, D. J. and Thomas, K. W. (1983). Half-life of $^{26}$Al. Journal of Geophysical Research: Solid Earth, 88(S01), B331-B333. https://doi.org/10.1029/JB088iS01p0B331

Omenda, P., Ebinger, C., Nelson, W., Delvaux, D., Cumming, W., Marini, L., Halldórsson, S., Varet, J., Árnason, K., Ruempker, G. and Alexander, K. (2016). Characteristics and important factors that influence the development of geothermal systems in the western branch of East African Rift System”. In 6th African Rift Geothermal Conference 2016.

Perron, J. T. and Royden, L. (2012). An integral approach to bedrock river profile analysis. Earth Surface Processes and Landforms, 38(6), 570-576. https://doi.org/10.1002/esp.3302

Ring, U. (1994). The influence of preexisting structure on the evolution of the Cenozoic Malawi rift (East African rift system). Tectonics, 13(2), 313-326. https://doi.org/10.1029/93TC03188

Rotevatn, A., Jackson, C. A. L., Tvedt, A. B., Bell, R. E. and Blækkan, I. (2019). How do normal faults grow?. Journal of Structural Geology, 125, 174-184. https://doi.org/10.1016/j.jsg.2018.08.005

Rugel, G., Pavetich, S., Akhmadaliev, S., Baez, S. M. E., Scharf, A., Ziegenrücker, R. and Merchel, S. (2016). The first four years of the AMS-facility DREAMS: Status and developments for more accurate radionuclide data. Nuclear Instruments and Methods in Physics Research B, 370, 94-100. https://doi.org/10.1016/j.nimb.2016.01.012

Saria, E., Calais, E., Stamps, D. S., Delvaux, D. and Hartnady, C. J. H. (2014). Present-day kinematics of the East African Rift. Journal of Geophysical Research: Solid Earth, 119(4), 3584-3600. https://doi.org/10.1016/0301-9268(84)90032-9

Schlische, R. W., Young, S. S., Ackermann, R. V. and Gupta, A. (1996). Geometry and scaling relations of a population of very small rift-related normal faults. Geology, 24(8), 683-686. https://doi.org/10.1130/0091-7613(1996)024<0683:GASROA>2.3.CO;2

Schlüter, T. (1997). Geology of East Africa. In: Bender, F., Jacobshagen, V. and Lüttig, G. (Eds.), Beiträge zur Regionalen Geologie der Erde, Band 27. Gebrüder Borntraeger, Berlin, Stuttgart, 484 pp.

Schultz, R. A., Soliva, R., Fossen, H., Okubo, C. H. and Reeves, D. M. (2008). Dependence of displacement–length scaling relations for fractures and deformation bands on the volumetric changes across them. Journal of Structural Geology, 30(11), 1405-1411. https://doi.org/10.1016/j.jsg.2008.08.001

Schwanghart, W. and Scherler, D. (2014). TopoToolbox 2–MATLAB-based software for topographic analysis and modeling in Earth surface sciences. Earth Surface Dynamics, 2(1), 1-7. doi:10.5194/esurf-2-1-2014

Schwarzer, J., Misof, B., Ifuta, S. N. and Schliewen, U. K. (2011). Time and origin of cichlid colonization of the lower Congo rapids. Plos one, 6(7), e22380. https://doi.org/10.1371/journal.pone.0022380

Seiler, M., Anjar, J., Værnes, E., Nadeau, M. J. and Scognamiglio, G. (2018). First $^{10}$Be measurements at Trondheim 1 MV AMS. Nuclear Instruments and Methods in Physics, B 437, 123-129. https://doi.org/10.1016/j.nimb.2018.08.013

Shudofsky, G. N. (1985). Source mechanisms and focal depths of East African earthquakes using Rayleigh-wave inversion and body-wave modelling. Geophysical Journal International, 83(3), 563-614. https://doi.org/10.1111/j.1365-246X.1985.tb04328.x

Shuman, B., Henderson, A. K., Colman, S. M., Stone, J. R., Fritz, S. C., Stevens, L. R., Power, M. J. and Whitlock, C. (2009). Holocene lake-level trends in the Rocky Mountains, USA. Quaternary Science Reviews, 28(19-20), 1861-1879. https://doi.org/10.1016/j.quascirev.2009.03.003

Stamps, D. S., Calais, E., Saria, E., Hartnady, C., Nocquet, J. M., Ebinger, C. J. and Fernandes, R. M. (2008). A kinematic model for the East African Rift. Geophysical Research Letters, 35(5), L05304. https://doi.org/10.1029/2007GL032781

Strecker, M. R., Blisniuk, P. M. and Eisbacher, G. H. (1990). Rotation of extension direction in the central Kenya Rift. Geology, 18(4), 299-302. https://doi.org/10.1130/0091-7613(1990)018<0299:ROEDIT>2.3.CO;2

Tack, L., Fernandez-Alonso, M., Trefois, P., Lavreau, J. and Cailteux, J. L. H. (2003). New data raise new questions on the regional geology of the Katanga Province as figured on the 1974 Geological Map (1/2000000) of the Democratic Republic of Congo (DRC). In Proterozoic Base Metal Deposits of Western Gondwana. 3rd IGCP-450 Conference and Guide Book of the Field Workshop, Lumbumbashi, Congo, 78-82.

Thieme, J.G. (1971). The Geology of Musonda Falls Area, Explanation of Sheet 1028, SE Quarter. Geological Survey of Zambia, Report No. 32, 25.

Tiercelin, J. J. and Lezzar, K. E. (2002). A 300 million years history of rift lakes in Central and East Africa: an updated broad review. In The East African great lakes: limnology, palaeolimnology and biodiversity. Springer, Dordrecht, 3-60. https://doi.org/10.1007/0-306-48201-0_1

Tiercelin, J. J., Chorowicz, J., Bellon, H., Richert, J. P., Mwanbene, J. T. and Walgenwitz, F. (1988). East African Rift System: offset, age and tectonic significance of the Tanganyika-

Rukwa-Malawi intracontinental transcurrent fault zone. Tectonophysics, 148(3-4), 241-252. https://doi.org/10.1016/0040-1951(88)90133-3

Torabi, A. and Berg, S. S. (2011). Scaling of fault attributes: A review. Marine and Petroleum Geology, 28(8), 1444-1460. https://doi.org/10.1016/j.marpetgeo.2011.04.003

Trauth, M. H., Maslin, M. A., Deino, A. and Strecker, M. R. (2005). Late Cenozoic moisture history of East Africa. Science, 309(5743), 2051-2053. https://doi.org/10.1126/science.1112964

Trauth, M. H., Maslin, M. A., Deino, A. L., Junginger, A., Lesoloyia, M., Odada, E. O., Olago, D. O., Olaka, L.A., Strecker, M. R. and Tiedemann, R. (2010). Human evolution in a variable environment: the amplifier lakes of Eastern Africa. Quaternary Science Reviews, 29(23-24), 2981-2988. https://doi.org/10.1016/j.quascirev.2010.07.007

Unrug, R. (1984). The mid-Proterozoic Mporokoso Group of northern Zambia: stratigraphy, sedimentation and regional position. Precambrian Research, 24(2), 99-121.

Van Damme, D. and Pickford, M. (2003). The late Cenozoic Thiaridae (Mollusca, Gastropoda, Cerithioidea) of the Albertine Rift Valley (Uganda-Congo) and their bearing on the origin and evolution of the Tanganyikan thalassoid malacofauna. Hydrobiologia, 498(1-3), 1-83. https://doi.org/10.1023/A:1026298512117

van der Merwe, P.D., Cotterill, F.P.D., Kandziora, M., Watters, B.R., Nagy, B., Genade, T., Flügel, T.J., Svendsen D. and Bellstedt, D. U. (2021). Genomic Fingerprints of Palaeogeographic History: The tempo and mode of Rift tectonics across tropical Africa has shaped the diversification of the killifish genus *Nothobranchius* (Teleostei: Cyprinodontiformes). Molecular Phylogenetics and Evolution, In Press. https://doi.org/10.1016/j.ympev.2020.106988

Vermeesch, P. (2007). CosmoCalc: An Excel add-in for cosmogenic nuclide calculations. Geochemistry, Geophysics, Geosystems, 8(8), https://doi.org/10.1029/2006GC001530

von Blanckenburg, F., Hewawasam, T. and Kubik, P. W. (2004). Cosmogenic nuclide evidence for low weathering and denudation in the wet, tropical highlands of Sri Lanka. Journal of Geophysical Research: Earth Surface, 109(F3), F03008. https://doi.org/10.1029/2003JF000049

Walsh, J. J. and Watterson, J. (1988). Analysis of the relationship between displacements and dimensions of faults. Journal of Structural geology, 10(3), 239-247. https://doi.org/10.1016/0191-8141(88)90057-0

Walsh, J. J., Nicol, A. and Childs, C. (2002). An alternative model for the growth of faults. Journal of Structural Geology, 24(11), 1669-1675. https://doi.org/10.1016/S0191-8141(01)00165-1

Walsh, J. J. and Watterson, J. (1991). Geometric and kinematic coherence and scale effects in normal fault systems. Geological Society, London, Special Publications, 56(1), 193-203. https://doi.org/10.1144/GSL.SP.1991.056.01.13

Watterson, J., Walsh, J. J., Gillespie, P. A. and Easton, S. (1996). Scaling systematics of fault sizes on a large-scale range fault map. Journal of Structural Geology, 18(2-3), 199-214. https://doi.org/10.1016/S0191-8141(96)80045-9

Wells, D. L. and Coppersmith, K. J. (1994). New empirical relationships among magnitude, rupture length, rupture width, rupture area, and surface displacement. Bulletin of the seismological Society of America, 84(4), 974-1002.

Wesnousky, S. G. (2008). Displacement and geometrical characteristics of earthquake surface ruptures: Issues and implications for seismic-hazard analysis and the process of earthquake rupture. Bulletin of the Seismological Society of America, 98(4), 1609-1632. https://doi.org/10.1785/0120070111

Whipple, K. X. and Tucker, G. E. (1999). Dynamics of the stream- power river incision model: Implications for height limits of mountain ranges, landscape response timescales, and research needs. Journal of Geophysical Research: Solid Earth, 104(B8), 17661-17674. https://doi.org/10.1029/1999JB900120

Whipple, K. X., Snyder, N. P. and Dollenmayer, K. (2000). Rates and processes of bedrock incision by the Upper Ukak River since the 1912 Novarupta ash flow in the Valley of Ten Thousand Smokes, Alaska. Geology, 28(9), 835-838. https://doi.org/10.1130/0091-7613(2000)28<835:RAPOBI>2.0.CO;2

Williamson, P. G. (1978). Evidence for the major features and development of Rift Palaeolakes in the Neogene of East Africa from certain aspects of Lacustrine Mollusc assemblages. Geological Society, London, Special Publications, 6(1), 507-527. https://doi.org/10.1144/GSL.SP.1978.006.01.35

## Figure Captions

Figure 1: Morphotectonic map of the Mweru-Mweru Wantipa Fault System (MMFS) in the southern East African Rift System. Normal faults are indicated by black lines while ticks indicate downfaulted side. Numbers next to each fault correspond to entries in Table A2 in the Appendix. Red lines indicate topographic profiles presented in Figures 4, 5 and 6. Green circles, yellow triangles and blue squares indicate sampling locations of the three different sampling groups. Inset shows location of study area in Africa. KUN: Kundabikwa Waterfalls; LUM: Lumangwe Waterfall; NTU: Ntumbachushi Waterfalls; MUM: Mumbuluma I Waterfalls; LUP: Lupupa Waterfall; LUO: Mumbuluma II Waterfall; LUZ: Lunzua Waterfalls.

Figure 2: A) Sampling of KUN01 from a vertical face on the banks of Kalungwishi River, downstream of Kundabikwa Waterfalls, Zambia; B) Sampling of bedrock (MUM04) directly from the horizontal surface of the knickpoint at Mumbuluma I Waterfalls, Zambia; C) View of Lumangwe Waterfall, Zambia; D) Sample location of ME09, Lwilwa River, DRC; E) Sampling of MWE01 from the face of fault 16, DRC.

Figure 3: A) Log-log plot illustrating the relationship between topographic fault length and total displacement for the faults in the MMFS (grey circles) and the Mpulungu basin (southern Tanganyika Fault System; black circles). B) Same as (a) but illustrating separately the NW dipping (circles) and the SE dipping (triangles) faults in the MMFS. C) Log-log plot illustrating the relationship between topographic fault length and the displacement rate for the faults in the MMFS (grey circles) and the Mpulungu basin (black circles). D) Global dataset of displacement vs. fault length (shaded area; Nicol et al., 2016b). Black circles show data for the same faults as in Figure 3A while white triangles represent single-event displacement rupture lengths for historical earthquakes (Wesnousky, 2008). Least squares lines of best fit and R2 values are also indicated for each dataset.

Figure 4: Five topographic profiles approximately perpendicular to the trend of the MMFS (for locality of the profiles see Figure 1). The SE dipping faults are indicated with red lines while the NW dipping faults with blue lines. Sample locations are indicated with yellow circles. Numbers with F next to faults correspond to numbered faults in Figure 1 and entries in Table A2 in the Appendix. Plain numbers next to the faults indicate the throw (m) of the respective fault. The total fault throw as well as the throw of the NW (blue) and SE (red) dipping faults are indicated on each profile. Blue dashed line indicates the potential water level of the paleo-lake Mweru.

Figure 5: Topographic profile along the trend of the MMFS. See Figure 1 for profile location and Figure 4 for explanations.

Figure 6: Reconstructed landscape based on the topographic profiles presented in Figures 4 and 5 and two additional profiles (Profiles 7 and 8) which are depicted in Figure 1. Subtracted throw resulted assuming a constant fault displacement rate (see Table A2 for values) during the last 2.6 Ma. Dashed black lines represent the current landscape. Grey dashed line indicates the approximate elevation of the reconstructed landscape about 2.6 Ma (rift's onset), while black solid line is the average elevation of the reconstructed landscape. The SE dipping faults are indicated by red triangles while blue circles indicate the NW dipping faults. The SW dipping faults are presented as green rhombuses, while yellow squares show the NE dipping faults.

Figure 7: A) Locations of river knickpoints for the Lake Mweru catchment. Symbol colours indicate knickpoint elevations and symbol sizes show knickpoint magnitudes (lips minus base elevation). Only river knickpoints with elevations between 900 and 1200 m asl are shown. Note the clustering of river knickpoints at ~925 (dark blue), ~1000, and ~1180 m asl that correspond to paleo-shorelines of paleo-lake Mweru. B) Hypsometric curve of Lake Mweru derived from a 30 m SRTM DEM (NASA JPL, 2020). All grid cells within the Lake Mweru catchment were binned into 10 m elevation bins and their respective surface areas were calculated (black line). The elevations were filtered to only show hillslope angles < 3° (blue line). Note the two distinctive peaks at ~925 m asl and ~1180 m asl that show the elevations of the paleo-lake Mweru. Knickpoint elevation shows a high number of river knickpoints at paleo-lake shorelines (only river knickpoints with at least 30 m offset are shown).

Figure 8: Two-nuclide diagrams showing $^{10}$Be concentrations (atoms/g, corrected for total shielding and scaled to common elevation) versus $^{26}$Al/$^{10}$Be ratios for samples of Group A. The black dashed line indicates the "steady state denudation line" and the solid black line the "constant exposure line" (e.g. Lal, 1991). Red lines show the temporal evolution of data at constant denudation rates and subsequent burial. Green lines indicate duration of burial under the assumption that samples were first exposed and later completely buried until present.

Samples are indicated with black error ellipses (1σ shown). Underlined labels indicate samples taken from vertical surfaces. A) Kundabikwa Waterfalls; B) Lumangwe Waterfall; C) Ntumbachushi Waterfalls; D) Mumbuluma I Waterfalls.

Figure 9: Schematic figure of successive landscape stages of Kalungwishi River at Kundabikwa Waterfalls and paleo-lake Mweru. T1: Initial river state with waterfall already in place. T2: Onset of paleo-lake Mweru below Kundabikwa Waterfalls. Areas downstream of the knickpoint are covered with water and sediment, while denudation at and upstream of the waterfalls is reduced due to lower energy environment. T3: Full establishment of paleo-lake Mweru resulting in water cover and sediment deposition on top horizontal surfaces. T4: Drainage of the paleo-lake, resulting in exposure of areas above the knickpoint with concomitant incision of lacustrine sediments at the waterfalls and deposition of these sediments into the remaining lake below the waterfalls. T5: Paleo-lake Mweru is completely drained and sediments deposited during T3 and T4 are removed through regional denudation, resulting in differential bedrock exposure. T6: Present day river course with limited sedimentary cover and ongoing down- and backwearing through increased denudation.

Figure 10: Two-nuclide diagrams showing $^{10}Be$ concentrations (atoms/g) versus $^{26}Al/^{10}Be$ ratios for samples of Group B. See Figure 8 for explanations. A) Lupupa Waterfall; B) Mumbuluma II Waterfall (Luongo River); C) Lunzua Waterfalls.

Figure 11: Two-nuclide diagram showing $^{10}Be$ concentration (atoms/g) versus $^{26}Al/^{10}Be$ ratios for samples of Group C. See Figure 8 for explanations.

Figure 12: Schematic representation of the possible maximum extent of paleo-lake Mweru during the Plio-Pleistocene (see blue contour at 1200 m asl). Shaded areas represent reconstructed paleo-topography that was present during the Plio-Pleistocene.

 

Table 1: Sampling details for samples from Northern Province, Zambia and Katanga Province, Democratic Republic of Congo. Total shielding factor includes surface dip, horizon shielding and self shielding.

| Name | Latitude ° S | Longitude ° E | Elevation (m) | Surface Dip (°) | Average Thickness (cm) | Total Shielding Factor |
|---|---|---|---|---|---|---|
| *Kundabikwa Waterfalls, Kalungwishi River, Zambia* | | | | | | |
| KUN01 | 9.21207 | 29.30468 | 1037 | 90 | 2.5 | 0.49 |
| KUN02 | 9.21201 | 29.30470 | 1043 | 0 | 2.5 | 0.97 |
| KUN03 | 9.20947 | 29.30399 | 1043 | 0 | 2.5 | 0.98 |
| KUN04 | 9.20949 | 29.30403 | 1039 | 90 | 2.5 | 0.49 |
| KUN05 | 9.20824 | 29.30189 | 1034 | 0 | 7 | 0.94 |
| KUN06 | 9.20849 | 29.30184 | 1030 | 90 | 2 | 0.49 |
| KUN07 | 9.21781 | 29.30395 | 1030 | 0 | 2.5 | 0.98 |
| *Lumangwe Waterfall, Kalungwishi River, Zambia* | | | | | | |
| LUM02 | 9.54023 | 29.38688 | 1150 | 86 | 2.5 | 0.53 |
| LUM03 | 9.54027 | 29.38696 | 1159 | 0 | 2.5 | 0.98 |
| *Ntumbachushi Waterfalls, Ngona River, Zambia* | | | | | | |
| NTU01 | 9.85439 | 28.94402 | 1157 | 75 | 2.5 | 0.65 |
| NTU02 | 9.85421 | 28.94397 | 1157 | 5 | 2.5 | 0.88 |
| NTU03 | 9.85481 | 28.94346 | 1167 | 90 | 2.5 | 0.49 |
| *Mumbuluma I Waterfalls, Mumbuluma River, Zambia* | | | | | | |
| MUM01 | 10.93031 | 28.73533 | 1182 | 90 | 2.5 | 0.49 |
| MUM02 | 10.93544 | 28.73293 | 1178 | 0 | 2.5 | 0.98 |
| MUM03 | 10.92980 | 28.73502 | 1177 | 90 | 8.5 | 0.46 |
| MUM04 | 10.93012 | 28.73532 | 1186 | 0 | 2.5 | 0.98 |
| *Lupupa Waterfall, Mukubwe River, Zambia* | | | | | | |
| LUP01 | 9.27355 | 29.78074 | 1361 | 90 | 2.5 | 0.49 |
| *Mumbuluma II Waterfall, Luongo River, Zambia* | | | | | | |
| LUO01 | 10.10907 | 29.57566 | 1371 | 45 | 2.5 | 0.90 |
| LUO02 | 10.10732 | 29.57449 | 1339 | 50 | 7.5 | 0.76 |
| *Lunzua Waterfalls, Lunzua River, Zambia* | | | | | | |
| LUZ01 | 8.91501 | 31.15994 | 1258 | 90 | 2.5 | 0.45 |
| LUZ02 | 8.91686 | 31.16070 | 1303 | 90 | 2.5 | 0.48 |
| *Luvua River, D.R.Congo* | | | | | | |
| ME04 | 8.48340 | 28.88423 | 937 | 90 | 2 | 0.49 |
| ME05 | 8.48366 | 28.88371 | 985 | 90 | 5 | 0.54 |
| *Musefwe River, D.R. Congo* | | | | | | |
| ME06 | 8.72807 | 28.68353 | 992 | 0 | 1 | 0.98 |
| *Lwilwa River, D.R. Congo* | | | | | | |
| ME09 | 8.82977 | 28.56613 | 1030 | 0 | 2 | 0.98 |
| *Fault scarp sample, D.R. Congo* | | | | | | |
| MWE01 | 8.74980 | 28.65532 | 1035 | 80 | 7.5 | 0.56 |

Table 2: $^{10}Be$ and $^{26}Al$ concentrations and minimum exposure ages ($T_{10}$, $T_{26}$) based thereon. Asterisk (*) indicates samples collected from vertical or subvertical surfaces. All uncertainties presented are 1σ. They include: measurement uncertainty (statistical), standard uncertainty (certification), reproducibility of standard analyses, carrier uncertainties. Age uncertainties do not include errors of production rates and scaling. See text for details on production rates and scaling method used. AMS labs where analyses were performed: D= HZDR, Dresden, Germany; T= NTNU, Trondheim, Norway; C= ASTER, CEREGE, Aix-en-Provence, France.

| Name | $^{10}Be$ ($10^6$ atoms $g^{-1}$) | $T_{10}$ (ka) | $^{10}Be$ AMS | $^{26}Al$ ($10^6$ atoms $g^{-1}$) | $T_{26}$ (ka) | $^{26}Al$ AMS |
|---|---|---|---|---|---|---|
| *Group A* | | | | | | |
| KUN01* | 1.178±0.024 | 514±11 | *D* | 4.03±0.15 | 244.0±9.1 | *D* |
| KUN02 | 0.725±0.015 | 145.1±3.0 | *D* | 2.91±0.11 | 82.1±3.2 | *D* |
| KUN03 | 1.751±0.035 | 367.3±7.4 | *D* | 5.81±0.22 | 169.2±6.3 | *D* |
| KUN04* | 1.305±0.027 | 577±12 | *D* | 5.63±0.23 | 360±15 | *D* |
| KUN05 | 1.491±0.030 | 326.5±6.6 | *D* | 7.59±0.28 | 240.9±9.0 | *D* |
| KUN06* | 0.2400±0.0055 | 94.6±2.2 | *D* | 1.256±0.060 | 70.2±3.3 | *D* |
| KUN07 | 1.570±0.032 | 329.3±6.7 | *D* | 8.07±0.30 | 360±13 | *D* |
| LUM02* | 0.657±0.025 | 225.4±8.6 | *T* | 3.64±0.26 | 181±13 | *C* |
| LUM03 | 1.074±0.028 | 198.2±5.1 | *T* | 6.93±0.30 | 186.9±8.0 | *C* |
| NTU01* | 0.0820±0.0032 | 21.70±0.85 | *D* | 0.525±0.056 | 19.6±2.1 | *C* |
| NTU02 | 1.754±0.046 | 376.0±9.8 | *T* | 10.43±0.58 | 335±19 | *C* |
| NTU03* | 0.2806±0.0076 | 100.4±2.7 | *D* | 1.52±0.12 | 77.3±5.9 | *C* |
| MUM01* | 0.1986±0.0059 | 68.9±2.0 | *D* | 1.25±0.07 | 61.5±3.5 | *C* |
| MUM02 | 1.479±0.035 | 271.1±6.5 | *D* | 8.77±0.41 | 236±11 | *C* |
| MUM03* | 0.3054±0.0082 | 113.8±3.0 | *D* | 1.91±0.12 | 101.8±6.5 | *C* |
| MUM04 | 0.643±0.016 | 112.8±2.8 | *D* | 3.78±0.17 | 94.6±4.3 | *C* |
| *Group B* | | | | | | |
| LUP01* | 0.1385±0.0041 | 42.5±1.3 | *D* | 0.957±0.062 | 41.6±2.7 | *C* |
| LUO01 | 0.484±0.019 | 81.0±3.2 | *T* | 3.06±0.13 | 72.7±3.1 | *C* |
| LUO02 | 3.441±0.080 | 830±19 | *T* | 20.72±0.97 | 844±40 | *C* |
| LUZ01* | 1.306±0.033 | 533±13 | *T* | 7.88±0.36 | 499±23 | *C* |
| LUZ02* | 0.309±0.010 | 102.6±3.4 | *T* | 2.128±0.091 | 101.5±4.3 | *C* |
| *Group C* | | | | | | |
| ME04* | 0.0292±0.0024 | 12.1±1.0 | *T* | 0.216±0.023 | 12.6±1.4 | *C* |
| ME05* | 0.0294±0.0024 | 10.72±0.88 | *T* | 0.258±0.024 | 13.2±1.2 | *C* |
| ME06 | 0.2136±0.0080 | 42.8±1.6 | *T* | 1.506±0.071 | 42.7±2.0 | *C* |
| ME09 | 0.2270±0.0079 | 44.5±1.5 | *T* | 1.69±0.10 | 46.9±2.9 | *C* |
| MWE01* | 0.0249±0.0026 | 7.89±0.81 | *T* | 0.173±0.020 | 7.67±0.90 | *C* |

Table 3: $^{10}Be$ and $^{26}Al$ maximum erosion rates ($\varepsilon_{10}$, $\varepsilon_{26}$) obtained for samples of Groups B and C. All uncertainties presented are 1σ.

| Name | Dip angle (°) | $\varepsilon_{10}$ (mm $ka^{-1}$) | $\varepsilon_{26}$ (mm $ka^{-1}$) |
|---|---|---|---|
| LUO01 | 45 | 5.65±0.22 | 6.39±0.27 |
| LUO02 | 50 | 0.4016±0.0094 | 0.317±0.015 |
| LUZ01 | 90 | 0.3906±0.0099 | 0.375±0.017 |
| LUZ02 | 90 | 2.367±0.079 | 2.40±0.10 |
| ME04 | 90 | 22.6±1.9 | 22.6±2.4 |
| ME05 | 90 | 25.4±2.1 | 21.3±2.0 |
| ME06 | 0 | 15.96±0.60 | 16.42±0.77 |
| ME09 | 0 | 15.26±0.53 | 14.79±0.91 |
| MWE01 | 80 | 39.2±4.0 | 41.9±4.9 |

Figure (Color)

Click here to access/download;Figure (Color);Figure 1.jpeg

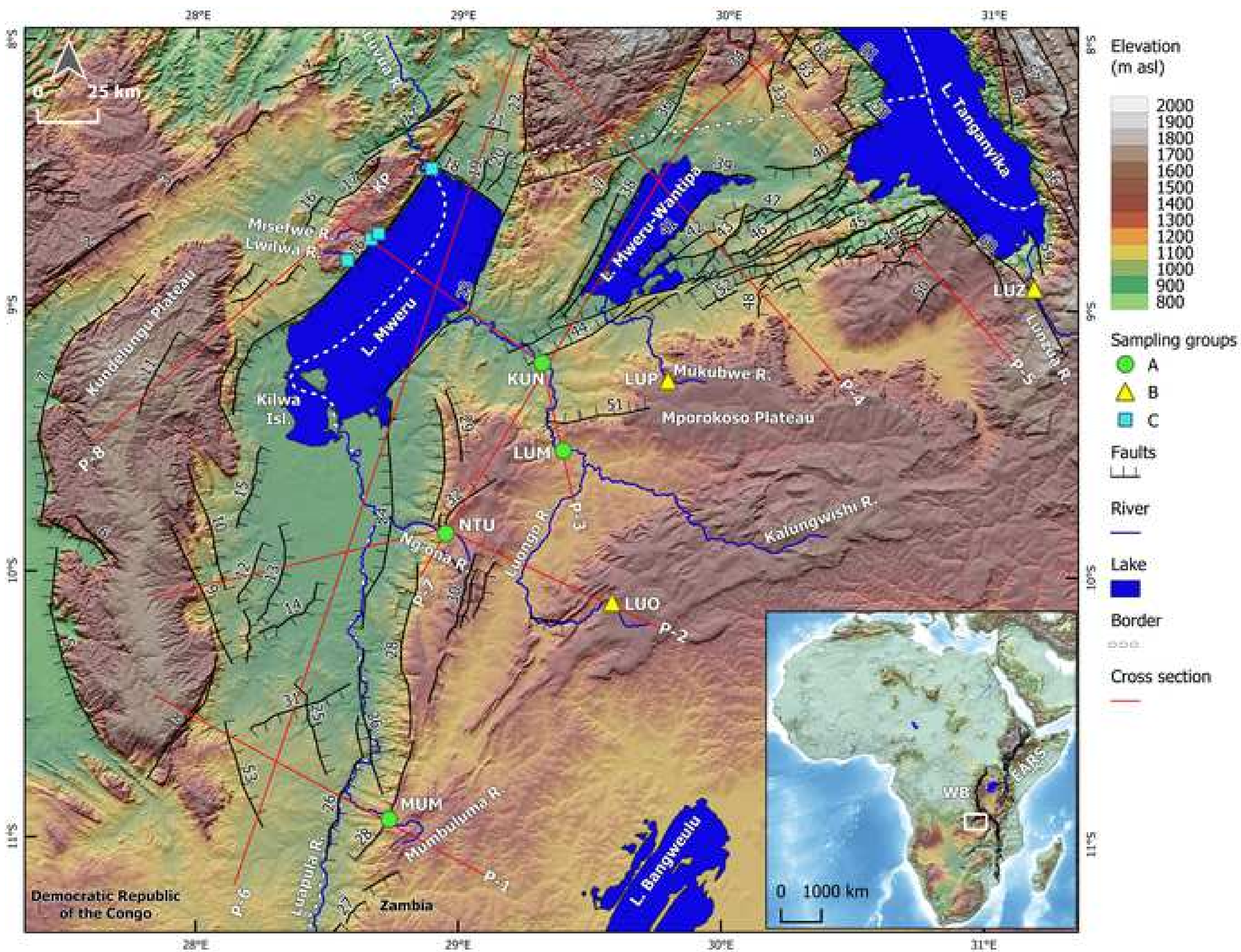

Figure (Color)

Click here to access/download;Figure (Color);Figure 2a.png

 

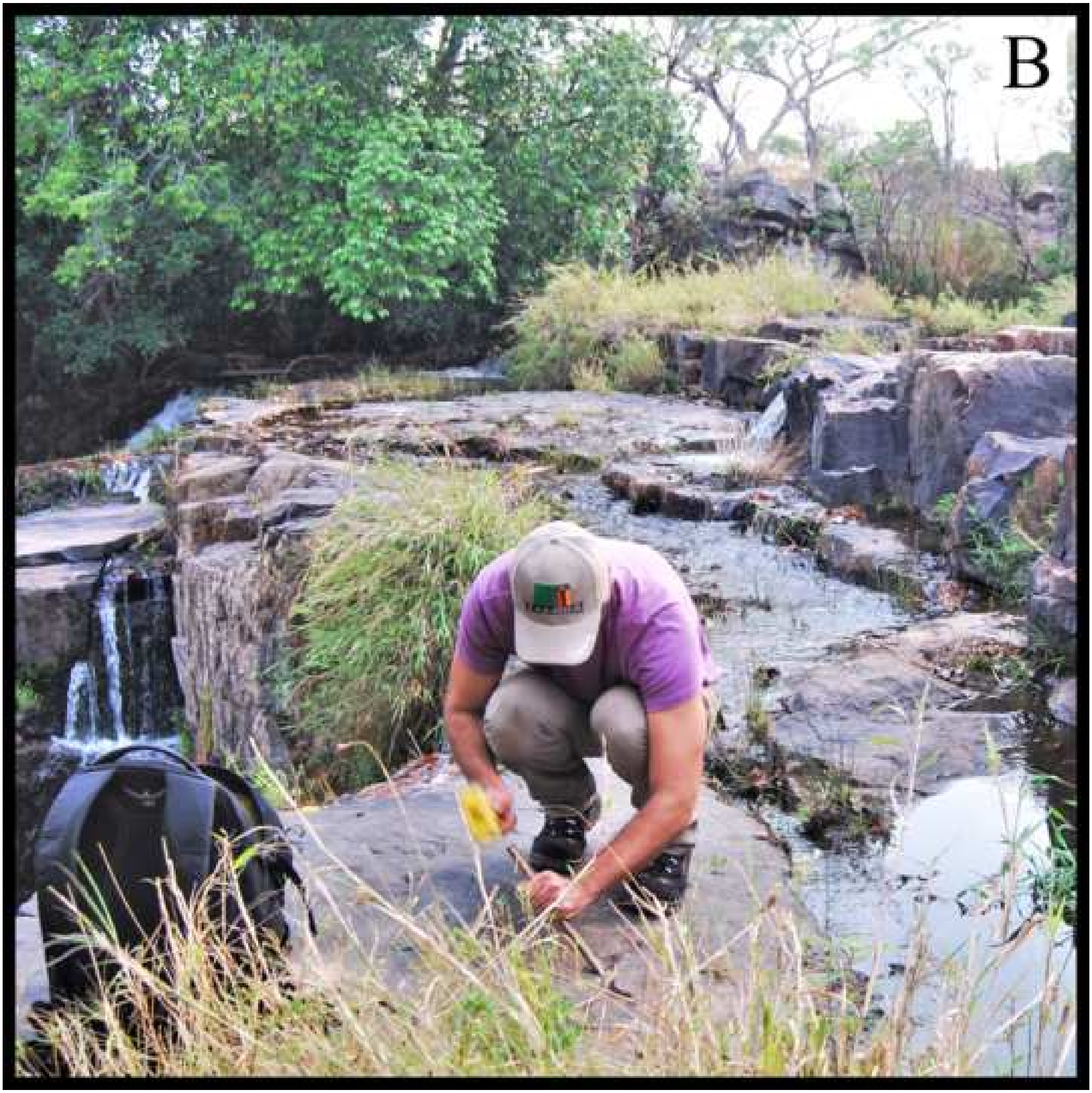
B


C

Figure (Color)

Click here to access/download;Figure (Color);Figure 2d.png

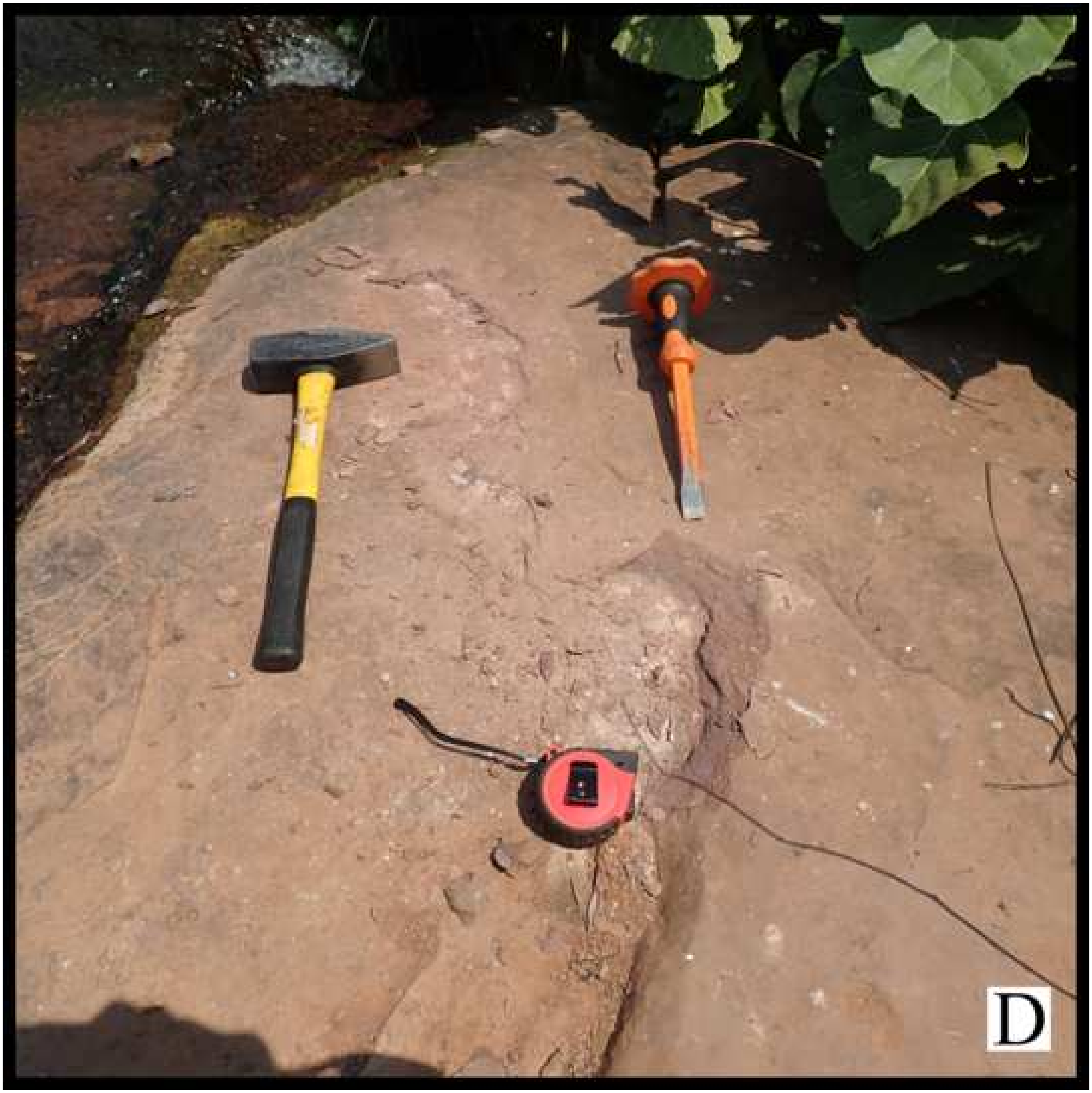

Figure (Color)

Click here to access/download;Figure (Color);Figure 2e.png

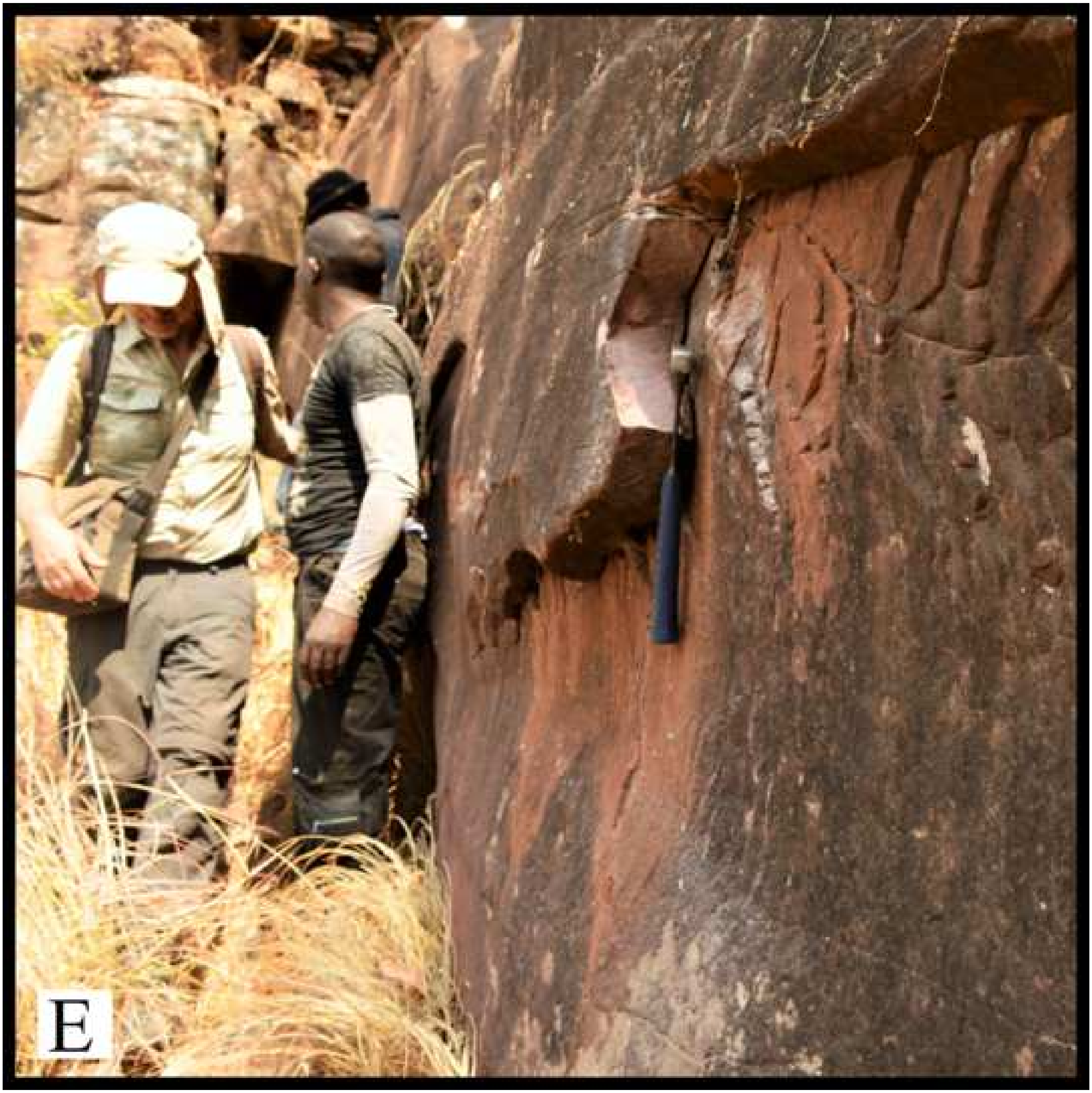

Figure (Color)

Click here to access/download;Figure (Color);Figure 3abc.png

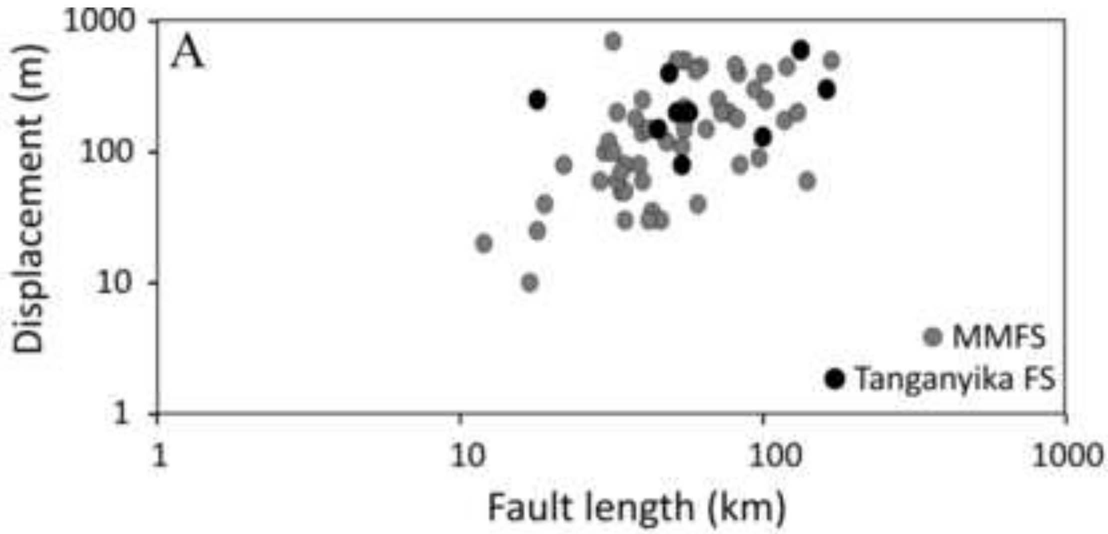


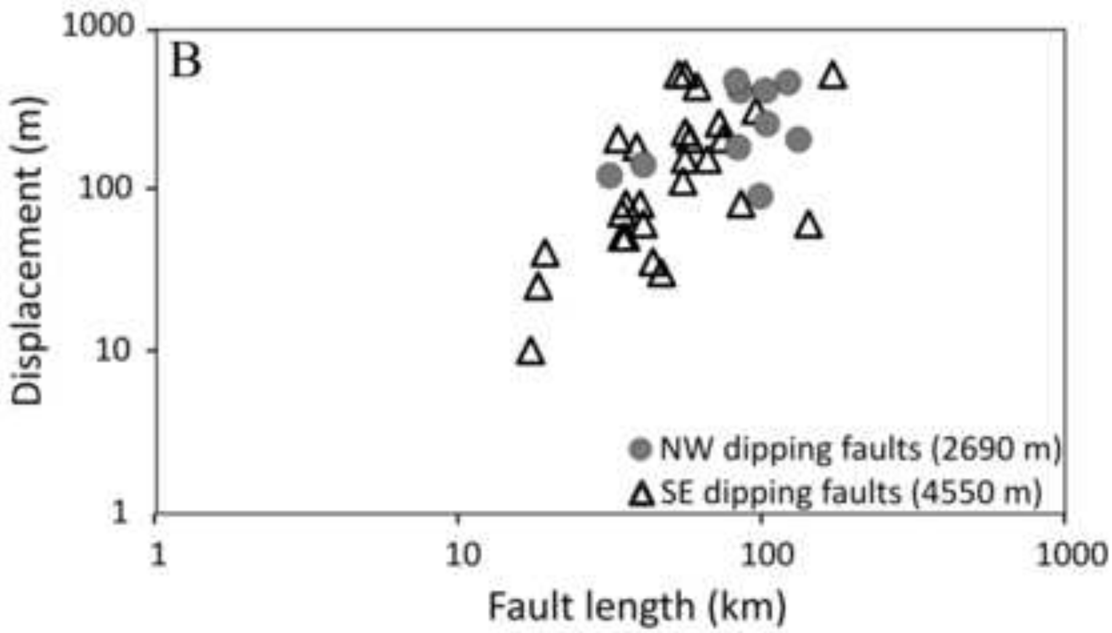


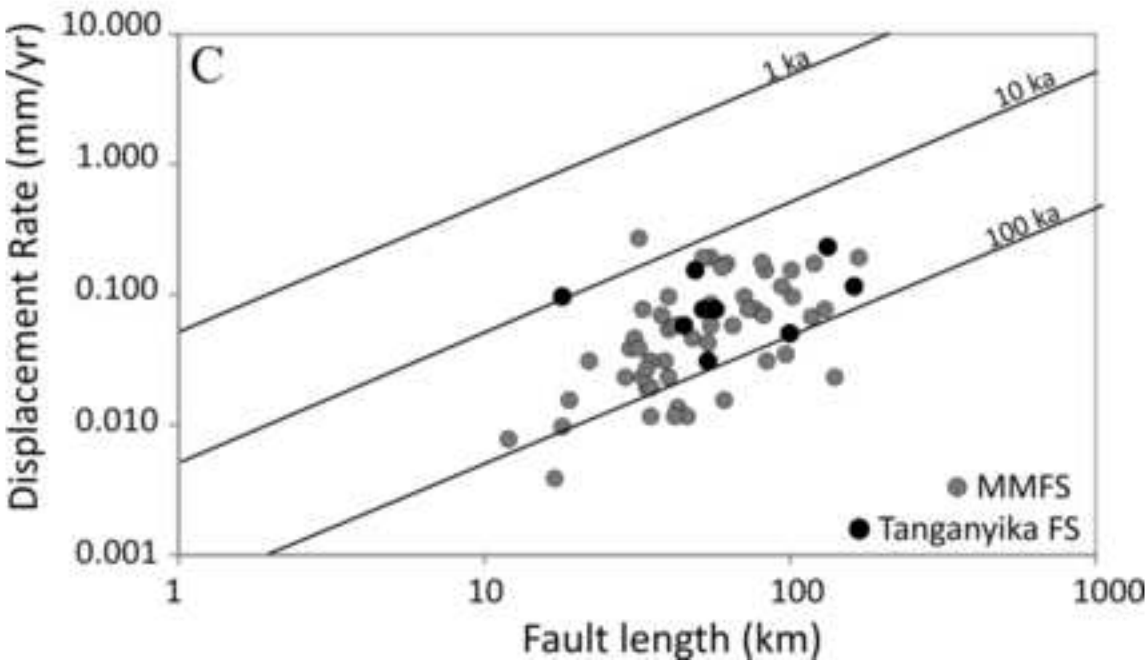

Figure (Color) Click here to access/download;Figure (Color);Figure 3d.png

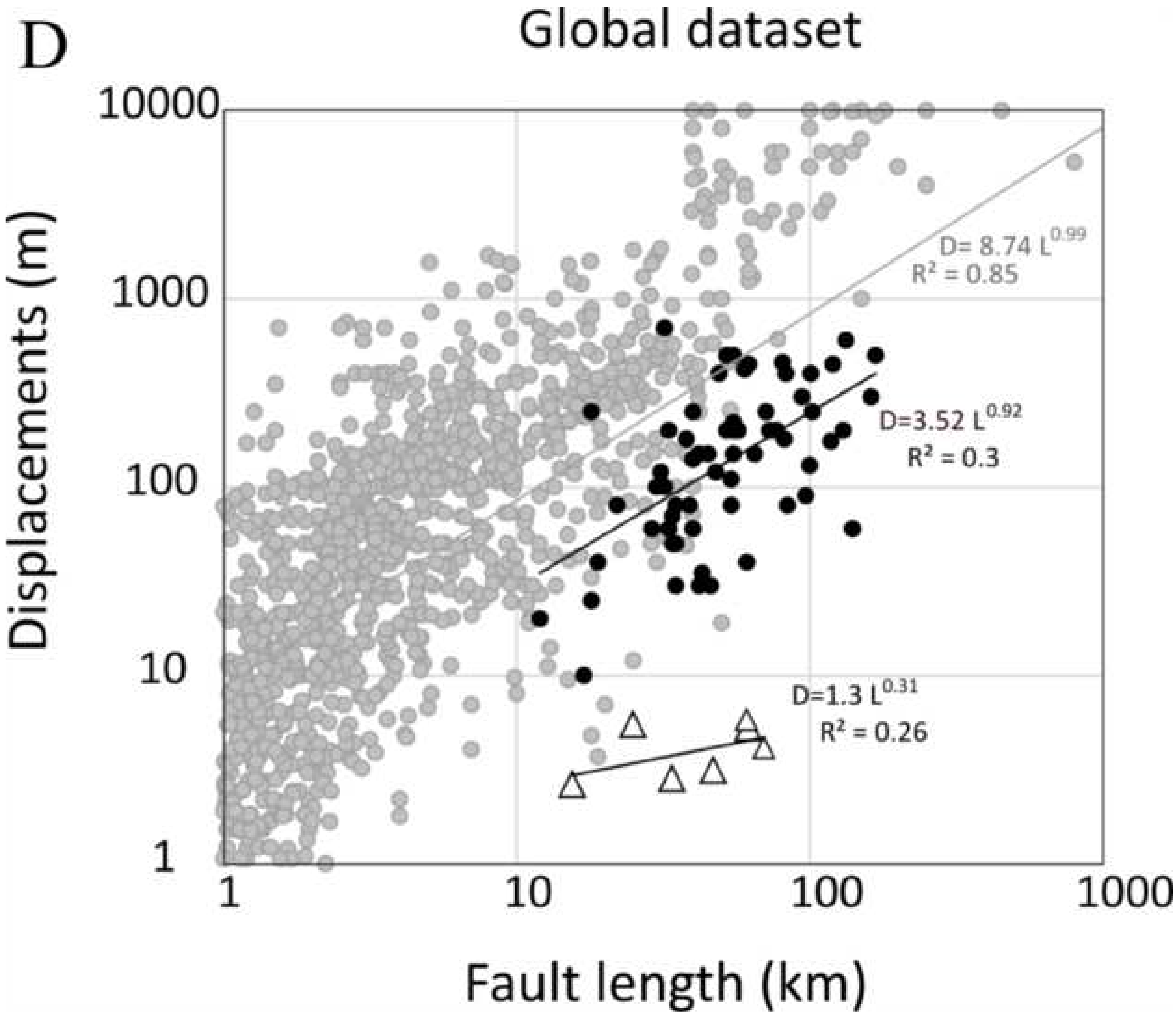

Figure (Color) Click here to access/download;Figure (Color);Figure 4.png

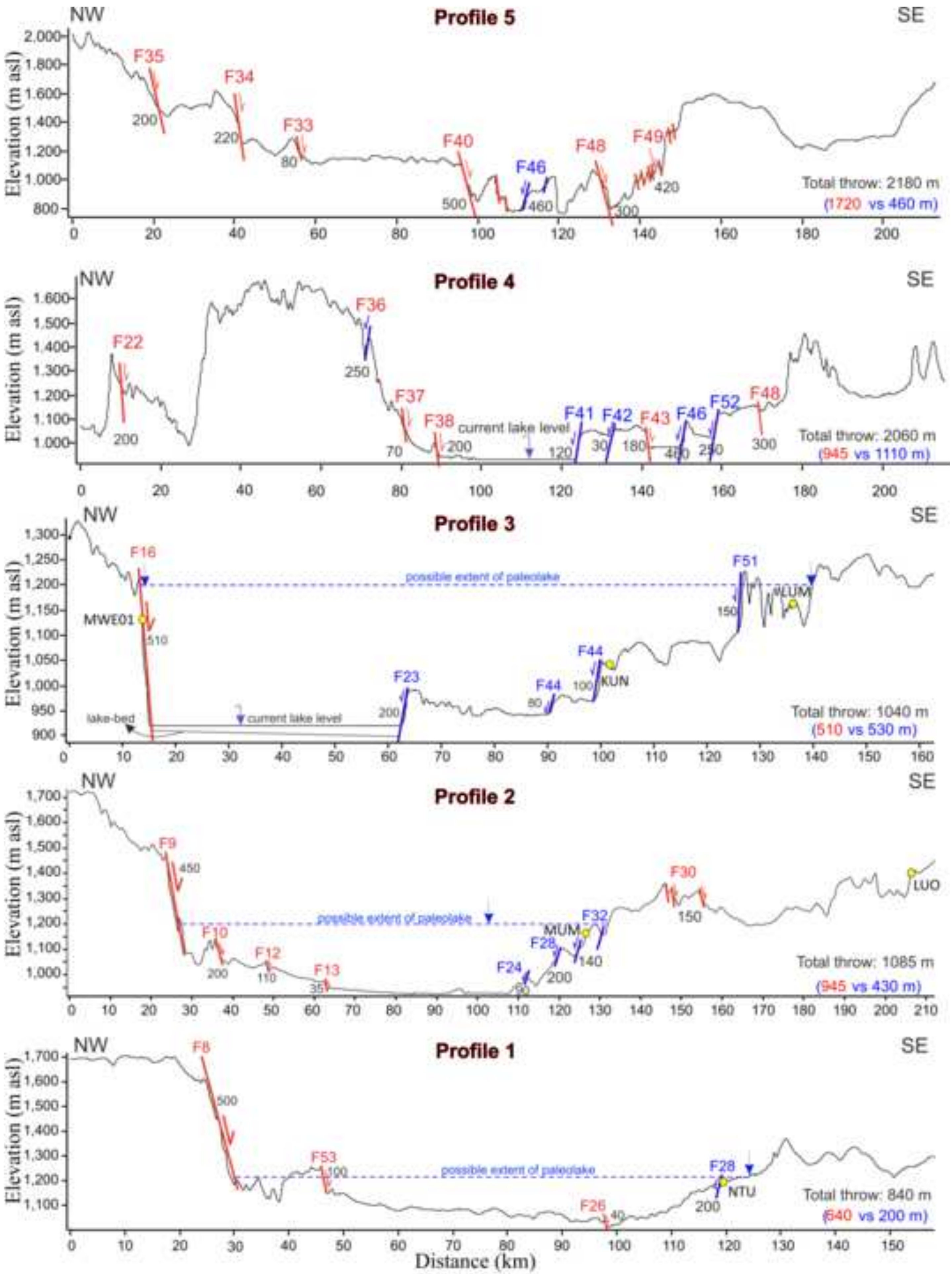

Figure (Color)

Click here to access/download;Figure (Color);Figure 5.png

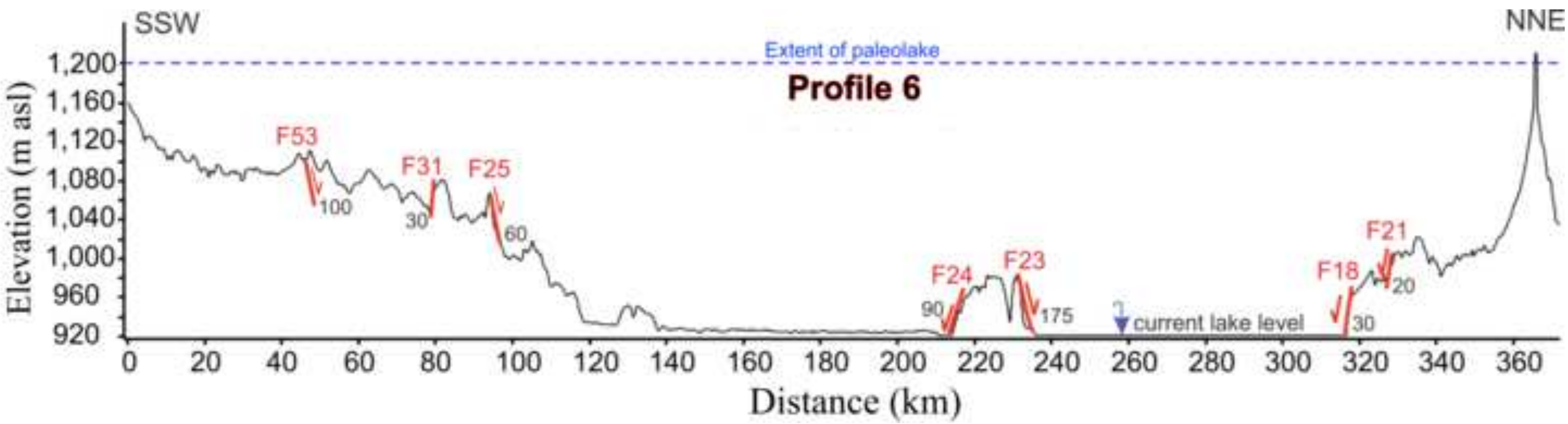

Figure (Color)

Click here to access/download;Figure (Color);Figure 6a.png

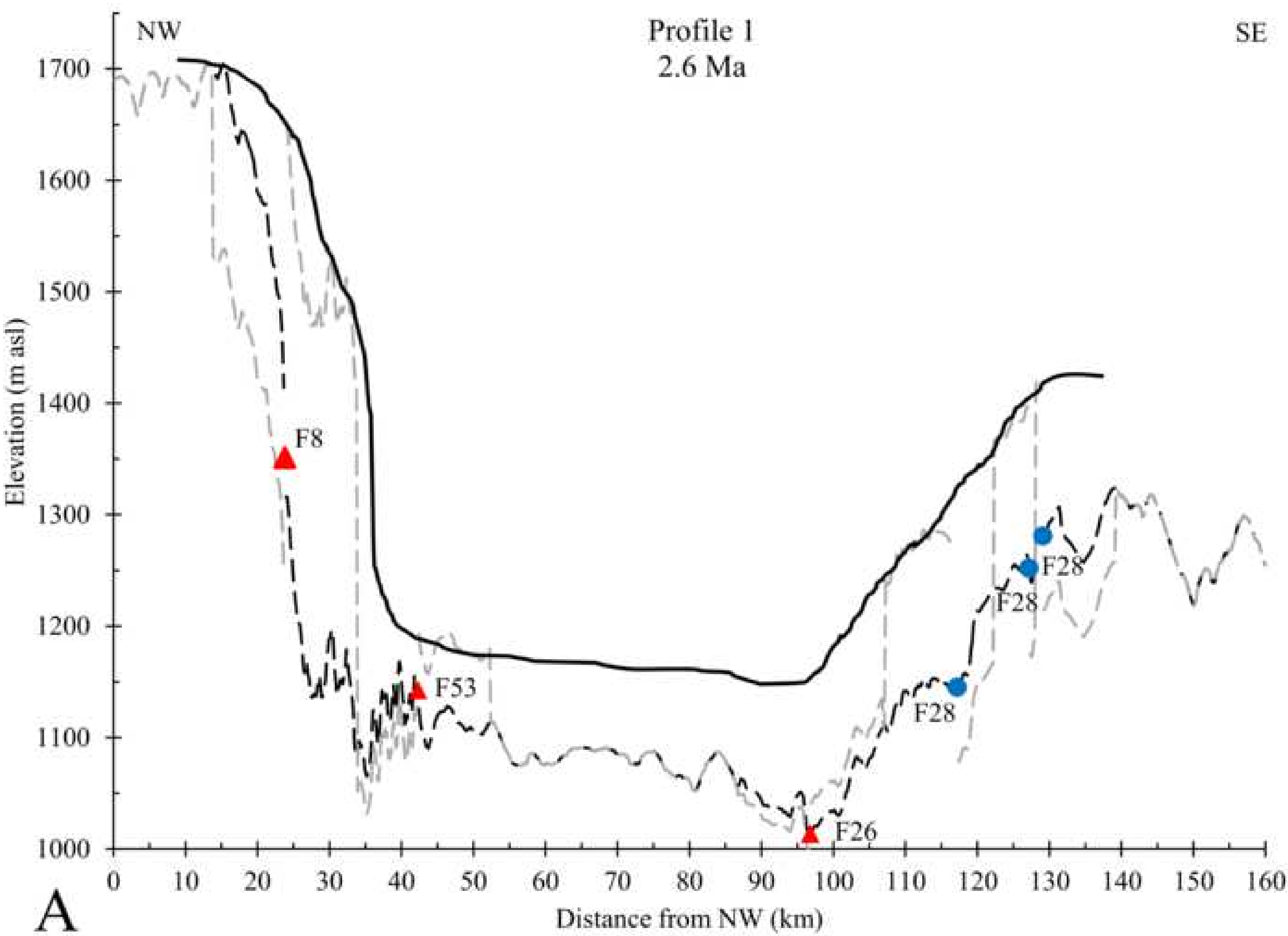

Figure (Color)

Click here to access/download;Figure (Color);Figure 6b.png

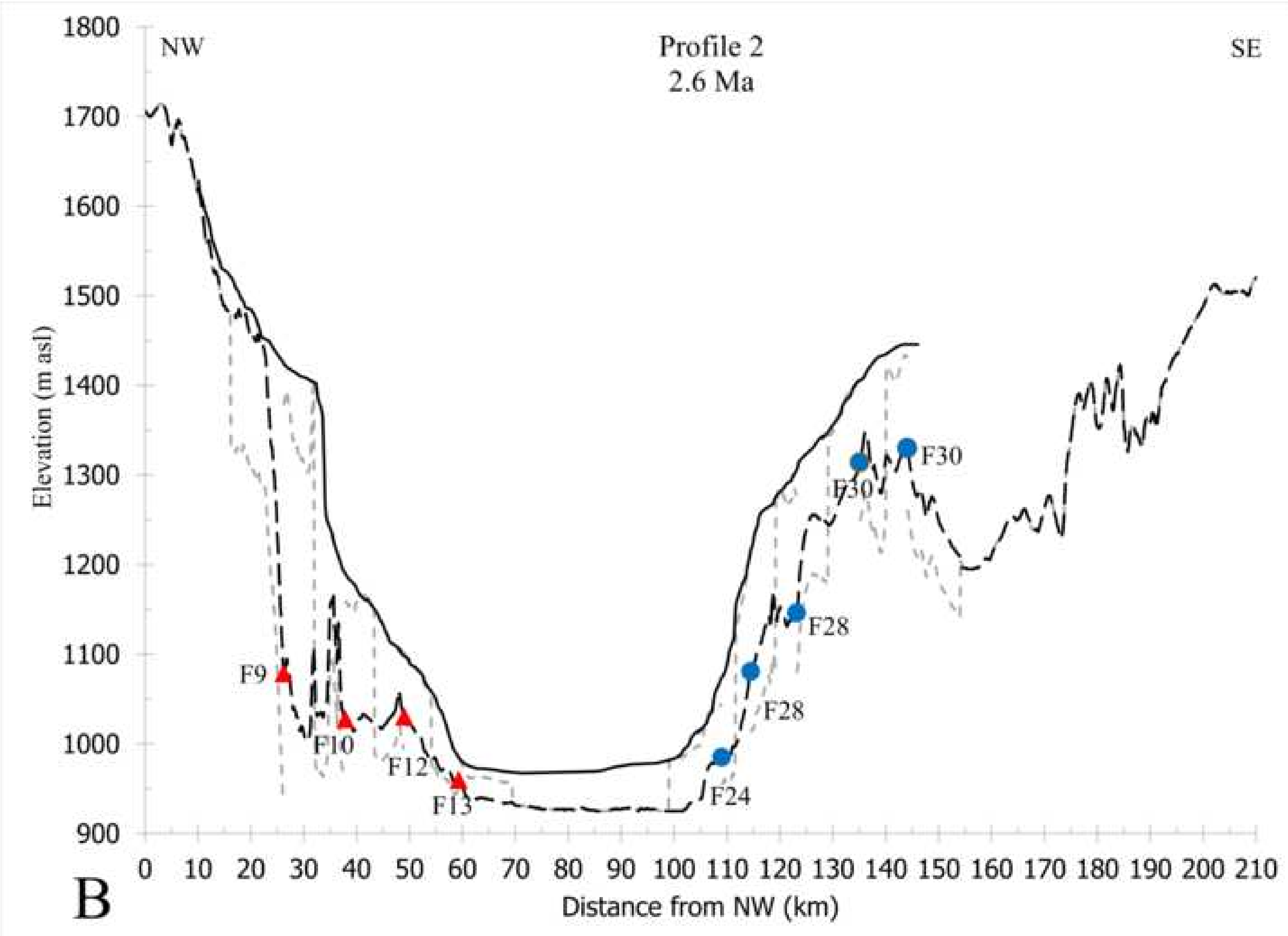

Figure (Color)

Click here to access/download;Figure (Color);Figure 6c.png

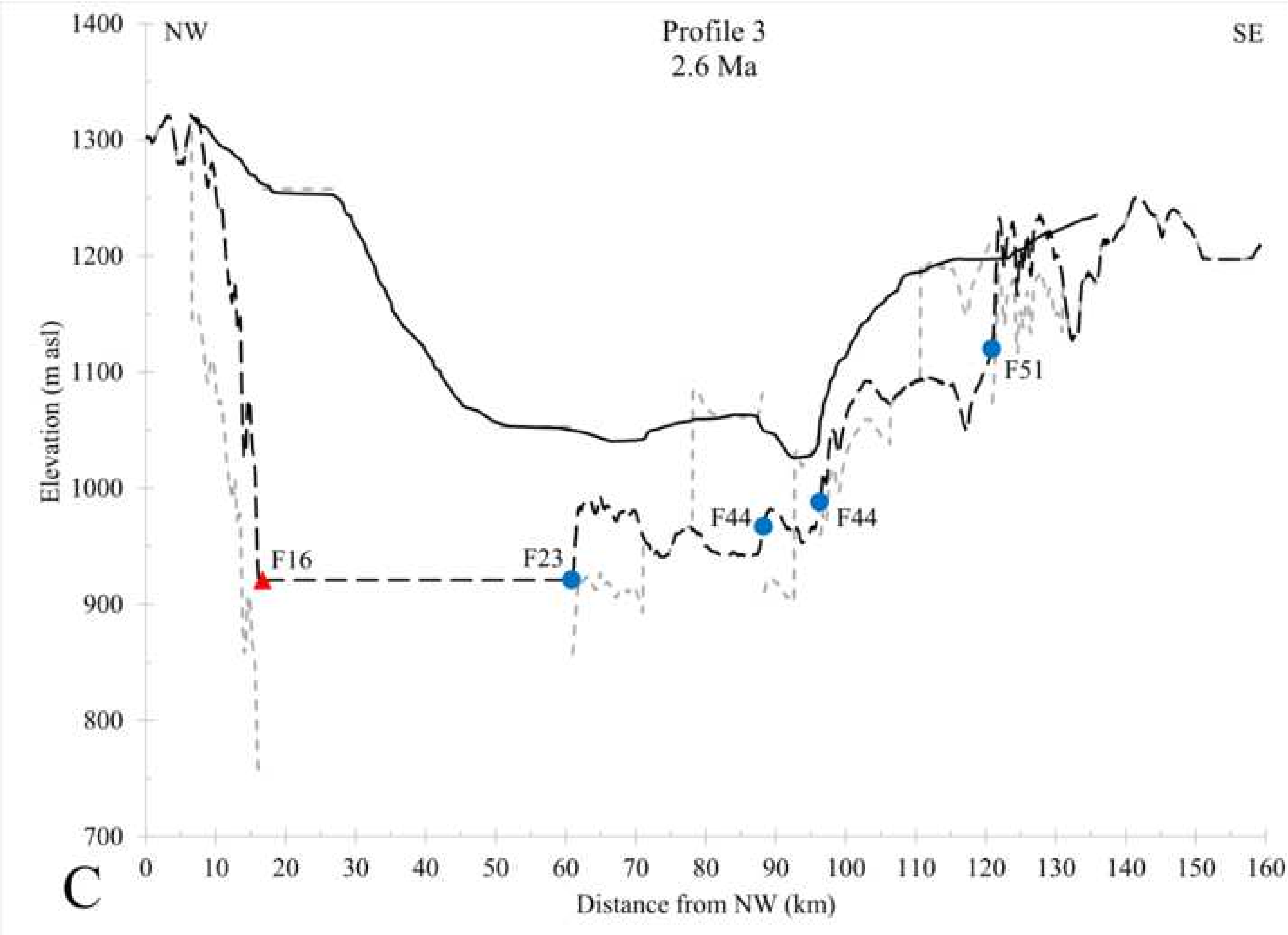

Figure (Color)

Click here to access/download;Figure (Color);Figure 6d.png

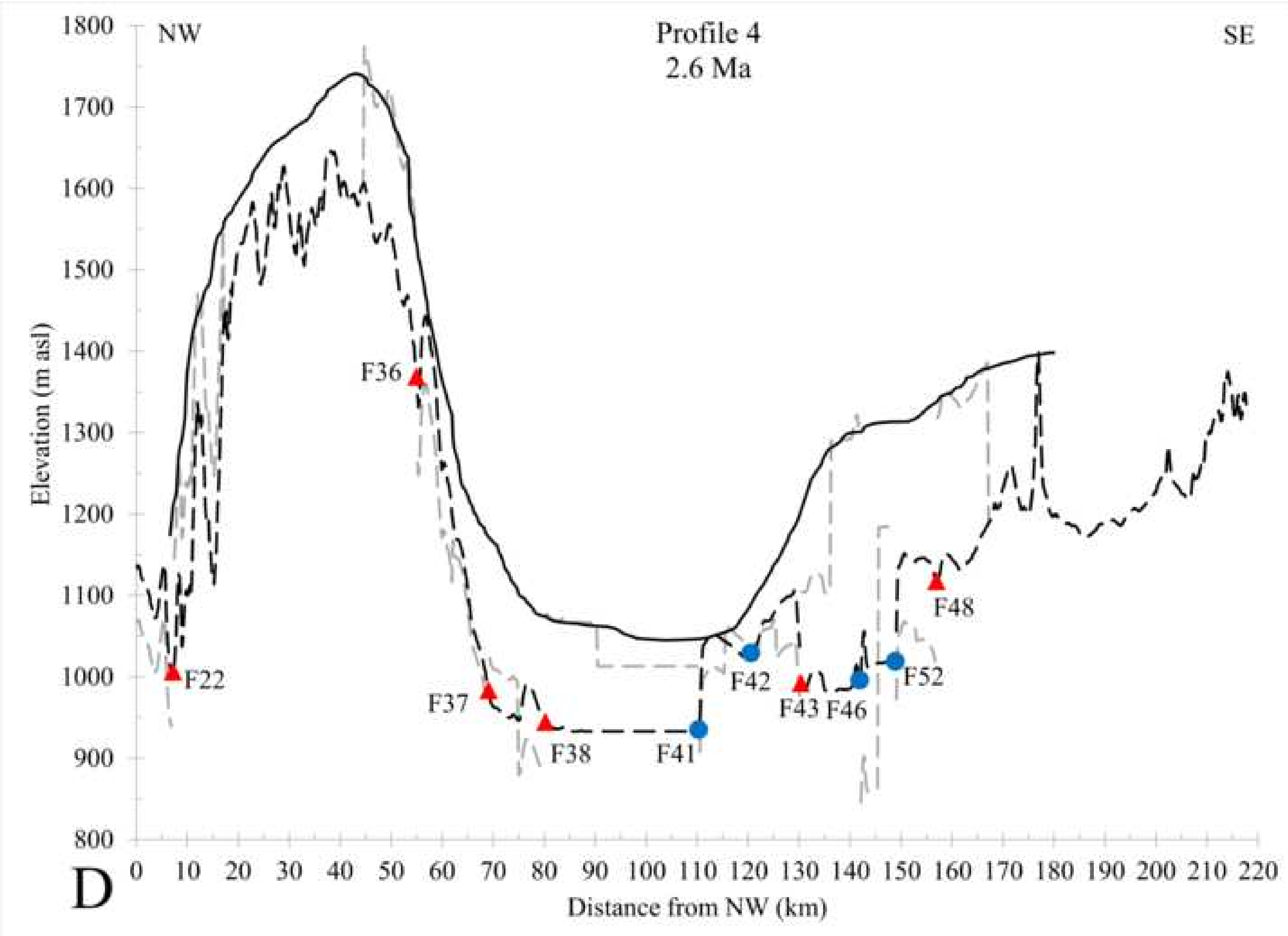

Figure (Color) Click here to access/download;Figure (Color);Figure 6e.png

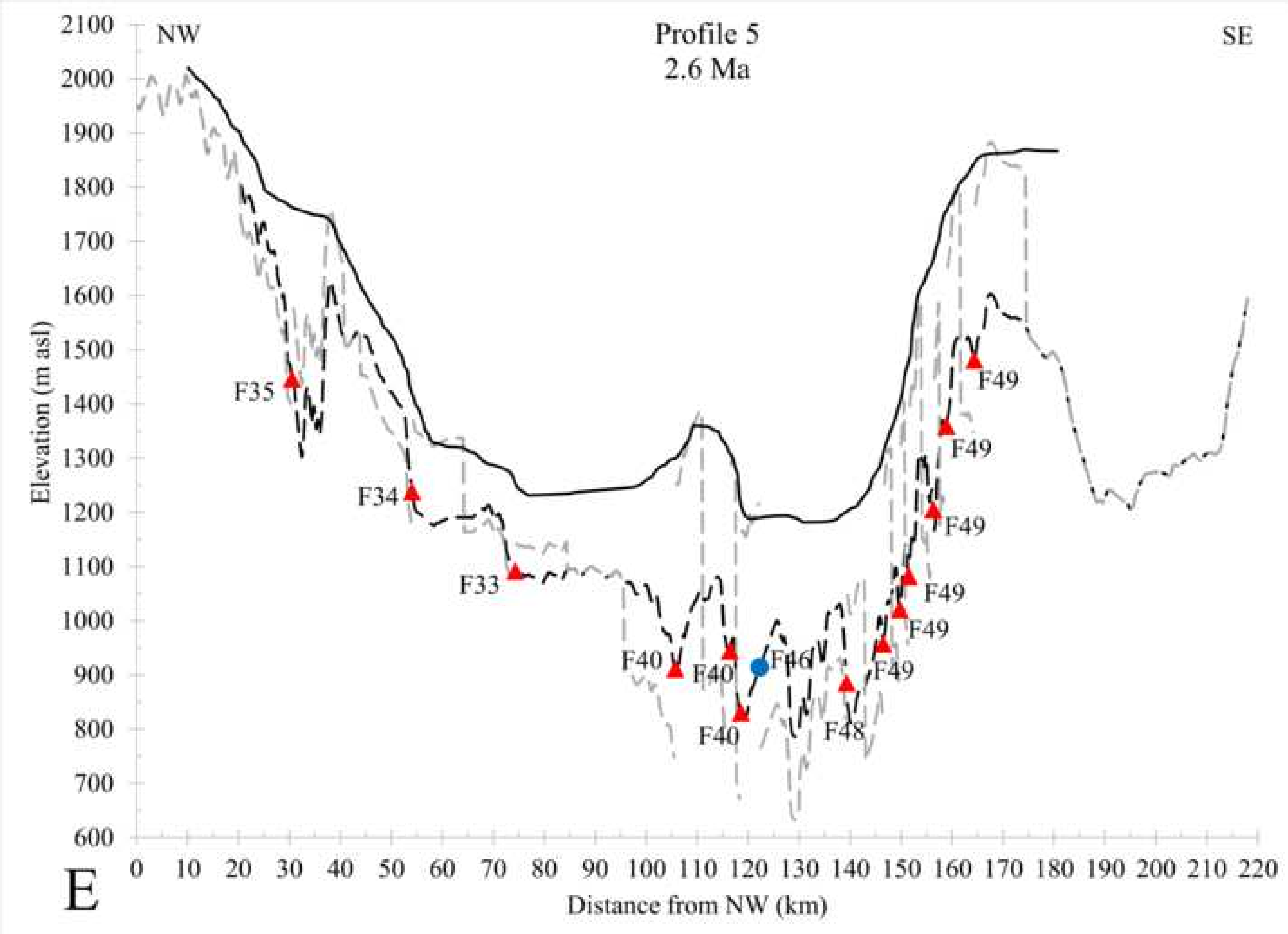

Figure (Color)

Click here to access/download;Figure (Color);Figure 6f.png

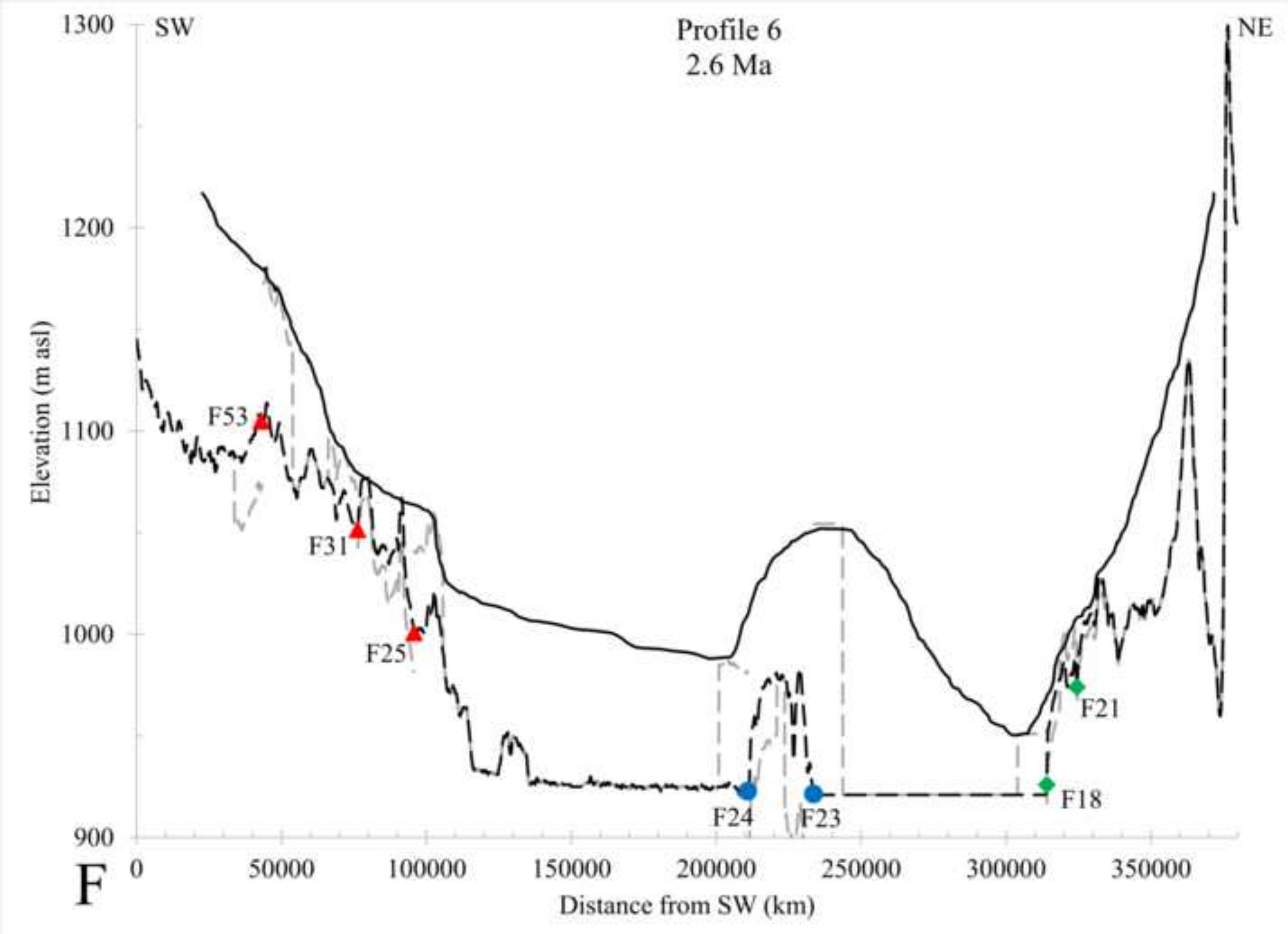

Figure (Color)

Click here to access/download;Figure (Color);Figure 6g.png

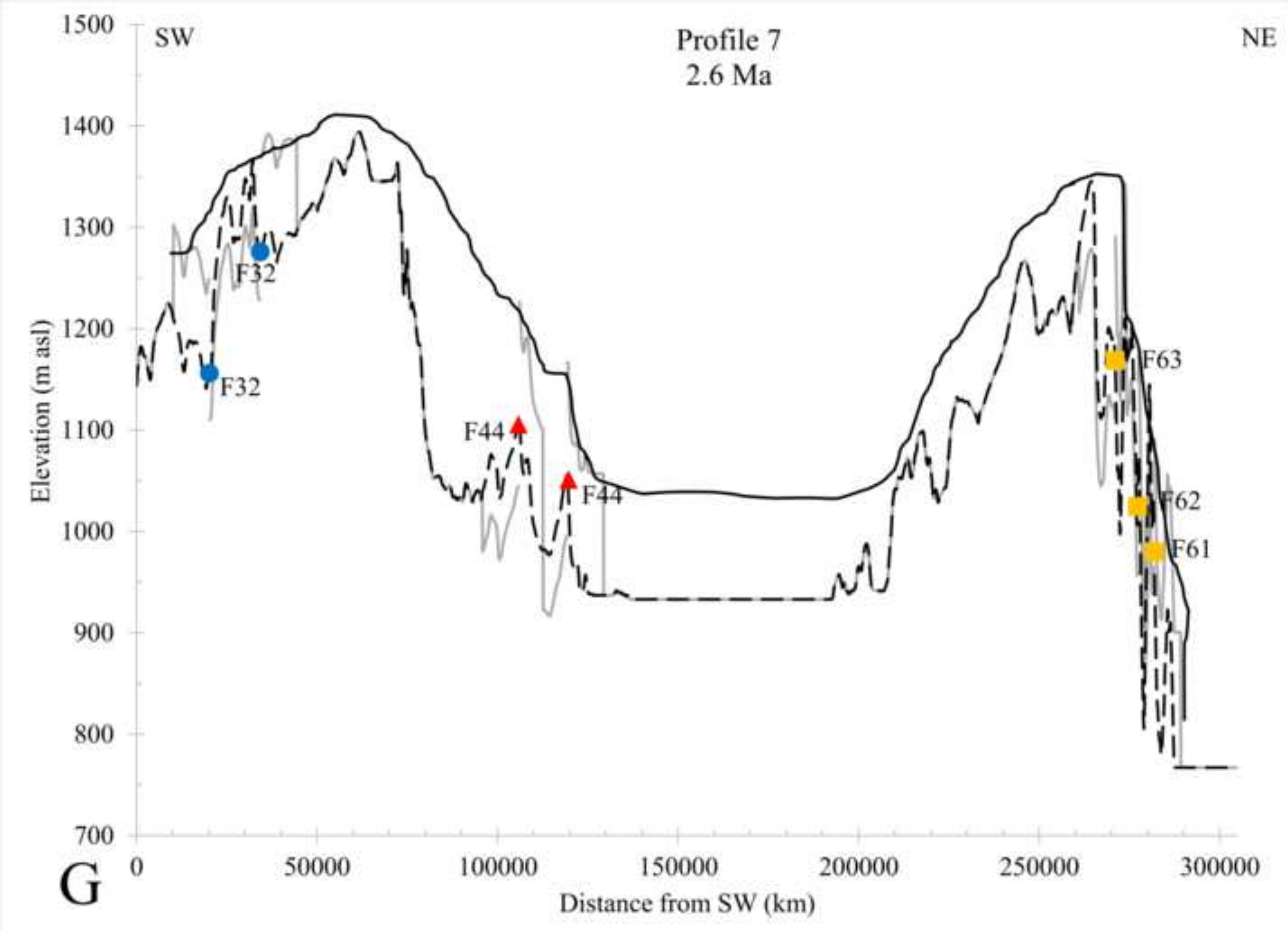

Figure (Color)

Click here to access/download;Figure (Color);Figure 6h.png

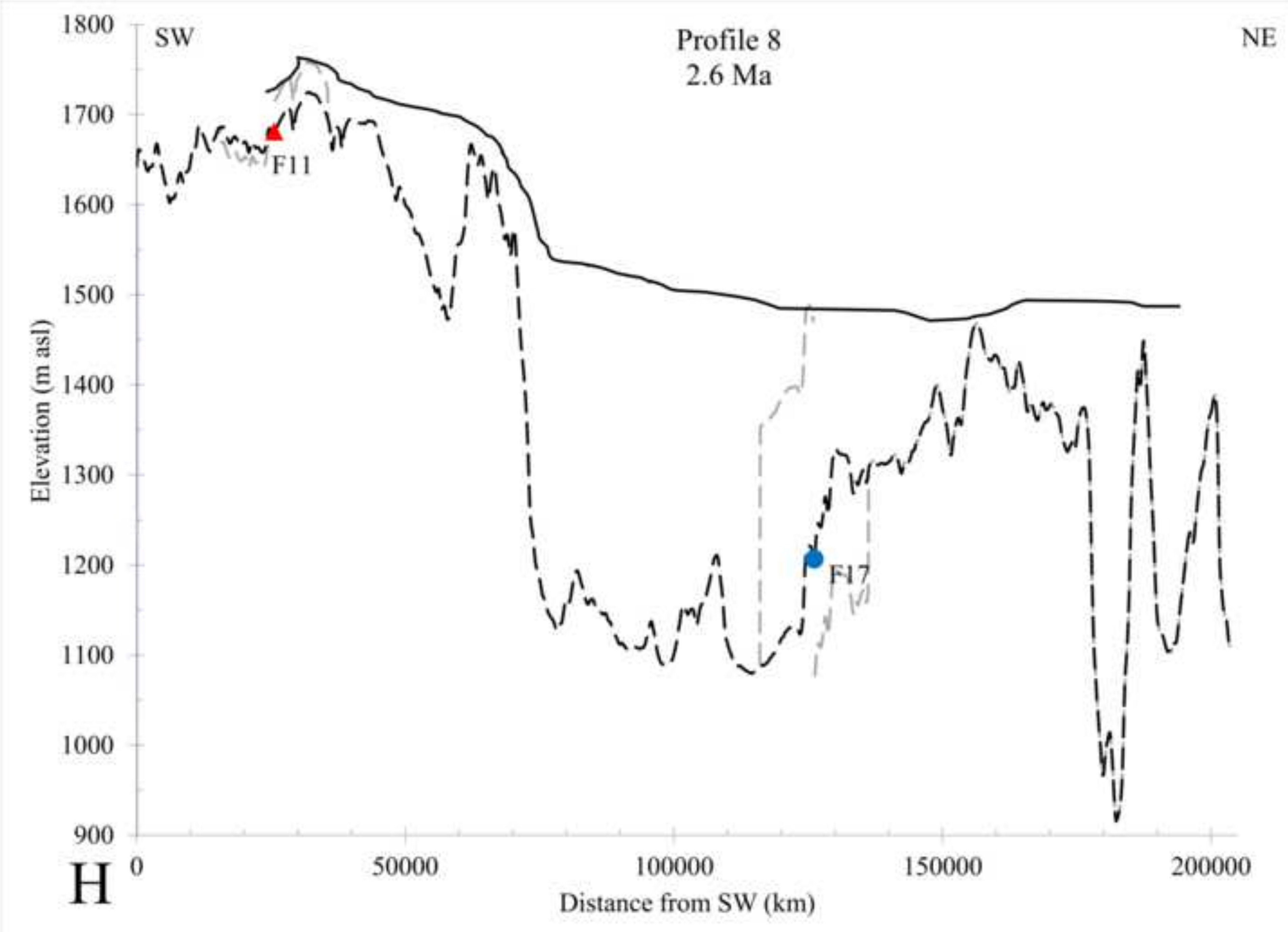

Figure (Color) Click here to access/download;Figure (Color);Figure 7a.png

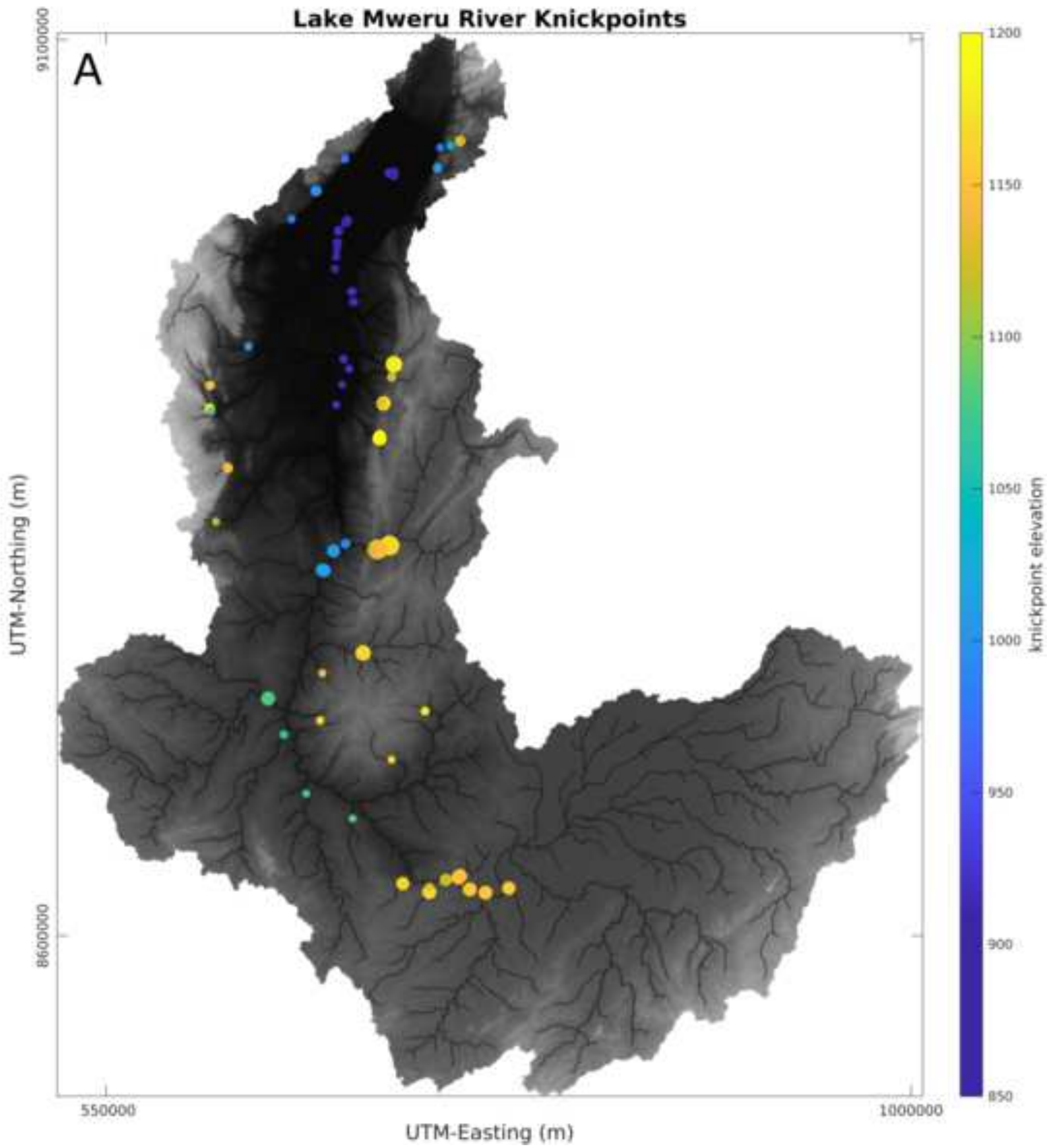

Figure (Color) Click here to access/download;Figure (Color);Figure 7b.png

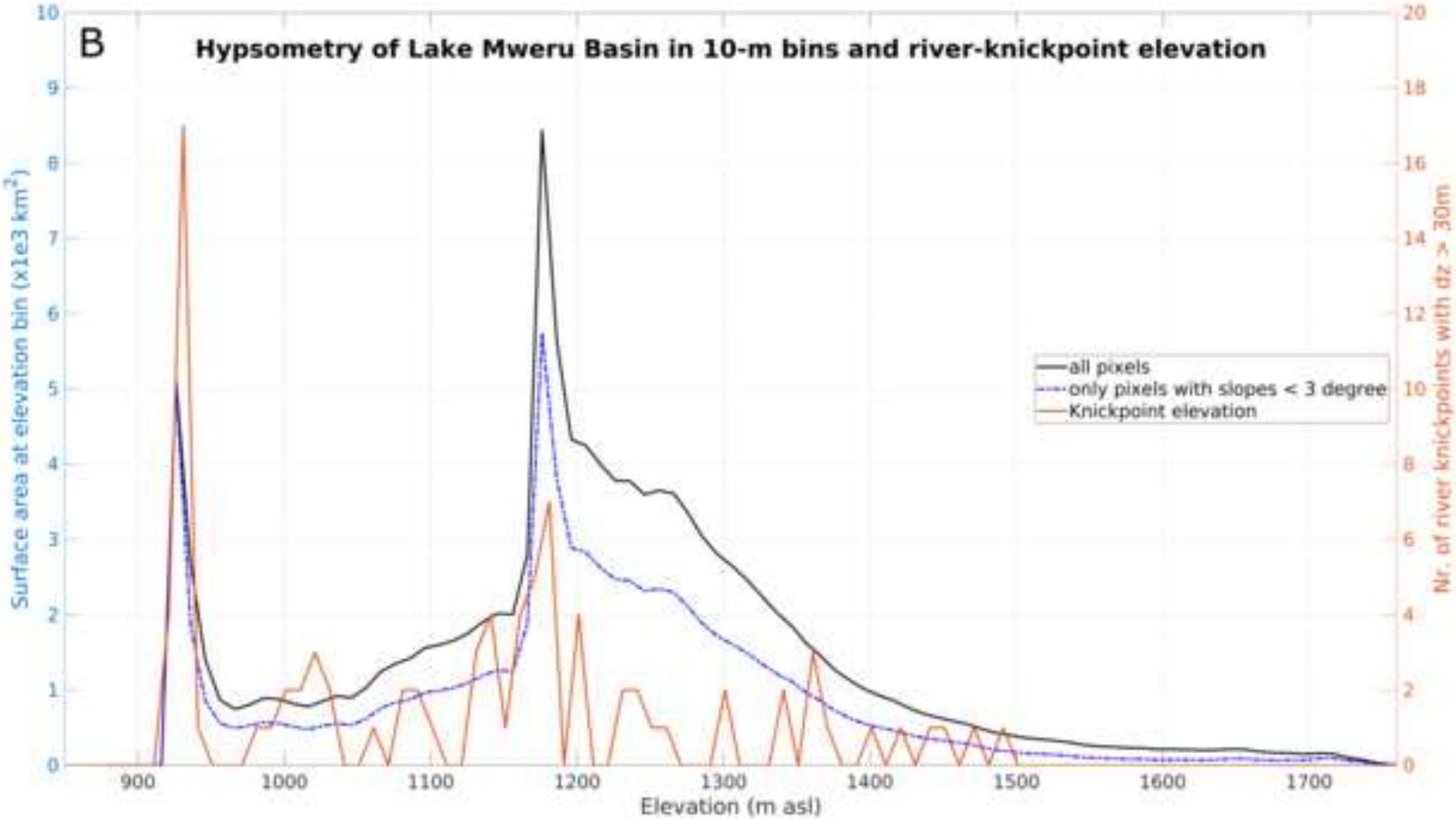

Figure (Color)

Click here to access/download;Figure (Color);Figure 8a.jpg

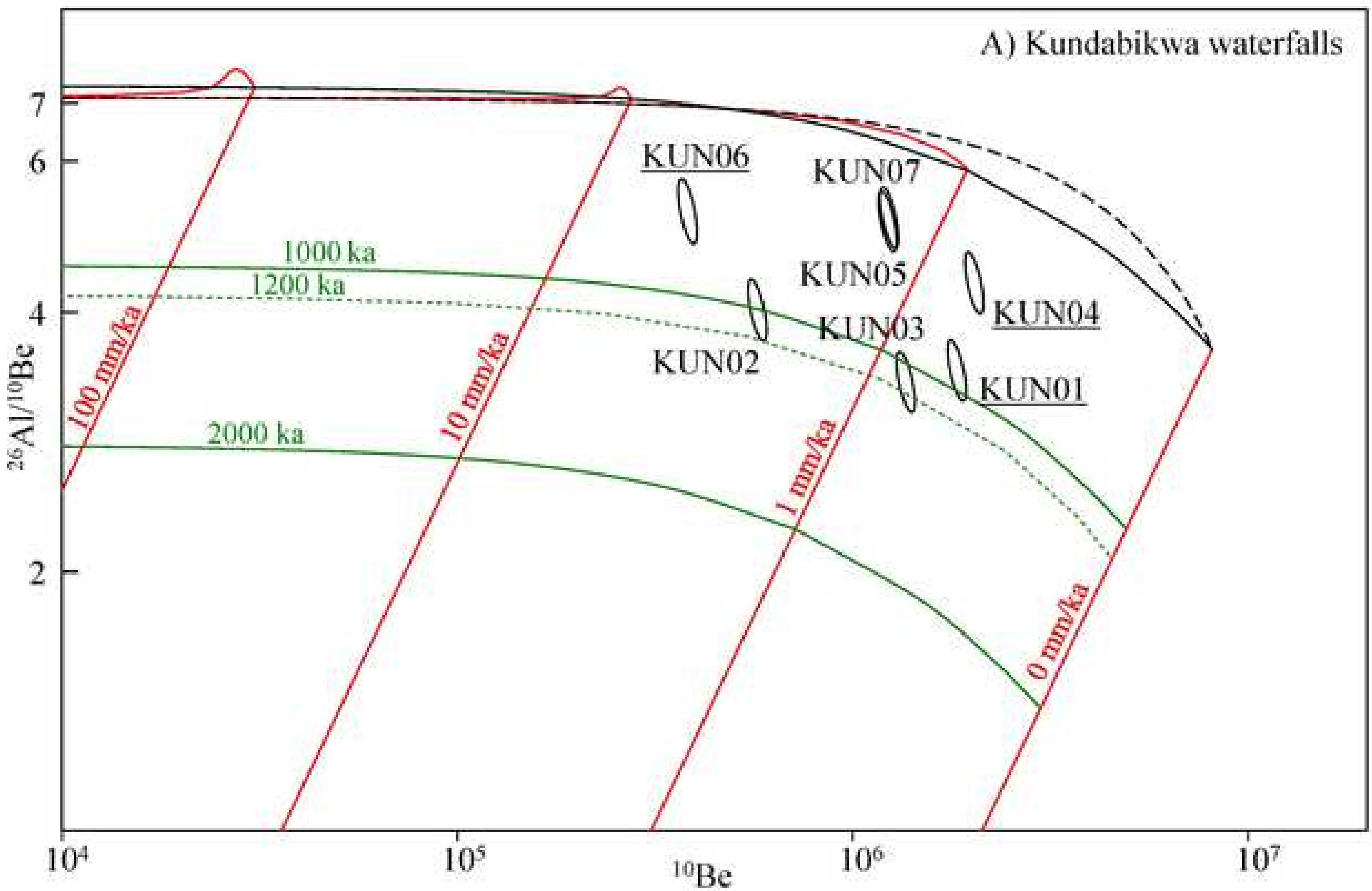

Figure (Color)

Click here to access/download;Figure (Color);Figure 8b.jpg

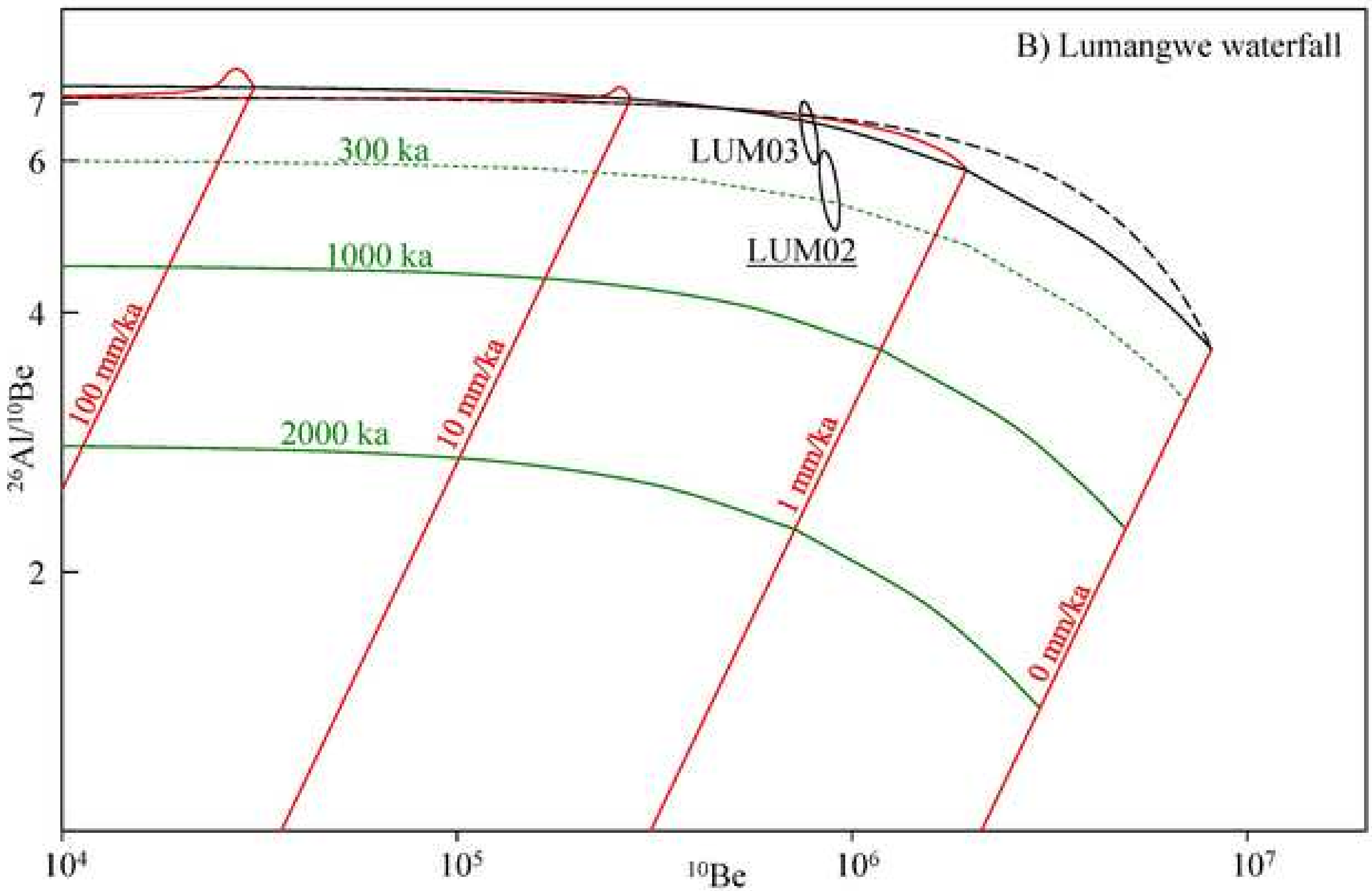

 

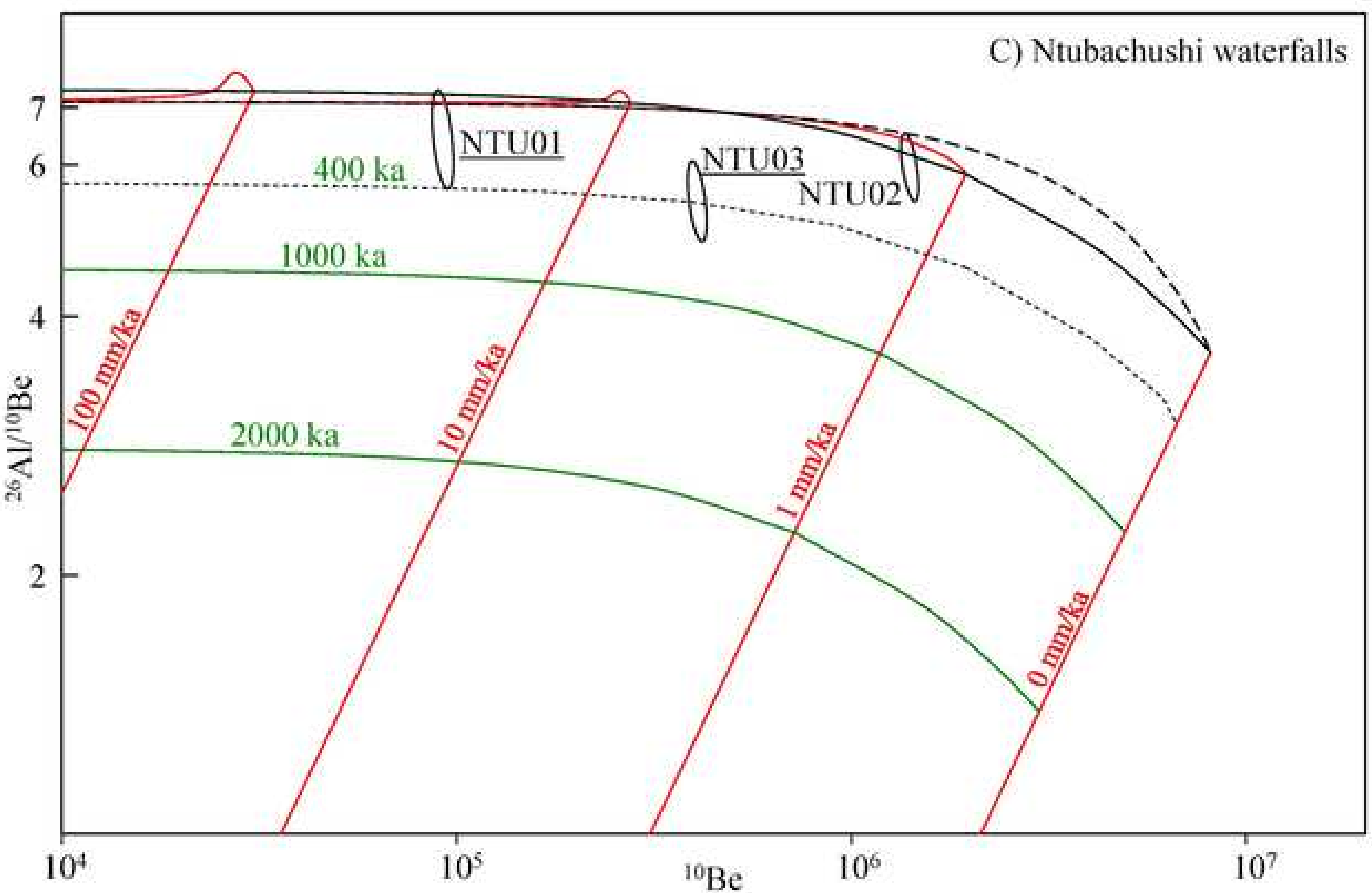
C) Ntubachushi waterfalls
NTU01
NTU03
NTU02
400 ka
1000 ka
2000 ka
100 mm/ka
10 mm/ka
1 mm/ka
0 mm/ka
7
6
4
2
$^{26}$Al/$^{10}$Be
$10^4$
$10^5$
$10^6$
$10^7$
$^{10}$Be

Figure (Color)

Click here to access/download;Figure (Color);Figure 8d.jpg

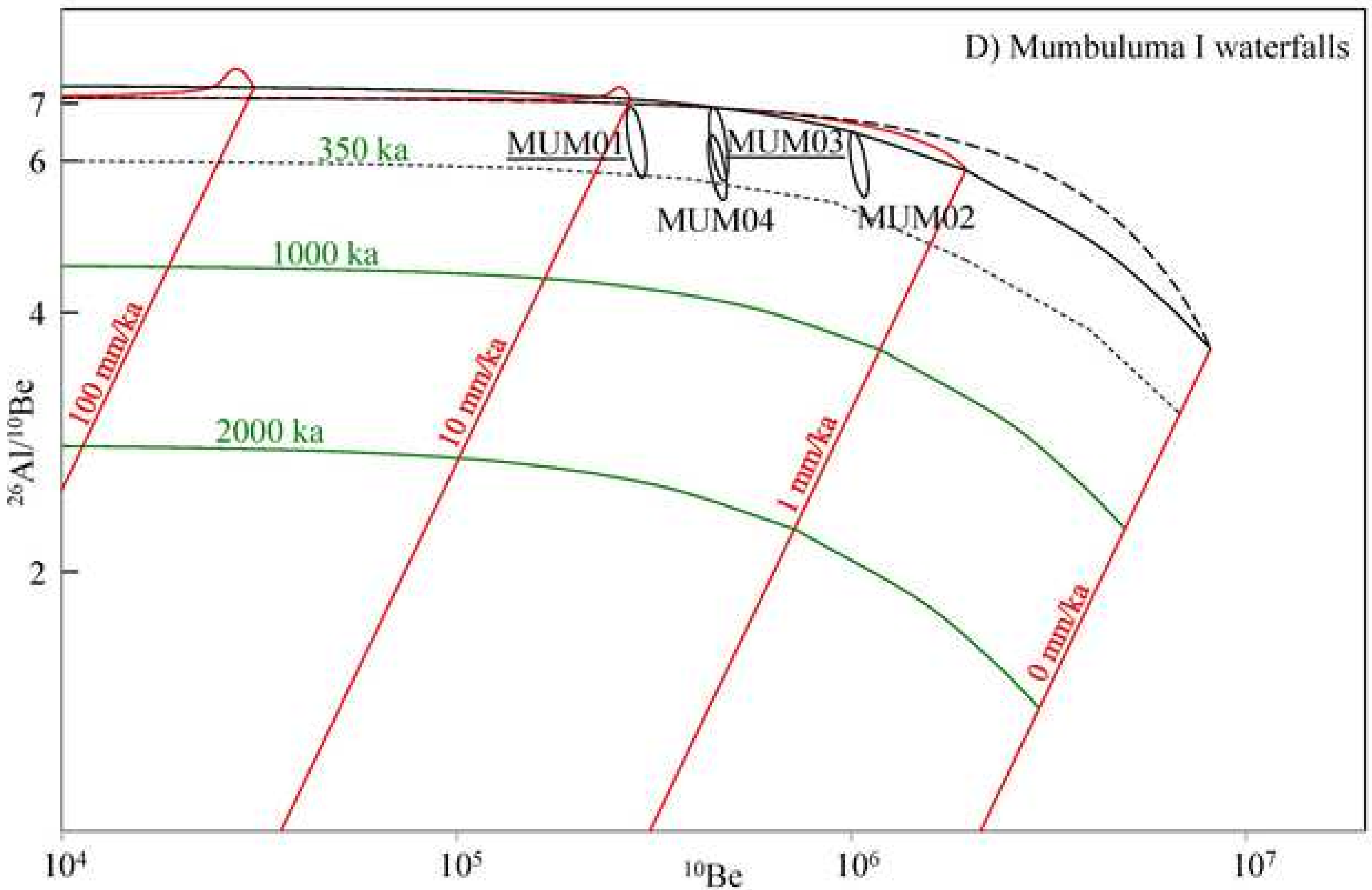

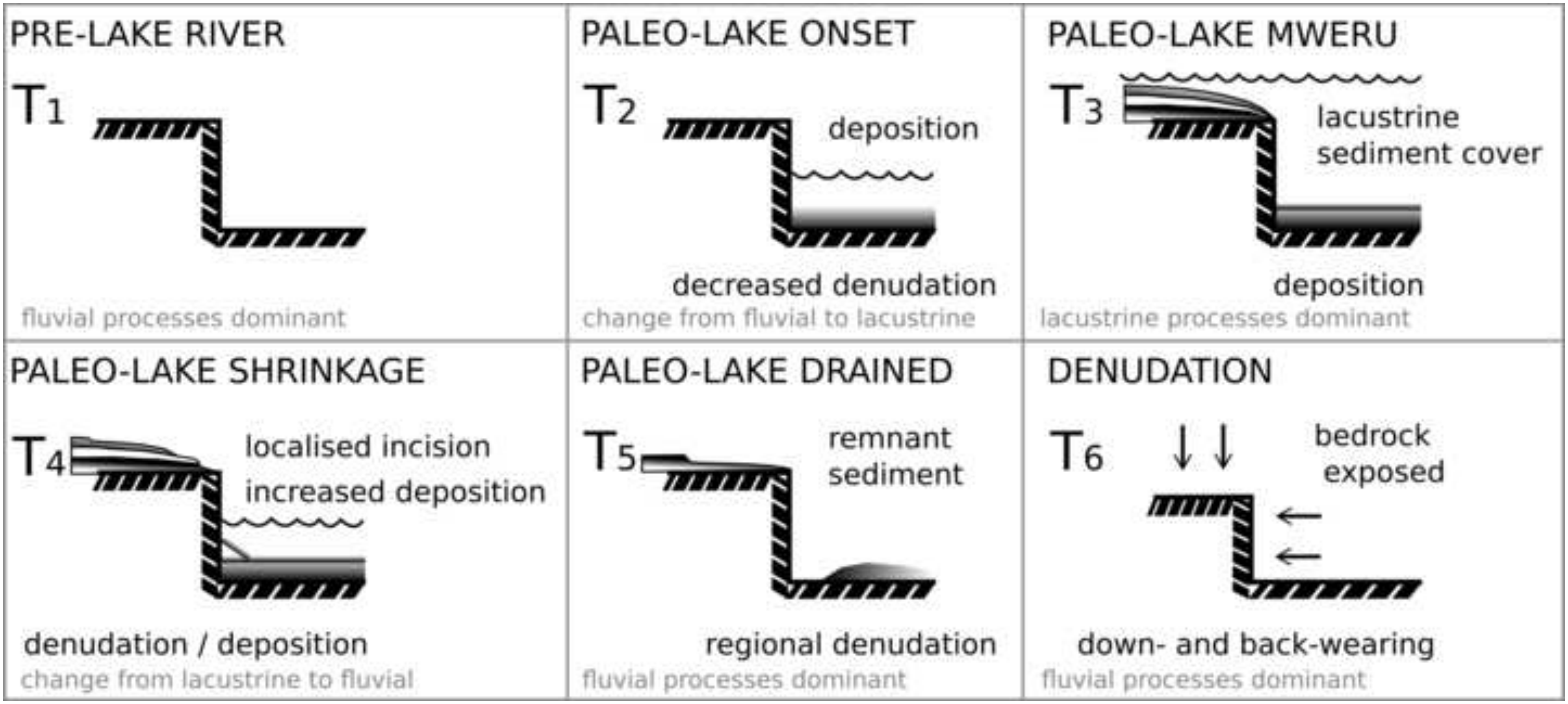
PRE-LAKE RIVER
T1
fluvial processes dominant
PALEO-LAKE ONSET
T2
deposition
decreased denudation
change from fluvial to lacustrine
PALEO-LAKE MWERU
T3
lacustrine sediment cover
deposition
lacustrine processes dominant
PALEO-LAKE SHRINKAGE
T4
localised incision
increased deposition
denudation / deposition
change from lacustrine to fluvial
PALEO-LAKE DRAINED
T5
remnant sediment
regional denudation
fluvial processes dominant
DENUDATION
T6
bedrock exposed
down- and back-wearing
fluvial processes dominant

Figure (Color) Click here to access/download;Figure (Color);Figure 10a.jpg

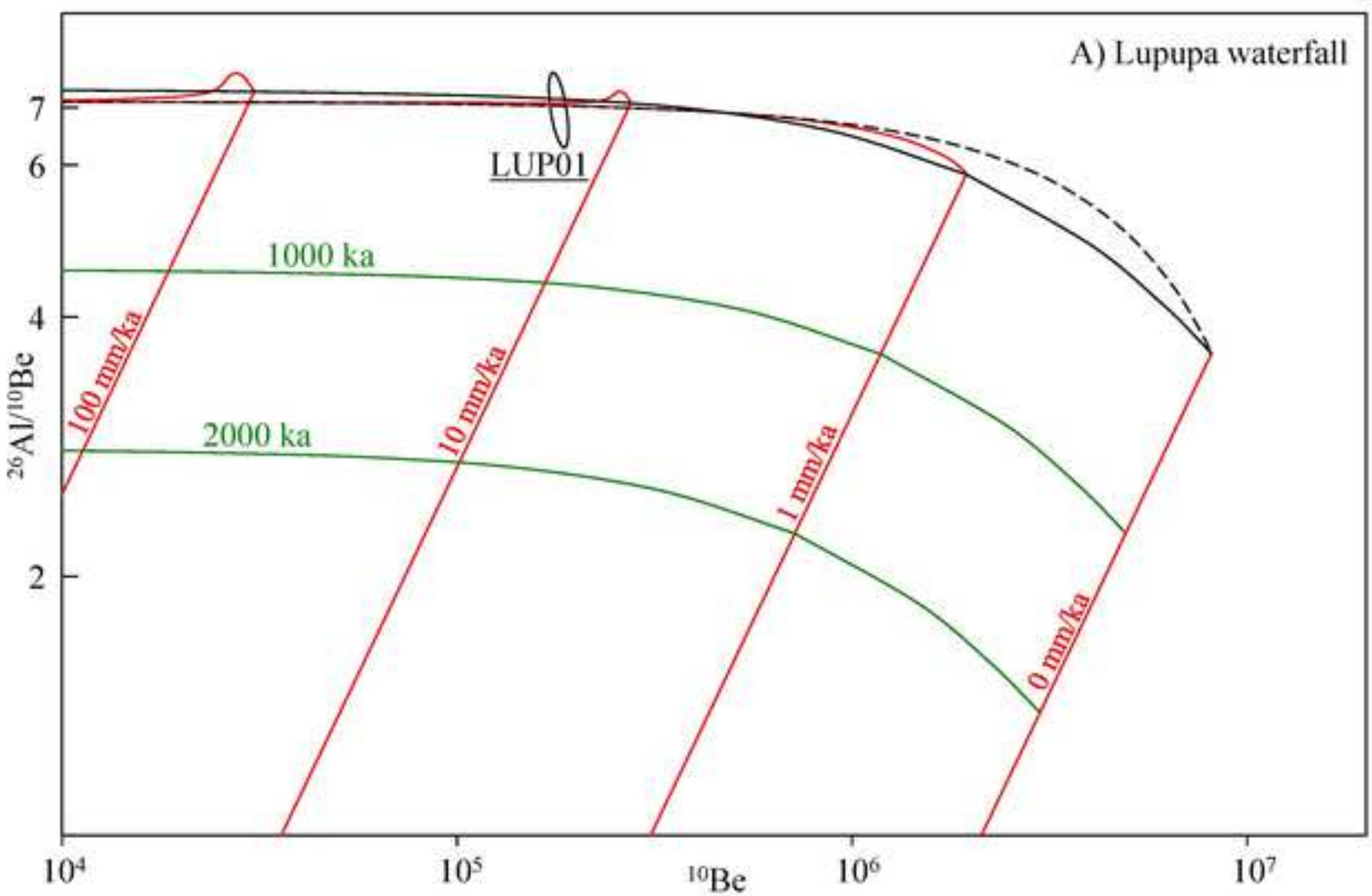

Figure (Color) Click here to access/download;Figure (Color);Figure 10b.jpg

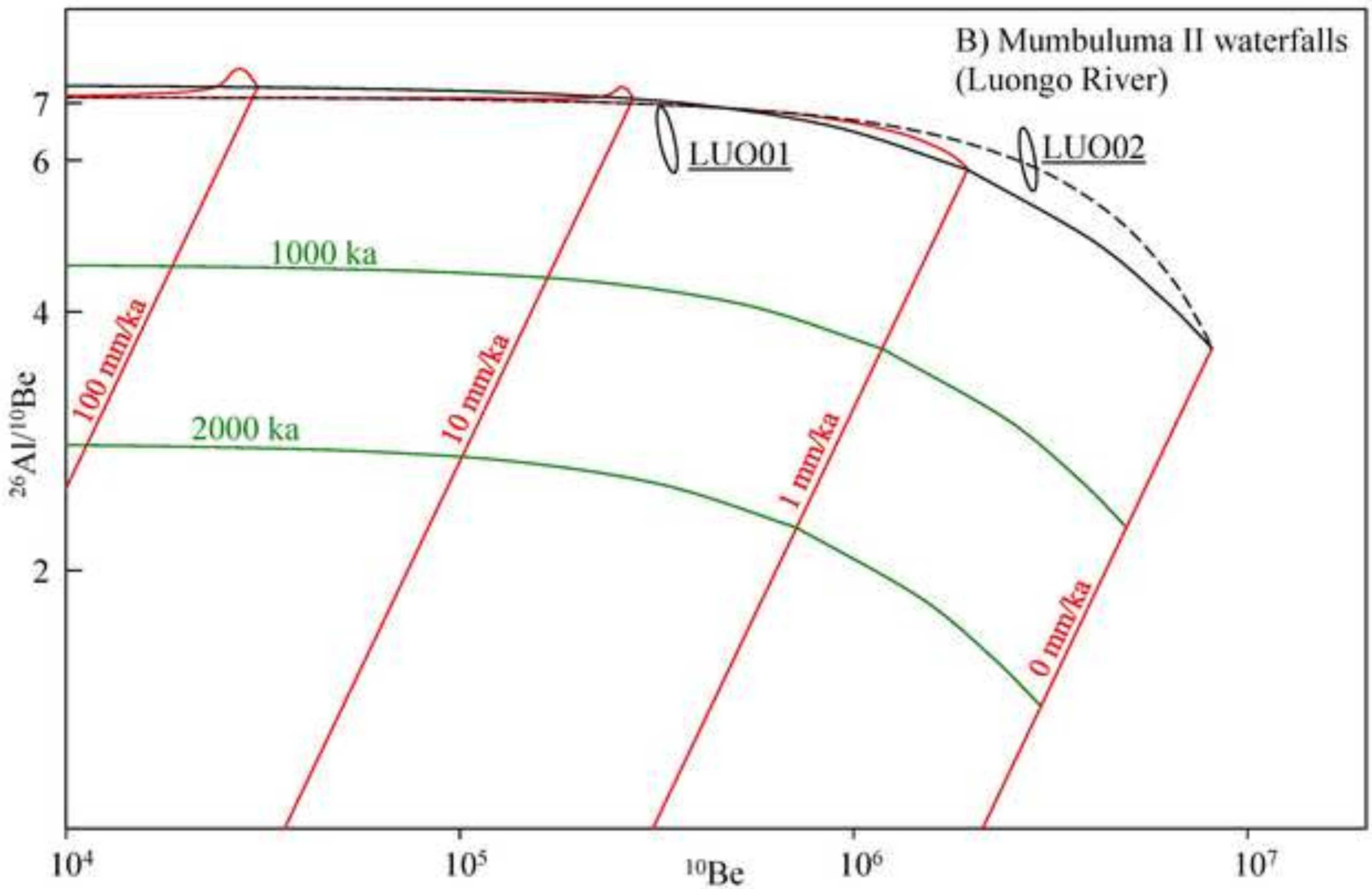

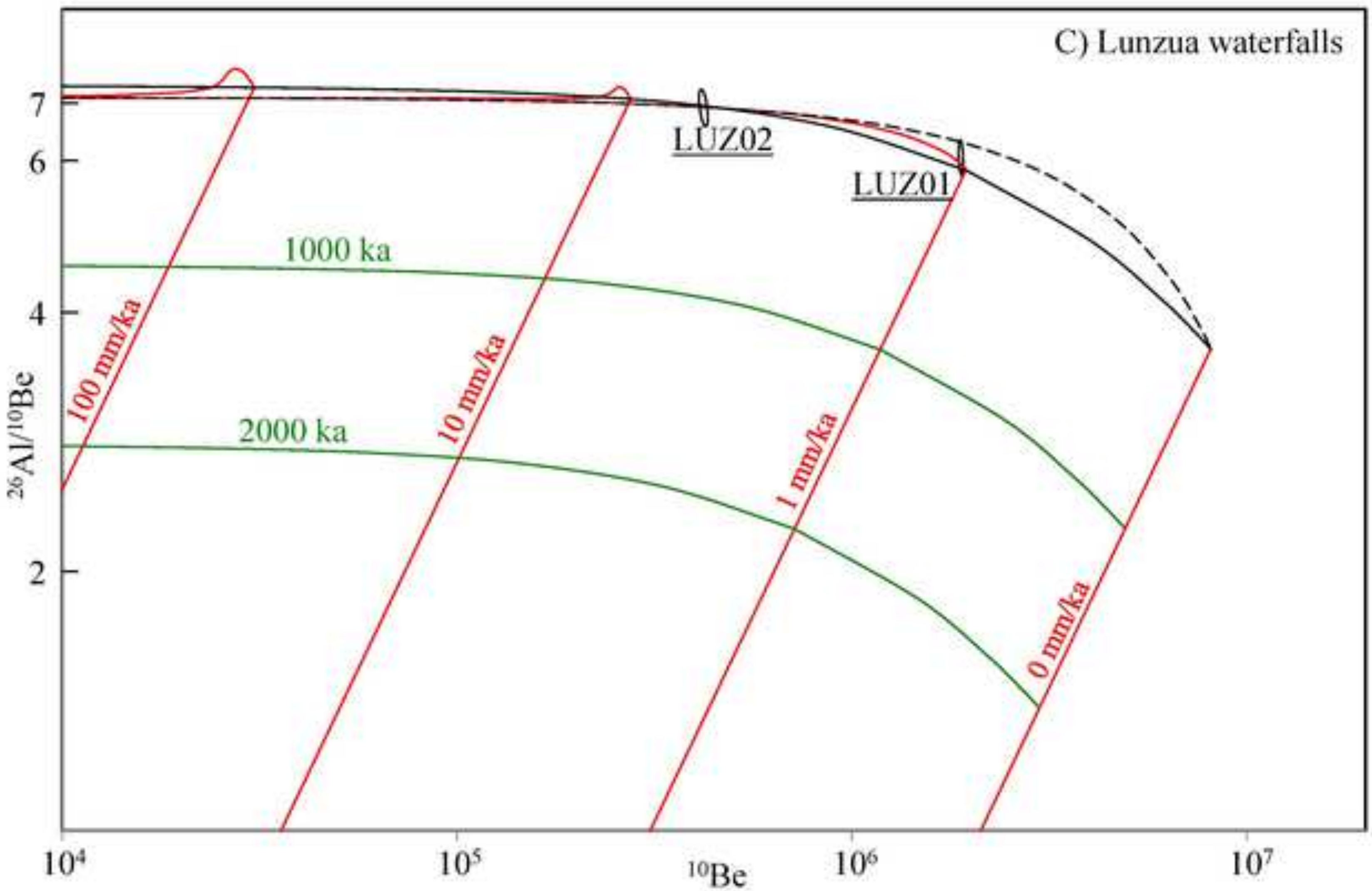
C) Lunzua waterfalls
7
6
4
2
$^{26}$Al/$^{10}$Be
LUZ02
LUZ01
1000 ka
2000 ka
100 mm/ka
10 mm/ka
1 mm/ka
0 mm/ka
10$^4$
10$^5$
10$^6$
10$^7$
$^{10}$Be

Figure (Color)

Click here to access/download;Figure (Color);Figure 11.jpg

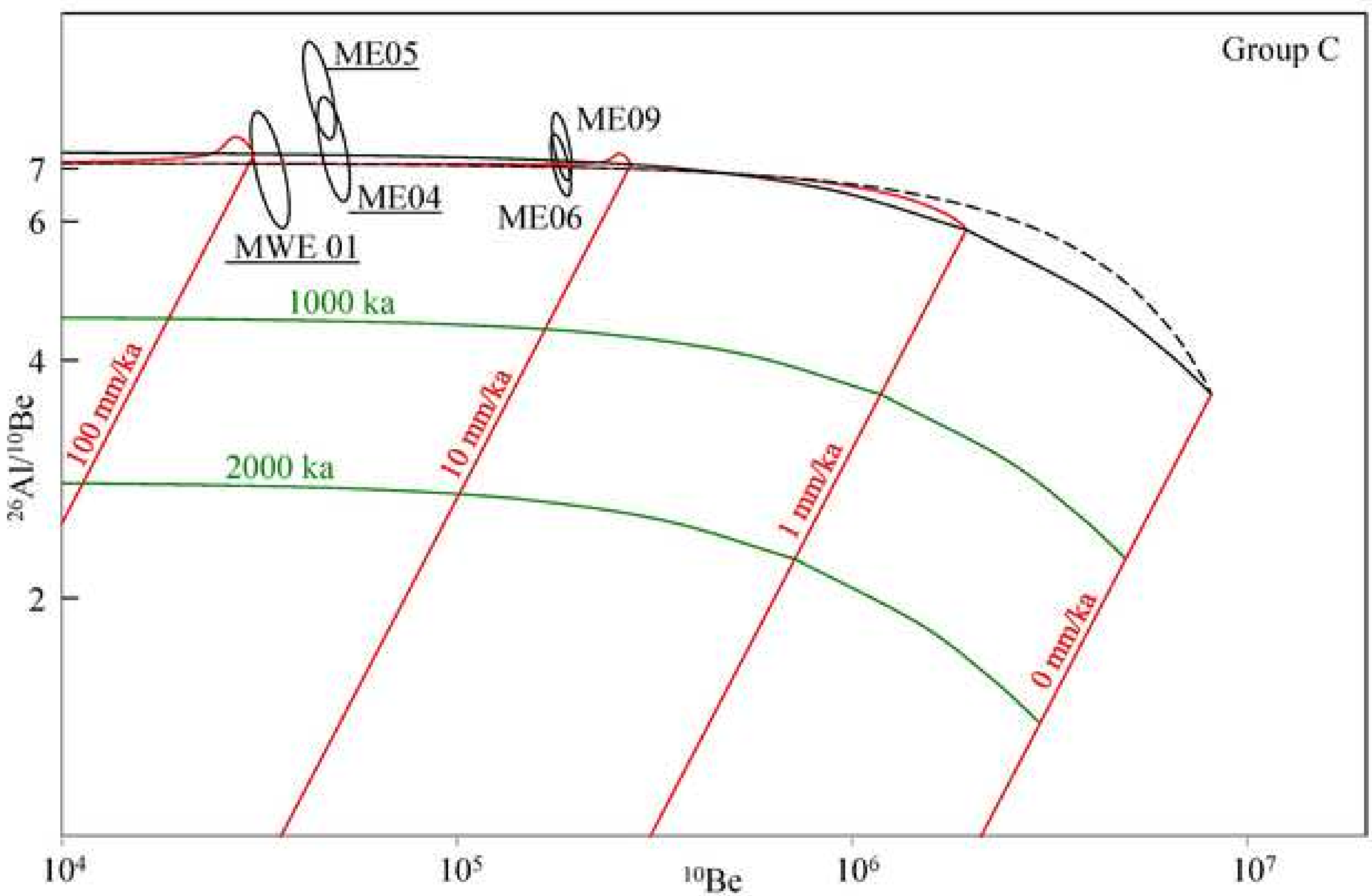

Figure (Color) Click here to access/download;Figure (Color);Figure 12.jpeg

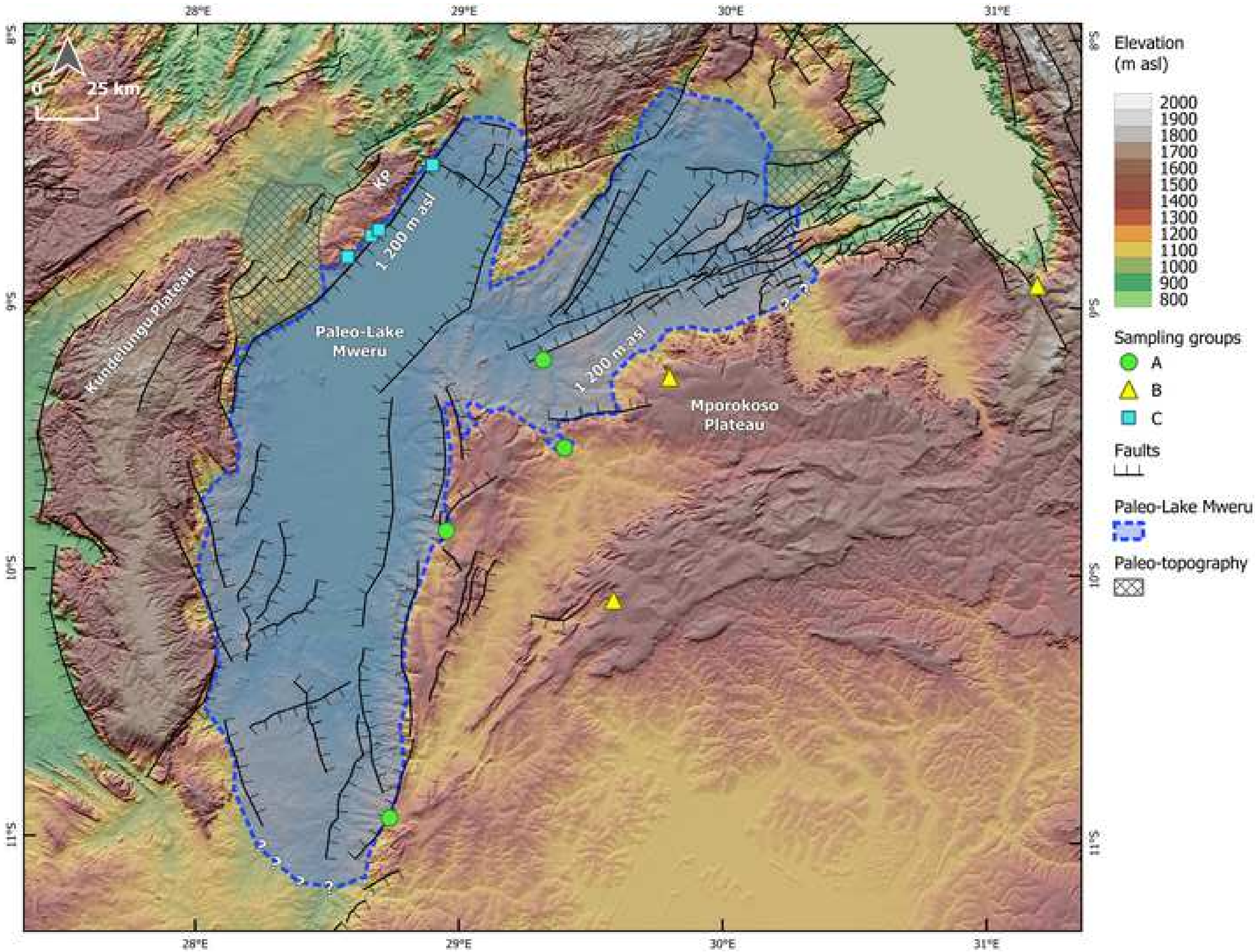

Figure (Greyscale) Click here to access/download;Figure (Greyscale);Figure 1_Greyscale.jpeg

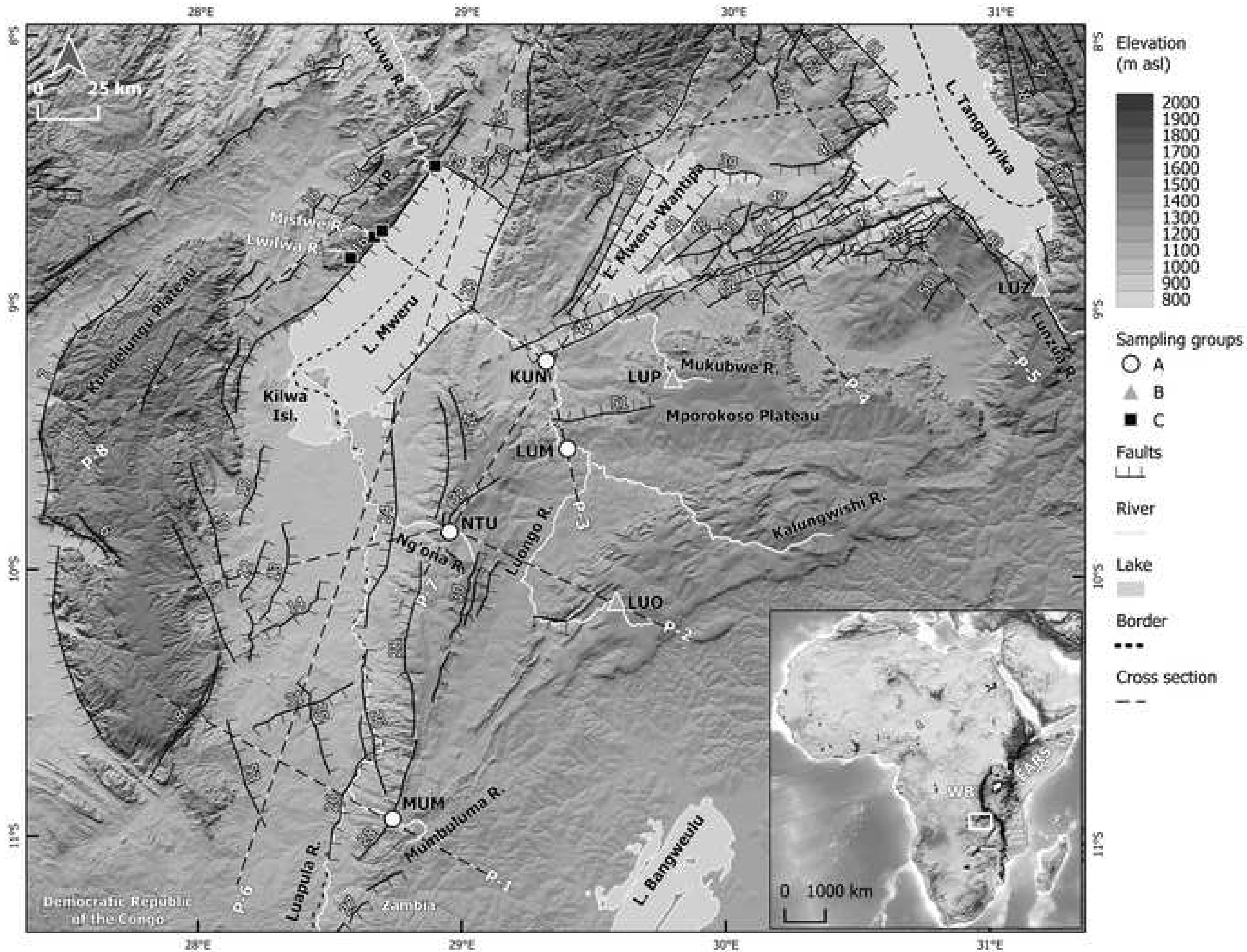

Figure (Greyscale)

Click here to access/download;Figure (Greyscale);Figure 2a_Greyscale.png

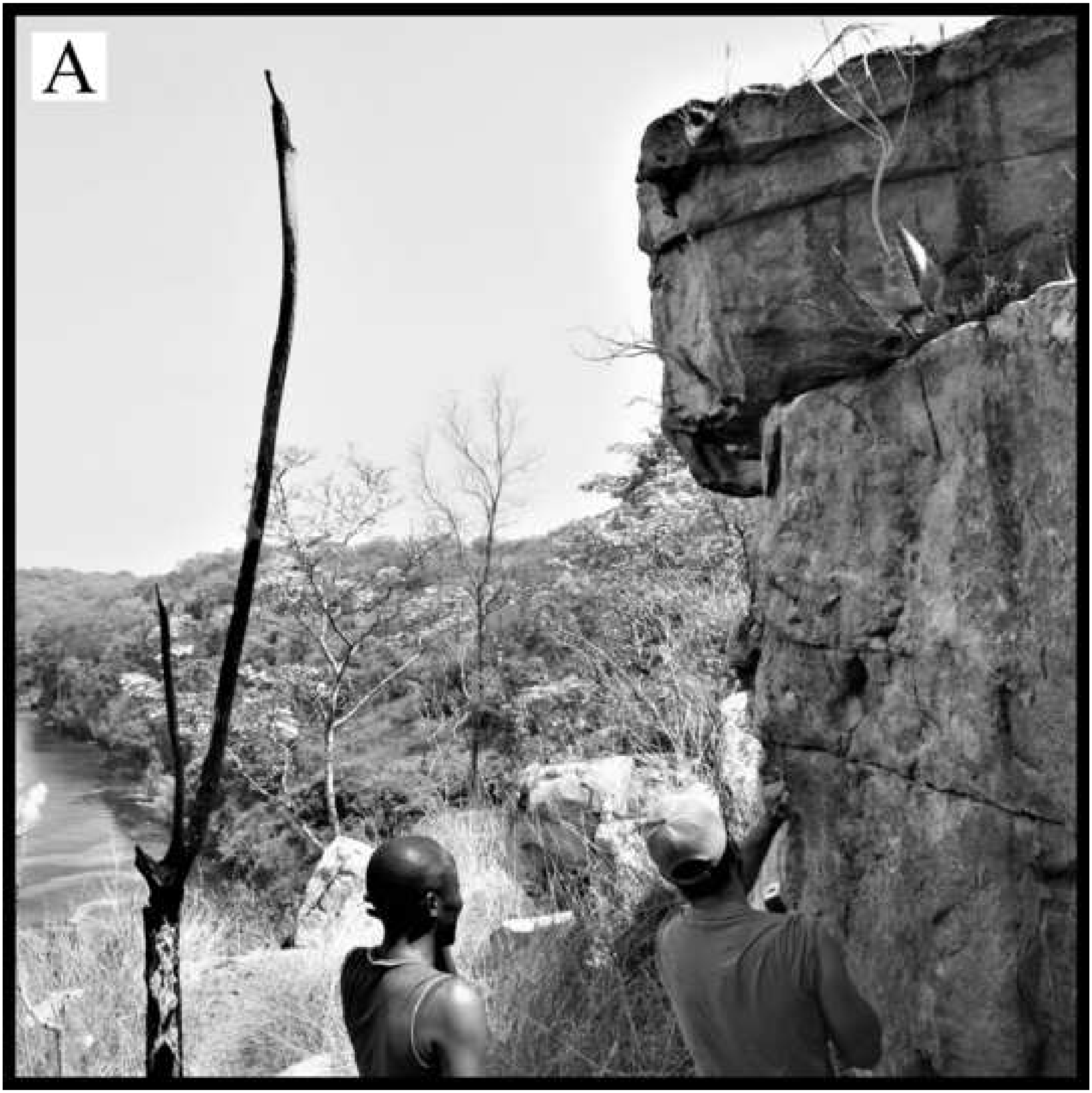

Figure (Greyscale)

Click here to access/download;Figure (Greyscale);Figure 2b_Greyscale.png

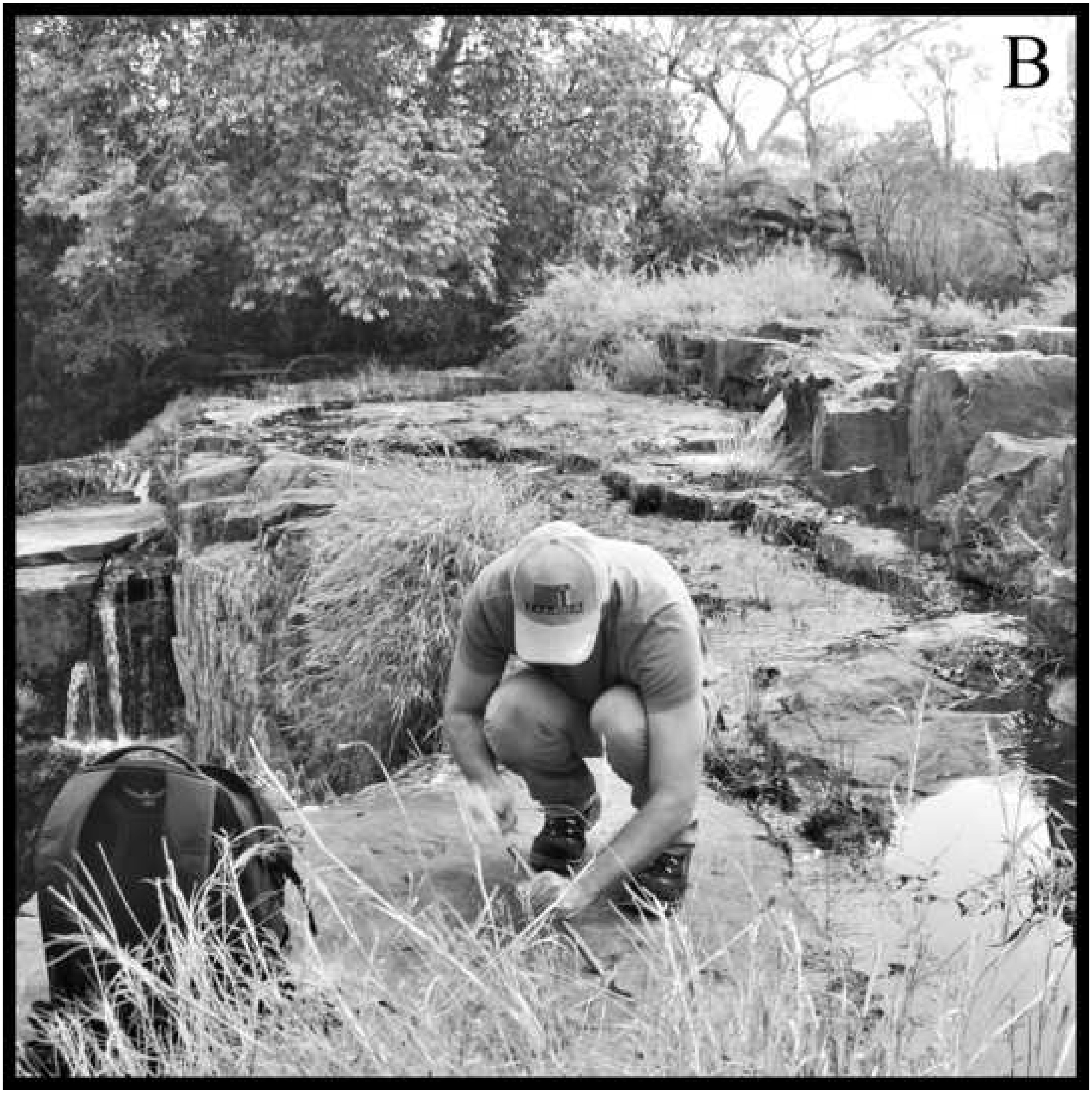

Figure (Greyscale)

Click here to access/download;Figure (Greyscale);Figure 2c_Greyscale.png

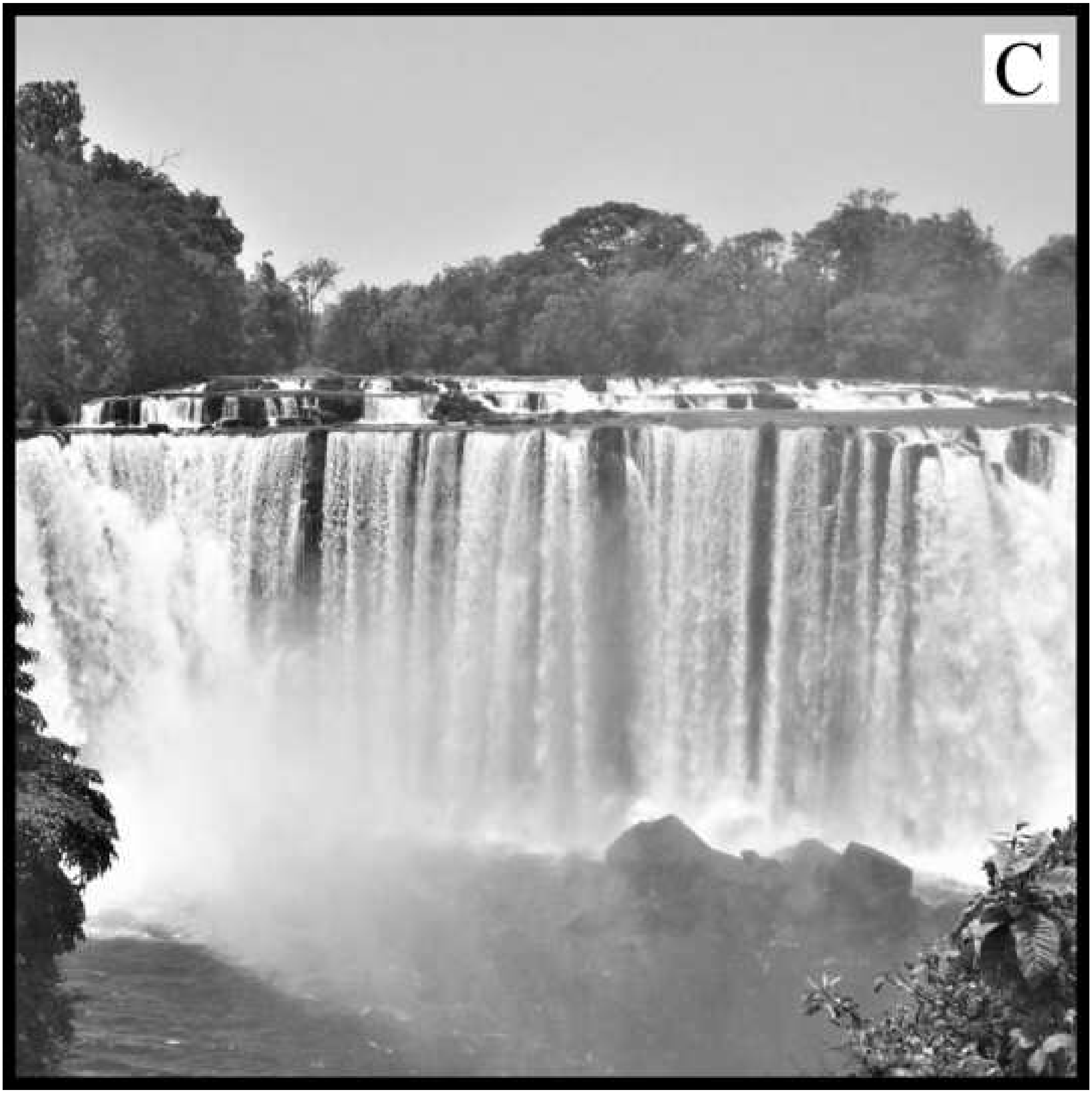

Figure (Greyscale)

Click here to access/download;Figure (Greyscale);Figure 2d_Greyscale.png

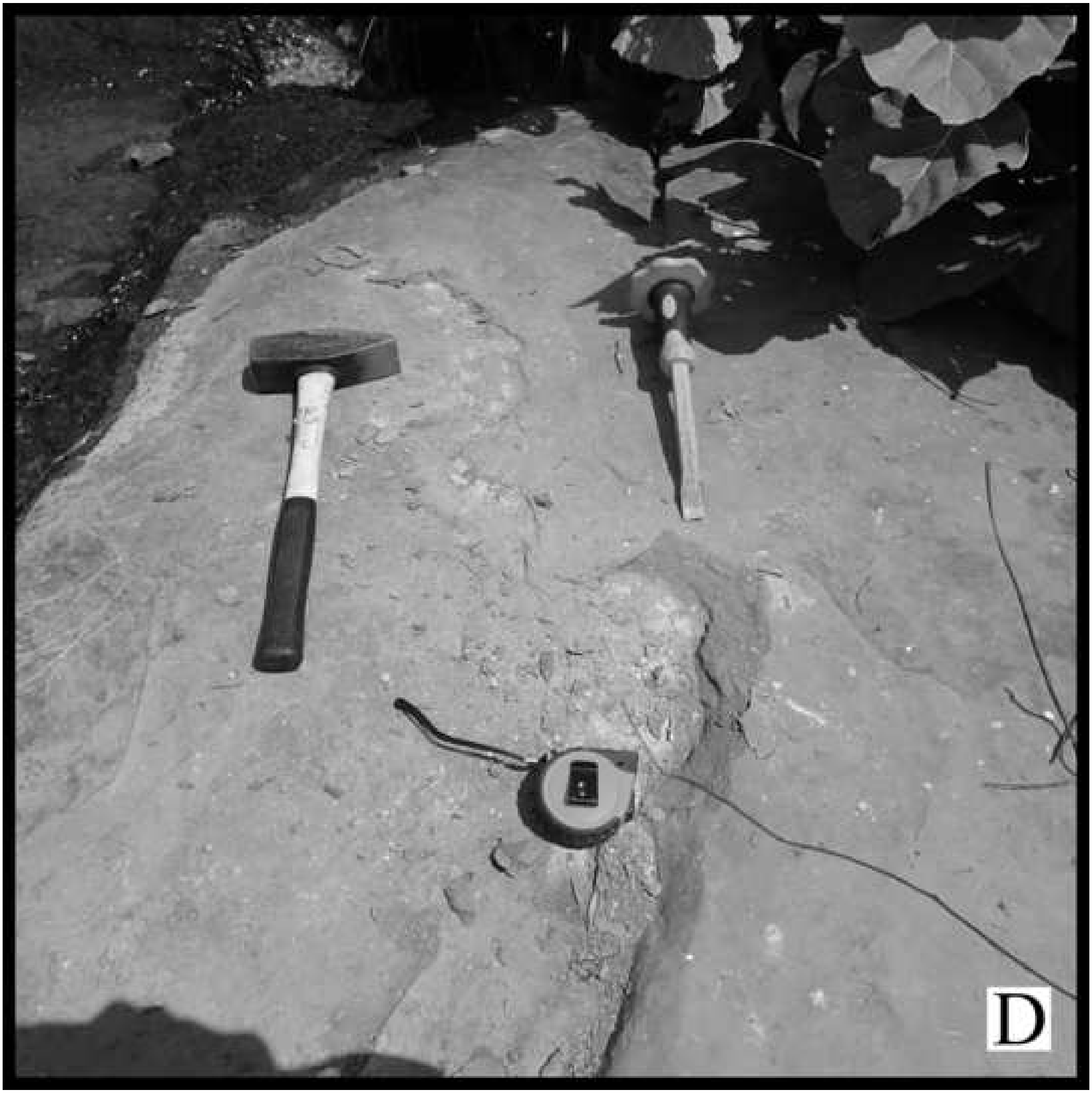

Figure (Greyscale)

Click here to access/download;Figure (Greyscale);Figure 2e_Greyscale.png

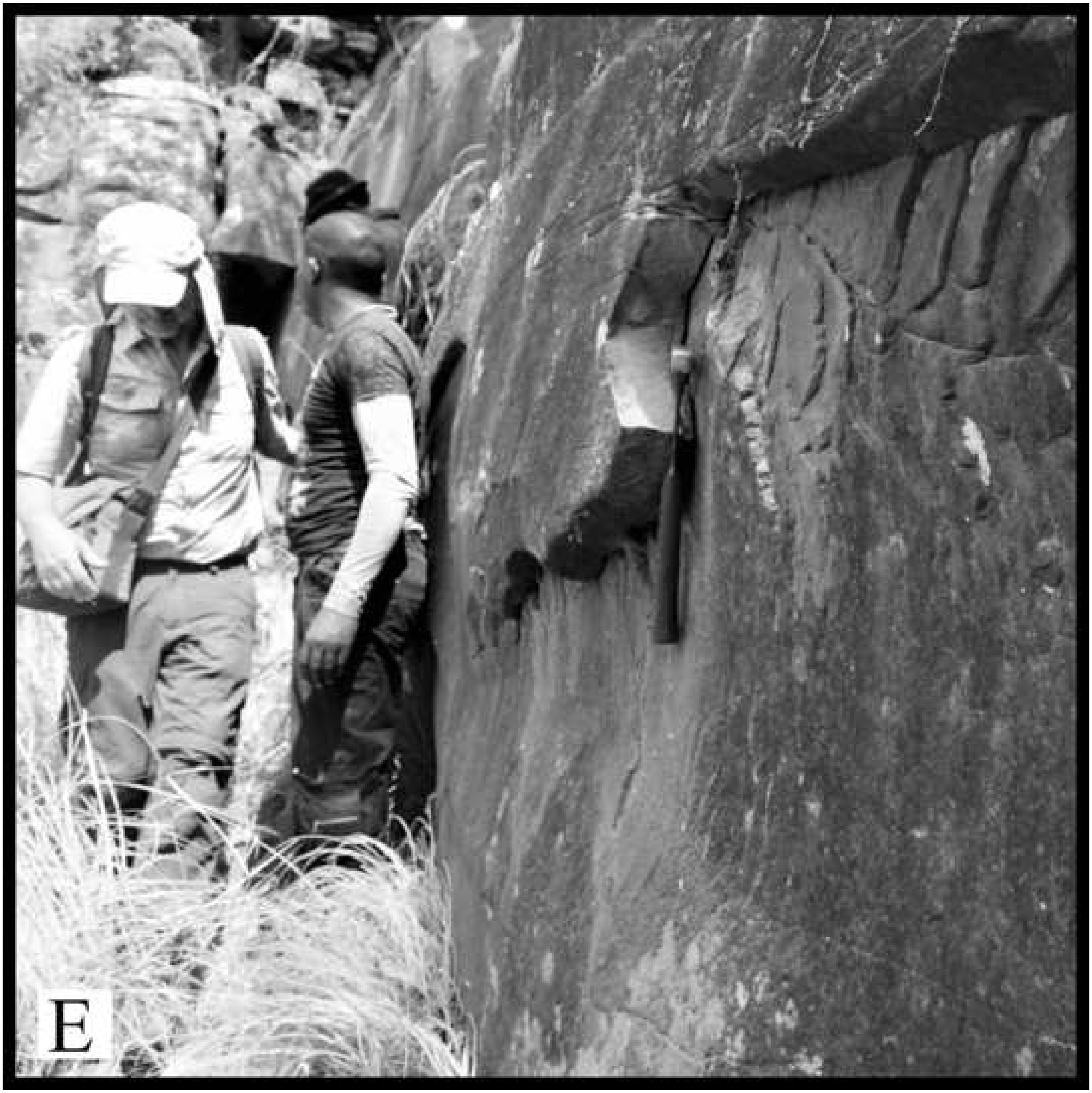

Figure (Greyscale)

Click here to access/download;Figure (Greyscale);Figure 3abc_Greyscale.png

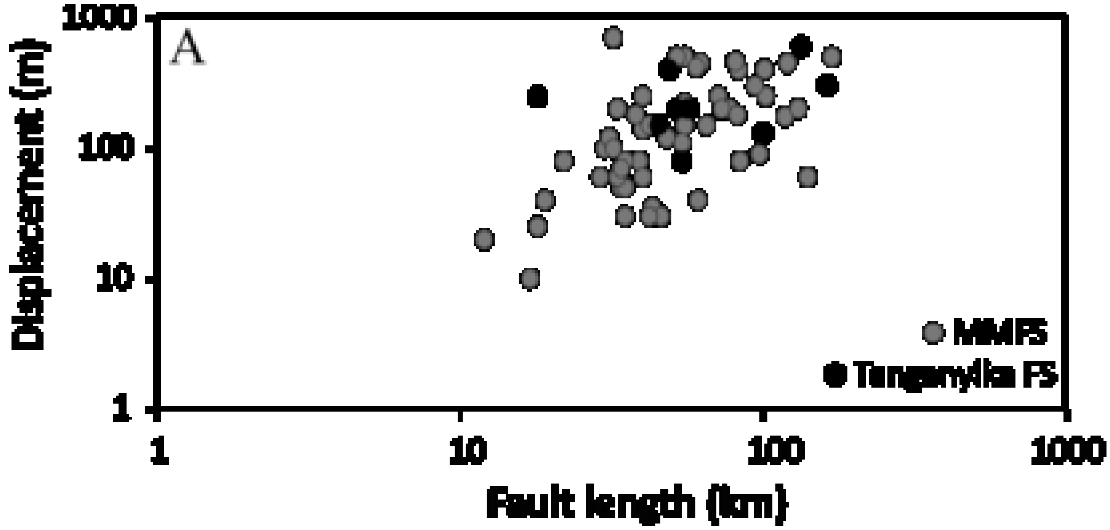


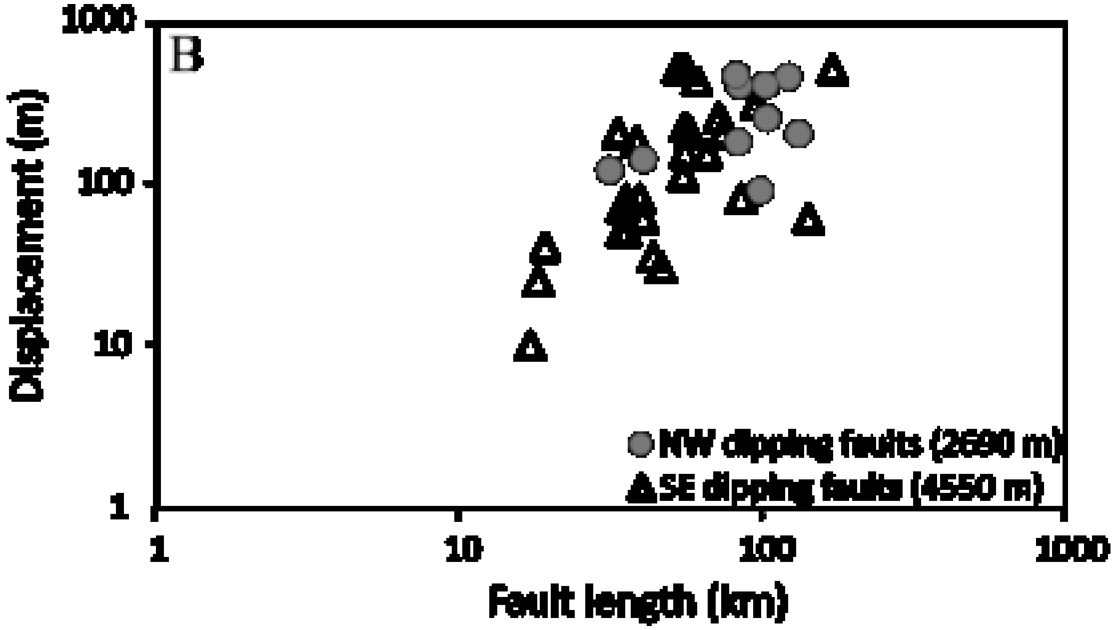


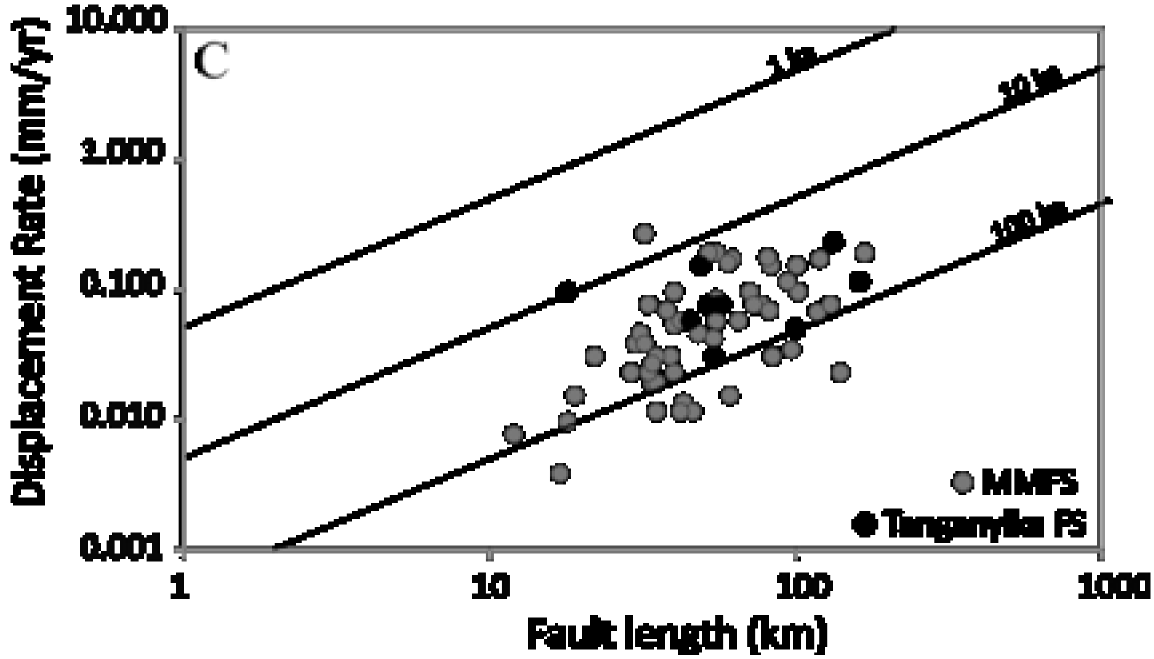

Figure (Greyscale)

Click here to access/download;Figure (Greyscale);Figure 3d_Greyscale.png

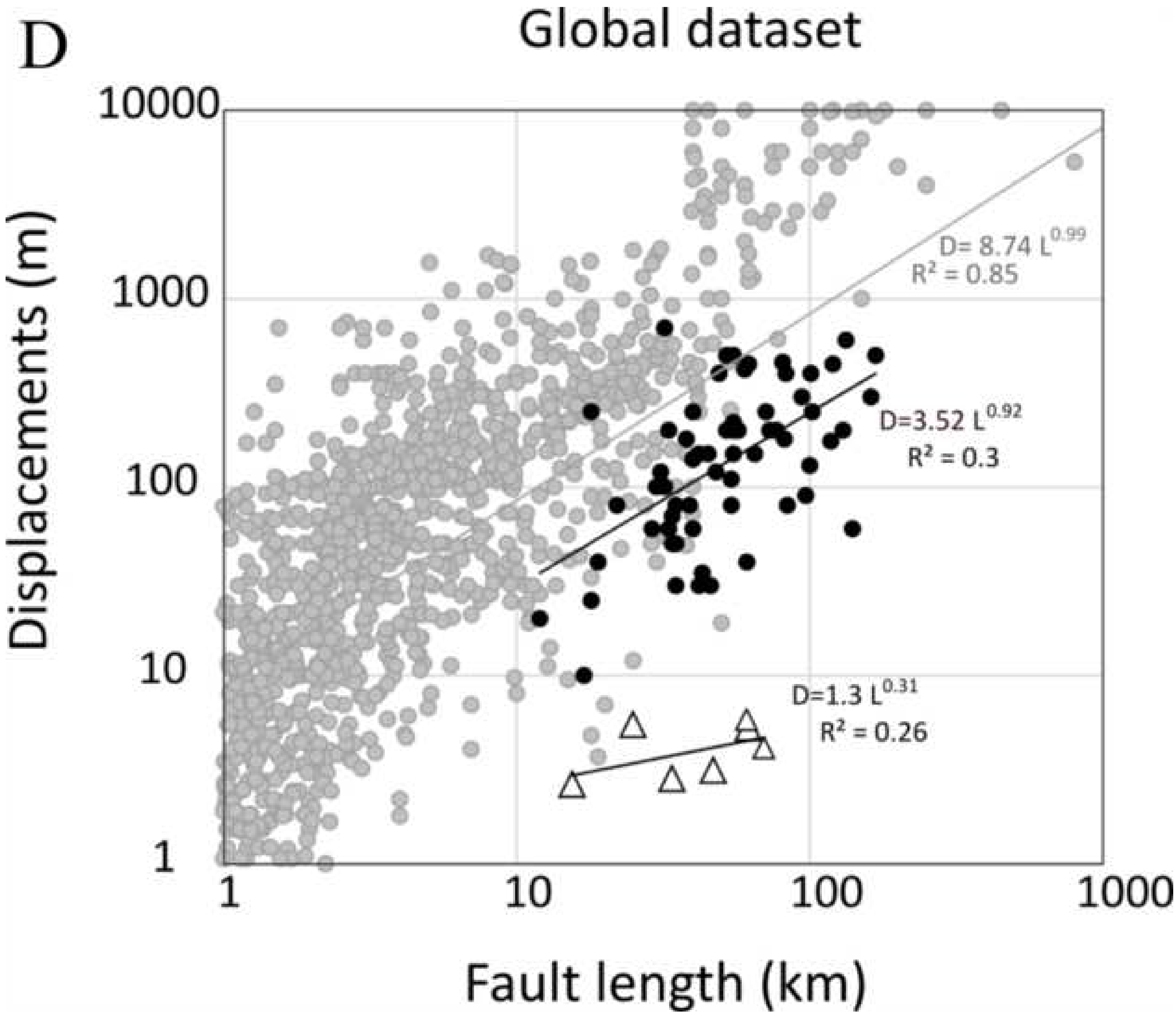

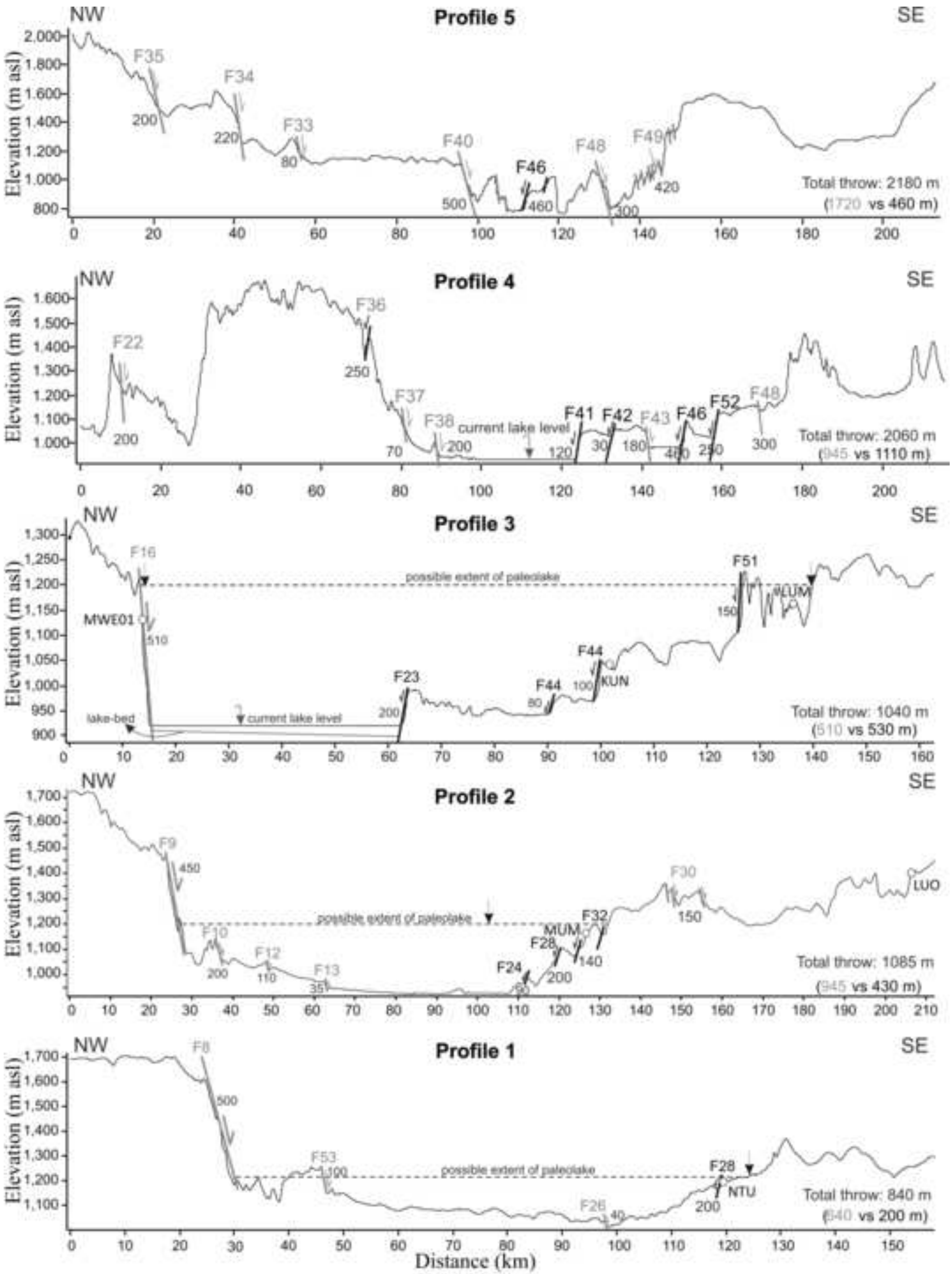
Profile 5
NW
SE
Elevation (m asl)
F35
F34
F33
F40
F46
F48
F49
200
220
80
500
460
300
420
Total throw: 2180 m
(1720 vs 460 m)
Profile 4
F22
F36
F37
F38
F41
F42
F43
F46
F52
F48
current lake level
250
70
200
120
30
180
460
250
300
Total throw: 2060 m
(945 vs 1110 m)
Profile 3
F16
F51
F23
F44
possible extent of paleolake
MWE01
510
LUM
150
KUN
100
80
lake-bed
current lake level
200
Total throw: 1040 m
(510 vs 530 m)
Profile 2
F9
F10
F12
F13
F24
F28
F32
F30
450
possible extent of paleolake
MUM
200
110
35
60
200
140
150
LUO
Total throw: 1085 m
(945 vs 430 m)
Profile 1
F8
F53
F26
F28
500
100
possible extent of paleolake
NTU
200
40
Total throw: 840 m
(640 vs 200 m)
Distance (km)

Figure (Greyscale) Click here to access/download;Figure (Greyscale);Figure 5_Greyscale.png

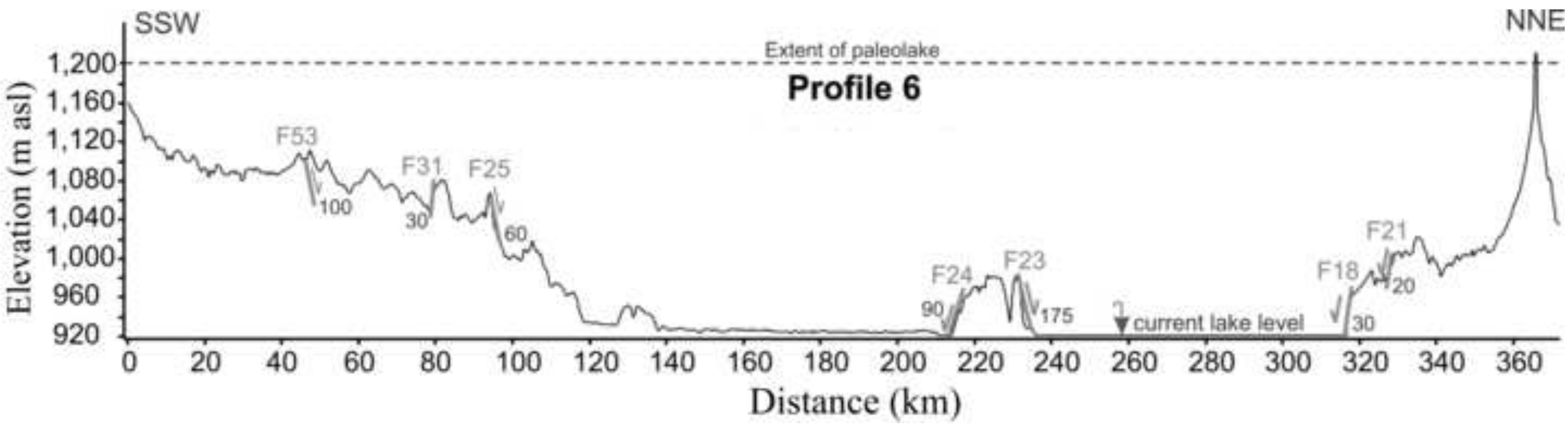

Figure (Greyscale)

Click here to access/download;Figure (Greyscale);Figure 7a_Greyscale.png

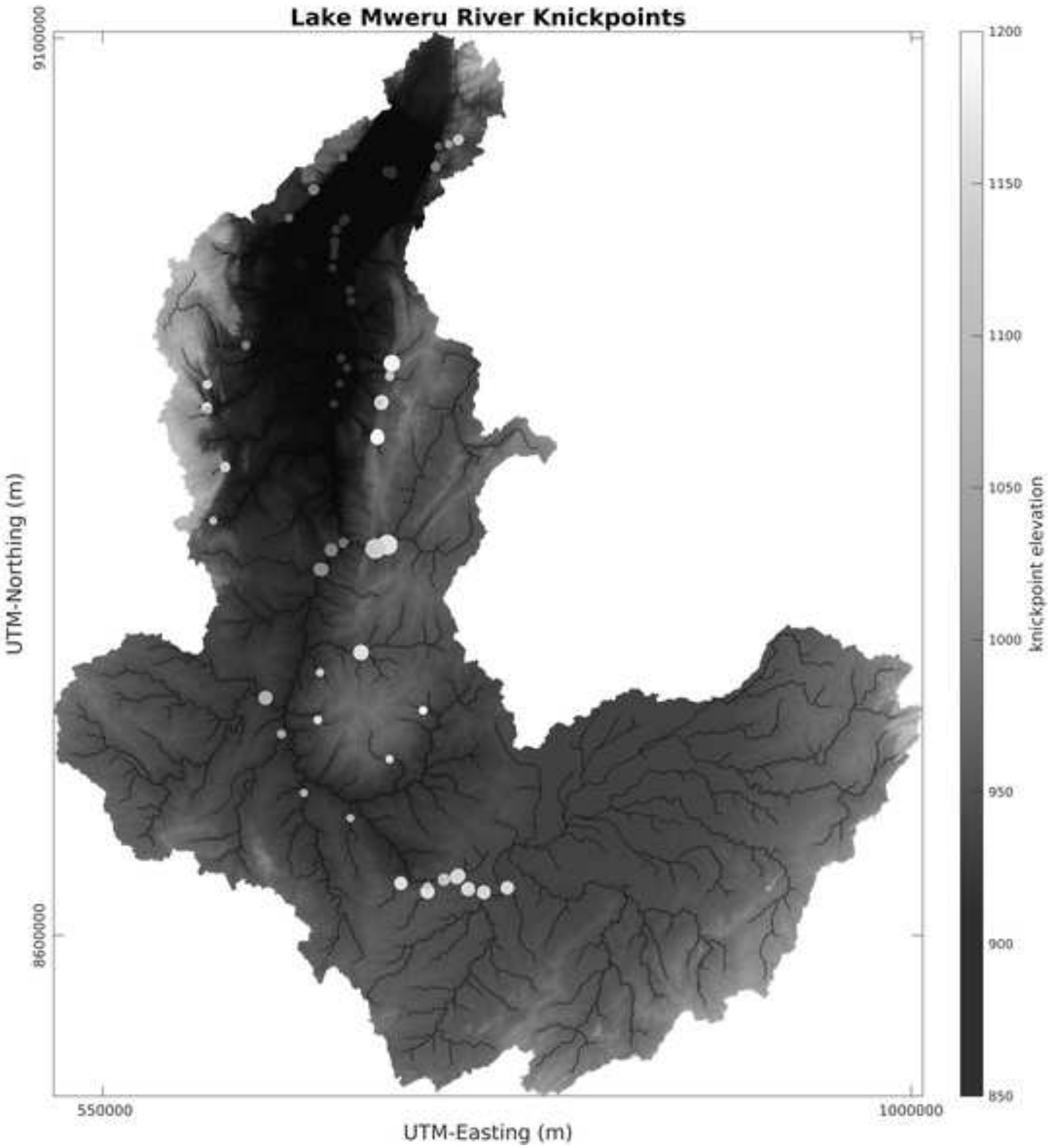

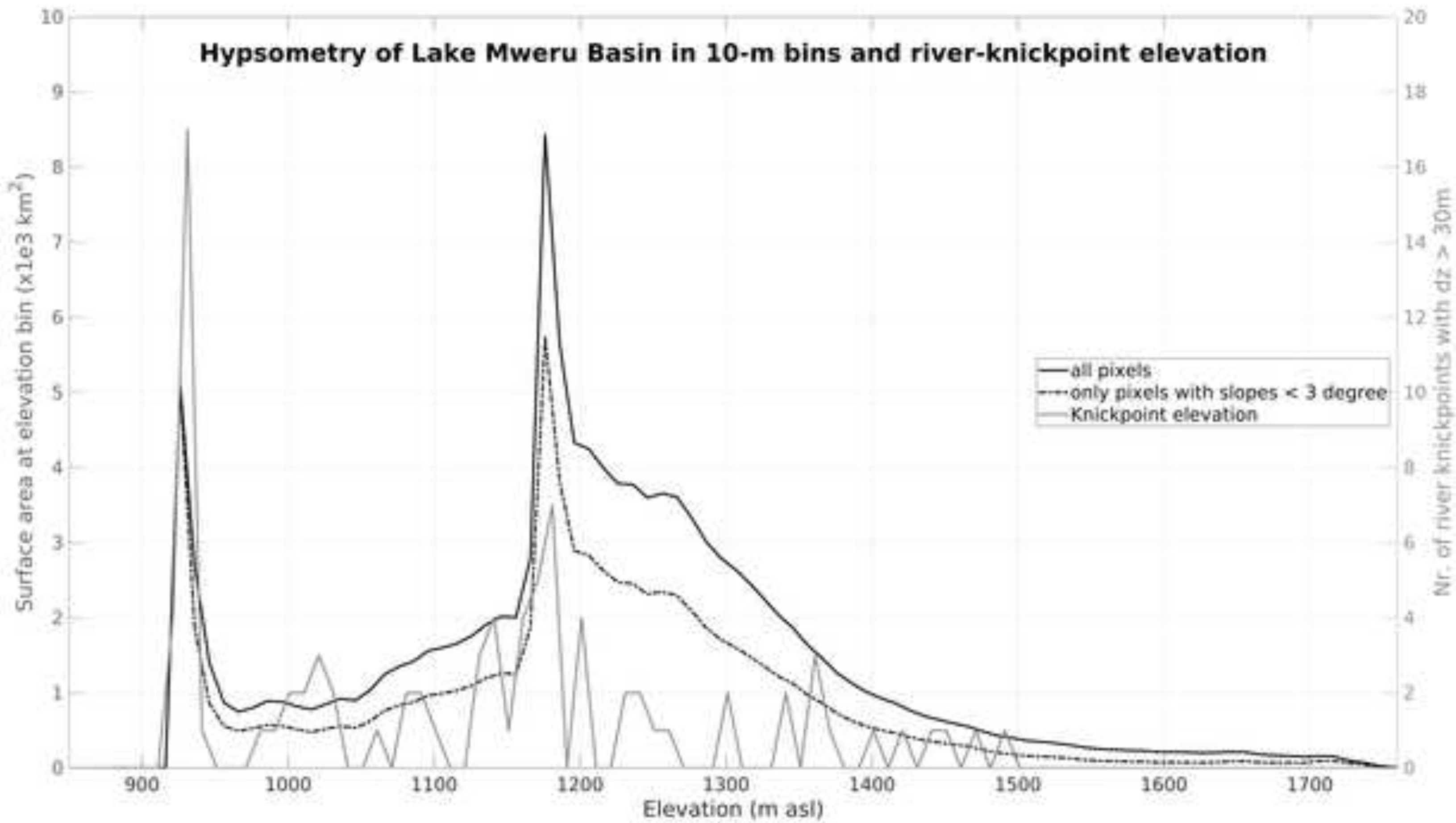

Hypsometry of Lake Mweru Basin in 10-m bins and river-knickpoint elevation
all pixels
only pixels with slopes < 3 degree
Knickpoint elevation
Surface area at elevation bin (x1e3 km²)
Nr. of river knickpoints with dz > 30m
Elevation (m asl)
0
1
2
3
4
5
6
7
8
9
10
900
1000
1100
1200
1300
1400
1500
1600
1700
0
2
4
6
8
10
12
14
16
18
20

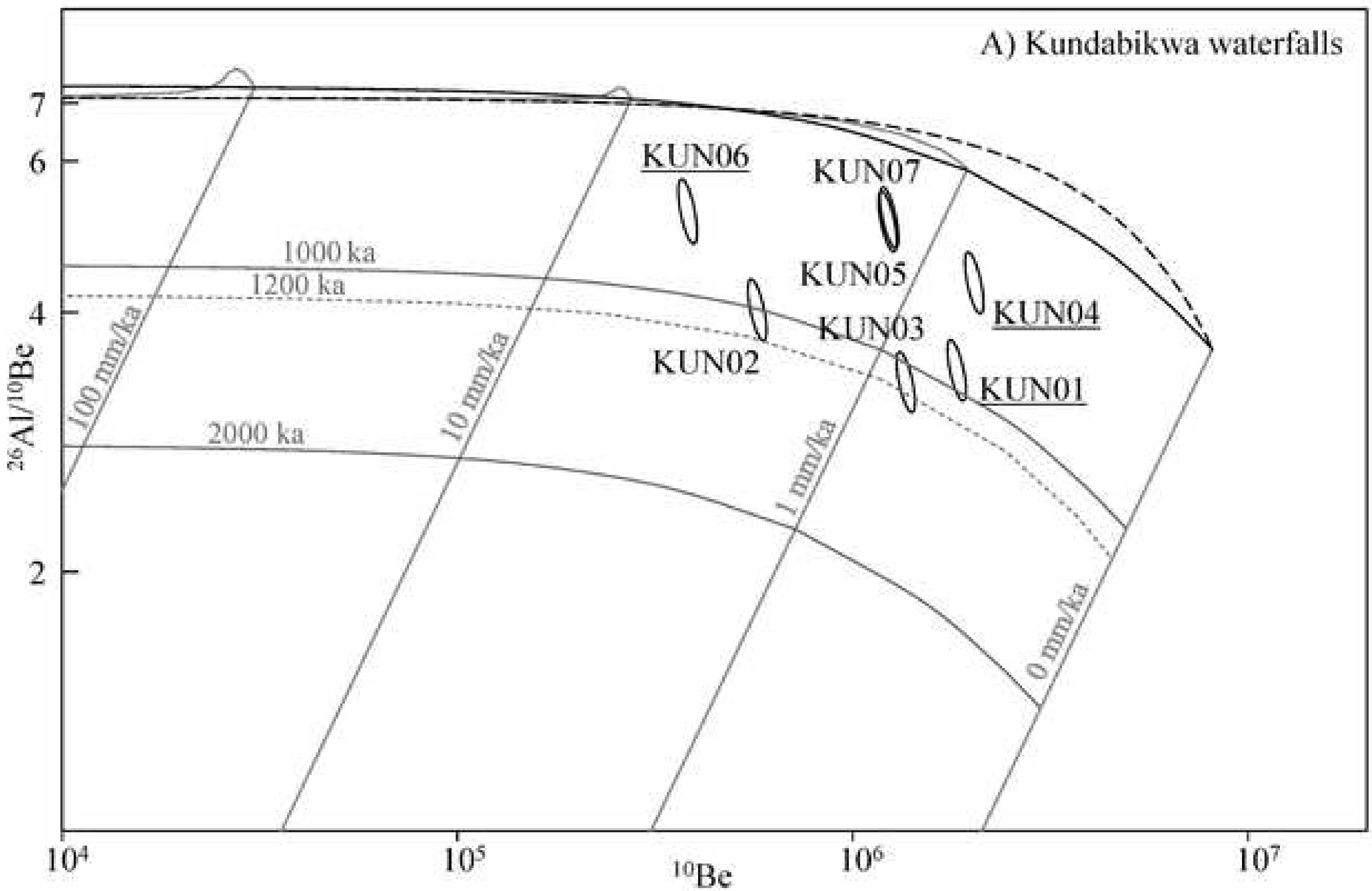
A) Kundabikwa waterfalls
KUN06
KUN07
KUN05
KUN04
KUN03
KUN02
KUN01
1000 ka
1200 ka
2000 ka
100 mm/ka
10 mm/ka
1 mm/ka
0 mm/ka
7
6
4
2
$^{26}$Al/$^{10}$Be
$10^4$
$10^5$
$10^6$
$10^7$
$^{10}$Be

Figure (Greyscale) Click here to access/download;Figure (Greyscale);Figure 8b_Greyscale.jpg

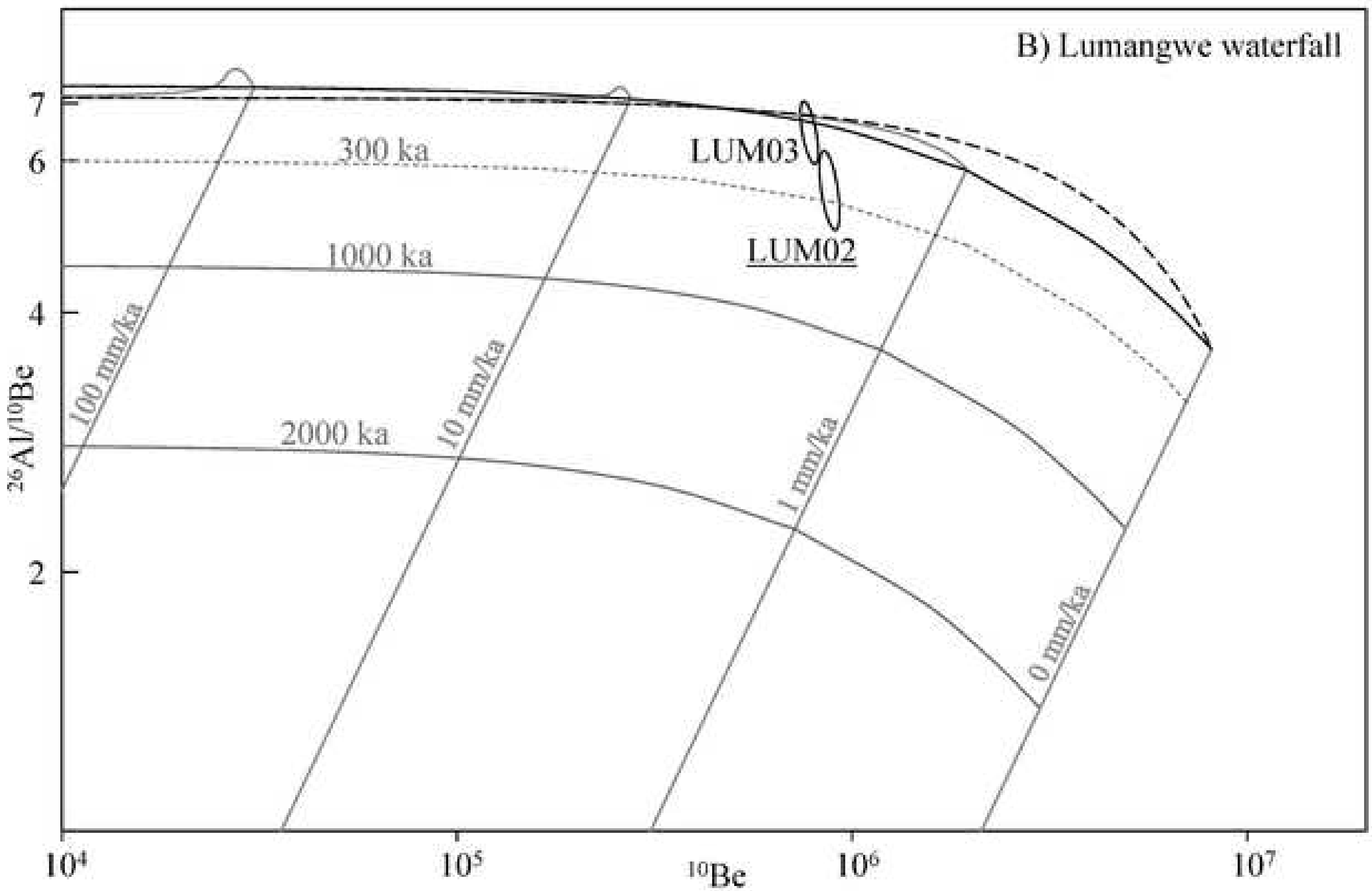

Figure (Greyscale) Click here to access/download;Figure (Greyscale);Figure 8c_Greyscale.jpg

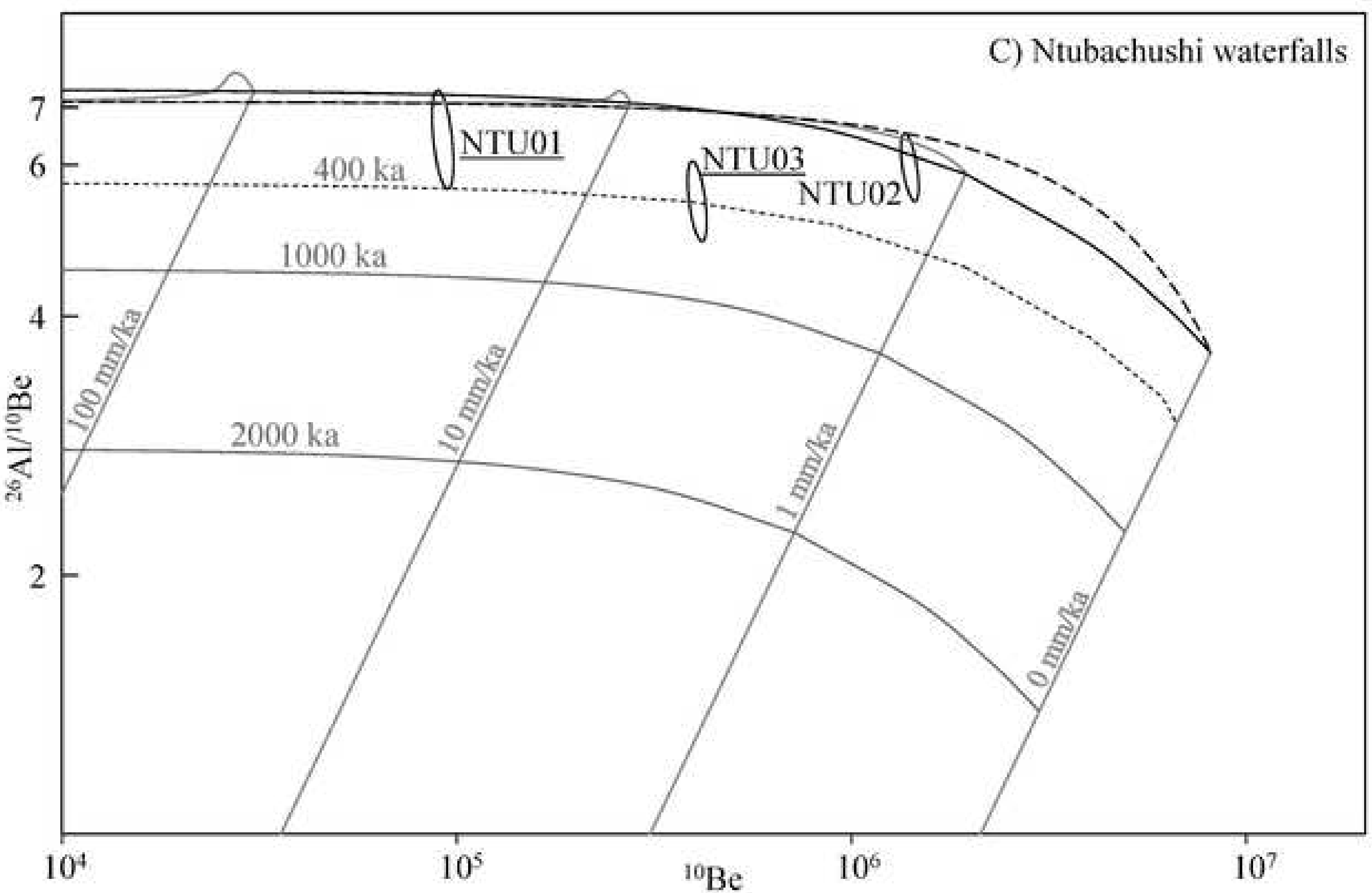

Figure (Greyscale) Click here to access/download;Figure (Greyscale);Figure 8d_Greyscale.jpg

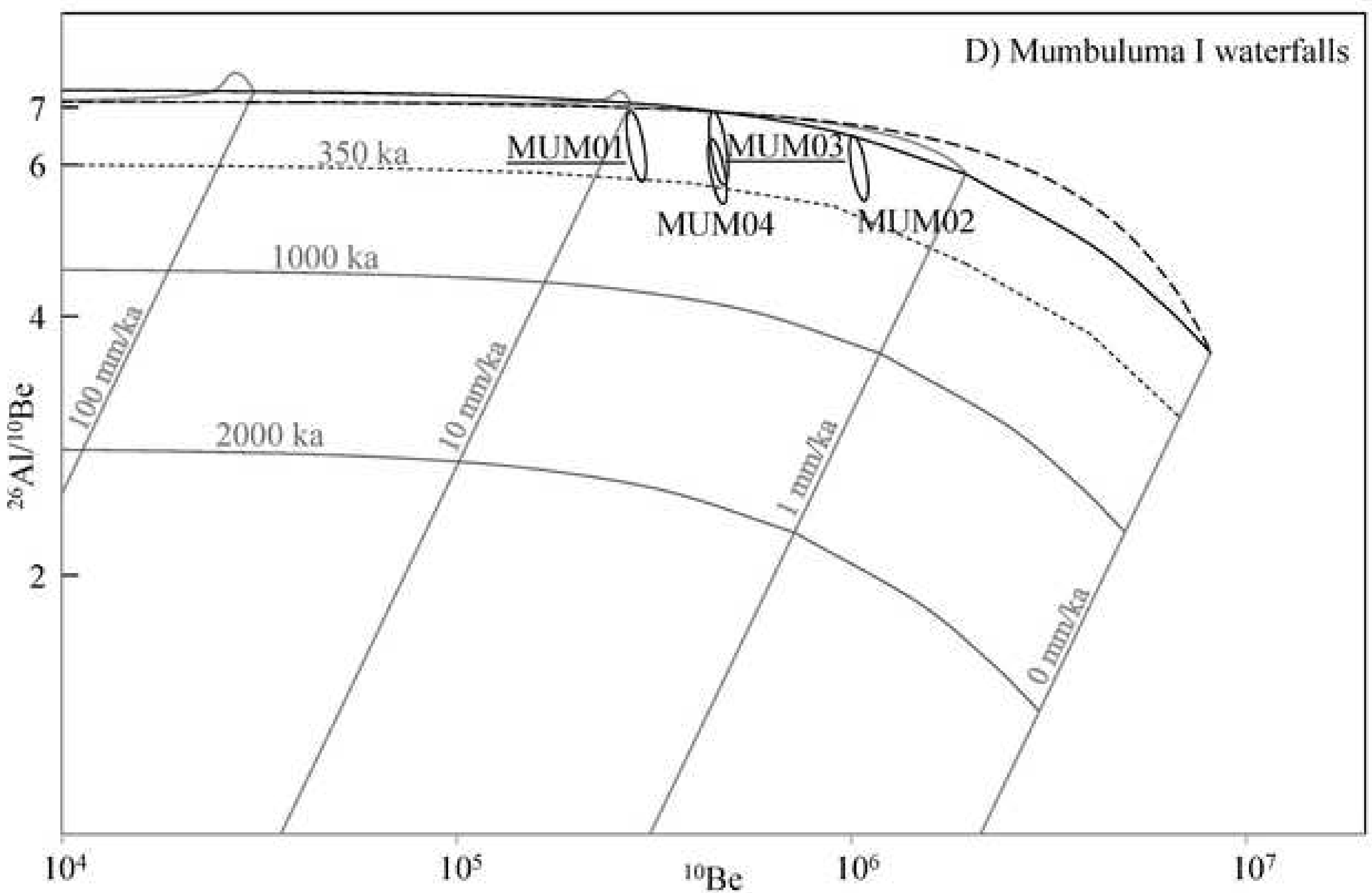

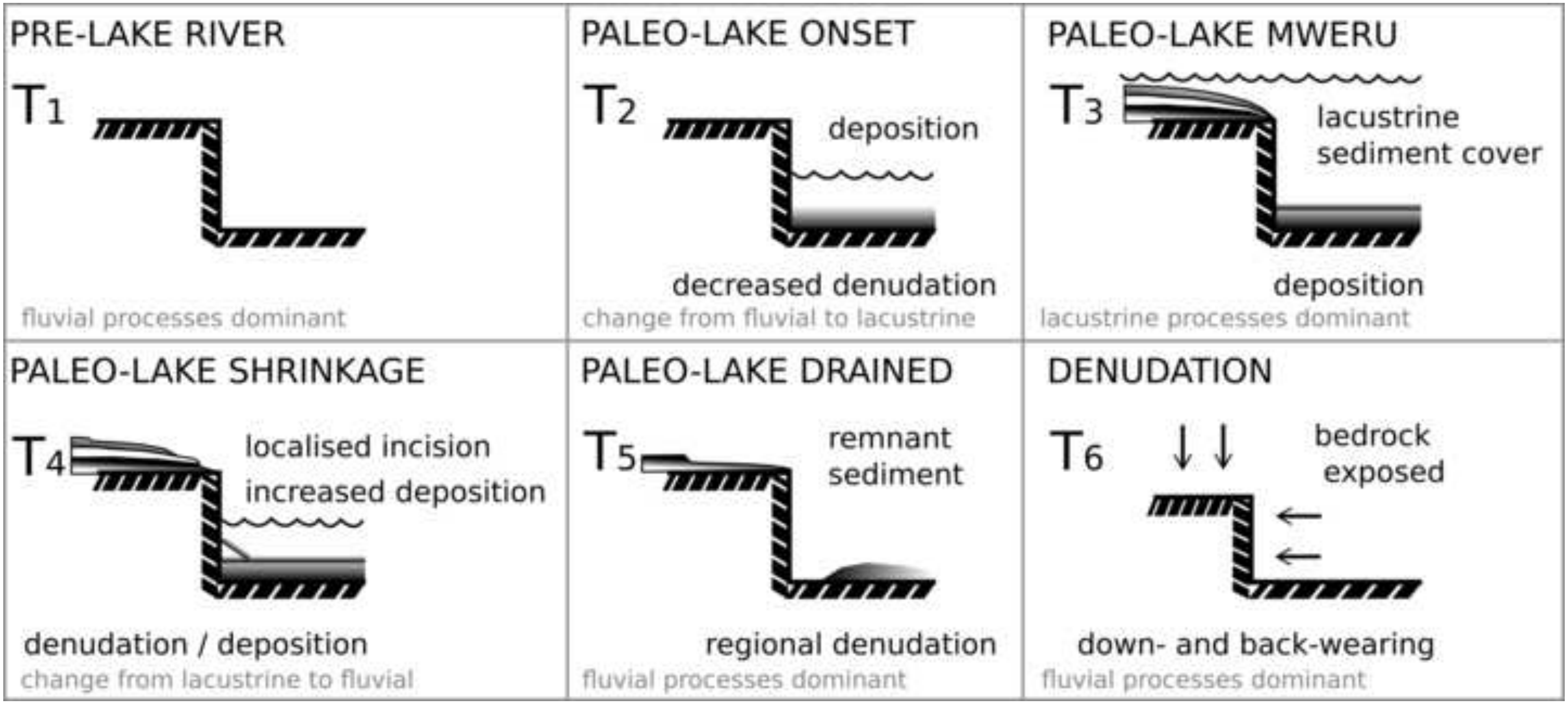
PRE-LAKE RIVER
T1
fluvial processes dominant
PALEO-LAKE ONSET
T2
deposition
decreased denudation
change from fluvial to lacustrine
PALEO-LAKE MWERU
T3
lacustrine sediment cover
deposition
lacustrine processes dominant
PALEO-LAKE SHRINKAGE
T4
localised incision
increased deposition
denudation / deposition
change from lacustrine to fluvial
PALEO-LAKE DRAINED
T5
remnant sediment
regional denudation
fluvial processes dominant
DENUDATION
T6
bedrock exposed
down- and back-wearing
fluvial processes dominant

Figure (Greyscale) Click here to access/download;Figure (Greyscale);Figure 11_Greyscale.jpg

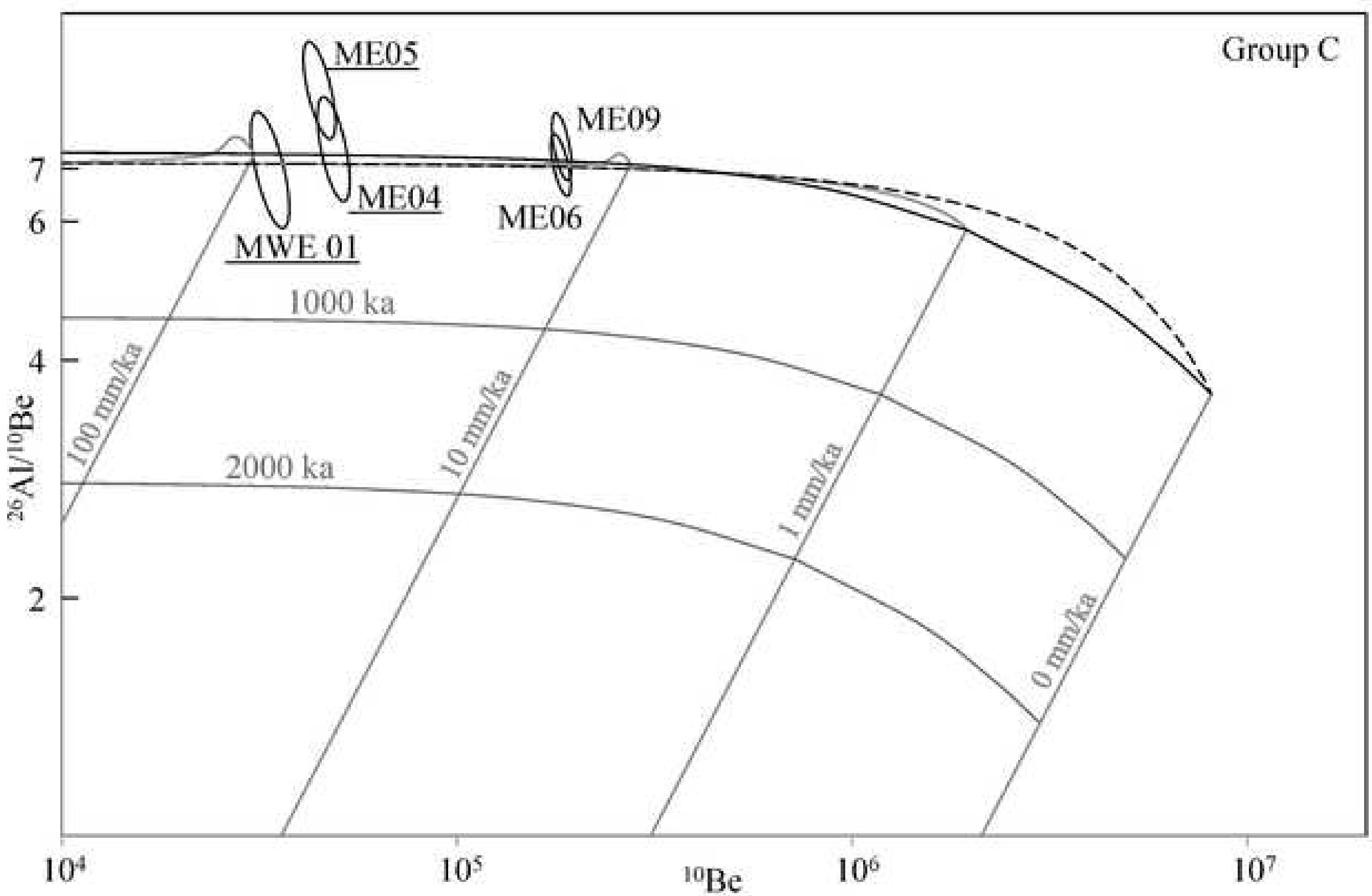

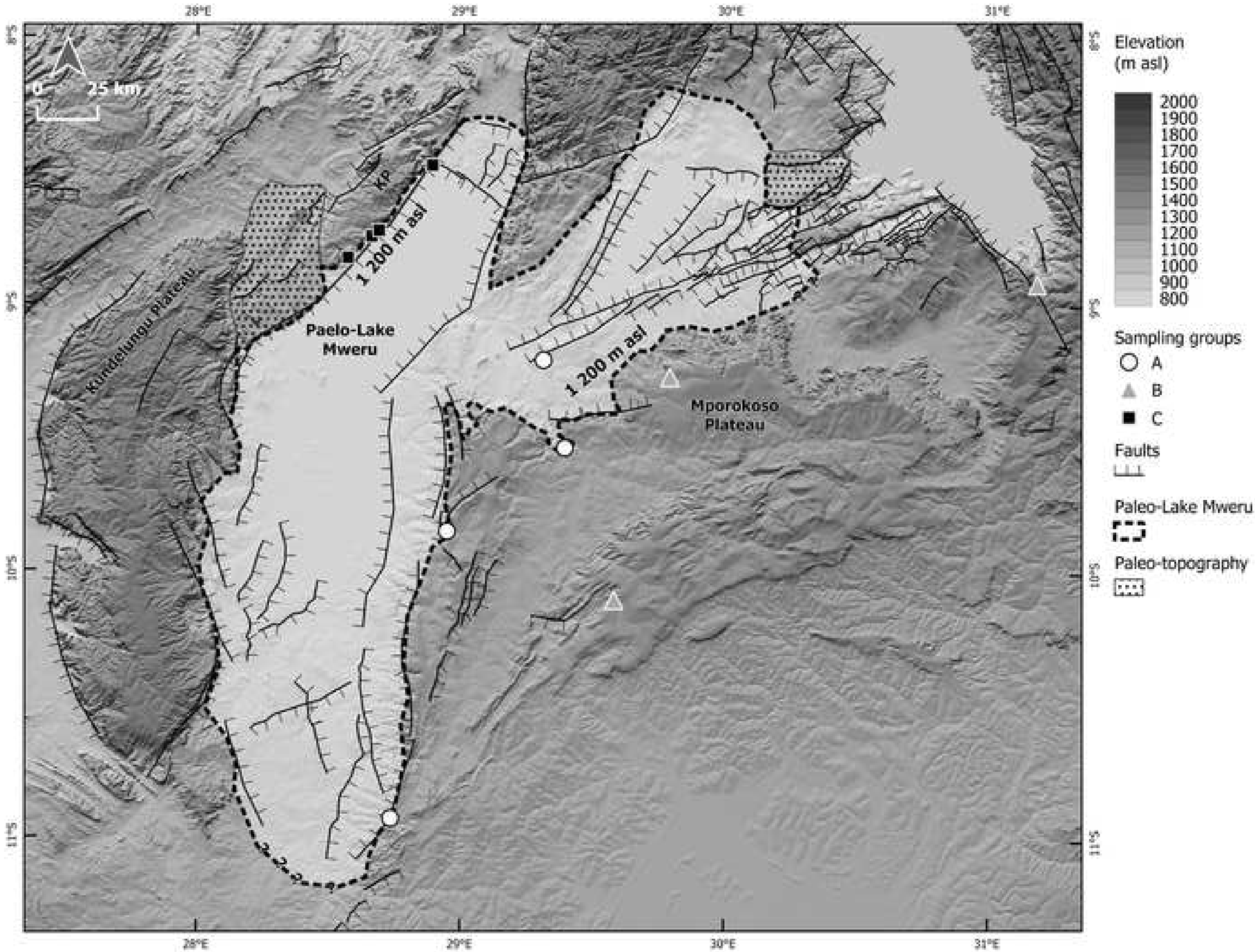
28°E
29°E
30°E
31°E
8°S
9°S
10°S
11°S
0 25 km
KP
1 200 m asl
Kundelungu Plateau
Paelo-Lake Mweru
1 200 m asl
Mporokoso Plateau
Elevation (m asl)
2000
1900
1800
1700
1600
1500
1400
1300
1200
1100
1000
900
800
Sampling groups
A
B
C
Faults
Paleo-Lake Mweru
Paleo-topography

Figure (Greyscale) Click here to access/download;Figure (Greyscale);Figure 10a_Greyscale.jpg

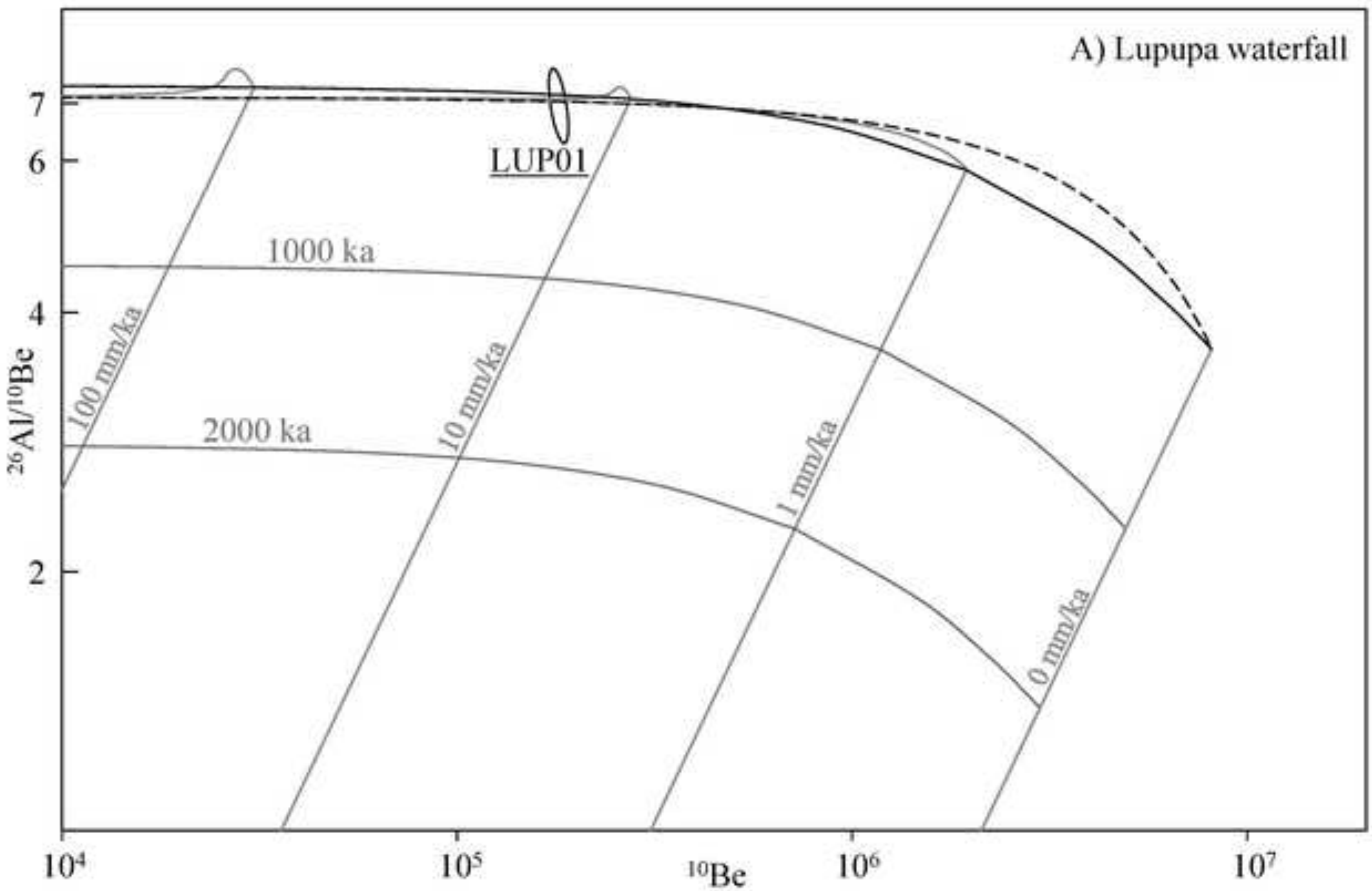

Figure (Greyscale) Click here to access/download;Figure (Greyscale);Figure 10b_Greyscale.jpg

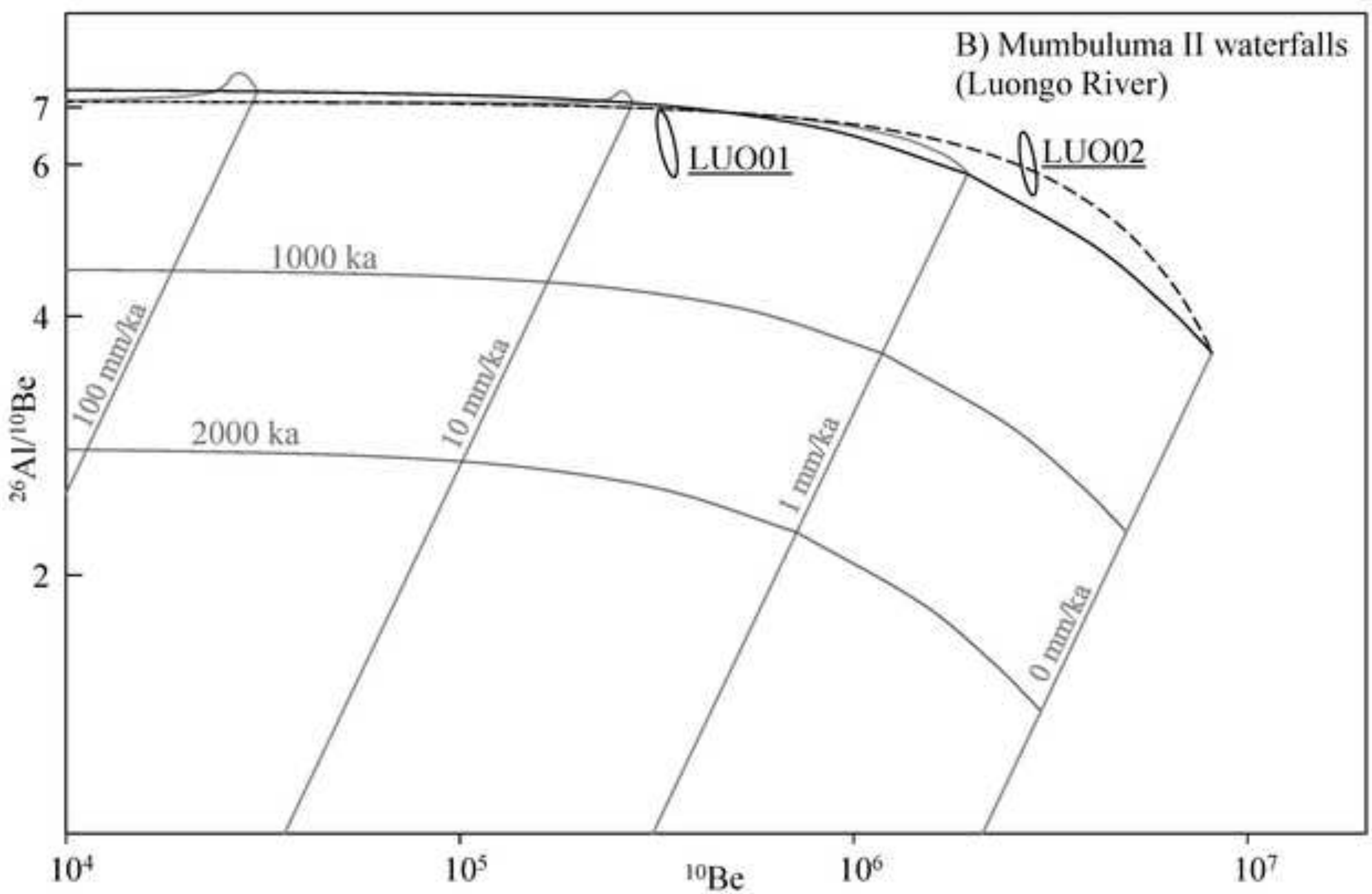

Figure (Greyscale) Click here to access/download;Figure (Greyscale);Figure 10c_Greyscale.jpg

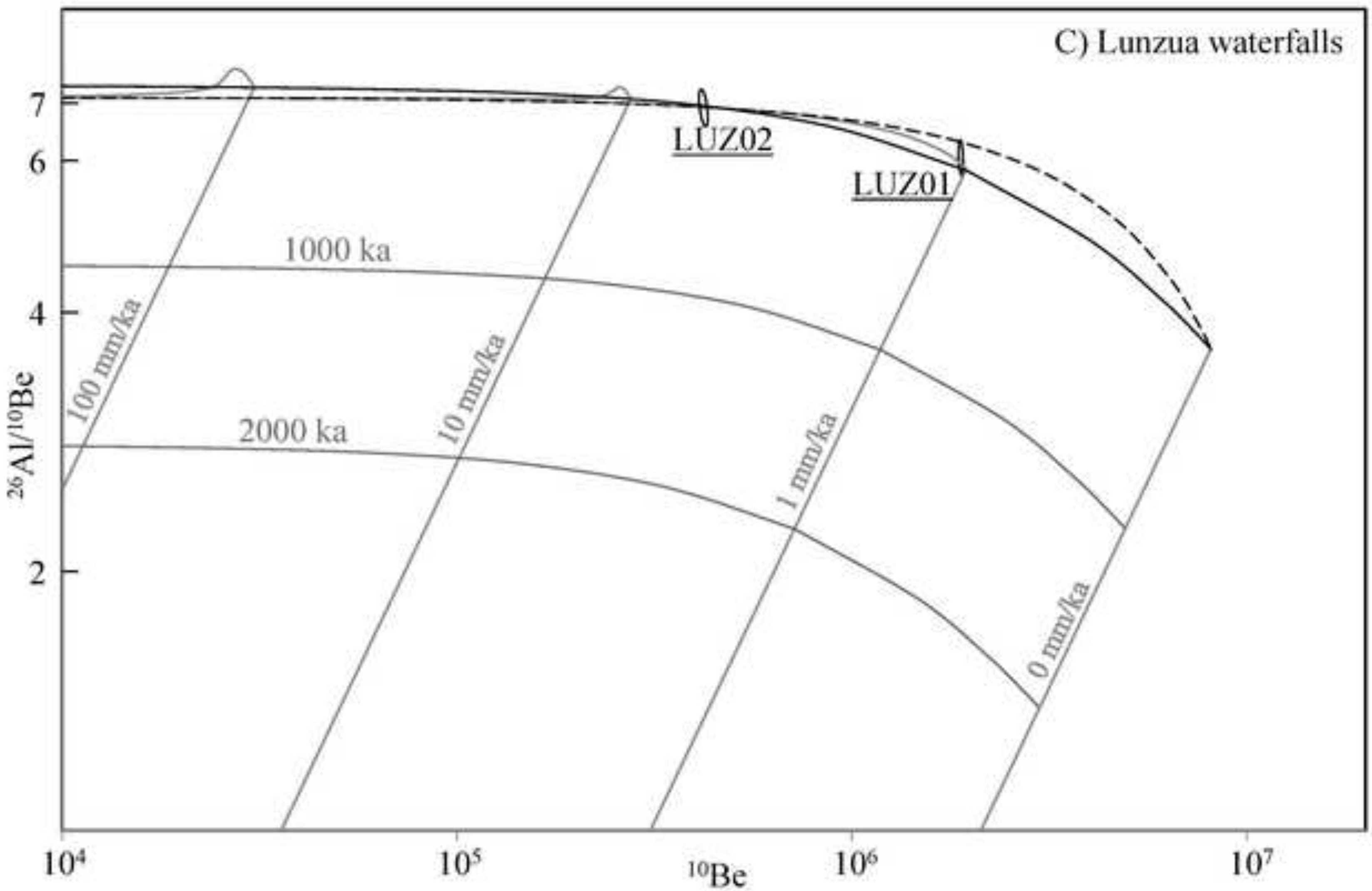

Figure (Greyscale)
Click here to access/download;Figure (Greyscale);Figure 6a_Greyscale.png

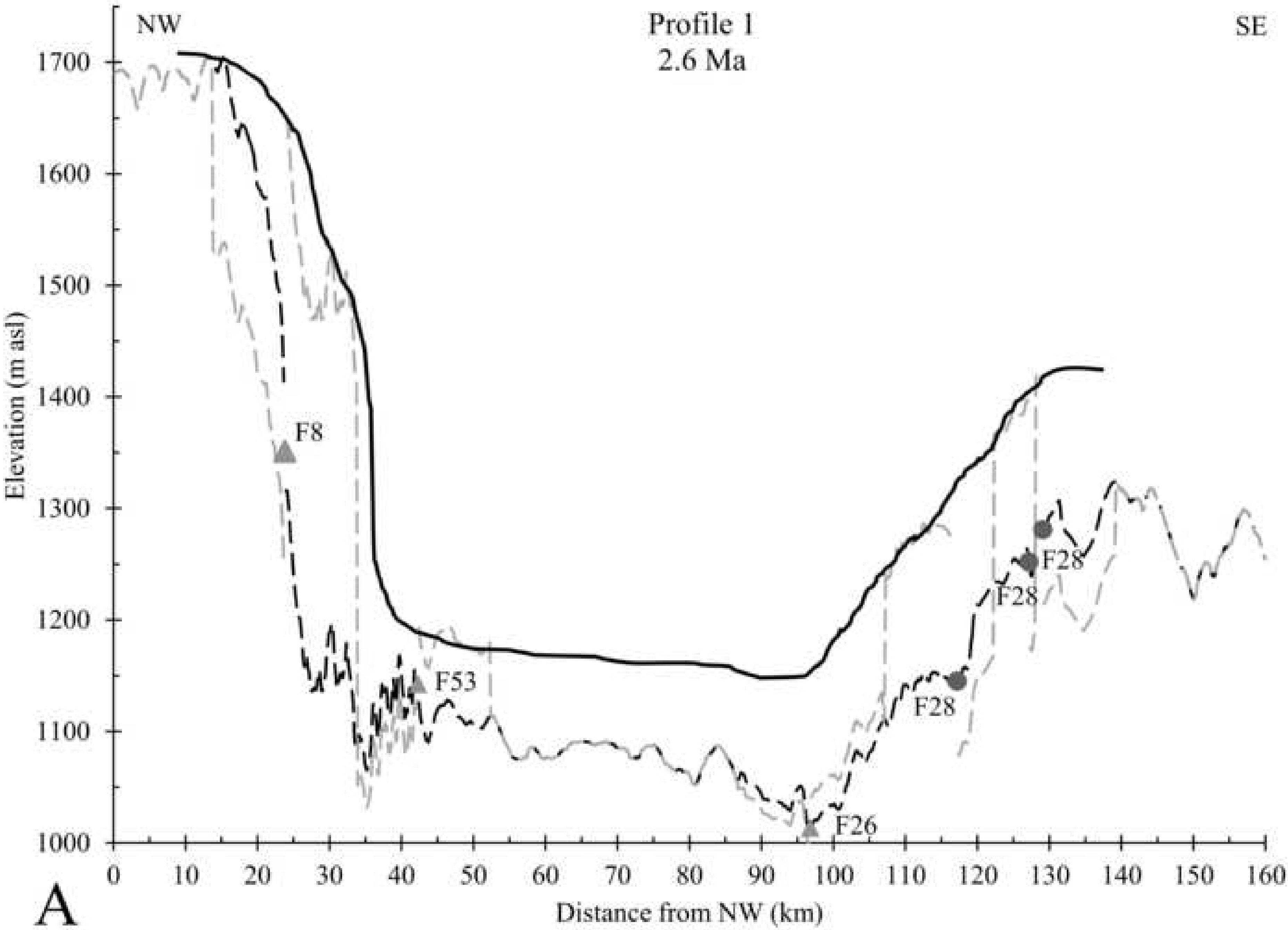

Figure (Greyscale)

Click here to access/download;Figure (Greyscale);Figure 6b_Greyscale.png

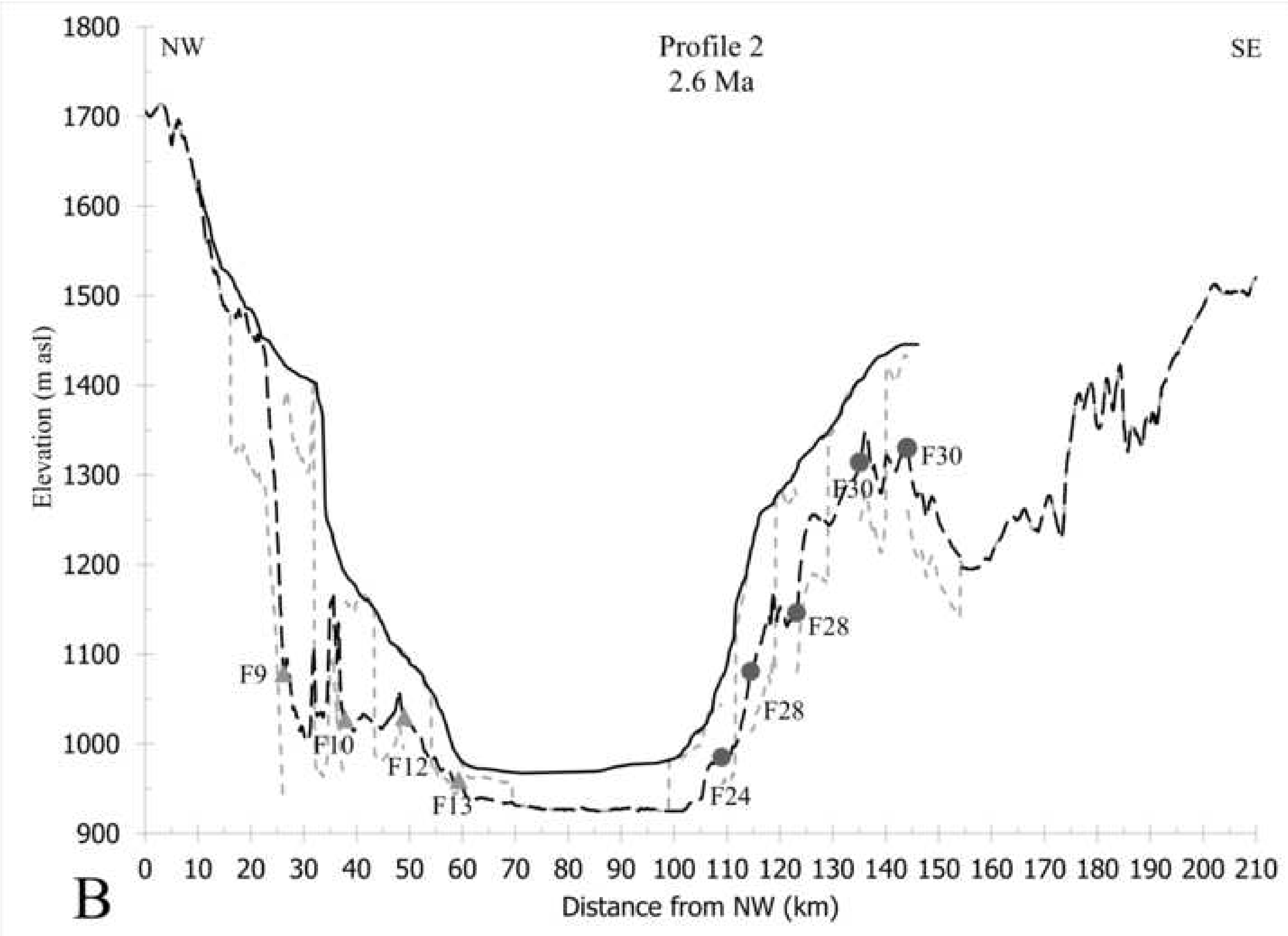

Figure (Greyscale)

Click here to access/download;Figure (Greyscale);Figure 6c_Greyscale.png

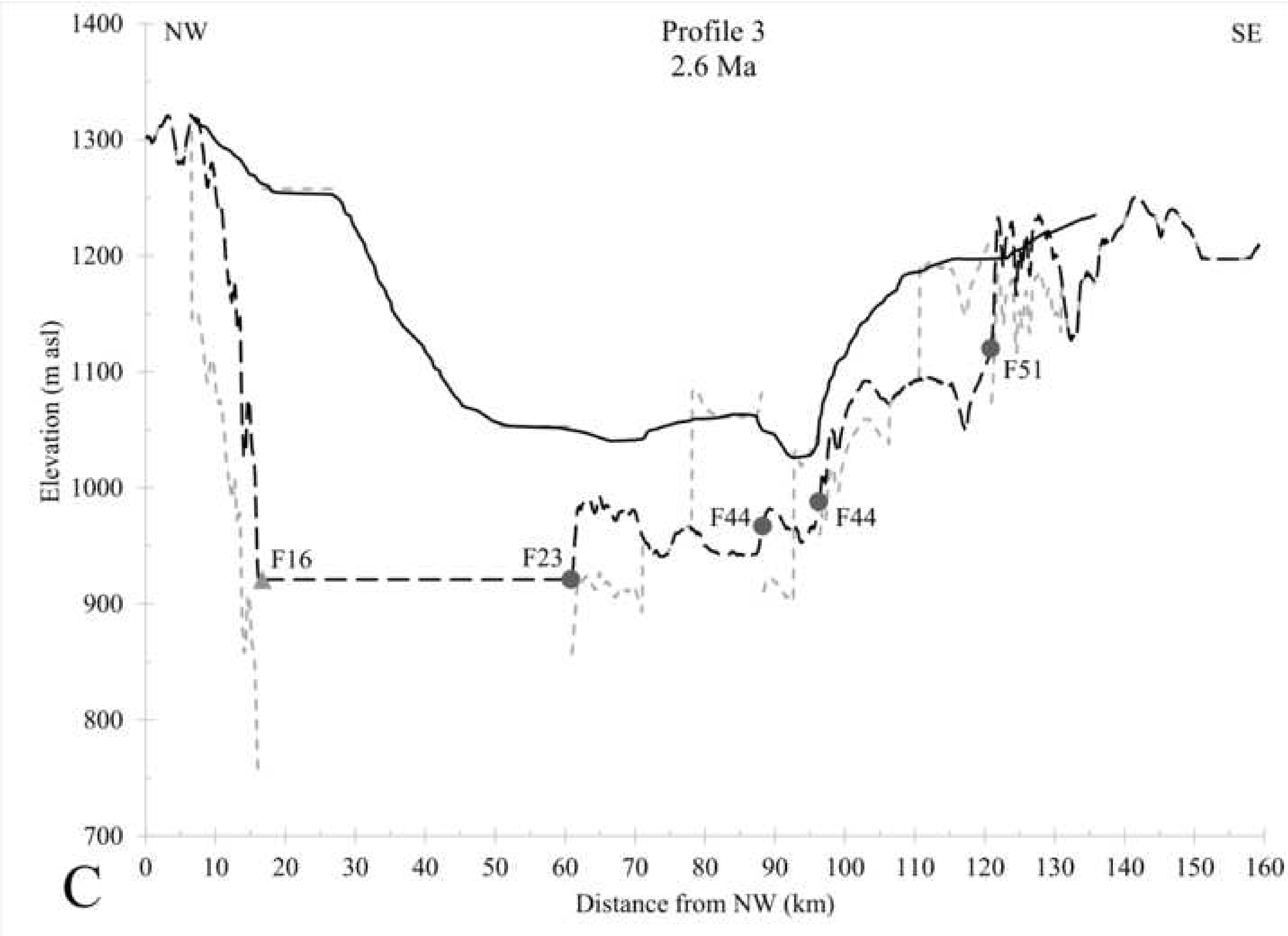

Figure (Greyscale)

Click here to access/download;Figure (Greyscale);Figure 6d_Greyscale.png

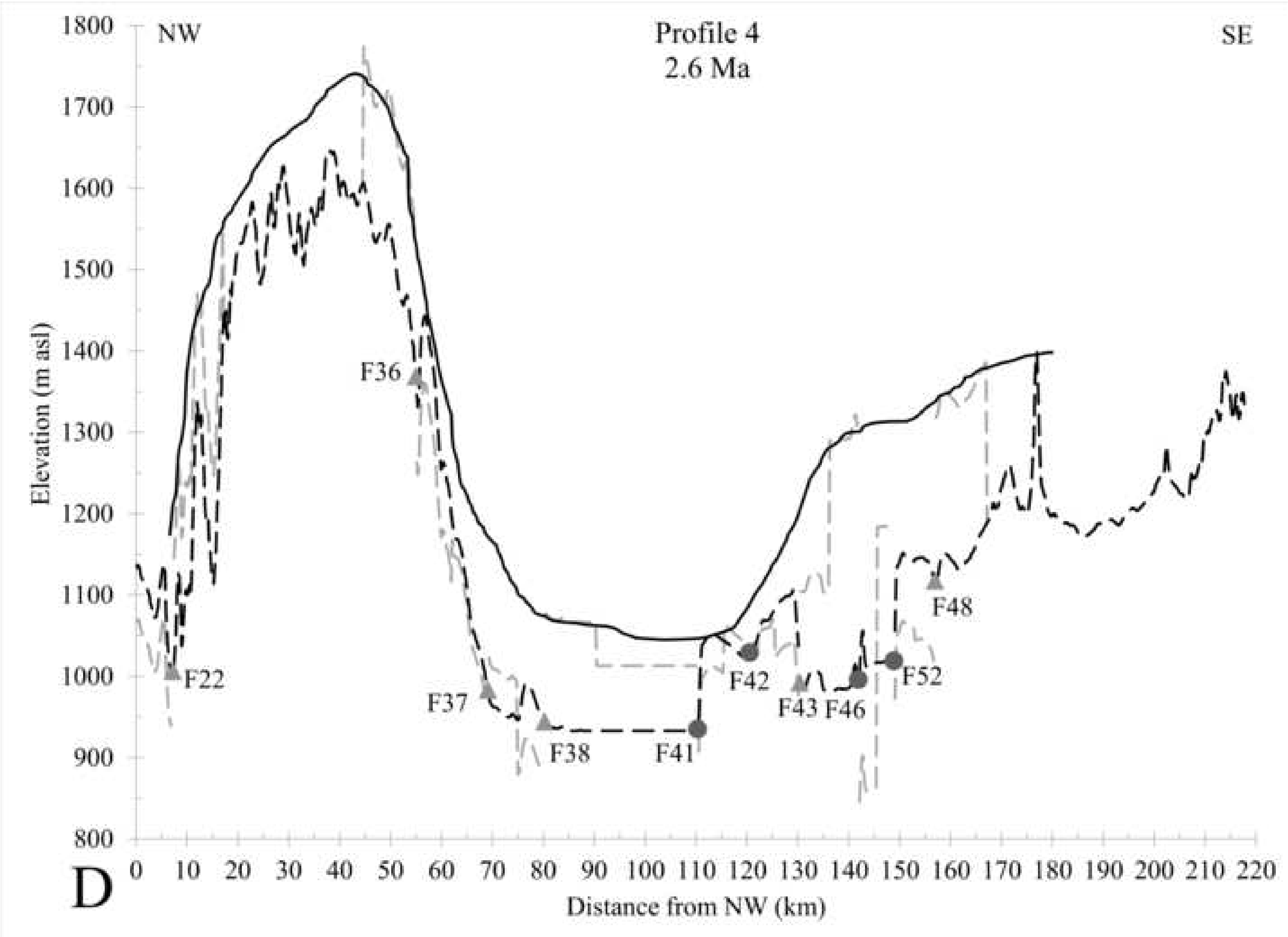

Figure (Greyscale) Click here to access/download;Figure (Greyscale);Figure 6e_Greyscale.png

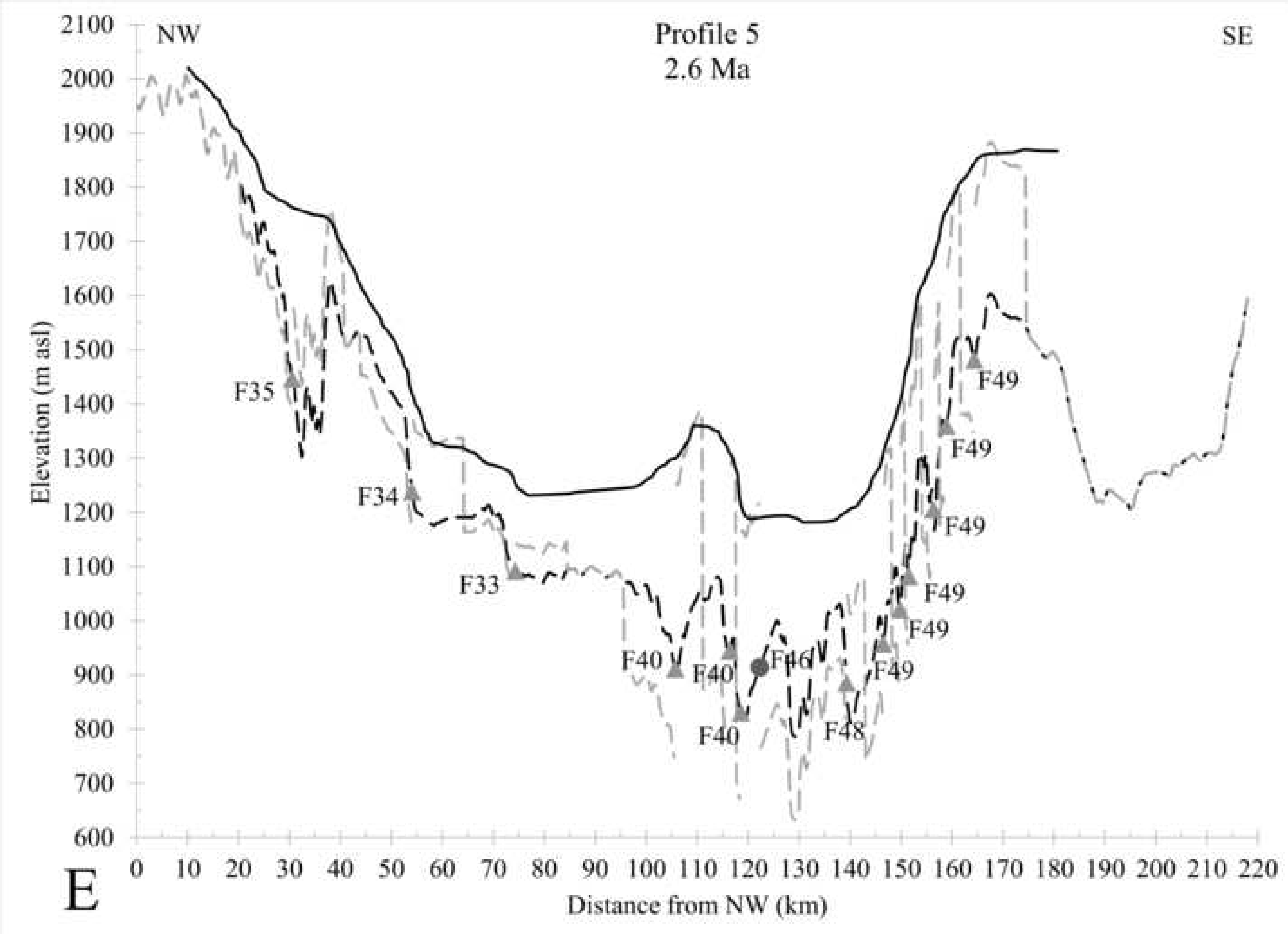

Figure (Greyscale) Click here to access/download;Figure (Greyscale);Figure 6f_Greyscale.png

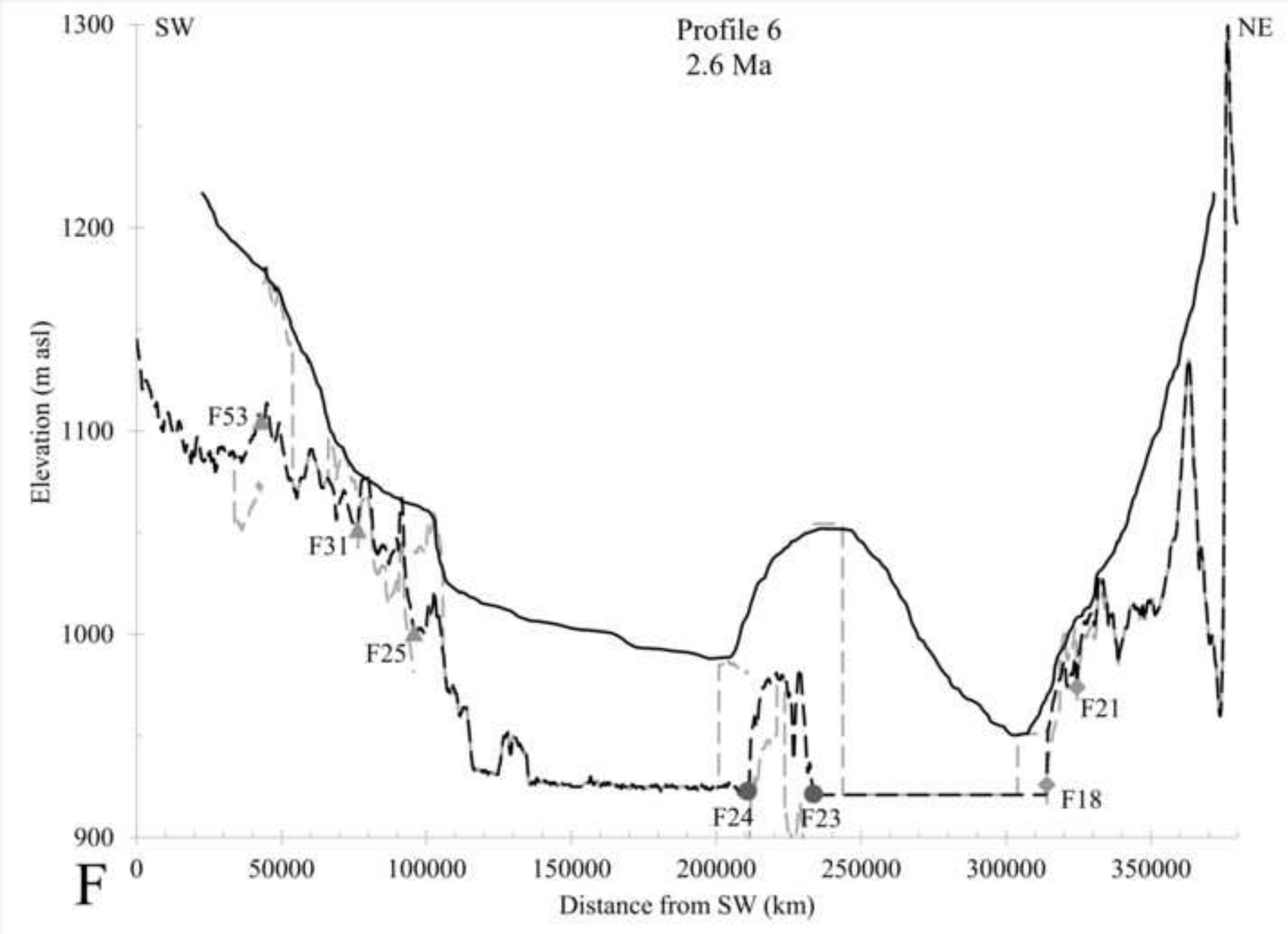

Figure (Greyscale)

Click here to access/download;Figure (Greyscale);Figure 6g_Greyscale.png

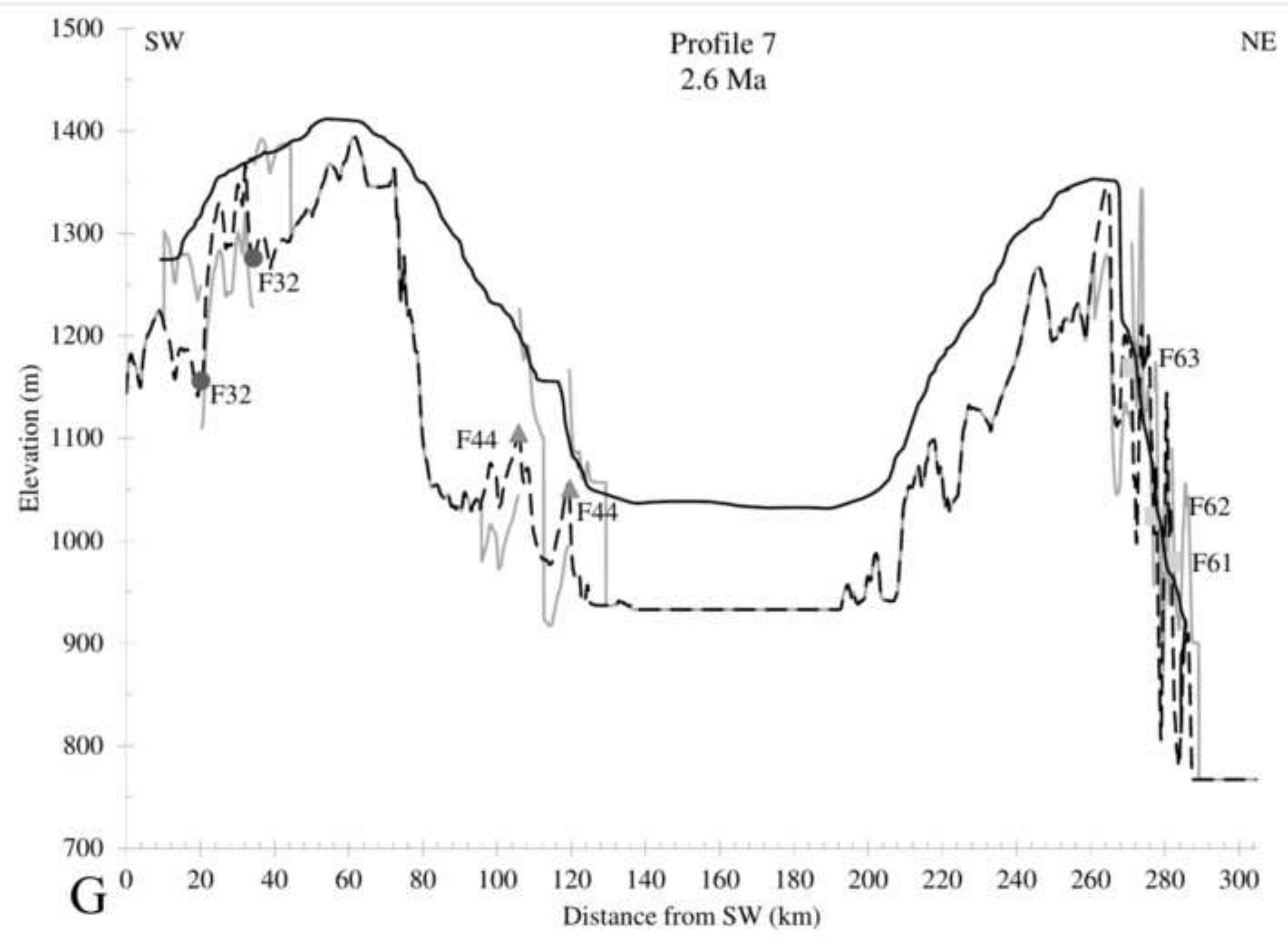

Figure (Greyscale)

Click here to access/download;Figure (Greyscale);Figure 6h_Greyscale.png

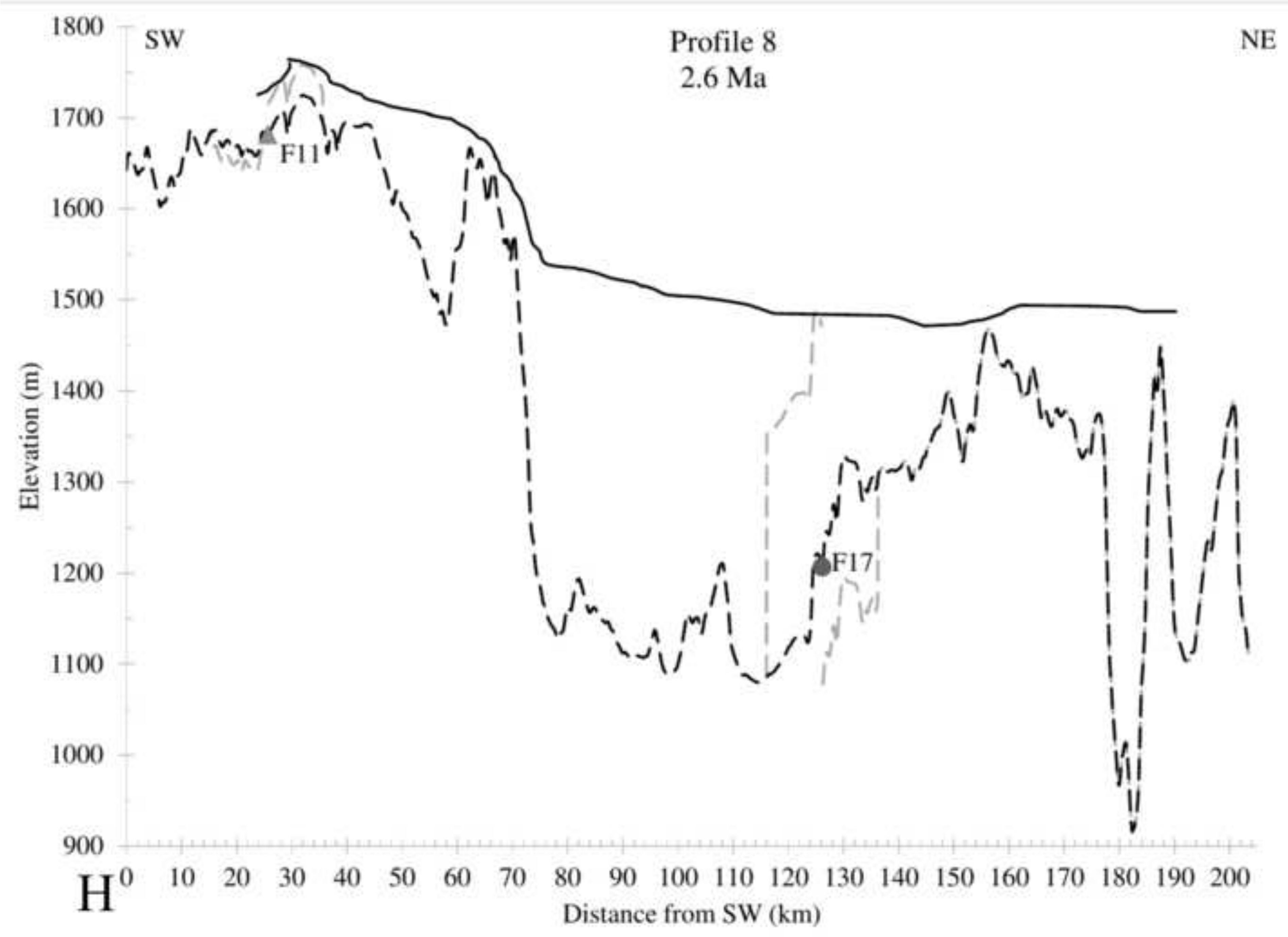

Click here to access/download

**Supplementary material for online publication only**

Figure A2.png

Click here to access/download
**Supplementary material for online publication only**
Figure A3a.jpg

Click here to access/download
**Supplementary material for online publication only**
Figure A3b.jpg

Click here to access/download
**Supplementary material for online publication only**
Figure A3c.jpg

Click here to access/download

**Supplementary material for online publication only**

Figure A4a.jpg

Click here to access/download
**Supplementary material for online publication only**
Figure A5e.png

**Declaration of interests**

☒ The authors declare that they have no known competing financial interests or personal relationships that could have appeared to influence the work reported in this paper.

☐The authors declare the following financial interests/personal relationships which may be considered as potential competing interests: